

The art of simulating the early Universe

A dissertation on lattice techniques for the simulation of scalar and gauge field dynamics in an expanding Universe

Part I: Integration Techniques and Canonical Cases

Daniel G. Figueroa¹

Instituto de Física Corpuscular (IFIC), Consejo Superior de Investigaciones Científicas (CSIC) and Universitat de Valencia (UV), Valencia, Spain.

Adrien Florio²

Institute of Physics, Laboratory of Particle Physics and Cosmology (LPPC), École Polytechnique Fédérale de Lausanne (EPFL), CH-1015 Lausanne, Switzerland.

Francisco Torrenti³

Department of Physics, University of Basel, Klingelbergstr. 82, CH-4056 Basel, Switzerland.

Wessel Valkenburg⁴

Institute of Physics, Laboratory of Particle Physics and Cosmology (LPPC), École Polytechnique Fédérale de Lausanne (EPFL), CH-1015 Lausanne, Switzerland.

¹daniel.figueroa@ific.uv.es

²adrien.florio@epfl.ch

³f.torrenti@unibas.ch

⁴wessel.valkenburg@epfl.ch

The art of simulating the early Universe – Part I

Daniel G. Figueroa¹, Adrien Florio², Francisco Torrentí³ and Wessel Valkenburg⁴

¹*Instituto de Física Corpuscular (IFIC), CSIC-Universitat de Valencia, Spain.*

^{2,4}*Institute of Physics, Laboratory of Particle Physics and Cosmology (LPPC),
École Polytechnique Fédérale de Lausanne (EPFL), CH-1015 Lausanne, Switzerland.*

³*Department of Physics, University of Basel, Klingelbergstr. 82, CH-4056 Basel, Switzerland.*

Abstract

We present a comprehensive discussion on lattice techniques for the simulation of scalar and gauge field dynamics in an expanding universe. After reviewing the continuum formulation of scalar and gauge field interactions in Minkowski and FLRW backgrounds, we introduce the basic tools for the discretization of field theories, including *lattice gauge invariant* techniques. Following, we discuss and classify numerical algorithms, ranging from methods of $\mathcal{O}(\delta t^2)$ accuracy like *staggered leapfrog* and *Verlet integration*, to *Runge-Kutta* methods up to $\mathcal{O}(\delta t^4)$ accuracy, and the *Yoshida* and *Gauss-Legendre* higher-order integrators, accurate up to $\mathcal{O}(\delta t^{10})$. We adapt these methods for their use in classical lattice simulations of the non-linear dynamics of scalar and gauge fields in an expanding grid in $3+1$ dimensions, including the case of ‘self-consistent’ expansion sourced by the volume average of the fields’ energy and pressure densities. We present lattice formulations of canonical cases of: *i) Interacting scalar fields*, *ii) Abelian $U(1)$ gauge theories*, and *iii) Non-Abelian $SU(2)$ gauge theories*. In all three cases we provide symplectic integrators, with accuracy ranging from $\mathcal{O}(\delta t^2)$ up to $\mathcal{O}(\delta t^{10})$. For each algorithm we provide the form of relevant observables, such as energy density components, field spectra and the Hubble constraint. We note that all our algorithms for gauge theories always respect the Gauss constraint to machine precision, even in the case of ‘self-consistent’ expansion. As a numerical example we analyze the post-inflationary dynamics of an oscillating inflaton charged under $SU(2) \times U(1)$. We note that the present manuscript is meant as part of the theoretical basis for the code *CosmoLattice*, a multi-purpose MPI-based package for simulating the non-linear evolution of field theories in an expanding universe, to be released in 2020.

Contents

1	Introduction	4
1.1	The <i>Numerical Early Universe</i> : a laboratory for non-linear high energy physics	4
1.2	Purpose of this manuscript. Introducing <i>CosmoLattice</i>	6
1.3	Conventions and notation	9
2	Field dynamics in the continuum	9
2.1	Scalar and Gauge field interactions in flat space-time	9
2.2	Field dynamics in an expanding background	12
2.3	Dynamics of the expanding background	13
3	Field dynamics in a computer: the lattice approach	14
3.1	Lattice definition and discrete Fourier transform	14
3.2	Lattice representation of differential operators	16
3.2.1	Derivative operators and lattice momenta	16
3.2.2	Lattice gauge invariant techniques	17
3.3	Evolution algorithms	19
3.3.1	Staggered leapfrog	21
3.3.2	Verlet integration	23
3.3.3	Explicit Runge-Kutta methods	25

3.4	Higher-order integrators	26
3.4.1	Yoshida method: recursive Verlet integration	26
3.4.2	Gauss-Legendre methods: Implicit Runge-Kutta	27
3.5	Integrator properties	29
4	Lattice formulation of interacting scalar fields	30
4.1	Continuum formulation and natural variables	30
4.2	Lattice formulation of interacting scalar fields: $\mathcal{O}(dt^2)$ accuracy methods	33
4.2.1	Staggered leapfrog from a lattice action	33
4.2.2	Staggered leapfrog <i>à la LatticeEasy</i>	35
4.2.3	Synchronized Leapfrog: Position- and Velocity-Verlet	37
4.3	$\mathcal{O}(dt^n)$ Lattice formulation of interacting scalar fields	39
4.3.1	Explicit Runge-Kutta 4th order	39
4.3.2	Verlet Integration n th order	40
4.3.3	Gauss-Legendre n th order	41
4.4	Observables	42
4.4.1	Energy components	42
4.4.2	Spectra	42
5	Lattice formulation of gauge fields, I: $U(1)$ interactions	42
5.1	Continuum formulation and natural variables	43
5.2	Non-compact Lattice formulation of scalar-gauge dynamics	43
5.2.1	Staggered Leap-Frog	44
5.2.2	Velocity-Verlet	45
5.2.3	Velocity-Verlet n th order	45
5.3	Compact Lattice formulation of scalar-gauge dynamics	46
5.3.1	Staggered Leap-Frog	47
5.3.2	Velocity-Verlet	47
5.3.3	Velocity-Verlet n th order	48
5.4	Observables	49
5.4.1	Energy components	49
5.4.2	Spectra	49
6	Lattice formulation of gauge fields, II: $SU(N)$ interactions	50
6.1	Continuum formulation and natural variables	50
6.2	Lattice formulation of scalar-gauge dynamics	50
6.2.1	Staggered Leap-Frog	51
6.2.2	Velocity Verlet	52
6.2.3	Velocity Verlet n th order	52
6.3	Observables	53
6.3.1	Energy components	53
6.3.2	Spectra	54
7	Initial conditions	54
7.1	Stochastic spectrum of scalar fluctuations	54
7.2	Charged scalars and gauge fields	56
8	A working example: the $SU(2) \times U(1)$ gauge invariant inflaton	59
8.1	Model details	59
8.1.1	Preheating	61
8.2	Lattice simulations: $U(1)$ gauge interactions	63
8.2.1	Accuracy tests	68
8.3	Lattice simulations: $SU(2) \times U(1)$ gauge interactions	69

1 Introduction

1.1 The Numerical Early Universe: a laboratory for non-linear high energy physics

Compelling evidence [1] supports the idea of *inflation*, a phase of accelerated expansion in the early universe, which provides both a solution to the shortcomings of the hot Big Bang framework [2–8], and an explanation for the origin of the primordial density perturbations [9–13]. Inflation is often assumed to be driven by a scalar field, the *inflaton*, with potential and initial conditions appropriately chosen to sustain a long enough period of accelerated expansion. To switch to the standard hot Big Bang cosmology, a *reheating* period must be ensured after inflation, converting the energy available into light degrees of freedom (*dof*), which eventually thermalize and dominate the universe energy budget. This transition process is an integral part of the inflationary paradigm, although observationally much less constrained than the inflationary period itself. For reviews on inflation and reheating, see [14–17] and [18–21].

In many scenarios, the inflaton oscillates around the minimum of its potential following the end of inflation, initially in the form of a homogeneous condensate. Particle species coupled sufficiently strongly to it are then created in energetic bursts. If the particles are bosons, their production is driven by parametric resonance, resulting in an exponential transfer of energy within few oscillations of the inflaton [22–29]. If the particles are fermion species, there can also be a significant transfer of energy [30–33], albeit no resonance can be developed due to Pauli blocking. Particle production in this way, of either bosons or fermions, corresponds to a non-perturbative effect, which cannot be described with standard quantum field theory (QFT) perturbative techniques. Furthermore, particle species created by these effects are typically far away from thermal equilibrium, and in the case of bosonic species their production is exponential, so they eventually backreact onto the inflaton, breaking apart its initial homogeneous condition. The dynamics of the system becomes non-linear from that moment onward. All of these effects, from the initial particle production to the eventual development of non-linearities in the system, represent what is referred to as a *preheating* stage. In order to fully capture the non-perturbative, out-of-equilibrium and eventual non-linearities of preheating, we need to study such phenomena on a lattice. This requires the use of classical field theory real-time simulations, an approach valid as long as the particle species involved in the problem have large occupation numbers $n_k \gg 1$, so that their quantum nature can be neglected [34, 35].

Parametric particle production can also be developed in the early universe, in circumstances other than preheating. For instance, in the curvaton scenario [36–39], the initially homogeneous curvaton (a spectator field during inflation) may decay after inflation via parametric resonance, transferring abruptly all its energy to other particle species [40–43]. If the Standard Model (SM) Higgs is weakly coupled to the inflationary sector, the Higgs can be excited either during inflation [44–46], or towards the end of it [47, 48], in the form of a condensate with large amplitude. The Higgs then decays naturally into the rest of the SM species via parametric effects [45, 48–53], some time after inflation¹. In supersymmetric (SUSY) extensions of the SM we encounter flat directions [62, 63], configurations in field space where the renormalizable part of the scalar potential is exactly flat (as SUSY must be broken, the exact flatness is however typically uplifted by various effects [64]). During inflation, due to quantum fluctuations, field configurations can be developed with a large expectation value along these directions [63, 65]. If such scalar condensates have a soft mass, its amplitude starts oscillating after inflation once the Hubble rate becomes smaller than its mass [64, 66], possibly ensuing an explosive decay of the field condensate due to non-perturbative resonant effects [67–69].

In certain types of inflationary models where spontaneous symmetry breaking plays a central role, tachyonic effects can also lead to non-perturbative and out-of-equilibrium particle production, eventually driving the system into a non-linear regime. One example of this is Hybrid inflation [70], a family of models where the inflationary stage is sustained by the vacuum energy of a Higgs-like field. During inflation, the effective

¹Note that this differs from the Higgs-Inflation scenario [54, 55], where the Higgs also decays after inflation into SM fields via parametric effects [50, 56–61], but as the Higgs plays the role of the inflaton, this scenario belongs to the category of preheating.

squared mass of the Higgs field is positive defined, but becomes negative when the inflaton eventually crosses around a critical point. The Higgs then sustains a tachyonic mass that leads into an exponential growth of the occupation number of its most infrared (IR) modes below its own tachyonic mass scale [71–74]. This continues until the mass square becomes positive again, due to the Higgs own self-interactions. In Hilltop-inflation, inflation is sustained while the inflaton slowly rolls from close to a maximum of its potential (the ‘hilltop’) towards its minimum, located at some non-vanishing scale. When the inflaton amplitude crosses a certain threshold, inflation ends, and the inflaton starts oscillating around its minimum. Its effective squared mass then alternates between positive and negative values, as the inflaton rolls back and forth between the minimum of its potential and the region of negative curvature where inflation ended. Fluctuations of the inflaton then grow exponentially during successive tachyonic phases.

Preheating effects have been also studied in models with gravitationally non-minimal coupled fields [60, 75–80], and in particular, recently, in multi-field inflation scenarios [81–85]. In the latter, a single-field attractor behavior is developed during inflation, later persisting during preheating. Due to this, particle production after inflation becomes more efficient than in multi-field models with minimal couplings, where a *de-phasing* effect of the background fields’ oscillations leads to a damping of the resonances [20, 86–89].

Furthermore, as gauge fields are naturally present in the SM and in many of its extensions, their presence in inflationary scenarios has also been considered. Due to their bosonic nature, gauge fields can exhibit highly nonlinear dynamics during preheating. For instance, if the inflaton enjoys a shift-symmetry, a topological coupling to a gauge sector is allowed. In the case of $U(1)$ gauge fields, preheating effects have been studied in axion-inflation scenarios [90–95], showing that an interaction $\phi F\tilde{F}$ leads to an extremely efficient way to reheat the universe, as well as to very interesting (potentially observable) phenomenology. In [93, 96, 97] an improved lattice formulation of an interaction $\phi F\tilde{F}$ between an axion-like field and a $U(1)$ gauge sector was constructed, demonstrating that the topological nature of $F\tilde{F}$ as a total derivative $\partial_\mu \mathcal{K}^\mu$, can be actually realized exactly on a lattice (hence preserving exactly the shift symmetry at the lattice level). Interactions between a singlet inflaton and an Abelian gauge sector, via $f(\phi)F^2$, or a non-Abelian $SU(2)$ gauge sector, via $f(\phi)\text{Tr} G^2$, have also been explored in the context of preheating [98, 99].

In Hybrid inflation models, the presence and excitation of gauge fields have also been addressed extensively, both for Abelian and non-Abelian scenarios, obtaining a very rich phenomenology, see e.g. [100–110]. The case of preheating via parametric resonance, with a charged inflaton under a gauge symmetry, has however not been considered very often in the literature². Nothing is wrong *per se* about considering an inflaton charged under a gauge group [and hence coupled to some gauge field(s)], as long as one constructs a viable working model, respecting the observational constraints. In such a case, when the inflaton starts oscillating following the end of inflation, the corresponding gauge bosons will be parametrically excited. This has been studied in detail in Ref. [111], for both Abelian $U(1)$ and non-Abelian $SU(2)$ gauge groups. Actually, in this manuscript we also consider a similar model for which we compute the preheating stage via parametric resonance effects into $U(1)$ and $U(1) \times SU(2)$ sectors. A natural realization of an inflationary set-up where the inflaton is charged under a gauge group is the Higgs-Inflation scenario [54, 55], where the SM Higgs is the inflaton. There the electroweak gauge bosons and charged fermions of the SM are coupled to the Higgs, and thus they experience parametric excitation effects during the oscillations of the Higgs after inflation [50, 56–61]. If the SM Higgs is rather a spectator field during inflation, the post-inflationary decay of the Higgs into SM fields has also been considered in [52, 53, 112–114].

In general, the non-linear dynamics characteristic of preheating scenarios and in general of non-perturbative particle production phenomena, are interesting not only by themselves, but also because they may lead to cosmologically relevant and potentially observable phenomena. Among these, we highlight:

- The generation of scalar metric perturbations [115–124], possibly leading to the formation of primordial black holes [125–133].
- The production of stochastic gravitational wave backgrounds by parametric effects [94, 95, 109, 134–150]. For a recent review see [151].

²Possibly, this is partially due to the fact that there is no particular need to ‘gauge’ the inflationary sector, and partially because of the potential danger that gauge couplings may induce large radiative corrections in the inflaton potential, spoiling the conditions to sustain inflation.

- The creation of topological defects, like cosmic string networks [71, 109, 152–154], and their evolution during the scaling regime [155–161] and corresponding emission of GWs [162].
- The creation of soliton-like structures like oscillons [140, 143, 144, 146, 149, 153, 163–168] and similar structures [122, 169–171].
- The realization of magnetogenesis [91, 107, 108, 172–175] and baryogenesis mechanisms [91, 100–102, 102–104, 176–183].
- The determination of the post-inflationary equation of state, and its implications for the CMB inflationary observables [164, 184–188], or for the dark matter relic abundance [189].

In general, the details of nonlinear phenomena are difficult to grasp, when not impossible, by analytic calculations. In order to fully understand the non-linearities developed in a given model, the use of numerical techniques becomes necessary. The non-trivial results arising from the non-linear dynamics of early universe high-energy phenomena, represents an important perspective in determining the best observational strategies to probe the unknown physics from this era. It is therefore crucial to develop numerical techniques, as efficient and robust as possible, to simulate these phenomena. Numerical algorithms developed for this purpose must satisfy a number of physical constraints (e.g. energy conservation), and keep the numerical integration errors under control. It is actually useful to develop as many techniques as possible, to validate and double check results from simulations. Only in this way, we will achieve a certain robustness in the predictions of the potentially observational implications from non-linear high energy phenomena. Furthermore, the techniques developed for studying nonlinear dynamics of classical fields, are common to many other non-linear problems in the early universe, like the dynamics of phase transitions [73, 74, 97, 190, 190–194] and their emission of gravitational waves [195–201], cosmic defect formation [109, 154, 202–209], their later evolution [155–161, 210, 211] and gravitational wave emission [109, 162, 212], axion-like field dynamics [166, 170, 213–216], moduli dynamics [217, 218], etc. These techniques can also be used in applications of interest not only to cosmology, but also to other high energy physics areas. For example, classical-statistical simulations have been used to compute quantities such as the sphaleron-rate [219–234] and to study the Abelian [97, 192, 235–238] and non-Abelian [239] dynamics associated to the chiral anomaly, as well as for spectral quantities [240, 241], and some properties of the quark-gluon plasma [242–245].

1.2 Purpose of this manuscript. Introducing *CosmoLattice*

As just reviewed in the previous section, the phenomenology of high-energy non-linear processes in the early universe is vast and very rich. In order to make reliable predictions of their potentially observable consequences, we need appropriate numerical tools. The *Numerical Early Universe*, i.e. the study of high-energy non-linear field theory phenomena with numerical techniques, is an emerging field, and it is increasingly gaining relevance, especially as a methodology to assess our capabilities to experimentally constrain (or even determine) the physics of this (yet) unknown epoch. It is because we recognize the importance of this, that we have created this dissertation, the content and purpose of which we explain next.

The present manuscript is part of the theoretical basis for the code *CosmoLattice*, a modern multi-purpose MPI-based C++ package, to be publicly released in 2020 as a user-friendly software for lattice simulations of the non-linear dynamics of scalar and gauge field *dof* in an expanding background, with the expansion rate of the universe ‘self-consistently’ sourced by the fields themselves. Of course, exploring numerically the nonlinear dynamics of interacting fields during the early universe is not a new idea, as witnessed by the increasing number of lattice codes dedicated to this purpose that have appeared within the last years. With the exception of the recent *GFIRE* code [154], that includes integrators for Abelian gauge theories, previous public packages were dedicated only to interacting scalar fields, either with finite difference techniques in real space, like *Latticeeasy* [246], *Clustereasy* [247], *Defrost* [248], *CUDAeasy* [249], *HLattice* [250], *PyCOOL* [251] and *GABE* [252], or pseudo-spectral codes like *PSpectRe* [253] and *Stella* [165]. In most of the mentioned codes, metric perturbations (whenever present) are sourced passively, neglecting backreaction effects on the dynamics of the scalar fields. Notable exceptions to this are *HLATTICE v2.0*, and especially the recent *GABERel* [123], which allows for the full general relativistic evolution of non-linear

scalar field dynamics. Given that all these codes are already available, one may wonder what is the point of releasing yet a new one. In order to answer this, let us explain the purpose of *CosmoLattice*, which is actually twofold:

1. *CosmoLattice* is meant to be a ‘platform’ for users to implement any system of equations suitable for discretization on a lattice. That is, *CosmoLattice* is not a code for doing one type of simulation with one specific integration technique, such as e.g. the real-time evolution of interacting scalar fields sourcing self-consistently the expansion of the universe. The idea is rather something else: *CosmoLattice* is a package that introduces its own *symbolic language*, by defining field variables and operations over them. Therefore, once the user becomes familiar with the basic ‘vocabulary’ of the new language, they can write their own code: be it for the time evolution of the field variables in a given model of interest, or for some other operation, like a Monte-Carlo generator for thermal configurations. One of the main advantages of *CosmoLattice* is that it clearly separates the *physics* (i.e. fields living on a lattice and operations between them) from the *implementation details*, such as the handling of the parallelization or the Fourier transforms. For example, let us imagine a beginner user with little experience in programming, and with no experience at all in parallelization techniques. With *CosmoLattice*, they will be able to run a fully parallelized simulation of their favourite model (say using hundreds of processors in a cluster), while being completely oblivious to the technical details. They will just need to write a basic *model file* in the language of *CosmoLattice*, containing the details of the model being simulated. If, on the contrary, the user is rather an experienced one and wants to look inside the core routines of *CosmoLattice* and modify, for example, the MPI-implementation, they can always do so, and perhaps even contribute to improving them. On top of this, *CosmoLattice* includes already a *library* of basic routines and field-theoretical operations. This constitutes a clear advantage of using *CosmoLattice* as a platform to implement a given scenario over writing your own code from scratch. In particular, *CosmoLattice* comes with symbolic scalar, complex and $SU(2)$ algebras, which allows to use vectorial and matrix notations without sacrificing performances. Furthermore, *CosmoLattice* is MPI-based and uses a discrete Fourier Transform parallelized in multiple spatial dimensions [254], making it very powerful for probing physical problems with well-separated scales, running very high resolution simulations, or simply very long ones. *CosmoLattice* will be made publicly available in 2020, and it will come with a detailed manual explaining its whole structure and the basic instructions to start running your own simulations.
2. *CosmoLattice* includes already a set of algorithms to evolve lattice scalar-gauge theories in real-time, which can be selected with a single ‘switch’ option. Part of this document can be actually considered as the theoretical basis for such algorithms. In fact, this manuscript is really meant to be a primer on lattice techniques for non-linear simulations, as we present a comprehensive discussion on such techniques, in particular for the simulation of scalar and gauge field dynamics in an expanding universe. In Section 2 we review first the formulation of scalar and gauge field interactions in the continuum, both in a flat space-time and in *Friedmann-Lemaître-Robertson-Walker* (FLRW) backgrounds. In Section 3 we introduce the basic tools for discretizing any bosonic field theory in an expanding background, including a discussion on *lattice gauge invariant* techniques for both *Abelian* and *non-Abelian* gauge theories. Next, we introduce and classify a series of numerical algorithms, starting from methods of $\mathcal{O}(\delta t^2)$ accuracy, *staggered leapfrog* and *Verlet integration*, passing through *Runge-Kutta* methods up to $\mathcal{O}(\delta t^4)$ accuracy, and finally covering higher-order integrators accurate up to $\mathcal{O}(\delta t^{10})$, such as the *Yoshida* and *Gauss-Legendre* methods. In the following Sections 4, 5 and 6, we adapt the previous algorithms to a specialized use for classical lattice simulations of scalar and gauge field dynamics in an expanding background in $3 + 1$ dimensions. We put special care to include the possibility of ‘self-consistent’ expansion of the universe, sourcing the evolution of the scale factor by the volume average of the fields’ energy and pressure densities, independently of whether the fields are scalars, Abelian gauge fields, or non-Abelian gauge fields. In Section 4, we present a variety of lattice formulations of *interacting scalar fields*, consisting in different integrators which can reproduce the continuum theory to an accuracy ranging from $\mathcal{O}(\delta t^2)$ to $\mathcal{O}(\delta t^{10})$. Analogously, in Sections 5 and 6, we present a set of algorithms for *Abelian $U(1)$ gauge theories*, and *Non-Abelian $SU(2)$ gauge theories*, respectively,

again with an accuracy ranging between $\mathcal{O}(\delta t^2)$ and $\mathcal{O}(\delta t^{10})$. In the case of interacting scalar field methods, we provide both symplectic and non-symplectic integrators, whereas for gauge fields only symplectic integrators are built. For every algorithm presented, we always provide the form of the most significant observables, such as the energy density components, relevant field spectra, and the form of the Hubble constraint. The latter is verified by our symplectic algorithms with an accuracy that depends on the integrator order, reaching even down to machine precision in the case of the highest order schemes. Furthermore, it is worth noting that our integration algorithms for gauge theories always respect exactly, down to machine precision, the Gauss constraint, independently of the order of the integrator. This remains true even in the case of self-consistent expansion, independently of whether the gauge sector is Abelian or non-Abelian. We note that all the explicit-in-time algorithms presented in Sections 4-6 are already implemented in *CosmoLattice*, and will be made therefore publicly available once *CosmoLattice* is released.

It should be also noticed that this manuscript represents only *Part I* of our intended discussion on lattice techniques for the simulation of scalar and gauge dynamics in an expanding universe. In this document we focus on the presentation of general integration techniques (Section 3), and in their use to build explicit-in-time integration algorithms for *canonical* scalar-gauge theories, i.e. for field theories with canonically normalized kinetic terms and standard scalar potential (Section 4) and scalar-gauge Abelian (Section 5) and non-Abelian (Section 6) interactions. We would like to highlight that we present higher-order integration algorithms for interacting scalar fields, similar to those in *HLattice* [250], which built algorithms with accuracy up to $\mathcal{O}(\delta t^6)$. We go a step beyond building also explicit implementations for all the orders, including the highest ones $\mathcal{O}(\delta t^8)$ and $\mathcal{O}(\delta t^{10})$. Analogously, we also present higher-order integration algorithms for Abelian $U(1)$ gauge theories, similar to those in *GFiRe* [154]. We demonstrate explicitly for the first time their numerical implementation for all accuracy orders, including now $\mathcal{O}(\delta t^6)$, $\mathcal{O}(\delta t^8)$ and $\mathcal{O}(\delta t^{10})$. Furthermore, we also present here, to the best of our knowledge for the first time, an algorithm for non-Abelian $SU(N)$ gauge theories, which is symplectic, explicit in time, of arbitrary order, and preserving exactly the Gauss constraint, while solving for the expansion of the universe self-consistently. As a numerical example to test our algorithms in scalar-gauge canonical theories, we analyze the post-inflationary preheating dynamics of an oscillating inflaton charged under $SU(2) \times U(1)$ in Section 8. We postpone the discussion about methods for non-canonical scenarios for *Part II* of our dissertation on lattice techniques, to be published elsewhere [255], together with the public release of their implementation in *CosmoLattice*. Non-canonical scenarios are theories e.g. with non-minimal gravitational couplings, or more generally with kinetic terms with non-trivial field metrics, as considered e.g. in [84, 85, 252]. Non-canonical scenarios may also include interactions between field variables and their conjugate momenta, as naturally arising in exact derivative couplings between an axion-like field and gauge fields, as considered e.g. in [93]. Non-canonical interactions can be numerically complicated to deal with, and usually require integration techniques which are either non-symplectic or simply more involved, typically with high memory requirements, and often not explicit in time. It is precisely because of these circumstances that we naturally separate the methods for canonical scalar-gauge theories presented here in *Part I*, in Sections 4-6, from the numerical integrators that we will present for non-canonical interactions in *Part II* [255].

To conclude this section, let us mention that precisely because *CosmoLattice* is a platform rather than a specialized code for certain type of scenarios, there is a number of extensions (beyond the routines currently discussed here in *Part I*, or planned to be presented in *Part II*), which we would like to add in *CosmoLattice* in the mid-term, as we go updating and improving the code in time. We hope to eventually consider (perhaps in collaboration with you?) the following aspects:

- Addition of fermions. Even though this is numerically very costly, one can simulate out-of-thermal-equilibrium dynamics of classical bosonic fields coupled to quantum fermions. This has been done by [256] and successive works [257–259], combining the lattice implementation based on the the quantum mode equations proposed in [260], with the ‘low cost’ fermions introduced in [261].
- Computation of metric perturbations. This could be done for scalar and vector perturbations following [250], whereas tensor perturbations representing gravitational waves (GW), can be obtained following [262] (based on the idea originally proposed in [137]), as this allows for general GW sources built from

either scalar and gauge fields (or even fermions if they were present).

- Addition of *relativistic hydrodynamics*. This can be useful to describe scenarios where a classical scalar field, playing the role of an *order parameter* in a phase transition, is coupled to a relativistic fluid by means of a phenomenological friction term. This is the basis to describe numerically the dynamics of first order phase transitions [73, 74, 97, 190, 190–194] and their emission of gravitational waves [195–201].

- Addition of new ‘initializer’ routines. So far we have only considered the initialization of field fluctuations in Fourier space (on top of homogeneous field values), given a theoretical spectrum as an input. However, in order to simulate e.g. the dynamics of a network of cosmic strings or other type of topological defects, different algorithms have been used to create initially the defect network in configuration space, see e.g. [155–162, 210, 211, 263].

- Addition of ‘importance sampling’ algorithms. Monte-Carlo algorithms and Langevin dynamics are used to generate fields according to some probability distributions. They can be used to set up thermal initial conditions to study e.g. chiral charge dynamics in gauge theories at finite temperature [97, 192]. Alternatively, one could turn *CosmoLattice* into a general platform to sample positive definite path integrals. While specific and highly optimized open-source codes exist to simulate lattice QCD [264, 265], to the best of our knowledge, there is no truly versatile software to easily simulate other theories.

1.3 Conventions and notation

Unless otherwise specified, throughout the document we use the following conventions. We use natural units $c = \hbar = 1$ and choose metric signature $(-1, +1, +1, +1)$. We use interchangeably the Newton constant G , the full Planck mass $M_p \simeq 1.22 \cdot 10^{19}$ GeV, and the reduced Planck mass $m_p \simeq 2.44 \cdot 10^{18}$ GeV, related through $M_p^2 = 8\pi m_p^2 = 1/G$. Concerning space-time coordinates, Latin indices $i, j, k, \dots = 1, 2, 3$ are reserved for spatial dimensions, and Greek indices $\alpha, \beta, \mu, \nu, \dots = 0, 1, 2, 3$ for space-time dimensions. We use the *Einstein convention* of summing over repeated indices only in the continuum, whereas in the lattice, in general, repeated indices do not represent summation. We consider a flat FLRW metric $ds^2 = -a^{2\alpha}(\eta)d\eta^2 + a^2(\eta)\delta_{ij}dx^i dx^j$ with $\alpha \in \mathcal{R}e$ a constant chosen conveniently in each scenario. For $\alpha = 0$, η denotes the *coordinate time* t , whereas for $\alpha = 1$, η denotes the *conformal time* $\tau = \int \frac{dt'}{a(t')}$. For arbitrary α , we will refer to the time variable as the α -time. We reserve the notation (\cdot) for derivatives with respect to cosmic time with $\alpha = 0$, and $(\cdot)'$ for derivatives with respect to α -time with arbitrary α . Physical momenta are represented by \mathbf{p} , comoving momenta by \mathbf{k} , the α -time Hubble rate is given by $\mathcal{H} = a'/a$, whereas the physical Hubble rate is denoted by $H = \mathcal{H}|_{\alpha=0}$. Cosmological parameters are fixed to the CMB values given in [1, 266]. Our Fourier transform convention in the continuum is given by

$$f(\mathbf{x}) = \frac{1}{(2\pi)^3} \int d^3\mathbf{k} f(\mathbf{k}) e^{-i\mathbf{k}\mathbf{x}} \iff f(\mathbf{k}) = \int d^3\mathbf{x} f(\mathbf{x}) e^{+i\mathbf{k}\mathbf{x}}. \quad (1)$$

2 Field dynamics in the continuum

In this section, we describe briefly the formulation of scalar and gauge field dynamics in the continuum. We review first the case of interacting fields in a Minkowski background in Section 2.1, starting with scalar fields only, and then introducing gauge symmetries and the corresponding gauge field degrees of freedom (*dof*). We then promote the background metric into a curved manifold, and specialize our study to the case of a spatially-flat, homogeneous, and isotropic space-time, described by the FLRW metric. We consider the dynamics of scalar and gauge fields living in a FLRW background in Section 2.2, and the dynamics of the background itself, as sourced by the fields that live within it, in Section 2.3.

2.1 Scalar and Gauge field interactions in flat space-time

Let us consider first a set of N_s relativistic interacting scalar fields with action in flat space-time

$$S_S = - \int d^4x \left\{ \frac{1}{2} \partial^\mu \phi_i \partial_\mu \phi_i + V(\{\phi_j\}) \right\}, \quad (2)$$

where $i, j = 1, \dots, N_s$ label the fields, and the potential $V(\{\phi_j\})$ characterizes the interactions and self-interactions among fields. Because of the normalization constant $1/2$ in front of the kinetic terms $\partial^\mu \phi_i \partial_\mu \phi_i$, we will refer to these fields as *canonically normalized scalar fields*. We note that space-time indices are raised with the Minkowski metric, e.g. $\partial^\mu \phi \equiv \eta^{\mu\nu} \partial_\nu \phi$. The equations of motion (EOM) of the system are obtained from minimizing Eq. (2). This leads to

$$-\square_\eta \phi_i + \frac{\partial V}{\partial \phi_i} = 0, \quad \text{with } \square_\eta \equiv \eta^{\mu\nu} \partial_\mu \partial_\nu = \partial^\alpha \partial_\alpha. \quad (3)$$

In a more explicit form, the EOM can be written as

$$\ddot{\phi}_i - \vec{\nabla}^2 \phi_i + \frac{\partial V}{\partial \phi_i} = 0 \quad \Longleftrightarrow \quad \begin{cases} \dot{\phi}_i & \equiv \pi_i, \\ \dot{\pi}_i & = \vec{\nabla}^2 \phi_i - \frac{\partial V}{\partial \phi_i}. \end{cases} \quad (4)$$

Let us now consider a general scalar-gauge theory in the continuum, including three types of (canonically normalized) scalar fields: a singlet ϕ , a $U(1)$ -charged field φ , and a $[SU(N) \times U(1)]$ -charged field Φ ; as well as the corresponding Abelian A_μ and non-Abelian $B_\mu = C_\mu^a T_a$ gauge vector bosons. Here $\{T_a\}$ are the $N^2 - 1$ group generators of $SU(N)$, satisfying the properties of the $SU(N)$ Lie algebra

$$[T_a, T_b] = if_{abc} T_c, \quad \text{Tr}(T_a) = 0, \quad \text{Tr}(T_a T_b) = \frac{1}{2} \delta_{ab}, \quad T_a^\dagger = T_a, \quad (5)$$

with f_{abc} the totally anti-symmetric *structure constants* of $SU(N)$. In the particular case of $SU(2)$, $T_a \equiv \sigma_a/2$ ($a = 1, 2, 3$), with σ_a the *Pauli matrices*

$$\sigma_1 = \begin{pmatrix} 0 & 1 \\ 1 & 0 \end{pmatrix}, \quad \sigma_2 = \begin{pmatrix} 0 & -i \\ i & 0 \end{pmatrix}, \quad \sigma_3 = \begin{pmatrix} 1 & 0 \\ 0 & -1 \end{pmatrix}. \quad (6)$$

For later convenience we also write some of their properties,

$$[\sigma_a, \sigma_b] = 2i\epsilon_{abc} \sigma_c, \quad \text{Tr}(\sigma_a) = 0, \quad \text{Tr}(\sigma_a \sigma_b) = 2\delta_{ab}, \quad \sigma_a^\dagger = \sigma_a, \quad (7)$$

with ϵ_{abc} the total anti-symmetric tensor.

We can write a gauge invariant action as

$$\begin{aligned} S &= - \int d^4x \left\{ \frac{1}{2} \partial_\mu \phi \partial^\mu \phi + (D_\mu^A \varphi)^* (D_\mu^A \varphi) + (D_\mu \Phi)^\dagger (D_\mu \Phi) + \frac{1}{4} F_{\mu\nu} F^{\mu\nu} + \frac{1}{2} \text{Tr}\{G_{\mu\nu} G^{\mu\nu}\} + V \right\} \\ &= \int d^4x \left\{ \frac{\dot{\phi}^2}{2} - \frac{|\vec{\nabla} \phi|^2}{2} + |D_0 \varphi|^2 - |\vec{D} \varphi|^2 + |D_0 \Phi|^2 - |\vec{D} \Phi|^2 + \frac{|\vec{\mathcal{E}}|^2}{2} - \frac{|\vec{\mathcal{B}}|^2}{2} + \sum_a \left(\frac{|\vec{\mathcal{E}}_a|^2}{2} - \frac{|\vec{\mathcal{B}}_a|^2}{2} \right) - V \right\}, \end{aligned} \quad (8)$$

with a potential $V \equiv V(\phi, |\varphi|, |\Phi|)$ describing the interactions among the scalar fields,

$$\phi \in \mathcal{R}e, \quad \varphi \equiv \frac{1}{\sqrt{2}}(\varphi_0 + i\varphi_1), \quad \Phi = \begin{pmatrix} \varphi^{(0)} \\ \varphi^{(1)} \\ \vdots \\ \varphi^{(N-1)} \end{pmatrix} = \frac{1}{\sqrt{2}} \begin{pmatrix} \varphi_0 + i\varphi_1 \\ \varphi_2 + i\varphi_3 \\ \vdots \\ \varphi_{2N-2} + i\varphi_{2N-1} \end{pmatrix}, \quad (9)$$

and where we have introduced standard definitions of *covariant derivatives* (denoting Q_A and Q_B the Abelian and non-Abelian charges) and *field strength* tensors,

$$D_\mu^A \equiv \partial_\mu - i\frac{1}{2} Q_A g_A A_\mu, \quad (10)$$

$$D_\mu \equiv \mathcal{I} D_\mu^A - ig_B Q_B B_\mu^a T_a, \quad (11)$$

$$F_{\mu\nu} \equiv \partial_\mu A_\nu - \partial_\nu A_\mu, \quad (12)$$

$$G_{\mu\nu} \equiv \partial_\mu B_\nu - \partial_\nu B_\mu - i[B_\mu, B_\nu], \quad (13)$$

with \mathcal{I} the $N \times N$ identity matrix. In the second line of (8) we have used the properties of the generators, displayed in Eq. (5), to obtain

$$G_{\mu\nu} \equiv G_{\mu\nu}^a T_a \quad \Rightarrow \quad \frac{1}{2} \text{Tr}(G_{\mu\nu} G^{\mu\nu}) \equiv \frac{1}{2} G_{\mu\nu}^a G_a^{\mu\nu}; \quad G_{\mu\nu}^a \equiv \partial_\mu B_\nu^a - \partial_\nu B_\mu^a + f^{abc} B_\mu^b B_\nu^c, \quad (14)$$

and introduced Abelian and non-Abelian electric and magnetic fields as

$$\mathcal{E}_i \equiv F_{0i}, \quad \mathcal{B}_i = \frac{1}{2} \epsilon_{ijk} F^{jk}, \quad \mathcal{E}_i^a \equiv G_{0i}^a, \quad \mathcal{B}_i^a = \frac{1}{2} \epsilon_{ijk} G_a^{jk}. \quad (15)$$

The equations of motion (EOM) of the system can be obtained from minimizing Eq. (8). They are

$$\begin{aligned} \partial^\mu \partial_\mu \phi &= \frac{\partial V}{\partial \phi} && [\text{Singlet}] \\ D_A^\mu D_\mu \varphi &= \frac{\partial V}{\partial |\varphi|} \frac{\varphi}{|\varphi|} && [U(1)\text{-charged}] \\ D^\mu D_\mu \Phi &= \frac{\partial V}{\partial |\Phi|} \frac{\Phi}{|\Phi|} && [U(1) \times SU(N)] , \\ \partial_\nu F^{\mu\nu} &= J_A^\mu && [\text{Abelian vector}] \\ (\mathcal{D}_\nu)_{ab} G_b^{\mu\nu} &= J_a^\mu && [\text{Yang-Mills vector}] \end{aligned} \quad (16)$$

where $(\mathcal{D}_\nu O)_a = (\mathcal{D}_\nu)_{ab} O_b \equiv (\delta_{ab} \partial_\nu - f_{abc} B_\nu^c) O_b$, and the currents are given by

$$J_A^\mu \equiv g_A Q_A^{(\varphi)} \mathcal{I}m[\varphi^* (D_A^\mu \varphi)] + g_A Q_A^{(\Phi)} \mathcal{I}m[\Phi^\dagger (D^\mu \Phi)], \quad (17)$$

$$J_a^\mu \equiv 2g_B Q_B \mathcal{I}m[\Phi^\dagger T_a (D^\mu \Phi)]. \quad (18)$$

It is straightforward to show that both action (8) and the EOM (16) are invariant under the following set of gauge transformations,

$$\begin{aligned} \phi(x) &\longrightarrow \phi(x), \quad [\text{singlet}] \\ \varphi(x) &\longrightarrow \omega(x) \varphi(x), \quad \omega(x) = e^{-i \frac{g_A}{2} Q_A^{(\varphi)} \alpha(x)}, \\ \Phi(x) &\longrightarrow \omega(x) \Omega(x) \Phi(x), \quad \Omega(x) \equiv e^{-i g_B Q_B \beta_a(x) T_a}, \quad \omega(x) = e^{-i \frac{g_A}{2} Q_A^{(\Phi)} \alpha(x)}, \\ A_\mu(x) &\longrightarrow A_\mu(x) - \partial_\mu \alpha(x) \\ B_\mu(x) &\longrightarrow \Omega(x) B_\mu(x) \Omega^\dagger(x) - \frac{i}{g_B Q_B} [\partial_\mu \Omega(x)] \Omega^\dagger(x) \\ G_{\mu\nu}(x) &\longrightarrow \Omega(x) G_{\mu\nu}(x) \Omega^\dagger(x), \end{aligned} \quad (19)$$

with $\alpha(x)$ and $\beta_a(x)$ arbitrary real functions, $Q_A^{(\varphi)}$ and $Q_A^{(\Phi)}$ the Abelian charges of φ and Φ , and Q_B the non-Abelian charge of Φ .

Using the definitions in Eq. (15), we can also write the EOM in vectorial form, making more explicit the individual terms in each equation:

$$\ddot{\phi} - \vec{\nabla}^2 \phi = -V_{,\phi}, \quad (20)$$

$$\ddot{\varphi} - \vec{D}_A^2 \varphi = -V_{,|\varphi|} \cdot (\varphi/|\varphi|), \quad (21)$$

$$\ddot{\Phi} - \vec{D}^2 \Phi = -V_{,|\Phi|} \cdot (\Phi/|\Phi|), \quad (22)$$

$$\vec{\mathcal{E}} - \vec{\nabla} \times \vec{\mathcal{B}} = \vec{J}_A \equiv g_A Q_A^{(\varphi)} \mathcal{I}m[\varphi^* \vec{D}_A \varphi] + g_A Q_A^{(\Phi)} \mathcal{I}m[\Phi^\dagger \vec{D} \Phi], \quad (23)$$

$$(\vec{\mathcal{D}}_0 \vec{\mathcal{E}})_a - (\vec{\mathcal{D}} \times \vec{\mathcal{B}})_a = \vec{J}_a \equiv 2g_B Q_B^{(\Phi)} \mathcal{I}m[\Phi^\dagger T_a \vec{D} \Phi], \quad (24)$$

$$-\vec{\nabla} \cdot \vec{\mathcal{E}} = J_0^A \equiv g_A Q_A^{(\varphi)} \mathcal{I}m[\varphi^* (D_0^A \varphi)] + g_A Q_A^{(\Phi)} \mathcal{I}m[\Phi^\dagger (D_0 \Phi)], \quad (25)$$

$$-(\vec{\mathcal{D}} \cdot \vec{\mathcal{E}})_a = (J_0)_a \equiv 2g_B Q_B^{(\Phi)} \mathcal{I}m[\Phi^\dagger T_a (D_0 \Phi)]. \quad (26)$$

We note that the last two equations in Eq. (26) represent constraint equations, as they correspond to the equations associated with the temporal component of the gauge field, which is not dynamical. These constraints are equivalent to the standard *Gauss Law* of electromagnetism $\vec{\nabla} \cdot \vec{\mathcal{E}} = \rho$. In particular, they are the generators of gauge transformations [267].

2.2 Field dynamics in an expanding background

To describe the expansion of the Universe we consider a flat *Friedmann-Lemaître-Robertson-Walker* (FLRW) metric, with line element

$$ds^2 = g_{\mu\nu} dx^\mu dx^\nu = -a(\eta)^{2\alpha} d\eta^2 + a(\eta)^2 \delta_{ij} dx^i dx^j . \quad (27)$$

where $a(\eta)$ is the scale factor, δ_{ij} is the Euclidean metric, and α is a constant parameter that will be chosen conveniently in a case by case basis. The choice $\alpha = 0$ identifies η with the *coordinate time* t , whereas $\alpha = 1$ makes η the *conformal time* $\tau \equiv \int \frac{dt'}{a(t')}$. For the time being, we will consider α as an unspecified constant, and we will refer to η as the α -time variable.

Note -. Recall that we reserve the symbol $\dot{f} \equiv df/dt$ for derivatives with respect to the coordinate time, whereas $f' \equiv df/d\eta$ will indicate derivative with respect to any α -time variable.

For later convenience we write explicitly the metric and inverse metric elements,

$$g_{00} = -a(\eta)^{2\alpha} ; \quad g_{ij} = a(\eta)^2 \delta_{ij} ; \quad g^{00} = -a(\eta)^{-2\alpha} ; \quad g^{ij} = a(\eta)^{-2} \delta^{ij} . \quad (28)$$

To obtain the EOM in curved space, we follow the *minimal gravitational coupling* prescription, making the following replacements into the flat space-time equations,

$$\eta_{\mu\nu} \rightarrow g_{\mu\nu} , \quad (29)$$

$$\partial_\gamma V_{\mu\nu}^{\alpha\beta..} \equiv V_{\mu\nu..,\gamma}^{\alpha\beta..} \rightarrow \nabla_\gamma V_{\mu\nu}^{\alpha\beta..} \equiv V_{\mu\nu..;\gamma}^{\alpha\beta..} = V_{\mu\nu..,\gamma}^{\alpha\beta..} + \Gamma_{\gamma\sigma}^\alpha V_{\mu\nu..}^{\sigma\beta..} - \Gamma_{\gamma\mu}^\sigma V_{\sigma\nu..}^{\alpha\beta..} + \dots , \quad (30)$$

where $V_{;\mu} = \nabla_\mu V$ represents a (gravitational) covariant derivative, $\Gamma_{\alpha\beta}^\mu$ are the Christoffel symbols, and $V_{\mu\nu..}^{\alpha\beta..}$ is an arbitrary tensor. Using the non-vanishing Christoffel symbols of the FLRW metric,

$$\Gamma_{00}^0 = \alpha \frac{a'(\eta)}{a(\eta)} , \quad \Gamma_{ij}^0 = a^{-2\alpha+2} \frac{a'(\eta)}{a(\eta)} \delta_{ij} , \quad \Gamma_{i0}^i = \frac{a'(\eta)}{a(\eta)} , \quad (31)$$

we can obtain, via the minimal coupling prescription, the EOM in an expanding Universe. In practice, we can obtain directly the transformation of the derivative terms in the scalar and gauge field EOM, by making use of the following identities for the divergence of a vector and a rank-2 anti-symmetric tensor,

$$\nabla_\sigma V^\sigma = \frac{1}{\sqrt{g}} \frac{\partial(V^\sigma \sqrt{g})}{\partial x^\sigma} = \frac{1}{a^{3+\alpha}} \frac{\partial(V^\sigma a^{3+\alpha}(t))}{\partial x^\sigma} = g^{\sigma\lambda} \partial_\sigma V_\lambda + (3+\alpha) \frac{a'}{a} V^0 , \quad (32)$$

$$\nabla_\sigma F^{\sigma\lambda} = \frac{1}{\sqrt{g}} \frac{\partial(F^{\sigma\lambda} \sqrt{g})}{\partial x^\sigma} = \frac{1}{a^{3+\alpha}} \frac{\partial(F^{\sigma\lambda} a^{3+\alpha}(t))}{\partial x^\sigma} = (3+\alpha) \frac{a'}{a} g^{0\lambda} g^{\alpha\beta} F_{\lambda\beta} + \partial_\sigma (g^{\sigma\lambda} g^{\alpha\beta} F_{\lambda\beta}) , \quad (33)$$

where $g = -\det(g_{\mu\nu})$. This leads to

$$\partial_\mu \partial^\mu \phi \rightarrow \nabla_\mu [\partial^\mu \phi] = a^{-2\alpha} \phi'' - a^{-2} \partial_i \partial_i \phi + (3-\alpha) \frac{a'}{a} \phi' , \quad (34)$$

$$\partial_\mu F^{\mu\nu} \rightarrow \nabla_\mu F^{\mu\nu} = g^{\nu\nu} \left(-a^{-2\alpha} \partial_0 F_{0\nu} + a^{-2} \partial_i F_{i\nu} - (3-\alpha) a^{-2\alpha} \frac{a'}{a} F_{0\nu} \right) - a^{-2\alpha} F_{0\nu} \partial_0 g^{\nu\nu} . \quad (35)$$

Using these identities and the metric elements (28), we obtain the EOM in an expanding background as

$$\phi'' - a^{-2(1-\alpha)} \vec{\nabla}^2 \phi + (3-\alpha) \frac{a'}{a} \phi' = -a^{2\alpha} V_{,\phi} , \quad (36)$$

$$\varphi'' - a^{-2(1-\alpha)} \vec{D}_A^2 \varphi + (3-\alpha) \frac{a'}{a} \varphi' = -a^{2\alpha} V_{,|\varphi|} \cdot (\varphi/|\varphi|) , \quad (37)$$

$$\Phi'' - a^{-2(1-\alpha)} \vec{D}^2 \Phi + (3-\alpha) \frac{a'}{a} \Phi' = -a^{2\alpha} V_{,|\Phi|} \cdot (\Phi/|\Phi|) , \quad (38)$$

$$\partial_0 F_{0i} - a^{-2(1-\alpha)} \partial_j F_{ji} + (1-\alpha) \frac{a'}{a} F_{0i} = a^{2\alpha} J_i^A , \quad (39)$$

$$(\mathcal{D}_0)_{ab} (G_{0i})^b - a^{-2(1-\alpha)} (\mathcal{D}_j)_{ab} (G_{ji})^b + (1-\alpha) \frac{a'}{a} (G_{0i})^b = a^{2\alpha} (J_i)_a , \quad (40)$$

$$\partial_i F_{0i} = a^2 J_0^A , \quad (41)$$

$$(\mathcal{D}_i)_{ab} (G_{0i})^b = a^2 (J_0)_a , \quad (42)$$

where the currents on the *rhs* of the gauge field EOM are still given by Eqs. (17)-(18). We note that Eqs. (41) and (42) are the generalization of the $U(1)$ and $SU(2)$ Gauss constraints in an expanding background. When we discretize the system of equations later on, we will use them as an indicator of the correctness of the discretization scheme, by checking whether the constraints are preserved at all times during the field evolution.

2.3 Dynamics of the expanding background

If the expansion of the Universe is dictated by some external *dof* different than the fields we are evolving, say e.g. a fluid with a given equation of state, we will refer to this case as *fixed background*. If on the contrary, the matter fields (scalar or gauge) for which we are solving their dynamics are the ones which govern the expansion of the Universe, we will refer to this case as *self-consistent expansion*. In general, the evolution of the scale factor $a(\eta)$ is dictated by the stress-energy tensor of matter fields via the Friedmann equations. Denoting the background energy and pressure densities as $\bar{\rho}$ and \bar{p} , the stress-energy tensor of a background *perfect fluid* is given by

$$\bar{T}_{\mu\nu} \equiv (\bar{\rho} + \bar{p})u_\mu u_\nu + \bar{p}g_{\mu\nu} , \quad g_{\mu\nu}u^\mu u^\nu = -1 \quad \Rightarrow \quad \begin{cases} \bar{\rho} = a^{-2\alpha} \bar{T}_{00} , \\ \bar{p} = \frac{1}{3a^2} \sum_j \bar{T}_{jj} , \end{cases} \quad (43)$$

where we have used $u_\mu = (a^\alpha, 0, 0, 0)$ and $u^\mu = -(a^{-\alpha}, 0, 0, 0)$. The evolution of the scale factor is then determined by the Friedmann equations, which, in α -time, read as

$$\mathcal{H}^2 \equiv \left(\frac{a'}{a}\right)^2 = a^{2\alpha} \frac{\bar{\rho}}{3m_p^2} , \quad \frac{a''}{a} = \frac{a^{2\alpha}}{6m_p^2} [(2\alpha - 1)\bar{\rho} - 3\bar{p}] . \quad (44)$$

Let us consider first the case of a fixed background. If the expansion of the Universe is created by an external fluid with constant equation of state $w \equiv p/\rho$, the two Friedmann equations can be combined into a single equation as

$$2a'' + (1 + 3w - 2\alpha) \frac{a'^2}{a} = 0 , \quad (45)$$

with solution

$$a(\eta) = a(\eta_i) \left(1 + \frac{1}{p} \mathcal{H}_i (\eta - \eta_i)\right)^p , \quad \mathcal{H}(\eta) = \frac{\mathcal{H}_i}{\left(1 + \frac{1}{p} \mathcal{H}_i (\eta - \eta_i)\right)} = \frac{\mathcal{H}_i}{\sqrt[p]{a(\eta)/a(\eta_i)}} , \quad p \equiv \frac{2}{3(1 + w) - 2\alpha} , \quad (46)$$

where η_i is some initial time. In order to solve the scalar/gauge field dynamics, we just need then to plug in the above expressions for $a(\eta)$ and $\mathcal{H}(\eta)$ into the EOM of the matter fields.

In the case of self-consistent expansion, we need an expression for the energy momentum-tensor of the scalar/gauge matter fields, and then take a volume average of the corresponding local expressions of the energy and pressure densities, which source the Friedmann equations. From the Lagrangian in Eq. (8) we can actually derive a local expression for the stress-energy tensor of the scalar and gauge fields as

$$\begin{aligned} T_{\mu\nu} &= -\frac{2}{\sqrt{g}} \frac{\delta(\sqrt{g}\mathcal{L})}{\delta g^{\mu\nu}} = g_{\mu\nu} \mathcal{L} - 2 \frac{\delta \mathcal{L}}{\delta g^{\mu\nu}} \\ &= -g_{\mu\nu} \left(g^{\alpha\beta} \left[(D_\alpha \Phi)^\dagger (D_\beta \Phi) + (D_\alpha^A \varphi)^* (D_\beta^A \varphi) + \frac{1}{2} (\partial_\alpha \phi) (\partial_\beta \phi) \right] + \frac{1}{4} g^{\alpha\delta} g^{\beta\lambda} (G_{\alpha\beta}^a G_{\delta\lambda}^a + F_{\alpha\beta} F_{\delta\lambda}) + V \right) \\ &\quad + \left[2(D_\mu \Phi)^\dagger (D_\nu \Phi) + 2(D_\mu^A \varphi)^* (D_\nu^A \varphi) + (\partial_\mu \phi) (\partial_\nu \phi) \right] + g^{\alpha\beta} (G_{\mu\alpha}^a G_{\nu\beta}^a + F_{\mu\alpha} F_{\nu\beta}) , \end{aligned} \quad (47)$$

where in the first equality we used³ $\delta(\sqrt{g}) = -\frac{1}{2} g_{\mu\nu} \delta g^{\mu\nu}$, and in the second we used $\delta g^{\alpha\beta} = -g^{\alpha\mu} g^{\beta\nu} \delta g_{\mu\nu}$. Using $F^{\mu\nu} F_{\mu\nu} = -\frac{2}{a^{2(1+\alpha)}} \sum_i F_{0i}^2 + \frac{1}{a^4} \sum_{i,j} F_{ij}^2$ (similarly for $G_{\mu\nu}^a$), and $(D_\mu \Phi)^\dagger (D^\mu \Phi) = -a^{-2\alpha} (D_0 \Phi)^\dagger (D_0 \Phi) +$

³Had we wanted to obtain $T^{\mu\nu}$ with the space-time indices above, then we should use instead $\delta(\sqrt{g}) = +\frac{1}{2} g^{\mu\nu} \delta g_{\mu\nu}$.

$a^{-2}(D_i\Phi)^\dagger(D_i\Phi)$ (similarly for the $U(1)$ -charged and singlet scalar fields), we obtain for the energy and pressure densities,

$$\rho = K_\phi + K_\varphi + K_\Phi + G_\phi + G_\varphi + G_\Phi + K_{U(1)} + G_{U(1)} + K_{SU(2)} + G_{SU(2)} + V, \quad (48)$$

$$p = K_\phi + K_\varphi + K_\Phi - \frac{1}{3}(G_\phi + G_\varphi + G_\Phi) + \frac{1}{3}(K_{U(1)} + G_{U(1)}) + \frac{1}{3}(K_{SU(2)} + G_{SU(2)}) - V, \quad (49)$$

with V the interacting scalar potential, whereas the kinetic and gradient energy densities are

$$\begin{aligned} K_\phi &= \frac{1}{2a^{2\alpha}}\phi'^2 & G_\phi &= \frac{1}{2a^2}\sum_i(\partial_i\phi)^2 & K_{U(1)} &= \frac{1}{2a^{2+2\alpha}}\sum_i F_{0i}^2 \\ K_\varphi &= \frac{1}{a^{2\alpha}}(D_0^A\varphi)^*(D_0^A\varphi) \ ; & G_\varphi &= \frac{1}{a^2}\sum_i(D_i^A\varphi)^*(D_i^A\varphi) \ ; & K_{SU(2)} &= \frac{1}{2a^{2+2\alpha}}\sum_{a,i}(G_{0i}^a)^2 \\ K_\Phi &= \frac{1}{a^{2\alpha}}(D_0\Phi)^\dagger(D_0\Phi) & G_\Phi &= \frac{1}{a^2}\sum_i(D_i\Phi)^\dagger(D_i\Phi) & G_{U(1)} &= \frac{1}{2a^4}\sum_{i,j<i}F_{ij}^2 \\ & & & & G_{SU(2)} &= \frac{1}{2a^4}\sum_{a,i,j<i}(G_{ij}^a)^2. \end{aligned} \quad (50)$$

(Kinetic-Scalar) (Gradient-Scalar) (Electric & Magnetic)

Whenever dealing with scenarios with self-consistent expansion of the Universe, we then need to take first a volume average of the local expressions in Eqs. (48), (49), so that we obtain the background energy and pressure densities $\bar{\rho}$ and \bar{p} , within a given volume. Plugging back the background quantities into the Friedmann Eqs. (44), will determine then the evolution of the universe within the chosen volume, namely

$$\left(\frac{a'}{a}\right)^2 = \frac{a^{2\alpha}}{3m_p^2} \langle K_\phi + K_\varphi + K_\Phi + G_\phi + G_\varphi + G_\Phi + K_{U(1)} + G_{U(1)} + K_{SU(2)} + G_{SU(2)} + V \rangle, \quad (51)$$

$$\begin{aligned} \frac{a''}{a} &= \frac{a^{2\alpha}}{3m_p^2} \langle (\alpha - 2)(K_\phi + K_\varphi + K_\Phi) + \alpha(G_\phi + G_\varphi + G_\Phi) + (\alpha + 1)V \\ &\quad + (\alpha - 1)(K_{U(1)} + G_{U(1)} + K_{SU(2)} + G_{SU(2)}) \rangle, \end{aligned} \quad (52)$$

where $\langle \dots \rangle$ represents volume averaging. As long as the volume is sufficiently large compared to the scales excited in the matter fields, this approximation should lead to a well-defined notion of a 'homogeneous and isotropic' expanding background, within the given volume.

3 Field dynamics in a computer: the lattice approach

3.1 Lattice definition and discrete Fourier transform

In order to simulate the dynamics of interacting fields, we will consider a cubic lattice with N sites per dimension. As we are interested in three spatial dimensions, the lattice will have therefore N^3 points in total, labeled as

$$\mathbf{n} = (n_1, n_2, n_3), \quad \text{with } n_i = 0, 1, \dots, N-1, \quad i = 1, 2, 3. \quad (53)$$

We will often refer to this set of points simply as the lattice, the *grid*, or even more colloquially, as the *box*. For convenience we define

$$\hat{1} \equiv (1, 0, 0), \quad \hat{2} \equiv (0, 1, 0), \quad \hat{3} \equiv (0, 0, 1), \quad (54)$$

as unit vectors in the lattice, corresponding to positive displacements of length

$$\delta x \equiv \frac{L}{N}, \quad (55)$$

in each of the independent directions in the continuum. We will refer to δx as the *lattice spacing*.

A continuum function $\mathbf{f}(\mathbf{x})$ in space is represented by a lattice function $f(\mathbf{n})$, which has the same value as $\mathbf{f}(\mathbf{x})$ at $\mathbf{x} = \mathbf{n}\delta x$. We note that whereas in a flat background, positions $\{\mathbf{x}\}$ and their corresponding lattice sites $\{\mathbf{n}\}$ represent physical spatial coordinates, in an expanding background they will rather represent *comoving* spatial coordinates. Unless specified otherwise, we will always consider *periodic boundary conditions* in the three spatial directions, so that $f(\mathbf{n} + iN) = f(\mathbf{n})$, $i = 1, 2$ or 3 .

The periodic boundary conditions in coordinate space imply that momenta must be discretized, whereas the discretization of the spatial coordinates implies that any definition of a discrete Fourier transform must be periodic. For each lattice we can then consider always a reciprocal lattice representing *Fourier* modes, with sites labeled as

$$\tilde{\mathbf{n}} = (\tilde{n}_1, \tilde{n}_2, \tilde{n}_3), \quad \text{with } \tilde{n}_i = -\frac{N}{2} + 1, -\frac{N}{2} + 2, \dots, -1, 0, 1, \dots, \frac{N}{2} - 1, \frac{N}{2}, \quad i = 1, 2, 3. \quad (56)$$

We then define the discrete Fourier transform (DFT) as

$$f(\mathbf{n}) \equiv \frac{1}{N^3} \sum_{\tilde{\mathbf{n}}} e^{-i\frac{2\pi}{N}\tilde{\mathbf{n}}\mathbf{n}} f(\tilde{\mathbf{n}}) \quad \Leftrightarrow \quad f(\tilde{\mathbf{n}}) \equiv \sum_{\mathbf{n}} e^{+i\frac{2\pi}{N}\mathbf{n}\tilde{\mathbf{n}}} f(\mathbf{n}), \quad (57)$$

from where we obtain

$$\sum_{\mathbf{n}} e^{i\frac{2\pi}{N}\mathbf{n}\tilde{\mathbf{n}}} = N^3 \delta_{\mathbf{n}, \tilde{\mathbf{n}}}. \quad (58)$$

As expected, it follows that Fourier-transformed functions are periodic in the reciprocal lattice, with periodic boundary conditions as $f(\tilde{\mathbf{n}} + \hat{i}N) = f(\tilde{\mathbf{n}})$, with \hat{i} analogous unit vectors as in Eq. (54), but defined in the reciprocal lattice.

Let us emphasize that from the above discussion, it follows that we can only represent momenta down to a minimum infrared (IR) cut-off

$$k_{\text{IR}} = \frac{2\pi}{L} = \frac{2\pi}{N\delta x}, \quad (59)$$

such that $\tilde{\mathbf{n}}$ labels the continuum momentum values $\mathbf{k} = (\tilde{n}_1, \tilde{n}_2, \tilde{n}_3) k_{\text{IR}}$. Furthermore, there is also a maximum ultraviolet (UV) momentum that we can capture in each spatial dimension,

$$k_{i,\text{UV}} = \frac{N}{2} k_{\text{IR}} = \frac{\pi}{\delta x}. \quad (60)$$

The maximum momentum we can capture in a three-dimensional reciprocal lattice is therefore

$$k_{\text{max}} = \sqrt{k_{1,\text{UV}}^2 + k_{2,\text{UV}}^2 + k_{3,\text{UV}}^2} = \frac{\sqrt{3}}{2} N k_{\text{IR}} = \sqrt{3} \frac{\pi}{\delta x}. \quad (61)$$

In many situation, it will useful to define the *power – spectrum* of f , with ensemble average $\langle f^2 \rangle$ in the continuum defined as

$$\langle f^2 \rangle = \int d \log k \mathcal{P}_f(k) \quad , \quad \langle f_k f_{k'} \rangle = (2\pi)^3 \frac{2\pi^2}{k^3} \mathcal{P}_f(k) \delta(\mathbf{k} - \mathbf{k}'). \quad (62)$$

In a lattice, the ensemble average is substituted by a volume average,

$$\langle f^2 \rangle_V = \frac{dx^3}{V} \sum_{\mathbf{n}} f^2(n) \quad , \quad (63)$$

so that using the discrete Fourier transform we just defined, we obtain

$$\langle f^2 \rangle_V = \frac{1}{2\pi^2} \sum_{|\tilde{\mathbf{n}}|} \Delta \log k(\tilde{\mathbf{n}}) k^3(\tilde{\mathbf{n}}) \left(\frac{\delta x}{N} \right)^3 \langle |f(\tilde{n})|^2 \rangle_{R(\tilde{n})} \quad , \quad (64)$$

with $\langle (\dots) \rangle \equiv \frac{1}{4\pi|\tilde{\mathbf{n}}|^2} \sum_{\tilde{\mathbf{n}}' \in R(\tilde{\mathbf{n}})} (\dots)$ an angular average over the spherical shell of radius $\tilde{\mathbf{n}}' \in [|\tilde{\mathbf{n}}|, |\tilde{\mathbf{n}} + \Delta\tilde{\mathbf{n}}|]$, and $\Delta\tilde{\mathbf{n}}$ a given radial binning. We also defined $\Delta \log k(\tilde{\mathbf{n}}) \equiv \frac{k_{\text{IR}}}{k(\tilde{\mathbf{n}})}$. Identifying this with Eq. (62), we obtain the following expression for the discrete power spectrum

$$\mathcal{P}_f(k) \equiv \frac{k^3(\tilde{\mathbf{n}})}{2\pi^2} \left(\frac{\delta x}{N} \right)^3 \langle |f(\tilde{\mathbf{n}})|^2 \rangle_{R(\tilde{\mathbf{n}})}. \quad (65)$$

Finally, let us notice that we will be dealing in general with spatially dependent functions representing field amplitudes at a given time. As time goes by in the simulation, the amplitude of the functions will change. We can therefore think of the above functions depending not only on their coordinates \mathbf{n} (or reciprocal coordinates $\tilde{\mathbf{n}}$), but also depending on a discrete variable $n_0 = 0, 1, 2, \dots$ counting the number of time iterations in a simulation. In general, n_0 labels a time $\eta = \eta_* + n_0 \delta\eta$, where $\delta\eta$ is the temporal step chosen in the evolution, and η_* denotes an initial time. We will think therefore of the above functions as 4-dimensional functions, and we will often write them as $f(n) = f(n_0, \mathbf{n})$, or $f(\tilde{n}) = f(n_0, \tilde{\mathbf{n}})$. We will use the notation $\hat{0}$ to represent the advance of one time step, so e.g. $f(n + \hat{0}) = f(n_0 + 1, \mathbf{n})$.

3.2 Lattice representation of differential operators

3.2.1 Derivative operators and lattice momenta

The action or the equations of motion contain continuum derivatives, so we need to replace these with lattice expressions that have the correct continuum limit. A simple and symmetric definition of a lattice derivative is e.g. the *centered* or *neutral* derivative

$$[\nabla_\mu^{(0)} f] = \frac{f(n + \hat{\mu}) - f(n - \hat{\mu})}{2\delta x^\mu} \longrightarrow \partial_i \mathbf{f}(x)|_{x \equiv \mathbf{n}\delta x + n_0\delta\eta} + \mathcal{O}(\delta x_\mu^2), \quad (66)$$

where in the case of spatial derivatives δx^μ refers to the lattice spacing δx , whereas for temporal derivatives it refers to the time step $\delta\eta$ (typically bounded to be smaller than δx). The expression to the right-hand side of the arrow indicates where and to what order in the lattice spacing/time step the continuum limit is recovered. The neutral derivative in Eq. (66) has the drawback that it is insensitive to spatial variations at the smallest scale we can probe, $\sim \delta x$, or temporal variations within a time of the order of the actual time step $\sim \delta\eta$. Because of this, a definition involving the nearest spatial/temporal neighbors can be preferable. A standard way to do this, is to define the *forward* and *backward* derivatives

$$[\nabla_\mu^\pm f] = \frac{\pm f(n \pm \hat{\mu}) \mp f(n)}{\delta x^\mu} \longrightarrow \begin{cases} \partial_i \mathbf{f}(x)|_{x \equiv \mathbf{n}\delta x + n_0\delta\eta} + \mathcal{O}(\delta x_\mu) \\ \partial_i \mathbf{f}(x)|_{x \equiv (n \pm \hat{\mu}/2)\delta x^\mu} + \mathcal{O}(\delta x_\mu^2) \end{cases}, \quad (67)$$

which recover the continuum limit to linear or to quadratic order in the lattice spacing/time step, depending on whether we interpret that the discrete operator lives in n or in between the two lattice sites involved $n \pm \hat{\mu}/2$. This shows that in order to recover a continuum differential operation in the lattice, not only it is important to use a suitable discrete operator, but also to determine where it 'lives'. Depending on this choice, the operator might be symmetric or not with respect to the given location, hence recovering the continuum limit up to an even or an odd order in the lattice spacing/time step, respectively. To improve accuracy, one could also consider lattice derivatives which involve more points, typically leading to definitions that have a symmetry either around a lattice site or around half-way between lattice sites, see for instance [248].

Depending on the choice of lattice operator ∇_i for the spatial derivatives, the discrete Fourier transform will lead to different *lattice momenta*. In general, for any given derivative operator, the value of the derivative $[\nabla_i f]$ will be a linear combination of the field values at different lattice sites, $[\nabla_i f](\mathbf{l}) = \sum_{\mathbf{m}} D_i(\mathbf{l}, \mathbf{m}) f(\mathbf{m})$, with $D_i(\mathbf{l}, \mathbf{m})$ a real-valued function of two variables on the lattice. Since we want the derivative to be translation invariant, $D_i(\mathbf{l}, \mathbf{m})$ can only be a function of the difference $\mathbf{l} - \mathbf{m}$, i.e. $D_i(\mathbf{l}, \mathbf{m}) = D_i(\mathbf{l} - \mathbf{m})$, and we can write

$$[\nabla_i f](\mathbf{l}) = \sum_{\mathbf{m}} D_i(\mathbf{l}, \mathbf{m}) f(\mathbf{m}) = \sum_{\mathbf{m}} D_i(\mathbf{l} - \mathbf{m}) f(\mathbf{m}) = \sum_{\mathbf{m}'} D_i(\mathbf{m}') f(\mathbf{l} - \mathbf{m}'). \quad (68)$$

For example, for the neutral derivative (66),

$$D_i^0(\mathbf{m}') = \frac{\delta_{\mathbf{m}', -\hat{i}} - \delta_{\mathbf{m}', \hat{i}}}{2\delta x}, \quad (69)$$

whereas for the nearest-neighbor derivative (67),

$$D_i^\pm(\mathbf{m}') = \frac{\pm \delta_{\mathbf{m}', \mp \hat{i}/2} \mp \delta_{\mathbf{m}', \pm \hat{i}/2}}{\delta x} \quad \text{if } \mathbf{l} = \mathbf{n} + \frac{\hat{i}}{2}; \quad D_i^\pm(\mathbf{m}') = \frac{\pm \delta_{\mathbf{m}', \mp \hat{i}} \mp \delta_{\mathbf{m}', 0}}{\delta x} \quad \text{if } \mathbf{l} = \mathbf{n}. \quad (70)$$

The Fourier transform of the derivative $[\nabla_i f]$ is

$$\nabla_i f(\tilde{\mathbf{n}}) = \sum_{\mathbf{n}} e^{\frac{2\pi i}{N} \tilde{\mathbf{n}} \cdot \mathbf{n}} \sum_{\mathbf{m}} D_i(\mathbf{n} - \mathbf{m}) f(\mathbf{m}) = \sum_{\mathbf{n}'} e^{\frac{2\pi i}{N} \tilde{\mathbf{n}} \cdot \mathbf{n}'} D_i(\mathbf{n}') \sum_{\mathbf{m}} e^{\frac{2\pi i}{N} \tilde{\mathbf{n}} \cdot \mathbf{m}} f(\mathbf{m}) \equiv -i \mathbf{k}_{\text{Lat}}(\tilde{\mathbf{n}}) f(\tilde{\mathbf{n}}), \quad (71)$$

leading to define the *lattice momentum* $\mathbf{k}_{\text{Lat}}(\tilde{\mathbf{n}})$ as

$$\mathbf{k}_{\text{Lat}}(\tilde{\mathbf{n}}) = i \sum_{\mathbf{n}'} e^{\frac{2\pi i}{N} \tilde{\mathbf{n}} \cdot \mathbf{n}'} D_i(\mathbf{n}'). \quad (72)$$

Conversely, any function $\mathbf{k}_{\text{Lat}}(\tilde{\mathbf{n}})$ with the correct leading behaviour $\mathbf{k}_{\text{Lat}}(\tilde{\mathbf{n}}) \approx \tilde{\mathbf{n}} k_{\text{IR}}$ in the IR limit $|\tilde{\mathbf{n}}| \ll N$, defines a lattice derivative through the inverse Fourier transform.

In practice, for the neutral derivative (66) we obtain

$$k_{\text{Lat},i}^0 = \frac{\sin(2\pi \tilde{n}_i/N)}{\delta x}, \quad (73)$$

whereas for the forward/backward derivatives (67),

$$k_{\text{Lat},i} = 2 \frac{\sin(\pi \tilde{n}_i/N)}{\delta x} \quad \text{if } \mathbf{l} = \mathbf{n} + \frac{\hat{i}}{2}; \quad k_{\text{Lat},i}^{\pm} = \frac{\sin(2\pi \tilde{n}_i/N)}{\delta x} \pm i \frac{1 - \cos(2\pi \tilde{n}_i/N)}{\delta x} \quad \text{if } \mathbf{l} = \mathbf{n}. \quad (74)$$

We note that for anti-symmetric lattice derivatives with $D_i(-\mathbf{m}') = -D_i(\mathbf{m}')$, the lattice momentum \mathbf{k}_{Lat} must be real.

3.2.2 Lattice gauge invariant techniques

Discretizing a gauge theory requires a special care in order to preserve gauge invariance at the lattice level. It is not enough to recover gauge invariance in the continuum, sending the lattice spacing/time step to zero, as gauge invariance is meant to remove spurious transverse degrees of freedom. If we were to discretize a gauge theory substituting all ordinary derivatives in the continuum EOM by finite differences like those in Eqs. (66), (67), the gauge symmetry would not be preserved in the lattice and these spurious degrees of freedom would be propagating.

In order to understand this, let us consider the simplest possible case of a gauge theory, say an Abelian-Higgs model in flat space-time, with Lagrangian $-\mathcal{L} = (\partial_\mu + ieA_\mu)\varphi^*(\partial^\mu - ieA^\mu)\varphi + \frac{1}{4}F_{\mu\nu}F^{\mu\nu} + V(\varphi^*\varphi)$. This system is invariant under continuum gauge transformations $\varphi(x) \rightarrow e^{-i\alpha(x)}\varphi(x)$, $A_\mu(x) \rightarrow A_\mu(x) - \frac{1}{e}\partial_\mu\alpha(x)$ simply because the transformation of $\partial_\mu(e^{-i\alpha(x)}\varphi(x))$ leads to a term $i\partial_\mu\alpha(x)e^{-i\alpha(x)}\varphi(x)$, whereas the transformation of the gauge field in $-ieA_\mu e^{-i\alpha(x)}$ leads to a term identical but of opposite sign, $+i\partial_\mu\alpha(x)e^{-i\alpha(x)}\varphi(x)$, which cancels out the previous one. However, if we discretized the system by simply promoting continuum derivatives into finite differences, say $\partial_\mu f(x) \rightarrow \Delta_\mu^+ f(x)$, then $\Delta_\mu^+(e^{-i\alpha(x)}\varphi(x)) \neq \Delta_\mu^+(e^{-i\alpha(x)})\varphi(x) + e^{-i\alpha(x)}\Delta_\mu^+\varphi(x)$, and thus the transformation of the field derivative does not produce a term compensated by the gauge field transformation in $-ieA_\mu e^{-i\alpha(x)}$. The reason is simple, the *Leibniz* rule $(fg)' = f'g + fg'$ does not hold for finite difference operators. The situation is no different in non-Abelian theories.

How can we restore gauge invariance in the lattice? To mimic a continuum gauge theory in the lattice, we must adopt a special discretization procedure that preserves some sort of discretized version of gauge transformations. Lattice gauge invariance is actually necessary in order to preserve constraints that follow from the EOM, in particular the Gauss laws. In order to introduce a general formalism valid for gauge theories (either Abelian or non-Abelian), let us consider the more general case of a $SU(N)$ invariant theory. We introduce then a *parallel transporter*, connecting two points in space-time

$$U(x, y) = P \exp \left\{ -i \int_x^y dx^\mu A_\mu \right\}, \quad (75)$$

where $P \exp \{ \dots \}$ means *path-ordered* along the trajectory. The crucial observation is that under a gauge transformation of the gauge fields, recall Eq. (19), the parallel transporter transforms as

$$U(x, y) \rightarrow \Omega(x) U(x, y) \Omega^\dagger(y), \quad (76)$$

which in the Abelian case reduces simply to $U(x, y) \rightarrow U(x, y)e^{-i(\alpha(x)-\alpha(y))}$. Therefore, according to Eq. (76), a parallel transporter transforms exactly as the field strength transforms for $x = y$, Eq. (19). Thus, considering the *minimal connector* between two space-time sites separated only by one lattice spacing/time step, $x(n) \equiv \mathbf{n}\delta x + n_0\delta t$, $x(n + \hat{\mu}) \equiv \mathbf{n}\delta x + n_0\delta t + \delta x_\mu$, we define the *link* variables as

$$U_{0,n} \equiv \text{Pexp} \left\{ -i \int_{x(n)}^{x(n+\hat{0})} dt' A_0 \right\} \approx e^{-i\delta t A_0}, \quad U_{i,n} \equiv \text{Pexp} \left\{ -i \int_{x(n)}^{x(n+\hat{i})} dx A_i \right\} \approx e^{-i\delta x A_i}, \quad (77)$$

where the gauge field, and hence the link, is considered to live in the point $n + \frac{\hat{\mu}}{2}$. We also define $U_{-\mu,n} = U_{\mu,n-\mu}^\dagger \equiv U_\mu^\dagger(n - \frac{1}{2}\hat{\mu})$. Before we continue, it will be useful at this point to establish some conventions to simplify the notation of upcoming expressions.

Convention -. From now on, unless stated otherwise, a scalar field living in a generic lattice site $n = (n_o, \mathbf{n}) = (n_o, n_1, n_2, n_3)$, i.e. $\varphi_n = \varphi(n)$, will be simply denoted as φ . If the point is displaced in the μ -direction by one unit lattice spacing/time step, $n + \hat{\mu}$, we will then use the notation $n + \mu$ or simply by $+\mu$ to indicate this, so that the field amplitude in the new point is expressed by $\varphi_{+\mu} \equiv \varphi(n + \hat{\mu})$. In the case of gauge fields, whenever represented explicitly in the lattice, we will automatically understand that they live in the middle of lattice points, i.e. $A_\mu \equiv A_\mu(n + \frac{1}{2}\hat{\mu})$. It follows then that e.g. $A_{\mu,+\nu} \equiv A_\mu(n + \frac{1}{2}\hat{\mu} + \hat{\nu})$. In the case of links, we will use the notation $U_\mu \equiv U_{\mu,n} \equiv U_\mu(n + \hat{\mu}/2)$, and hence $U_{\mu,\pm\nu} = U_{\mu,n\pm\nu} \equiv U_\mu(n + \hat{\mu}/2 \pm \hat{\nu})$. Even though the lattice spacing δx and the time step δt do not need to be equal, we will loosely speak of corrections of order $\mathcal{O}(\delta x)$, independently of whether we are referring to the lattice spacing or the time step (the latter is actually always forced to be smaller than the former). In lattice expressions we will never consider summation over repeated indices.

In the continuum limit, we recover the gauge fields simply from

$$\frac{(\mathcal{I} - U_{\mu,n})}{i\delta x^\mu} \rightarrow A_\mu(n + \frac{1}{2}\hat{\mu}) + \mathcal{O}(\delta x). \quad (78)$$

It turns out that we can actually build the action or EOM for any gauge theory, preserving a discretized version of the gauge symmetry, using only link variables and no gauge fields. That is known as the *compact formulation* of lattice gauge theories, which can be applied to both Abelian and non-Abelian gauge theories. Actually, in the case of non-Abelian theories, compact formulations are the only way to discretize them while respecting gauge invariance in the lattice. In Abelian gauge theories, however, it is still possible to make use of an explicit representation of the gauge fields, in the so called *non-compact formulation*. Below we provide both. We introduce now standard definitions for *links*, *plaquettes* and *lattice covariant derivatives*, specialized to both Abelian and non-Abelian gauge groups. We provide also basic definitions, together with useful approximations and expressions (in the case of Abelian theories for both compact and non-compact formulations):

— U(1) toolkit —

$$\begin{aligned} \text{Links : } V_\mu &\equiv e^{-id x_\mu A_\mu} = \cos(dx_\mu A_\mu) - i \sin(dx_\mu A_\mu); \quad V_{-\mu} \equiv V_{\mu,-\mu}^*; \quad V_\mu^* V_\mu = 1; \\ \text{Plaquettes : } V_{\mu\nu} &\equiv V_\mu V_{\mu,+\nu} V_{\mu,+\nu}^* V_\nu^* \simeq e^{-id x_\mu dx_\nu [F_{\mu\nu} + \mathcal{O}(\delta x)]}; \quad V_{\mu\nu}^* = V_{\nu\mu}; \\ \text{Covariant Derivs. : } (D_\mu^\pm \varphi)(\mathbf{l}) &= \pm \frac{1}{\delta x^\mu} (V_{\pm\mu} \varphi_{\pm\mu} - \varphi), \quad \mathbf{l} = \mathbf{n} \pm \frac{1}{2}\hat{\mu} \\ \text{Expansions : } \begin{cases} (D_\mu^\pm \varphi)(\mathbf{l}) &\rightarrow (D_\mu \varphi)(\mathbf{l}) + \mathcal{O}(\delta x^2) \quad \mathbf{l} = \mathbf{n} \pm \frac{1}{2}\hat{\mu} \\ \mathcal{R}e\{V_{\mu\nu}\} &\rightarrow 1 - \frac{1}{2} dx_\mu^2 dx_\nu^2 F_{\mu\nu}^2 + \mathcal{O}(\delta x^5), \quad \mathbf{l} = \mathbf{n} + \frac{1}{2}\hat{\mu} + \frac{1}{2}\hat{\nu} \\ \mathcal{I}m\{V_{\mu\nu}\} &\rightarrow -dx_\mu dx_\nu F_{\mu\nu} + \mathcal{O}(\delta x^3), \quad \mathbf{l} = \mathbf{n} + \frac{1}{2}\hat{\mu} + \frac{1}{2}\hat{\nu} \end{cases} \quad (79) \\ \text{Expressions : } \begin{cases} \sum_n \frac{1}{4} F_{\mu\nu}^2 \simeq -\frac{1}{2} \sum_n \frac{\mathcal{R}e\{V_{\mu\nu}\}}{dx_\mu^2 dx_\nu^2} = -\frac{1}{4} \sum_n \frac{(V_{\mu\nu} + V_{\mu\nu}^*)}{dx_\mu^2 dx_\nu^2} + \mathcal{O}(\delta x^2) \\ \sum_n \frac{1}{4} F_{\mu\nu}^2 \simeq \sum_n \frac{1}{4} \frac{\mathcal{I}m^2\{V_{\mu\nu}\}}{dx_\mu^2 dx_\nu^2} = -\sum_n \frac{1}{4} \frac{(V_{\mu\nu} - V_{\mu\nu}^*)^2}{dx_\mu^2 dx_\nu^2} + \mathcal{O}(\delta x^2) \end{cases} \quad (\text{Compact}) \\ \sum_n \frac{1}{4} F_{\mu\nu}^2 \simeq \frac{1}{4} \sum_n (\Delta_\mu^+ A_\nu - \Delta_\nu^+ A_\mu)^2 + \mathcal{O}(\delta x^2) \quad (\text{Non - Compact}) \end{cases}$$

$$\text{Gauge Trans} \left\{ \begin{array}{lll} \phi & \longrightarrow & e^{+i\alpha}\phi \\ A_\mu & \longrightarrow & A_\mu + \frac{1}{e}\Delta_\mu^+\alpha \\ U_{\pm\mu} & \longrightarrow & e^{+i\alpha}U_{\pm\mu}e^{-i\alpha\pm\mu} \end{array} \right\} \implies \left\{ \begin{array}{lll} D_\mu^\pm\phi & \longrightarrow & e^{+i\alpha}(D_\mu^\pm\phi) \\ U_{\mu\nu} & \longrightarrow & U_{\mu\nu} \text{ (gauge inv. !)} \end{array} \right\}$$

— SU(N) toolkit —

$$\text{Links : } U_\mu \equiv e^{-idxB_\mu} = e^{-idxB_\mu^a T_a}; \quad U_{-\mu} \equiv U_{\mu,-\mu}^\dagger; \quad U_\mu^\dagger U_\mu = \mathcal{I}$$

$$\text{Plaquettes : } U_{\mu\nu} \equiv U_\mu U_{\nu,+\mu} U_{\mu,+\nu}^\dagger U_\nu^\dagger \simeq e^{-id x_\mu dx_\nu [G_{\mu\nu}^a T_a + \mathcal{O}(dx_\mu)]}; \quad U_{\mu\nu}^\dagger = U_{\nu\mu}$$

$$\text{Covariant Derivs. : } (D_\mu^\pm \Phi)(\mathbf{l}) = \pm \frac{1}{\delta x^\mu} (U_{\pm\mu} \Phi_{\pm\mu} - \Phi) \longrightarrow (D_\mu \Phi)(\mathbf{l}) + \mathcal{O}(\delta x^2), \quad \mathbf{l} = \mathbf{n} \pm \frac{1}{2}\hat{\mu}$$

$$\text{Expansions : } \left\{ \begin{array}{ll} (D_\mu^\pm \Phi)(\mathbf{l}) & \longrightarrow (D_\mu \Phi)(\mathbf{l}) + \mathcal{O}(\delta x^2), \quad \mathbf{l} = \mathbf{n} \pm \frac{1}{2}\hat{\mu} \\ (U_{\mu\nu} - U_{\mu\nu}^\dagger) & \longrightarrow -2i\delta x_\mu \delta x_\nu G_{\mu\nu} + \mathcal{O}(dx_\mu^3), \quad \mathbf{l} = \mathbf{n} + \frac{1}{2}\hat{\mu} + \frac{1}{2}\hat{\nu} \\ \text{Tr}[U_{\mu\nu}] & \longrightarrow 2 - \frac{dx_\mu^2 dx_\nu^2}{4} \sum_a (G_{\mu\nu}^a)^2 + \mathcal{O}(dx_\mu^5), \quad \mathbf{l} = \mathbf{n} + \frac{1}{2}\hat{\mu} + \frac{1}{2}\hat{\nu} \end{array} \right. \quad (80)$$

$$\text{Expressions : } \left\{ \begin{array}{l} \frac{1}{2}\text{Tr}[G_{\mu\nu} G^{\mu\nu}] = \frac{1}{4} \sum_a (G_{\mu\nu}^a)^2 \simeq -\frac{\text{Tr}[U_{\mu\nu}]}{dx_\mu^2 dx_\nu^2} + \mathcal{O}(\delta x^2), \\ G_{\mu\nu} = G_{\mu\nu}^a T_a \simeq \frac{i}{2dx_\mu dx_\nu} (U_{\mu\nu} - U_{\mu\nu}^\dagger) + \mathcal{O}(\delta x^2), \\ G_{\mu\nu}^a \simeq \frac{1}{dx_\mu dx_\nu} \text{Tr}[(iT_a)(U_{\mu\nu} - U_{\mu\nu}^\dagger)] + \mathcal{O}(\delta x^2) \end{array} \right.$$

$$\text{Gauge Trans.} \left\{ \begin{array}{lll} \Phi & \longrightarrow & \Omega \Phi, \quad \Omega \equiv e^{+i\alpha_a T_a} \\ U_{\pm\mu} & \longrightarrow & \Omega U_{\pm\mu} \Omega_{\pm\mu}^\dagger \end{array} \right\} \implies \left\{ \begin{array}{lll} D_\mu^\pm \Phi & \longrightarrow & \Omega (D_\mu^\pm \Phi) \\ U_{\mu\nu} & \longrightarrow & \Omega U_{\mu\nu} \Omega^\dagger \\ \text{Tr}\{U_{\mu\nu}\} & \longrightarrow & \text{Tr}\{U_{\mu\nu}\} \end{array} \right.$$

In the of case of $SU(2)$, any element can be written as

$$U_\mu = c_{\mu 0} \mathcal{I} + \sum_{a=1}^3 i c_{\mu a} \sigma_a = \sum_{\nu=0}^3 c_{\mu\nu} \bar{\sigma}_a, \quad \bar{\sigma}_a \equiv (1, i\vec{\sigma}), \quad \sum_{\nu=0}^3 c_{\mu\nu}^2 = 1, \quad (81)$$

or, in matrix form (in the gauge $U_0 = \mathcal{I}$)

$$U_i \equiv U_i(c_{i0}, c_{i1}, c_{i2}, c_{i3}) = \begin{pmatrix} c_{i0} + i c_{i3} & c_{i2} + i c_{i1} \\ -c_{i2} + i c_{i1} & c_{i0} - i c_{i3} \end{pmatrix}, \quad U_i^\dagger = U_i(c_{i0}, -c_{i1}, -c_{i2}, -c_{i3}). \quad (82)$$

Useful expressions for the electric and magnetic fields are

$$\mathcal{E}_i^a = G_{0i}^a \approx \frac{1}{\delta t \delta x} \text{Tr}[(iT_a)(U_{0i} - U_{i0})] = \frac{1}{\delta t \delta x} \text{Tr}[(iT_a)(U_{0i} - U_{0i}^\dagger)], \quad (83)$$

$$\mathcal{B}_i^a = \frac{1}{2} \epsilon_{ijk} G_{jk}^a \approx \frac{\epsilon_{ijk}}{2\delta x^2} \text{Tr}[(iT_a)(U_{jk} - U_{kj})]. \quad (84)$$

3.3 Evolution algorithms

Solving the field dynamics in an expanding background in a lattice consists in writing some appropriate discrete version of the EOM [say Eqs. (36)-(38) for scalar fields, Eqs. (37)-(42) for gauge fields, and Eqs. (51)-(52) for the scale factor], and then iterate the discrete EOM for a finite number of time steps. In general we will have to follow the evolution in each spatial lattice site of a number of *dof* representing real field amplitudes, say one per singlet, two per complex field, four per doublet, etc, as well as the Lorentz components of each gauge field considered. Let us denote these *dof* collectively as the *field amplitudes* $\{f_j\}$, with j some index labeling all the real field amplitudes involved in a given scenario, and $\{\pi_j\}$ their *conjugate momenta*. As the scale factor is only a homogeneous *dof* (sourced by the volume averaged energy

and pressure densities built from the matter *dof*), we will not include it in the previous numbered list of *dof*'s, and we will rather treat it as a separate variable $a(\eta)$, with conjugate momenta $\pi_a \equiv a'(\eta)$. For example, in a theory with two singlet scalar fields, say ϕ and χ , and self-consistent expansion, we can consider $\{f_1, f_2\} \equiv \{\phi(x), \chi(x)\}$ and $\{\pi_1, \pi_2\} \equiv \{\phi'(x), \chi'(x)\}$, and then separately $a(\eta)$ and $\pi_a(\eta) = a'(\eta)$. Looking at the EOM in the continuum Eqs. (36)-(38) and scale factor Eqs. (51)-(52), we note the following structure in the system of equations (independently of the nature of fields involved),

$$\pi_a(\eta) = a'(\eta), \quad (85)$$

$$\pi'_a(\eta) = \mathcal{K}_a[a(\eta), \bar{V}(\eta), \bar{K}(\eta), \bar{G}(\eta)], \quad (86)$$

$$\pi_i(\mathbf{x}, \eta) = \mathcal{D}_i[f'_i(\mathbf{x}, \eta), a(\eta), \pi_a(\eta); \{f_j(\mathbf{x}, \eta)\}, \{f'_{j \neq i}(\mathbf{x}, \eta)\}], \quad (87)$$

$$\pi'_i(\mathbf{x}, \eta) = \mathcal{K}_i[f_i(\mathbf{x}, \eta), \pi_i(\mathbf{x}, \eta), a(\eta), \pi_a(\eta); \{f_{j \neq i}(\mathbf{x}, \eta)\}, \{\pi_{j \neq i}(\mathbf{x}, \eta)\}], \quad (88)$$

where $\mathcal{D}_i[\dots]$ is a functional – the *drift* – that defines the conjugate momentum of the *i*th *dof*, $\mathcal{K}_i[\dots]$ is another functional – the *kernel* or *kick* –, that determines the interactions of the *i*th *dof* with the rest of *dof*'s (possibly including itself), and finally $\mathcal{K}_a[\dots]$ is given by the square root of the *rhs* of Eq. (52), based on the volume averages $\langle \dots \rangle$ of the different *dof* contributions to the potential, kinetic and gradient energy densities, $\bar{V}(\eta) \equiv \langle V \rangle$, $\bar{K} \equiv \{\bar{K}_j(\eta); \bar{K}_j(\eta) \equiv \langle K_j \rangle\}$ and $\bar{G} \equiv \{\bar{G}_j(\eta); \bar{G}_j(\eta) \equiv \langle G_j \rangle\}$.

For canonical kinetic terms, \mathcal{D}_i depends on f'_i but not on any other $f'_{j \neq i}$. We note also that we have separated within the argument of each kernel \mathcal{K}_i , the amplitude and momentum of the *i*th *dof* itself, from the amplitudes and momenta of the rest of *dof*'s. The latter actually act merely as 'instantaneous' parameters for an infinitesimal evolution of the *i*th *dof*. Hence, in general, we will only care about the dependence of the *i*th kernel \mathcal{K}_i on f_i and π_i . Furthermore, we will encounter often that the time derivative π'_i of a given *dof* can (and often will) depend on its amplitude f_i , but not on π_i itself. This is actually not a physical requisite, but rather a mathematical requisite we will seek. In fact, the EOM in the continuum as written so far, lead to kernels \mathcal{K}_i that depend on π_i , see e.g. the friction terms in Eqs. (36)-(40). However, from the point of view of the stability of the numerical algorithms used to solve the discrete EOM, it will be convenient to 'massage' appropriately the EOM, so that we arrive into effective kernels \mathcal{K}_i that do not depend⁴ on π_i . We will see later on how to do this in a case by case basis. For the time being, we will consider that this condition has been achieved, implicitly assuming that pertinent manipulations (if any) of the field variables in the EOM have been made to grant it. Taking into account all the above considerations, the typical system of equations we will want to solve (for a theory with canonical kinetic terms) looks as follows

$$\pi_a(\eta) = a'(\eta), \quad (89)$$

$$\pi'_a(\eta) = \mathcal{K}_a[a(\eta), \bar{V}(\eta), \bar{K}(\eta), \bar{G}(\eta)], \quad (90)$$

$$\pi_i(\mathbf{x}, \eta) = \mathcal{D}_i[f'_i(\mathbf{x}, \eta), a(\eta); \dots], \quad (91)$$

$$\pi'_i(\mathbf{x}, \eta) = \mathcal{K}_i[f_i(\mathbf{x}, \eta), a(\eta), \pi_a(\eta); \dots]. \quad (92)$$

Let us note that, although any possible dependence of the drift \mathcal{D}_i on π_a would not pose a problem to the algorithms presented below, in practice we do not know of any theory that produces such dependence, so we have removed it as an explicit argument from \mathcal{D}_i . A discrete version of the EOM will then have a scheme similar to

$$\pi_a(\eta) = \Delta_0 a(\eta), \quad (93)$$

$$\Delta_0 \pi_a = \mathcal{K}_a[a(\eta), \bar{V}(\eta), \bar{K}(\eta), \bar{G}(\eta)], \quad (94)$$

$$\pi_i(\mathbf{x}, \eta) = \mathcal{D}_i[\Delta_0 f_i(\mathbf{x}, \eta), a(\eta); \dots], \quad (95)$$

$$\Delta_0 \pi_i(\mathbf{x}, \eta) = \mathcal{K}_i[f_i(\mathbf{x}, \eta), a(\eta), \pi_a(\eta); \dots], \quad (96)$$

⁴The kernel \mathcal{K}_i will typically also not depend on the rest of conjugate momenta $\{\pi_{i \neq j}\}$, except in the case of non-canonically normalized kinetic terms. As already said, we leave this case for future work.

with Δ_0 some discrete operator mimicking continuum time derivatives. As we will see in a moment, introducing time operators as simple as

$$(\Delta_0^{\pm r} f) = \frac{\pm f(n \pm r\delta t) \mp f(n)}{r\delta t} \longrightarrow \begin{cases} (\Delta_0^+ f) = \frac{f(n+\delta t) - f(n)}{\delta t} & , \text{ Standard Forward Deriv.} \\ (\Delta_0^- f) = \frac{f(n) - f(n-\delta t)}{\delta t} & , \text{ Standard Backward Deriv.} \\ (\Delta_0^{+\frac{1}{2}} f) = \frac{f(n+\delta t/2) - f(n)}{(\delta t/2)} & , +\frac{1}{2} \text{ Forward Deriv.} \\ (\Delta_0^{-\frac{1}{2}} f) = \frac{f(n) - f(n-\delta t/2)}{(\delta t/2)} & , -\frac{1}{2} \text{ Backward Deriv.} \end{cases} \quad (97)$$

will actually enable us to address all basic algorithms to iterate coupled finite difference equations like (93)-(96), mimicking continuum coupled differential equations like (89)-(92).

3.3.1 Staggered leapfrog

One of the simplest methods for solving second order differential equations is the *leapfrog* algorithm. Let us illustrate it by solving a simple one-dimensional problem, consisting in one *dof* $x(t)$ that depends only on a time variable t , with EOM

$$\ddot{x}(t) = \mathcal{K}[x(t)]. \quad (98)$$

Taylor expanding the position at the next step we obtain

$$x(t + \delta t) = x(t) + \dot{x}(t)\delta t + \frac{1}{2}\mathcal{K}[x(t)]\delta t^2 + \dots \equiv x(t) + \dot{x}(t + \delta t/2)\delta t + \dots, \quad (99)$$

where in the second equality we have substituted the Taylor expansion of the velocity at half time step

$$\dot{x}(t + \delta t/2) = \dot{x}(t) + \frac{\delta t}{2}\mathcal{K}[x(t)] + \dots \equiv \dot{x}(t - \delta t/2) + \mathcal{K}[x(t)]\delta t + \dots, \quad (100)$$

and where we have used that $\dot{x}(t) = \dot{x}(t - \delta t/2) + \mathcal{K}[x(t - \delta t/2)]\delta t + \mathcal{O}(\delta t^2)$ and $\mathcal{K}[x(t - \delta t/2)]\delta t + \mathcal{O}(\delta t^2) = \mathcal{K}[x(t)]\delta t + \mathcal{O}(\delta t^2)$. Applying recursively the above relations between velocity and position, we obtain

$$x(t) = x(t - \delta t) + \dot{x}(t - \delta t/2)\delta t, \quad (101)$$

$$\dot{x}(t + \delta t/2) = \dot{x}(t - \delta t/2) + \mathcal{K}[x(t)]\delta t, \quad (102)$$

$$x(t + \delta t) = x(t) + \dot{x}(t + \delta t/2)\delta t, \quad (103)$$

$$\dot{x}(t + 3\delta t/2) = \dot{x}(t + \delta t/2) + \mathcal{K}[x(t + \delta t)]\delta t, \quad (104)$$

....

The leapfrog method has an accuracy of order $\mathcal{O}(\delta t^2)$, because each step advances x or π_x in terms of its derivative at the middle of the step. This is better than the simpler *Euler* method, which has $\mathcal{O}(\delta t)$ accuracy. This can be demonstrated by simply noting the accuracy of the derivative expressions $(x(t + \delta t) - x(t))/\delta t \simeq \dot{x}(t + \delta t/2) + \mathcal{O}(\delta t^2)$ and $(\dot{x}(t + \delta t/2) - \dot{x}(t - \delta t/2))/\delta t \simeq \ddot{x}(t) + \mathcal{O}(\delta t^2)$. Let us label the initial time as t_0 , and start with initial conditions $x_0 \equiv x(t_0)$ and $\dot{x}_0 \equiv \dot{x}(t_0)$. We can obtain first $\dot{x}(t_0 + \delta t/2) = \dot{x}_0 + 1/2\mathcal{K}[x_0]\delta t$, and from then on, iterate as follows: $(x(t_0), \dot{x}(t_0 + \delta t/2)) \longrightarrow (x(t_1), \dot{x}(t_1 + \delta t/2)) \longrightarrow \dots \longrightarrow (x(t_n), \dot{x}(t_n + \delta t/2))$, with $t_n \equiv t_0 + n\delta t$, and n the number of iterations.

In terms of the previously introduced time derivative operators, we can simply write the algorithm as

$$\Delta_0^+ x_n = \pi_{n+1/2}, \quad (105)$$

$$\Delta_0^+ \pi_{n+1/2} = \mathcal{K}[x_{n+1}], \quad (106)$$

understanding that x_n lives at 'integer' times $t_n \equiv t_0 + n\delta t$ and π_x at 'semi-integer' times $t_{n+1/2} \equiv t_n + \delta t/2 = t_0 + (n + 1/2)\delta t$, so that $\Delta_0^+ x_n \equiv (x_{n+1} - x_n)/\delta t$ lives at $t_{n+1/2}$, whereas $\Delta_0^+ \pi_{n+1/2} \equiv (\pi_{n+3/2} - \pi_{n+1/2})/\delta t$ lives at t_{n+1} . Due to this separation into variables that live at integer times and conjugate momenta that live at semi-integer times, sometimes people refer to this method as the 'staggered' leapfrog algorithm. We will content ourselves with simply referring to it as the leapfrog algorithm.

The leapfrog method, encapsulated in Eqs. (105)-(106) can be extended readily to multiple *dof*, simply labeling them with some index as x_n^i and $\pi_{n+1/2}^i$, with $i = 1, 2, 3, \dots$ counting the number of *dof*. Namely

$$\Delta_0^+ x_n^i = \pi_{n+1/2}^i, \quad (107)$$

$$\Delta_0^+ \pi_{n+1/2}^i = \mathcal{K}_i \left[x_{n+1}^i, \{x_{n+1}^{j \neq i}\} \right], \quad (108)$$

where the kernels \mathcal{K}_i represent the interaction of the i th *dof* x^i with the rest of *dofs* $\{x^{j \neq i}\}$. However, this method is only applicable to *conservative* forces⁵, i.e. to EOM with kernels that only depend on amplitude variables $\mathcal{K} \equiv \mathcal{K}[\{x^i(t)\}]$. This method can be therefore applied readily to our field theory EOM (93)-(96) in a flat space-time background. If the expansion of the Universe is switched off, i.e. $a = 1$ and $\dot{a} = \ddot{a} = 0$, we can ignore the first two Eqs. (93)-(94) and take care of evolving only (95)-(96), which represent the evolution of the matter field *dof* in a flat background. Switching back to our α -time variable, say $\eta(n_0) \equiv \eta_0 + n_0 \delta\eta$ with n_0 counting the number of time steps, we can solve Eqs. (95)-(96) with a leapfrog scheme simply as

$$\Delta_0^+ f_i(\mathbf{x}, n_0) = \pi_i(\mathbf{x}, n_0 + 1/2), \quad (109)$$

$$\Delta_0^+ \pi_i(\mathbf{x}, n_0 + 1/2) = \mathcal{K}_i[\{f_j(\mathbf{x}, n_0 + 1)\}], \quad (110)$$

with $i = 1, 2, 3, \dots$ counting our field theory *dof*, e.g. scalar field real components and gauge field Lorentz components.

We note now that in any set of discrete EOM mimicking continuum EOM, the spatial coordinates \mathbf{x} are discretized, being represented by a finite set of lattice sites $\mathbf{n} = (n_1, n_2, n_3)$ with $n_i = 0, 1, 2, \dots, N - 1$, and N the number of lattice sites per spatial dimension (recall Section 3.1 for definitions). This implies that spatial derivatives appearing in the discrete EOM, e.g. the Laplacian operator for scalar fields $\nabla^2 f$, will be substituted by lattice derivative operators like in Eq. (67). Due to this, the kernels in the discretized EOM are not functions of the point \mathbf{n} only, but also of its nearest neighbours, e.g. $\mathbf{n} \pm \hat{j}$, with $j = 1, 2, 3$. The correct form of the discretized field EOM in a flat background will then look like

$$\Delta_0^+ f_i(\mathbf{n}, n_0) = \pi_i(\mathbf{n}, n_0 + 1/2), \quad (111)$$

$$\Delta_0^+ \pi_i(\mathbf{n}, n_0 + 1/2) = \mathcal{K}_i[\{f_j(\mathbf{m}, n_0 + 1)\}], \quad (112)$$

with \mathbf{m} representing \mathbf{n} and its nearest neighbours (to be determined in each case depending on the choice of lattice spatial derivatives).

Note that the leapfrog algorithm cannot be applied directly to scenarios where the expansion of the universe is considered (either background or self-consistent expansion), without a careful choice of which *dof* to evolve. Indeed, the EOM of matter fields in FLRW, c.f. Eq. (87), have kernels $\mathcal{K}[\dots]$ containing conjugate momenta π_i , due to the presence of the friction terms $\propto (a'/a)f'_i$ in the field EOM, see e.g. Eqs. (36)-(40). Furthermore, the Friedmann equation $\pi'_a = \mathcal{K}_a[a, \bar{V}, \bar{K}, \bar{G}]$ [c.f. Eq. (86)], also contains the kinetic terms $\bar{K} \equiv \{K_j\}$, built from the conjugate momenta of the fields. As conjugate momenta π_i and π_a live, in a leapfrog algorithm, naturally at semi-integer times $\eta_{n+1/2}$, the leapfrog algorithm for kernels which contain conjugate momenta will not work, as they should rather live at integer times η_p for the algorithm to be stable and order $\mathcal{O}(\delta t^2)$. As we will show in Sections 4.2.1 and 4.2.2, it is possible to overtake this problem by means of field re-definitions and/or manipulations of the EOM, so that we can have a consistent iterative scheme with appropriate kernels, even in the presence of an expanding background. So for now, let us assume that we managed to obtain *dof* such that the kernels do not depend on the momenta. We then have the following leapfrog algorithm in an expanding universe

Leapfrog in an expanding background

$$\Delta_0^+ \pi_a(\mathbf{n}, n_0 - 1/2) = \mathcal{K}_a[a(n_0), \bar{V}(n_0), \bar{K}(n_0), \bar{G}(n_0)], \quad (113)$$

$$\Delta_0^+ \pi_i(\mathbf{n}, n_0 - 1/2) = \mathcal{K}_i[\{f_j(\mathbf{m}, n_0)\}, a(n_0)], \quad (114)$$

⁵In reality nothing prevents you from applying it to *non-conservative* forces with $\mathcal{K} = \mathcal{K}[x(t), \dot{x}(t)]$, but then its stability properties and its $\mathcal{O}(\delta t^2)$ accuracy will be lost.

$$\Delta_0^+ a(n_0) = \pi_a(n_0 + 1/2), \quad (115)$$

$$\Delta_0^+ f_i(\mathbf{n}, n_0) = \mathcal{D}_i[\pi_i(\mathbf{n}, n_0 + 1/2), a(n_0 + 1/2)], \quad (116)$$

Its concrete applications to the case of interacting scalar, Abelian and non-Abelian gauge fields are discussed in Section 4 through 6.

3.3.2 Verlet integration

Let us dig up again the one-dimensional problem of a single *dof* that depends only on time, $x(t)$, with EOM

$$\ddot{x}(t) = \mathcal{K}[x(t)], \quad (117)$$

say with initial condition $t_0 = 0$, $x(0) = x_0$ and $\dot{x}(0) = \pi_0$. Recall that in order to initiate the previously discussed leapfrog algorithm, we initially needed x_0 and $\pi_{1/2} \equiv \dot{x}(\delta t/2)$, so we proposed to obtain the initial half-time step displaced velocity as $\pi_{1/2} \simeq \pi_0 + \frac{1}{2}\delta t \mathcal{K}[x_0] + \mathcal{O}(\delta t^2)$ (or equivalently, from applying $\Delta_{0/2}^+ \pi_0 = \frac{1}{2}\mathcal{K}[x_0]$). Now, following the leapfrog prescription, we would apply $\Delta_0^+ x_0 = \pi_{1/2}$ leading to x_1 at order $\mathcal{O}(\delta t^2)$, and then $\Delta_0^+ \pi_{1/2} = \mathcal{K}[x_1]$ leading to $\pi_{3/2}$ at order $\mathcal{O}(\delta t^2)$, and so on and so forth with successive iterations. However, after obtaining x_1 , we might as well apply $\Delta_{0/2}^+ \pi_{1/2} = \frac{1}{2}\mathcal{K}[x_1]$, leading to π_1 , also at order $\mathcal{O}(\delta t^2)$. Essentially, by applying the velocity part of the leapfrog algorithm at two equal and successive half time steps (with one position update in between), we can simply jump from (x_0, π_0) to (x_1, π_1) , and from there to (x_2, π_2) , and so on and so forth. In other words, we can actually obtain the position and velocity always at integer times, up at order $\mathcal{O}(\delta t^2)$, with a 'kick - drift - kick' scheme as

$$\left. \begin{aligned} \pi_{n+1/2} &= \pi_n + \frac{1}{2}\delta t \mathcal{K}[x_n], \\ x_{n+1} &= x_n + \pi_{n+1/2} \delta t, \\ \pi_{n+1} &= \pi_{n+1/2} + \frac{1}{2}\delta t \mathcal{K}[x_{n+1}], \end{aligned} \right\} \iff \left\{ \begin{aligned} \Delta_{0/2}^+ \pi_n &= \mathcal{K}[x_n], \\ \Delta_0^+ x_n &= \pi_{n+1/2}, \\ \Delta_{0/2}^+ \pi_{n+1/2} &= \mathcal{K}[x_{n+1}]. \end{aligned} \right. \quad (118)$$

In reality, this method is nothing else than the leapfrog algorithm, but adding an 'extra' computation of the conjugate momenta at integer times in each iteration,

$$\left. \begin{aligned} x_{n+1} &= x_n + \pi_{n+1/2} \delta t, \\ \pi_{n+3/2} &= \pi_{n+1/2} + \delta t \mathcal{K}[x_{n+1}], \\ \left(\pi_{n+1} &= \pi_{n+1/2} + \frac{1}{2}\delta t \mathcal{K}[x_{n+1}] \right) \end{aligned} \right\} \iff \left\{ \begin{aligned} \Delta_0^+ x_n &= \pi_{n+1/2}, \\ \Delta_0^+ \pi_{n+1/2} &= \mathcal{K}[x_{n+1}], \\ \left(\Delta_{0/2}^+ \pi_{n+1/2} &= \mathcal{K}[x_{n+1}] \right). \end{aligned} \right. \quad (119)$$

Alternatively, since we may only care about the amplitudes and conjugate momenta at the same moment, say at integer times, the scheme can be put into a 'drift-kick' scheme, simply by

$$\left. \begin{aligned} x_{n+1} &= x_n + \pi_n \delta t + \frac{1}{2}\mathcal{K}[x_n] \delta t^2, \\ \pi_{n+1} &= \pi_n + \frac{1}{2}(\mathcal{K}[x_n] + \mathcal{K}[x_{n+1}]) \delta t, \end{aligned} \right\} \iff \left\{ \begin{aligned} \Delta_0^+ x_n &= \pi_n + \frac{\delta t}{2} \mathcal{K}[x_n], \\ \Delta_0^+ \pi_n &= \frac{1}{2}(\mathcal{K}[x_n] + \mathcal{K}[x_{n+1}]). \end{aligned} \right. \quad (120)$$

The method, represented by either scheme Eq. (118), Eq. (119) or Eq. (120), is known as the *velocity-Verlet* algorithm. Let us remark that the 2-step scheme has actually no advantage versus the 3-step scheme, as in reality the number of operations is the same: the 2-step scheme simply contains the 'third' step in the drift (i.e. in the right hand side of the amplitude updates). The 2-step scheme is only a convenient way of writing the algorithm in a more compact way.

If instead we apply the coordinate part of the leapfrog algorithm at two equal and successive half time steps (with one velocity update in between), then the method turns into the *position-Verlet* algorithm, which in a 'drift-kick-drift' scheme, has the form

$$\left. \begin{aligned} x_{n+1/2} &= x_n + \frac{1}{2}\pi_n \delta t, \\ \pi_{n+1} &= \pi_n + \delta t \cdot \mathcal{K}[x_{n+1/2}], \\ x_{n+1} &= x_{n+1/2} + \frac{1}{2}\pi_{n+1} \delta t, \end{aligned} \right\} \iff \left\{ \begin{aligned} \Delta_{0/2}^+ x_n &= \pi_n, \\ \Delta_0^+ \pi_n &= \mathcal{K}[x_{n+1/2}], \\ \Delta_{0/2}^+ x_{n+1/2} &= \pi_{n+1}. \end{aligned} \right. \quad (121)$$

As before, this is nothing more than a standard leapfrog algorithm (with variables half time step shifted), plus an extra computation at each time step. Position-Verlet is also an algorithm of order $\mathcal{O}(\delta t^2)$. The position-Verlet algorithm can also be put in a 2-step scheme like

$$\left. \begin{aligned} \pi_{n+1} &= \pi_n + \delta t \cdot \mathcal{K}[x_n + \frac{\delta t}{2} \pi_n], \\ x_{n+1} &= x_n + \frac{\delta t}{2}(\pi_n + \pi_{n+1}), \end{aligned} \right\} \iff \begin{cases} \Delta_0^+ \pi_n &= \mathcal{K}[x_n + \frac{\delta t}{2} \pi_n], \\ \Delta_0^+ x_n &= \frac{1}{2}(\pi_n + \pi_{n+1}), \end{cases} \quad (122)$$

which again is just a more compact manner to write the algorithm: the number of operations is still three at each time step, with the 'third' step now contained inside the argument of the kick.

The application of either Verlet algorithm to field theories in a flat space-time background is straightforward. Introducing again $\eta(n_0) \equiv \eta_i + n_0 \delta \eta$ as the discrete α -time variable (η_i some initial time), and $i = 1, 2, 3, \dots$ labeling the field theory *dof* (namely scalar field real components and gauge field Lorentz components), the velocity-Verlet algorithm reads

$$\Delta_{0/2}^+ \pi_i(\mathbf{n}, n_0) = \mathcal{K}_i[\{f_j(\mathbf{m}, n_0)\}], \quad (123)$$

$$\Delta_0^+ f_i(\mathbf{n}, n_0) = \pi_i(\mathbf{n}, n_0 + 1/2), \quad (124)$$

$$\Delta_{0/2}^+ \pi_i(\mathbf{n}, n_0 + 1/2) = \mathcal{K}_i[\{f_j(\mathbf{m}, n_0 + 1)\}], \quad (125)$$

whereas the position-Verlet algorithm is

$$\Delta_{0/2}^+ f_i(\mathbf{n}, n_0) = \pi_i(\mathbf{n}, n_0), \quad (126)$$

$$\Delta_0^+ \pi_i(\mathbf{n}, n_0) = \mathcal{K}_i[\{f_j(\mathbf{m}, n_0 + 1/2)\}], \quad (127)$$

$$\Delta_{0/2}^+ f_i(\mathbf{n}, n_0 + 1/2) = \pi_i(\mathbf{n}, n_0 + 1). \quad (128)$$

Here, like in the staggered leapfrog algorithm, \mathbf{m} on the *rhs* represents \mathbf{n} and its nearest neighbours, which are determined by the choice of lattice spatial derivatives.

As in the case of leapfrog algorithms, to apply these algorithms to the case of an expanding universe, a careful choice of *dof* has to be taken. This choice will again be presented in Sections 4-6. Assuming we have *dof* such that the kernels are independent of the momenta, the velocity- and position-Verlet algorithms in respective 'kick-drift-kick' and 'drift-kick-drift' schemes read as

Velocity-Verlet in an expanding background

$$\Delta_{0/2}^+ \pi_a(\mathbf{n}, n_0) = \mathcal{K}_a[a(n_0), \bar{V}(n_0), \bar{K}(n_0), \bar{G}(n_0)], \quad (129)$$

$$\Delta_{0/2}^+ \pi_i(\mathbf{n}, n_0) = \mathcal{K}_i[\{f_j(\mathbf{m}, n_0)\}, a(n_0)], \quad (130)$$

$$\Delta_0^+ a(n_0) = \pi_a(n_0 + 1/2), \quad (131)$$

$$a(n_0 + 1/2) = \frac{1}{2}(a(n_0) + a(n_0 + 1)), \quad (132)$$

$$\Delta_0^+ f_i(\mathbf{n}, n_0) = \mathcal{D}_i[\pi_i(\mathbf{n}, n_0 + 1/2), a(n_0 + 1/2)], \quad (133)$$

$$\Delta_{0/2}^+ \pi_i(\mathbf{n}, n_0 + 1/2) = \mathcal{K}_i[\{f_j(\mathbf{m}, n_0 + 1)\}, a(n_0 + 1)], \quad (134)$$

$$\Delta_{0/2}^+ \pi_a(\mathbf{n}, n_0 + 1/2) = \mathcal{K}_a[a(n_0 + 1), \bar{V}(n_0 + 1), \bar{K}(n_0 + 1), \bar{G}(n_0 + 1)], \quad (135)$$

Position-Verlet in an expanding background

$$\Delta_{0/2}^+ f_i(\mathbf{n}, n_0) = \mathcal{D}_i[\pi_i(\mathbf{n}, n_0), a(n_0)], \quad (136)$$

$$\Delta_{0/2}^+ a(n_0) = \pi_a(n_0), \quad (137)$$

$$\Delta_0^+ \pi_i(\mathbf{n}, n_0) = \mathcal{K}_i[\{f_j(\mathbf{m}, n_0 + 1/2)\}, a(n_0 + 1/2)], \quad (138)$$

$$\bar{K}(n_0 + 1/2) = \frac{1}{2} (\bar{K}(n_0 + 1) + \bar{K}(n_0)) \quad (139)$$

$$\Delta_0^+ \pi_a(\mathbf{n}, n_0) = \mathcal{K}_a \left[a(n_0 + 1/2), \bar{K}(n_0 + 1/2), \bar{G}(n_0 + 1/2), \bar{V}(n_0 + 1/2) \right], \quad (140)$$

$$\Delta_{0/2}^+ a(n_0 + 1/2) = \pi_a(n_0 + 1), \quad (141)$$

$$\Delta_{0/2}^+ f_i(\mathbf{n}, n_0 + 1/2) = \mathcal{D}_i[\pi_i(\mathbf{n}, n_0 + 1), a(n_0 + 1)], \quad (142)$$

It is important to note that in both position- and velocity-Verlet algorithms for an expanding background, the kernels $\mathcal{K}_i[\dots]$ of the matter *dof* must not depend on π_a , as the latter already depend on the conjugate momenta through the volume averaged kinetic energy $\bar{K}[\{\pi_j\}]$. An advantage of the Verlet algorithm(s) is that they can readily be turned into more accurate schemes, as will be explained in Section 3.4.1.

3.3.3 Explicit Runge-Kutta methods

Finally, let us consider a one-dimensional problem with a single *dof*, where the kernel of the EOM is also allowed to depend on the conjugate momenta,

$$\ddot{x}(t) = \mathcal{K}[x(t), \dot{x}(t)]. \quad (143)$$

We take initial conditions $x(0) = x_0$ and $\dot{x}(0) = \pi_0$ at the initial time $t_0 = 0$. First-order Runge-Kutta algorithms are the *Euler method*,

$$x_{n+1} = x_n + \pi_n \delta t, \quad (144)$$

$$\pi_{n+1} = \pi_n + \delta t \mathcal{K}[x_n], \quad (145)$$

and the *Euler-Cromer method*,

$$x_{n+1} = x_n + \pi_n \delta t, \quad (146)$$

$$\pi_{n+1} = \pi_n + \delta t \mathcal{K}[x_{n+1}]. \quad (147)$$

Both methods have an accuracy of $\mathcal{O}(\delta t)$. They are also less stable than, for instance, Leapfrog methods when integrated over many steps, as they are not *symplectic* algorithms⁶, see Section 3.5.

More accurate algorithms are the Runge-Kutta second-order *modified Euler* algorithm [RK2],

$$\left. \begin{aligned} k_1 &\equiv \mathcal{K}[x_n, \pi_n], \\ k_2 &\equiv \mathcal{K}[x_n + \pi_n \delta t, \pi_n + k_1 \delta t], \end{aligned} \right\} \implies \left\{ \begin{aligned} x_{n+1} &= x_n + \pi_n \delta t + \frac{1}{2} k_1 \delta t^2, \\ \pi_{n+1} &= \pi_n + \frac{\delta t}{2} (k_1 + k_2), \end{aligned} \right. \quad (148)$$

and the Runge-Kutta fourth-order method [RK4]

$$\left. \begin{aligned} k_1 &= \mathcal{K}[x_n, \pi_n], \\ k_2 &= \mathcal{K}[x_n + \frac{1}{2} \pi_n \delta t, \pi_n + \frac{1}{2} k_1 \delta t], \\ k_3 &= \mathcal{K}[x_n + \frac{1}{2} \pi_n \delta t + \frac{1}{4} k_1 \delta t^2, \pi_n + \frac{1}{2} k_2 \delta t], \\ k_4 &= \mathcal{K}[x_n + \pi_n \delta t + \frac{1}{2} k_2 \delta t^2, \pi_n + k_3 \delta t], \end{aligned} \right\} \implies \left\{ \begin{aligned} x_{n+1} &= x_n + \pi_n \delta t + \frac{1}{6} (k_1 + k_2 + k_3) \delta t^2, \\ \pi_{n+1} &= \pi_n + \frac{1}{6} (k_1 + 2k_2 + 2k_3 + k_4) \delta t, \end{aligned} \right. \quad (149)$$

accurate to $\mathcal{O}(\delta t^5)$.

Adapting RG2 to the EOM of our field theory, we obtain

$$\left\{ \begin{aligned} a^{(1)} &= a, & f_i^{(1)} &= f_i, & \pi_i^{(1)} &= \pi_i, & \pi_a^{(1)} &= \pi_a, \\ a^{(2)} &= a^{(1)} + \delta \eta \pi_a^{(1)}, & f_j^{(2)} &= f_j^{(1)} + \delta \eta \pi_j^{(1)}, & \pi_i^{(2)} &= \pi_i^{(1)} + \delta \eta k_{1,i}, & \pi_a^{(2)} &= \pi_a^{(1)} + \delta \eta k_{1,a}, \end{aligned} \right\} \implies \left\{ \begin{aligned} k_{1,i} &= \mathcal{K}_i[a^{(1)}, \pi_a^{(1)}, \{f_j^{(1)}\}, \{\pi_j^{(1)}\}], & k_{1,a} &= \mathcal{K}_a[a^{(1)}, \bar{K}^{(1)}, \bar{G}^{(1)}, \bar{V}^{(1)}], \\ k_{2,i} &= \mathcal{K}_i[a^{(2)}, \pi_a^{(2)}, \{f_j^{(2)}\}, \{\pi_j^{(2)}\}], & k_{2,a} &= \mathcal{K}_a[a^{(2)}, \bar{K}^{(2)}, \bar{G}^{(2)}, \bar{V}^{(2)}], \end{aligned} \right\}$$

⁶By shifting the conjugate momenta in the Euler-Cromer method by half time step, we can actually turn it into a symplectic algorithm, as we simply recover once again the staggered leapfrog algorithm.

$$\Rightarrow \begin{cases} \Delta_0^+ f_i(\mathbf{n}, n_0) &= \pi_i(\mathbf{n}, n_0) + \frac{1}{2} k_{1,i} \delta\eta, \\ \Delta_0^+ a(n_0) &= \pi_a(n_0) + \frac{1}{2} k_{1,a} \delta\eta, \\ \Delta_0^+ \pi_i(\mathbf{n}, n_0) &= \frac{1}{2} (k_{1,i} + k_{2,i}), \\ \Delta_0^+ \pi_a(n_0) &= \frac{1}{2} (k_{1,a} + k_{2,a}), \end{cases} \quad (150)$$

On the other hand, RG4 leads to

$$\begin{aligned} & \left\{ \begin{array}{llll} a^{(1)} = a, & f_i^{(1)} = f_i, & \pi_i^{(1)} = \pi_i, & \pi_a^{(1)} = \pi_a, \\ a^{(2)} = a^{(1)} + \frac{\delta\eta}{2} \pi_a^{(1)}, & f_j^{(2)} = f_j^{(1)} + \frac{\delta\eta}{2} \pi_j^{(1)}, & \pi_i^{(2)} = \pi_i^{(1)} + \frac{\delta\eta}{2} k_{1,i}, & \pi_a^{(2)} = \pi_a^{(1)} + \frac{\delta\eta}{2} k_{1,a}, \\ a^{(3)} = a^{(1)} + \frac{\delta\eta}{2} \pi_a^{(2)}, & f_j^{(3)} = f_j^{(1)} + \frac{\delta\eta}{2} \pi_j^{(2)}, & \pi_i^{(3)} = \pi_i^{(1)} + \frac{\delta\eta}{2} k_{2,i}, & \pi_a^{(3)} = \pi_a^{(1)} + \frac{\delta\eta}{2} k_{2,a}, \\ a^{(4)} = a^{(1)} + \delta\eta \pi_a^{(3)}, & f_j^{(4)} = f_j^{(1)} + \delta\eta \pi_j^{(3)}, & \pi_i^{(4)} = \pi_i^{(1)} + \delta\eta k_{3,i}, & \pi_a^{(4)} = \pi_a^{(1)} + \delta\eta k_{3,a}, \end{array} \right\} \Rightarrow \\ & \left\{ \begin{array}{ll} k_{1,i} = \mathcal{K}_i[a^{(1)}, \pi_a^{(1)}, \{f_j^{(1)}\}, \{\pi_j^{(1)}\}], & k_{1,a} = \mathcal{K}_a[a^{(1)}, \bar{K}^{(1)}, \bar{G}^{(1)}, \bar{V}^{(1)}], \\ k_{2,i} = \mathcal{K}_i[a^{(2)}, \pi_a^{(2)}, \{f_j^{(2)}\}, \{\pi_j^{(2)}\}], & k_{2,a} = \mathcal{K}_a[a^{(2)}, \bar{K}^{(2)}, \bar{G}^{(2)}, \bar{V}^{(2)}], \\ k_{3,i} = \mathcal{K}_i[a^{(3)}, \pi_a^{(3)}, \{f_j^{(3)}\}, \{\pi_j^{(3)}\}], & k_{3,a} = \mathcal{K}_a[a^{(3)}, \bar{K}^{(3)}, \bar{G}^{(3)}, \bar{V}^{(3)}], \\ k_{4,i} = \mathcal{K}_i[a^{(4)}, \pi_a^{(4)}, \{f_j^{(4)}\}, \{\pi_j^{(4)}\}], & k_{4,a} = \mathcal{K}_a[a^{(4)}, \bar{K}^{(4)}, \bar{G}^{(4)}, \bar{V}^{(4)}], \end{array} \right\} \\ & \Rightarrow \begin{cases} \Delta_0^+ f_i(\mathbf{n}, n_0) &= \pi_i(\mathbf{n}, n_0) + \frac{1}{6} (k_{1,i} + k_{2,i} + k_{3,i}) \delta\eta, \\ \Delta_0^+ a(n_0) &= \pi_a(n_0) + \frac{1}{6} (k_{1,a} + k_{2,a} + k_{3,a}) \delta\eta, \\ \Delta_0^+ \pi_i(\mathbf{n}, n_0) &= \frac{1}{6} (k_{1,i} + 2k_{2,i} + 2k_{3,i} + k_{4,i}), \\ \Delta_0^+ \pi_a(n_0) &= \frac{1}{6} (k_{1,a} + 2k_{2,a} + 2k_{3,a} + k_{4,a}). \end{cases} \quad (151) \end{aligned}$$

3.4 Higher-order integrators

Here we show the construction of higher-order integrators with accuracy $\mathcal{O}(\delta t^4)$, $\mathcal{O}(\delta t^6)$, $\mathcal{O}(\delta t^8)$ and even $\mathcal{O}(\delta t^{10})$, based on the use of $\mathcal{O}(\delta t^2)$ staggered/synchronous leapfrog algorithms as building blocks, or on generalizing the previous explicit Runge-Kutta equations into an implicit problem.

3.4.1 Yoshida method: recursive Verlet integration

The $\mathcal{O}(\delta t^2)$ Verlet integration methods, introduced in Section 3.3.2 to solve the problem $\ddot{x}(t) = \mathcal{K}[x(t)]$ with initial conditions $x(t_0) = x_0$, $\dot{x}(t_0) = \pi_0$, can be used recursively as building blocks to conveniently construct integrators of higher (even) order $\mathcal{O}(\delta t^n)$. The idea is to decompose appropriately a single time step δt into s sub-steps $\delta t_i = w_i \delta t$ (with $\sum_{i=1}^s w_i = 1$), in such a way that the errors of the intermediate steps cancel up to order n . In practice, the only thing that has to be done is to iterate s -times the Verlet algorithm (118) or (121), using each time the appropriate δt_i sub-step. For example, using (118) as the building block, one full step δt of the algorithm must be divided in the sum of different δt_i 's as follows,

$$\begin{cases} t^{(0)} = t_n \\ \pi^{(0)} \equiv \pi_n \\ x^{(0)} \equiv x_n \end{cases} \Rightarrow \left\{ \begin{array}{l} \pi_{1/2}^{(i)} = \pi^{(i-1)} + \omega_i \frac{\delta t}{2} \mathcal{K}[x^{(i-1)}] \\ x^{(i)} = x^{(i-1)} + \pi_{1/2}^{(i)} \omega_i \delta t \\ \pi^{(i)} = \pi_{1/2}^{(i)} + \omega_i \frac{\delta t}{2} \mathcal{K}[x^{(i)}] \end{array} \right\}_{i=1, \dots, s} \Rightarrow \begin{cases} t_{n+1} = t_n + \delta t \\ \pi_{n+1} \equiv \pi^{(s)} \\ x_{n+1} \equiv x^{(s)}. \end{cases}$$

For information about how to construct a specific algorithm, i.e. how to find the corresponding weights ω_i , we refer the interested reader to the original paper by Yoshida [268]. Here we simply collect in Table 1 sets of

δt_i 's characterizing algorithms of order $O(\delta t^4)$, $O(\delta t^6)$, $O(\delta t^8)$ and $O(\delta t^{10})$, see [268, 269] for their derivation. We will refer to these algorithms as *VV4*, *VV6*, *VV8* and *VV10*, while we will refer to the standard velocity Verlet building block as *VV2*.

Some comments are, however, in order. First, the number of steps required to reach a given accuracy grows quickly. For example, *VV4* requires only 3 times more operations than *VV2*, while *VV10* requires 31 times more operations than *VV2*. Actually, to go from one algorithm to the next, the number of steps in each iteration is slightly more than doubled every time. This gives a rule of thumb as of when it is beneficial to use the next more accurate algorithm: if in order to reach some target precision, the time step must be decreased by more than a factor two, then we should consider using the next more accurate algorithm.

This said, let us write for completeness how this algorithm reads for our expanding fields, again assuming that a clever choice of *dof* has been made

$$\begin{aligned}
 \left\{ \begin{array}{l} \pi_i^{(0)} \equiv \pi_i(\mathbf{n}, n_0) \\ f_i^{(0)} \equiv f_i(\mathbf{n}, n_0) \\ a^{(0)} \equiv a(n_0) \\ \pi_a^{(0)} \equiv \pi_a(n_0) \end{array} \right. & \Rightarrow \left\{ \begin{array}{l} \pi_{a,1/2}^{(p)} = \pi_a^{(p-1)} + \frac{\omega_p \delta \eta}{2} \mathcal{K}_a \left[a^{(p-1)}, \bar{K}^{(p-1)}, \bar{G}^{(p-1)}, \bar{V}^{(p-1)} \right] \\ \pi_{i,1/2}^{(p)} = \pi_i^{(p-1)} + \frac{\omega_p \delta \eta}{2} \mathcal{K}_i [a^{(p-1)}, f_j^{(p-1)}] \\ a^{(p)} = a^{(p-1)} + \omega_p \delta \eta \pi_{a,1/2}^{(p)} \\ a_{1/2}^{(p)} = \frac{1}{2} (a^{(p)} + a^{(p-1)}) \\ f_i^{(p)} = f_i^{(p-1)} + \omega_p \delta \eta \mathcal{D} \left[a_{1/2}^{(p)}, \pi_{i,1/2}^{(p)} \right] \\ \pi_i^{(p)} = \pi_{i,1/2}^{(p)} + \frac{\omega_p \delta \eta}{2} \mathcal{K}_i [a^{(p)}, f_j^{(p)}] \\ \pi_a^{(p)} = \pi_{a,1/2}^{(p)} + \frac{\omega_p \delta \eta}{2} \mathcal{K}_a \left[a^{(p)}, \bar{K}^{(p)}, \bar{G}^{(p)}, \bar{V}^{(p)} \right] \end{array} \right\}_{p=1, \dots, s} \\
 & \Rightarrow \left\{ \begin{array}{l} \pi_i(\mathbf{n}, n_0 + 1) \equiv \pi_i^{(s)} \\ f_i(\mathbf{n}, n_0 + 1) \equiv f_i^{(s)} \\ a(n_0 + 1) \equiv a^{(s)} \\ b(n_0 + 1) \equiv b^{(s)} \end{array} \right. \quad (152)
 \end{aligned}$$

where $a_{1/2}^{(p)}$, $\pi_{i,1/2}^{(p)}$, $\pi_{a,1/2}^{(p)}$ are intermediates values and we explicitly wrote down the temporal derivatives. Note also that the same can be done using position-Verlet as a building block.

3.4.2 Gauss-Legendre methods: Implicit Runge-Kutta

The Runge-Kutta methods *RK2* and *RK4* (of order $\mathcal{O}(\delta t^2)$ and $\mathcal{O}(\delta t^4)$ respectively), that we introduced in Section 3.3.3 to solve the problem $\ddot{x}(t) = \mathcal{K}[x(t), \dot{x}(t)]$ with initial condition $x(t_0) = x_0$ and $\dot{x}(t_0) = \pi_0$, are actually only representative examples of a whole family of Runge-Kutta methods. Runge-Kutta methods are characterized in general by a one-step δt iteration algorithm of the form

$$x_{n+1} = x_n + \delta t \sum_{i=1}^s c_i \pi^{(i)}, \quad \pi_{n+1} = \pi_n + \delta t \sum_{i=1}^s c_i k^{(i)}, \quad (153)$$

with

$$x^{(i)} \equiv x_n + \delta t \sum_{j=1}^s b_{ij} \pi^{(j)}, \quad \pi^{(i)} \equiv \pi_n + \delta t \sum_{j=1}^s b_{ij} k^{(j)}, \quad k^{(i)} \equiv \mathcal{K}[x^{(i)}, \pi^{(i)}], \quad (154)$$

where a single step is subdivided in s sub-intervals, $\delta t = \sum_{i=1}^s \delta t_i$, with $\delta t_i \equiv c_i \delta t$, $c_i < 1$, and $\sum_{i=1}^s c_i = 1$. Schematically, each RK algorithm can be represented by a *Butcher tableau* as follows

$$\begin{array}{c|cccc}
 b_{11} & b_{12} & \cdots & b_{1s} \\
 b_{21} & b_{22} & \cdots & b_{2s} \\
 \vdots & \vdots & \cdots & \vdots \\
 b_{s1} & b_{s2} & \cdots & b_{ss} \\
 \hline
 c_1 & c_2 & \cdots & c_s
 \end{array} . \quad (155)$$

Nname	Order	$w_i = \frac{\delta t_i}{\delta t}$	q
VV4	$O(\delta t^4)$	$w_1 = w_3 = 1.351207191959657771818$ $w_2 = -1.702414403875838200264$	3
VV6	$O(\delta t^6)$	$w_1 = w_7 = 0.78451361047755726382$ $w_2 = w_6 = 0.23557321335935813368$ $w_3 = w_5 = -1.1776799841788710069$ $w_4 = 1.3151863206839112189$	7
VV8	$O(\delta t^8)$	$w_1 = w_{15} = 0.74167036435061295345$ $w_2 = w_{14} = -0.40910082580003159400$ $w_3 = w_{13} = 0.19075471029623837995$ $w_4 = w_{12} = -0.57386247111608226666$ $w_5 = w_{11} = 0.29906418130365592384$ $w_6 = w_{10} = 0.33462491824529818378$ $w_7 = w_9 = 0.31529309239676659663$ $w_8 = -0.79688793935291635402$	15
VV10	$O(\delta t^{10})$	$w_1 = w_{31} = -0.48159895600253002870$ $w_2 = w_{30} = 0.0036303931544595926879$ $w_3 = w_{29} = 0.50180317558723140279$ $w_4 = w_{28} = 0.28298402624506254868$ $w_5 = w_{27} = 0.80702967895372223806$ $w_6 = w_{26} = -0.026090580538592205447$ $w_7 = w_{25} = -0.87286590146318071547$ $w_8 = w_{24} = -0.52373568062510581643$ $w_9 = w_{23} = 0.44521844299952789252$ $w_{10} = w_{22} = 0.18612289547097907887$ $w_{11} = w_{21} = 0.23137327866438360633$ $w_{12} = w_{20} = -0.52191036590418628905$ $w_{13} = w_{19} = 0.74866113714499296793$ $w_{14} = w_{18} = 0.066736511890604057532$ $w_{15} = w_{17} = -0.80360324375670830316$ $w_{16} = 0.91249037635867994571$	31

Table 1: Time steps required to construct higher-order velocity Verlet algorithms. A given algorithm requires q iterations. The coefficients are symmetric, in each case, with respect to the intermediate ω_i parameter. Note that we reported here only the algorithms of a given order with the minimal number of steps. For others, see Ref. [269].

The *RK2* and *RK4* algorithms are represented by the following tables,

$$\begin{array}{c}
 \text{RK2 : } \begin{array}{|c|c|} \hline 0 & 0 \\ \hline 1 & 0 \\ \hline 1/2 & 1/2 \\ \hline \end{array} \quad , \quad \text{RK4 : } \begin{array}{|c|c|c|c|} \hline 0 & 0 & 0 & 0 \\ \hline 1/2 & 0 & 0 & 0 \\ \hline 0 & 1/2 & 0 & 0 \\ \hline 0 & 0 & 1 & 0 \\ \hline 1/6 & 1/3 & 1/3 & 1/6 \\ \hline \end{array} .
 \end{array} \tag{156}$$

These correspond to *explicit RK algorithms*, as they are characterized by $b_{ij} = 0 \ \forall \ i \leq j$, which allows to compute the successive $k_i, i = 1, 2, \dots, s$, as an explicit function of the previous ones. In any other circumstance, Eq. (153) corresponds to an *implicit RK algorithm*, as the k'_i s depend on the previous and following ones (even on themselves) through the implicit relations in Eq. (154). In a seminal paper [270], J. C. Butcher demonstrated that *i*) the coefficients c_i and b_{ij} in Eqs. (153) and (154) are unique (see appendix of [270]), and *ii*) the accuracy of the numerical solution of a method with s sub-steps is of order $O(\delta t^{2s})$. Furthermore, Butcher also determined the corresponding tableaux for the implicit *RK* methods with $s = 2, 3, 4$ and 5 sub-steps, which we reproduce in Table 2.

s = 2:	$\begin{array}{ c c } \hline \frac{1}{4} & \frac{1}{4} - \frac{\sqrt{3}}{6} \\ \hline \frac{1}{4} + \frac{\sqrt{3}}{6} & \frac{1}{4} \\ \hline \frac{1}{2} & \frac{1}{2} \\ \hline \end{array}$
s = 3:	$\begin{array}{ c c c } \hline \frac{5}{36} & \frac{2}{9} - \frac{\sqrt{15}}{15} & \frac{5}{36} - \frac{\sqrt{15}}{30} \\ \hline \frac{5}{36} + \frac{\sqrt{15}}{24} & \frac{2}{9} & \frac{5}{36} - \frac{\sqrt{15}}{24} \\ \hline \frac{5}{36} + \frac{\sqrt{15}}{30} & \frac{2}{9} + \frac{\sqrt{15}}{15} & \frac{5}{36} \\ \hline \frac{5}{18} & \frac{4}{9} & \frac{5}{18} \\ \hline \end{array}$
s = 4:	$\begin{array}{ c c c c } \hline \omega_1^- & \omega_1^+ - \omega_3^+ + \omega_4^- & \omega_1^+ - \omega_3^+ - \omega_4^- & \omega_1^- - \omega_5^+ \\ \hline \omega_1^- - \omega_3^- + \omega_4^+ & \omega_1^+ & \omega_1^+ - \omega_5^- & \omega_1^- - \omega_3^- - \omega_4^+ \\ \hline \omega_1^- + \omega_3^- + \omega_4^+ & \omega_1^+ + \omega_5^- & \omega_1^+ & \omega_1^- + \omega_3^- - \omega_4^+ \\ \hline \omega_1^- + \omega_5^+ & \omega_1^+ + \omega_3^+ + \omega_4^- & \omega_1^+ + \omega_3^+ - \omega_4^- & \omega_1^- \\ \hline 2\omega_1^- & 2\omega_1^+ & 2\omega_1^+ & 2\omega_1^- \\ \hline \left[\begin{array}{l} \omega_1^\pm = \frac{1}{8} \pm \frac{\sqrt{30}}{144}, \quad \omega_2^\pm = \frac{1}{2} \sqrt{\frac{15 \pm 2\sqrt{30}}{35}}, \quad \omega_3^\pm = \omega_2^\pm \left(\frac{1}{6} \pm \frac{\sqrt{30}}{24} \right), \\ \omega_4^\pm = \omega_2^\pm \left(\frac{1}{21} \pm \frac{5\sqrt{30}}{168} \right), \quad \omega_5^\pm = \omega_2^\pm - 2\omega_3^\pm, \end{array} \right] \\ \hline \end{array}$
s = 5:	$\begin{array}{ c c c c c } \hline \omega_1^- & \omega_1^+ - \omega_3^+ + \omega_4^- & \frac{32}{225} - \omega_5^- & \omega_1^+ - \omega_3^+ - \omega_4^- & \omega_1^- - \omega_6^+ \\ \hline \omega_1^- - \omega_3^- + \omega_4^+ & \omega_1^+ & \frac{32}{225} - \omega_5^+ & \omega_1^+ - \omega_6^- & \omega_1^- - \omega_3^- - \omega_4^+ \\ \hline \omega_1^- + \omega_7^+ & \omega_1^+ + \omega_7^- & \frac{32}{225} & \omega_1^+ - \omega_7^- & \omega_1^- - \omega_7^+ \\ \hline \omega_1^- + \omega_3^- + \omega_4^+ & \omega_1^+ + \omega_6^- & \frac{32}{225} + \omega_5^- & \omega_1^+ & \omega_1^- + \omega_3^- - \omega_4^+ \\ \hline \omega_1^- + \omega_6^+ & \omega_1^+ + \omega_3^+ + \omega_4^- & \frac{32}{225} - \omega_5^+ & \omega_1^+ + \omega_3^+ - \omega_4^- & \omega_1^- \\ \hline 2\omega_1^- & 2\omega_1^+ & \frac{64}{225} & 2\omega_1^+ & 2\omega_1^- \\ \hline \left[\begin{array}{l} \omega_1^\pm = \frac{322 \pm 13\sqrt{70}}{3600}, \quad \omega_2^\pm = \frac{1}{2} \sqrt{\frac{32 \pm 2\sqrt{70}}{63}}, \quad \omega_3^\pm = \omega_2^\pm \left(\frac{452 \pm 59\sqrt{70}}{3240} \right), \quad \omega_4^\pm = \omega_2^\pm \left(\frac{64 \pm 11\sqrt{70}}{1080} \right), \\ \omega_5^\pm = 8\omega_2^\pm \left(\frac{23 \pm \sqrt{70}}{405} \right), \quad \omega_6^\pm = \omega_2^\pm - 2\omega_3^\pm - \omega_5^\pm, \quad \omega_7^\pm = \omega_2^\pm \left(\frac{308 \pm 23\sqrt{70}}{960} \right), \end{array} \right] \\ \hline \end{array}$

Table 2: *Butcher tableaux* for the implicit RK methods with s sub-intervals and accuracy $\mathcal{O}(\delta t^{2s})$.

Adapting the implicit *RK* methods to the field theory of our interest, we obtain

$$\left. \begin{array}{l} \pi_i^{(l)} \equiv \pi_i(\mathbf{n}, n_0) + \delta\eta \sum_{m=1}^s b_{lm} k_i^{(m)}, \\ \pi_a^{(l)} \equiv \pi_a(n_0) + \delta\eta \sum_{m=1}^s b_{lm} k_a^{(m)}, \\ f_i^{(l)} \equiv f_i(\mathbf{n}, n_0) + \delta\eta \sum_{m=1}^s b_{lm} \pi_i^{(m)}, \\ a^{(l)} \equiv a(n_0) + \delta\eta \sum_{m=1}^s b_{lm} \pi_a^{(m)}, \\ k_i^{(l)} \equiv \mathcal{K}_i[a^{(l)}, \pi_a^{(l)}, \{f_j^{(l)}\}, \{\pi_j^{(l)}\}], \\ k_a^{(l)} \equiv \mathcal{K}_a[a^{(l)}, \bar{K}^{(l)}, \bar{G}^{(l)}, \bar{V}^{(l)}], \end{array} \right\} \Rightarrow \left\{ \begin{array}{l} \Delta_0^+ f_i(\mathbf{n}, n_0) = \sum_{m=1}^s c_m \pi_i^{(m)}, \\ \Delta_0^+ a(n_0) = \sum_{m=1}^s c_m \pi_a^{(m)}, \\ \Delta_0^+ \pi_i(\mathbf{n}, n_0) = \sum_{m=1}^s c_m k_i^{(m)}, \\ \Delta_0^+ \pi_a(n_0) = \sum_{m=1}^s c_m k_a^{(m)}, \end{array} \right. \quad (157)$$

3.5 Integrator properties

Finally, before we move into the discussion of applications of standard algorithms into our interactive field theories, let us mention the list of desired properties that we may want to demand in order to have a good numerical integrator:

- *Time reversal.* Dynamical processes are time-reversible if their EOM are invariant under a change in the sign of the time variable. Since this is an exact symmetry of the continuum EOM, it is desirable that a numerical approximation respects the same property. An evolution algorithm for discrete EOM respects time reversibility if we can integrate forward p steps, and then reverse the direction of integration and integrate backwards p steps, to arrive exactly at the original starting initial condition.
- *Symplectic nature.* Dynamical processes driven by conservative forces (i.e. from kernels that do not depend on conjugate momenta or on any time-dependent external function) respect the *Liouville's theorem*; the infinitesimal phase-space area per degree of freedom is preserved as the system evolves. As this area-preserving property is an exact feature of the continuum EOM which we want to solve, it is desirable that a numerical integrator respects such a conservation law. Numerical schemes that do so are referred to as *symplectic*. The relevance of having a symplectic integrator is that they possess a great stability: since the phase-space area is preserved during the evolution, there cannot be situations where the field amplitudes or their conjugate momenta (and hence their energy) increase without bound, because this would expand the phase-space area. Symplectic integrators offer therefore numerical conservation of energy⁷ to a good degree, which improves the higher the accuracy $\mathcal{O}(\delta t^p)$ of the integrator itself.
- *Integration accuracy.* Depending on the nature of a given numerical integrator method, we may obtain an accuracy in the integrated field amplitudes and conjugate momenta of the order $\mathcal{O}(\delta t^p)$, typically with $p = 2, 4, 6, 8$ or even 10. Our default algorithms have always an accuracy $\mathcal{O}(\delta t^2)$. However, basic $\mathcal{O}(\delta t^2)$ integrators can be converted into higher-order integrators using techniques due to *Haruo Yoshida*. Essentially, by applying the basic algorithm over a number of adjusted different timesteps chosen so that the errors cancel, far higher-order integrators can be obtained. For symplectic integrators this is particularly interesting, as the degree of conservation of energy (Hubble constraint for expanding backgrounds) will increase significantly as we improve the integrator accuracy.
- *Efficiency.* We obviously want to make our numerical integration as fast as possible, so if we need to choose between two integration methods with the same accuracy $\mathcal{O}(\delta t^p)$ but different levels of energy conservation, we might still prefer the faster integrator even if it has worse energy conservation (as long as it can be confronted against the outcome from other integrators with better energy conservation).

4 Lattice formulation of interacting scalar fields

4.1 Continuum formulation and natural variables

Let us consider a set of interacting real scalar fields $\{\phi_a\}$ with canonically normalized kinetic terms. If they live in a FLRW background $g_{\mu\nu} = \text{diag}(-a^{2\alpha}, a^2, a^2, a^2)$, with line element $ds^2 = -a^{2\alpha}\delta\eta^2 + a^2(\eta)d\vec{x}^2$ and α -time η , their action can be written like

$$S = - \int d^4x \sqrt{-g} \left(\frac{1}{2} \partial_\mu \phi_b \partial^\mu \phi_b + V(\{\phi_c\}) \right) = \left(\frac{f_*}{\omega_*} \right)^2 \tilde{S}, \quad (158)$$

with

$$\tilde{S} = \int d^3\tilde{x} d\tilde{\eta} \left\{ \frac{1}{2} a^{3-\alpha} \sum_b \tilde{\phi}_b'^2 - \frac{1}{2} a^{1+\alpha} \sum_{b,k} (\tilde{\nabla}_k \tilde{\phi}_b)^2 - a^{3+\alpha} \tilde{V}(\{\tilde{\phi}_c\}) \right\}, \quad (159)$$

the action expressed in the dimensionless variables

$$\tilde{\phi}_a \equiv \frac{\phi_a}{f_*}, \quad \delta\tilde{\eta} \equiv a^{-\alpha} \omega_* dt, \quad d\tilde{x}^i \equiv \omega_* dx^i, \quad (160)$$

⁷In the case of scenarios with an expanding background, by conservation of energy we actually mean the preservation of the Hubble constraint $3m_p^2 H^2 = \rho$.

where $' \equiv d/d\tilde{\tau}$ and $\tilde{\nabla}_i \equiv \partial/\partial\tilde{x}^i$, and where a dimensionless potential has been introduced as

$$\tilde{V}(\{\tilde{\phi}_c\}) \equiv \frac{1}{f_*^2 \omega_*^2} V(\{\phi_c\}) \Big|_{\phi_c = f_* \tilde{\phi}_c}. \quad (161)$$

The EOM in the dimensionless variables follow immediately from varying the action \tilde{S} ,

$$\tilde{\phi}_a'' - a^{-2(1-\alpha)} \tilde{\nabla}^2 \tilde{\phi}_a + (3-\alpha) \frac{a'}{a} \tilde{\phi}_a' + a^{2\alpha} \tilde{V}_{,\tilde{\phi}_a} = 0. \quad (162)$$

The expansion of the universe, on the other hand, is dictated by the Friedmann equations, sourced by the volume averaged energy and pressure densities $\langle \rho_\phi \rangle$, $\langle p_\phi \rangle$ of the fields. Writing the relevant part of Eqs. (51), (52) in program variables (160), we have

$$a'' = a^{2\alpha+1} \left(\frac{f_*}{m_p} \right)^2 \frac{1}{6} [(2\alpha-1)\langle \tilde{\rho}_\phi \rangle - 3\langle \tilde{p}_\phi \rangle], \quad a'^2 = a^{2\alpha+2} \left(\frac{f_*}{m_p} \right)^2 \frac{1}{3} \langle \tilde{\rho}_\phi \rangle, \quad (163)$$

with *program energy* and *pressure densities* defined as

$$\tilde{\rho}_\phi \equiv \frac{\rho}{f_*^2 \omega_*^2} = \tilde{K}_\phi + \tilde{G}_\phi + \tilde{V}, \quad ; \quad \tilde{p}_\phi \equiv \frac{p}{f_*^2 \omega_*^2} = \tilde{K}_\phi - \frac{1}{3} \tilde{G}_\phi - \tilde{V}, \quad (164)$$

where

$$\tilde{K}_\phi = \frac{1}{2a^{2\alpha}} \sum_i (\tilde{\phi}_i')^2, \quad \tilde{G}_\phi = \frac{1}{2a^2} \sum_{i,k} (\tilde{\nabla}_k \tilde{\phi}_i)^2. \quad (165)$$

As in reality we need the volume averages $\langle \dots \rangle$ of expressions (165), we define for convenience

$$E_K \equiv \frac{1}{2a^{2\alpha}} \sum_i \langle (\tilde{\phi}_i')^2 \rangle, \quad E_G \equiv \frac{1}{2a^2} \sum_{i,k} \langle (\tilde{\nabla}_k \tilde{\phi}_i)^2 \rangle, \quad E_V \equiv \langle \tilde{V}(\{\tilde{\phi}_j\}) \rangle, \quad (166)$$

so that the Friedmann equations read

$$\left(\frac{a'}{a} \right)^2 = \frac{a^{2\alpha}}{3} \left(\frac{f_*}{m_p} \right)^2 [E_K + E_G + E_V], \quad (167)$$

$$\frac{a''}{a} = \frac{a^{2\alpha}}{3} \left(\frac{f_*}{m_p} \right)^2 [(\alpha-2)E_K + \alpha E_G + (\alpha+1)E_V]. \quad (168)$$

If on the contrary the expansion of the universe is sourced by an external fluid, say with constant *barotropic* equation of state $w \equiv \langle p \rangle / \langle \rho \rangle$, then we obtain the scale factor simply from the analytical expression

$$a(\tilde{\eta}) = a_0 \left(1 + \frac{1}{p} \tilde{\mathcal{H}}_0 (\tilde{\eta} - \tilde{\eta}_0) \right)^p, \quad \text{with} \quad p = \frac{2}{3(1+w) - 2\alpha}, \quad (169)$$

where we fixed the initial conditions at an initial time $\tilde{\eta}_0$ ($= 0$, typically) to $a_0 = a(\tilde{\eta}_0)$ and $\tilde{\mathcal{H}}_0 \equiv \tilde{\mathcal{H}}(\tilde{\eta}_0)$, and introduced a dimensionless *program Hubble rate* $\tilde{\mathcal{H}} = \frac{a'}{a \omega_*}$, with $H \equiv \dot{a}/a$ the physical Hubble parameter.

Program variables –. We will refer to the dimensionless field and space-time variables in Eq. (160) as the *lattice* or *program variables*, and to the dimensionless potential in Eq. (161) as the *lattice* or *program potential*⁸. The values of α , f_* and ω_* can be chosen, in principle, arbitrarily. However, certain choices can be more convenient than others, depending on the form of the potential V . First, let us consider the choice of α . In principle, this could be chosen at will: we could take $\alpha = 0$ if we wanted to solve our dynamics in cosmic time, whereas we could choose $\alpha = 1$ if we wanted to solve it in conformal time (up to dimensionful constant factors). However, there are many situations in which an oscillatory field dominates the energy budget of the system for a long time, with a time-dependent oscillation period $T_{\text{osc}}(t)$. As the integration techniques introduced in the previous sections assume a constant time step, we would not be able to resolve

⁸We will also define dimensionless *program variables* for the charged scalars and gauge fields in Eqs. (277) and (360).

later oscillations of the field with the same accuracy as early ones. This could cause stability problems in the simulation at late times, if the oscillation period were to decrease with time. Therefore, if we were in such a situation, it would be extremely convenient to choose a value of α that makes the oscillation period constant in the new α -time variable. In Section 8 we show an example of this in the context of a scalar field oscillating around the minimum of a monomial potential.

Let us now consider f_* . For this, let us imagine a scenario in which one scalar field (say ϕ) has initially a homogeneous configuration with a certain initial amplitude Φ_* . A natural choice would be to fix the dimensionful normalization constant as $f_* = \Phi_*$, so that as long as that field dominates the energy budget during the dynamics, its normalized amplitude $\tilde{\phi}$ will be of order unity (modulo red-shifting dilution factors due to the expansion of the universe). This is often the case in models with parametric resonance, such as the preheating scenario presented in Section 8. If on the contrary, relevant field(s) in the dynamics start with vanishing (or small) amplitude but acquire a vacuum expectation value $\langle\phi\rangle = v$ later on, it might be convenient to take $f_* = v$. This will be the case e.g. in models with spontaneous symmetry breaking, like in phase transitions and cosmic defect formation. Finally, let us consider ω_* . If the dominant scalar field of the system oscillates say with a frequency $\Omega_{\text{osc}}(\eta)$ (possibly time-dependent), it can be convenient to take, for instance, $\omega_* = \Omega_{\text{osc}}(\eta_*)$, at the time $\eta = \eta_*$ of onset of field oscillations. However, if the time scale $\Delta\eta_*$ of excitation of other fields is rather the relevant time scale in the problem, it might be more convenient to choose ω_* of the order of $1/\Delta\eta_*$. Another possibility would be to simply set $f_* = \omega_*$, so we prevent ratios f_*/ω_* (naturally appearing e.g. in the initial condition of scalar field fluctuations) to become tiny or extremely large, see Section 7.

In summary, if the choice of α , f_* and ω_* is made judiciously, it will lead to order unity field amplitudes and time scales, in the naturally dimensionless program variables. This would achieve a twofold objective. first, a better handle of the program variables in the computer, as order unity numbers are more convenient to deal with from a computational point of view. And second, an easier and more transparent conversion of the dimensionless computer program variables into physical mass/time scales characteristic of each given scenario.

From now on, we assume that independently of the scenario we are dealing with, a convenient choice of (α, f_*, ω_*) has been made. In order to solve the dynamics of the interacting scalar fields on a computer, we need now to obtain some discretized version of the continuum EOM (162) expressed in the natural variables (160), (161). We need to do two things: first, to substitute somehow the time and spatial continuum derivatives by lattice operators mimicking such continuum differential operations up to some order $\mathcal{O}(\delta x^\mu)$; and second, to solve the resulting discrete lattice EOM with some algorithms. Our toolkit to address these two aspects was provided in Section 3, where we introduced both lattice differential operators and evolution algorithms. Armed with such toolkit, we have essentially two options:

1) *Lattice action approach.* This is based on discretizing the continuum action, so that it is substituted by a lattice version. Varying such lattice action with respect to the lattice field *dof*, leads to lattice EOM enjoying whichever symmetry the lattice action enjoyed in first place. Constraint equations (expected as a consequence of the symmetries) are then automatically satisfied at the lattice level.

2) *EOM discretization approach.* This is based on discretizing the continuum EOM directly. Here we simply substitute the partial derivatives involved in certain terms of the continuum EOM by appropriate lattice operators mimicking those continuum derivatives. This method allows to envisage lattice EOM adapted to essentially any evolution algorithm we wish to use.

Either approach 1) or 2) may have its advantages and disadvantages depending on the model and circumstances. Whereas for EOM in flat space-time the two approaches are essentially very similar, this might not be case in an expanding universe, particularly in the presence of gauge fields. As for the time being we only deal with scalar sectors in expanding backgrounds in this section, we will simply present next the series of algorithms that one can envisage to engineer lattice EOM that can be solved with the evolution algorithms we introduced in Section 3.

4.2 Lattice formulation of interacting scalar fields: $\mathcal{O}(dt^2)$ accuracy methods

4.2.1 Staggered leapfrog from a lattice action

A lattice version of action (159) can be written using e.g. forward derivatives [c.f. Eq. (67)] for the time derivatives and the spatial gradients. Promoting integrals into discrete sums $\int d\eta(\dots) \equiv \delta\eta \sum_{n_0}(\dots)$, $\int dx^3(\dots) \equiv \delta x^3 \sum_{\mathbf{n}}(\dots)$, we obtain

$$\tilde{S}_L = \delta\tilde{\eta}\delta\tilde{x}^3 \sum_{n_0} \sum_{\mathbf{n}} \left\{ \frac{1}{2} a_{+0/2}^{3-\alpha} \sum_b (\tilde{\Delta}_0^+ \tilde{\phi}^b)^2 - \frac{1}{2} a^{1+\alpha} \sum_{b,k} (\tilde{\Delta}_k^+ \tilde{\phi}^b)^2 - a^{3+\alpha} \tilde{V}(\{\tilde{\phi}_c\}) \right\}. \quad (170)$$

Note that we have not determined yet at what times the scale factor lives in, and we have rather referred to a scale factor at integer and half-integers times, whenever appropriate. The logic to specify where the scale factor lives in each term of the action, is to consider the time the operator it is multiplied to lives in. Thus, as $(\tilde{\Delta}_0^+ \tilde{\phi}^{(a)})^2$ lives at $n_0 + 1/2$, we write its pre-factor as $a_{+0/2}^{3-\alpha}$, whereas $(\tilde{\Delta}_k^+ \tilde{\phi}^{(a)})^2$ lives at n_0 , so we write its pre-factor as $a^{1+\alpha}$, etc. Varying this action with respect each field dof , $\delta_{\phi_a} S_L = 0$, leads to the discrete EOM

$$\tilde{\Delta}_0^- [a_{+0/2}^{3-\alpha} \tilde{\Delta}_0^+ \tilde{\phi}_b] = a^{1+\alpha} \sum_k \tilde{\Delta}_k^- \tilde{\Delta}_k^+ \tilde{\phi}_b - a^{3+\alpha} \tilde{V}_{,\tilde{\phi}_c}, \quad b = 1, 2, \dots, N_s \quad (171)$$

with N_s the total number of scalar fields.

Let us now deal with the expansion of the universe. We need to express the Friedmann equations as a function of program expressions for the volume averaged field energy and pressure densities $\langle \rho_\phi \rangle$, $\langle p_\phi \rangle$. We introduce first a discretized version of E_K, E_G and E_V , c.f. Eq. (166),

$$E_K \equiv \frac{1}{2a_{+0/2}^{2\alpha}} \sum_a \langle (\tilde{\Delta}_0^+ \tilde{\phi}_a)^2 \rangle, \quad E_G \equiv \frac{1}{2a^2} \sum_{a,k} \langle (\tilde{\Delta}_k^+ \tilde{\phi}_a)^2 \rangle, \quad E_V \equiv \langle \tilde{V}(\{\tilde{\phi}_c\}) \rangle \quad (172)$$

with E_G and E_V naturally living at integer times n_0 , and E_K at semi-integer times $n_0 + 1/2$. We need to decide now whether we consider a scale factor living 'naturally' at integer or semi-integer times. If we consider that a lives at semi-integer times, then it is natural to define the operator $b \equiv \tilde{\Delta}_0^+ a_{-0/2}$ living at integer times, and hence identify the first and second derivative [via the Friedmann equations in (167), (168)] of the scale factor as

$$a' \rightarrow \tilde{\Delta}_0^+ a_{-0/2} \equiv b, \quad (173)$$

$$a'' \rightarrow \tilde{\Delta}_0^+ b = \frac{1}{3} \left(\frac{f_*}{m_p} \right)^2 a_{+0/2}^{1+2\alpha} [(\alpha - 2)E_K + \alpha \overline{E_G} + (\alpha + 1)\overline{E_V}]. \quad (174)$$

with $\overline{E_G} \equiv (E_G + E_{G,+0/2})/2$ and $\overline{E_V} \equiv (E_V + E_{V,+0/2})/2$, so that they live at semi-integer times, like the scale factor and E_K . Alternatively, if we think of the scale factor living at integer times, we can define the operator $b_{+0/2} \equiv (\tilde{\Delta}_0^+ a)$ living at semi-integer times, and identify the first and second derivative of the scale factor as

$$a' \rightarrow \tilde{\Delta}_0^+ a \equiv b_{+0/2}, \quad (175)$$

$$a'' \rightarrow \tilde{\Delta}_0^+ b_{+0/2} = \frac{1}{6} \left(\frac{f_*}{m_p} \right)^2 a^{1+2\alpha} [(\alpha - 2)\overline{E_K} + \alpha E_G + (\alpha + 1)E_V], \quad (176)$$

with $\overline{E_K} \equiv (E_{K,-0/2} + E_{K,+0/2})/2$ living at integer times, as much as a, E_G and E_V .

From a practical or computational point of view, choosing a scale factor living at integer or semi-integer times, is actually irrelevant. If we choose that it lives at e.g. integer times, we will always be forced to obtain it also, within each iteration, at semi-integer times, from the semi-sum of its two values at the closest integer times. And vice versa. In order to provide an iterative scheme, we still need to decide on the *conjugate momenta* $\tilde{\pi}_{+0/2}^{(a)}$, which will be implemented through forward derivative operators. The question is whether

to choose that $\tilde{\pi}_{+0/2}^{(a)}$ represents the time-derivative of each field, i.e. ϕ'_a , or rather represents $a^{3-\alpha}\phi'_a$, as the EOM actually naturally suggest. It turns out that depending on this choice the integrator will be accurate to order $\mathcal{O}(\delta\eta)$ or $\mathcal{O}(\delta\eta^2)$. All together, we can obtain the following implementations of a staggered leapfrog algorithm (here *IC* stands for *Initial Condition*, and *HC* for *Hubble Constraint*):

I) *Iterative scheme for $\tilde{\pi}_{+0/2}^{(a)} \equiv \tilde{\Delta}_0^+ \tilde{\phi}_a$ and scale factor $a(n_0 + 1/2)$:*

$$IC : \quad \{\tilde{\phi}_a, b\} \text{ at } \tilde{\eta}_0, \quad \{\tilde{\pi}_{-0/2}^{(a)}, a_{-0/2}\} \text{ at } \tilde{\eta}_0 - 0.5\delta\tilde{\eta} \quad (177)$$

$$a_{+0/2} = a_{-0/2} + b\delta\tilde{\eta} \quad \longrightarrow \quad a \equiv (a_{+0/2} + a_{-0/2})/2 \quad (178)$$

$$\tilde{\pi}_{+0/2}^{(a)} = \left(\frac{a_{-0/2}}{a_{+0/2}}\right)^{3-\alpha} \tilde{\pi}_{-0/2}^{(a)} + a_{+0/2}^{-(3-\alpha)} \left(a^{1+\alpha} \sum_k \tilde{\Delta}_k^- \tilde{\Delta}_k^+ \tilde{\phi}^{(a)} - a^{3+\alpha} \tilde{V}_{\tilde{\phi}^{(a)}} \right) \quad (179)$$

$$\tilde{\phi}_{+0}^{(a)} = \tilde{\phi}^{(a)} + \delta\tilde{\eta} \tilde{\pi}_{+0/2}^{(a)} \quad (180)$$

$$b_{+0} = b + \frac{\delta\tilde{\eta}}{3} \left(\frac{f_*}{m_p}\right)^2 a_{+0/2}^{1+2\alpha} [(\alpha - 2)E_K + \alpha\overline{E_G} + (\alpha + 1)\overline{E_V}], \quad (181)$$

$$HC : \quad b^2 = \frac{1}{3} \left(\frac{f_*}{m_p}\right)^2 a^{2\alpha+1} (\overline{E_K} + E_G + E_V). \quad (182)$$

II) *Iterative scheme for $\tilde{\pi}^{(a)} \equiv \tilde{\Delta}_0^+ \tilde{\phi}_{-0/2}^{(a)}$ and scale factor $a(n_0)$*

$$IC : \quad \{\tilde{a}, \tilde{\pi}^{(a)}\} \text{ at } \tilde{\eta}_0, \quad \{\tilde{\phi}_{-0/2}^{(a)}, b_{-0/2}\} \text{ at } \tilde{\eta}_0 - 0.5\delta\tilde{\eta} \quad (183)$$

$$\tilde{\phi}_{+0/2}^{(a)} = \tilde{\phi}_{-0/2}^{(a)} + \delta\tilde{\eta} \tilde{\pi}^{(a)} \quad (184)$$

$$b_{+0/2} = b_{-0/2} + \frac{\delta\tilde{\eta}}{3} \left(\frac{f_*}{m_p}\right)^2 a^{1+2\alpha} [(\alpha - 2)E_K + \alpha\overline{E_G} + (\alpha + 1)\overline{E_V}], \quad (185)$$

$$a_{+0} = a + b_{+0/2} \delta\tilde{\eta} \quad \longrightarrow \quad a_{+0/2} \equiv (a_0 + a)/2, \quad (186)$$

$$\tilde{\pi}_{+0}^{(a)} = \left(\frac{a}{a_{+0}}\right)^{3-\alpha} \tilde{\pi}^{(a)} + a_{+0}^{-(3-\alpha)} \left(a_{+0/2}^{1+\alpha} \sum_k \tilde{\Delta}_k^- \tilde{\Delta}_k^+ \tilde{\phi}_{+0/2}^{(a)} - a_{+0/2}^{3+\alpha} \tilde{V}_{\tilde{\phi}^{(a)}} \Big|_{+0/2} \right), \quad (187)$$

$$HC : \quad b_{+0/2}^2 = \frac{1}{3} \left(\frac{f_*}{m_p}\right)^2 a_{+0/2}^{2\alpha+1} (\overline{E_K} + E_{G,+0/2} + E_{V,+0/2}), \quad (188)$$

III) *Iterative scheme for $\tilde{\pi}_{+0/2}^{(a)} \equiv a_{+0/2}^{3-\alpha} \tilde{\Delta}_0^+ \tilde{\phi}_a$ and scale factor $a(n_0)$*

$$IC : \quad \{\tilde{\phi}^{(a)}, a, \} \text{ at } \tilde{\eta}_0, \quad \{\tilde{\pi}_{-0/2}^{(a)}, b_{-0/2}\} \text{ at } \tilde{\eta}_0 - 0.5\delta\tilde{\eta} \quad (189)$$

$$\tilde{\pi}_{+0/2}^{(a)} = \tilde{\pi}_{-0/2}^{(a)} + \left(a^{1+\alpha} \sum_k \tilde{\Delta}_k^- \tilde{\Delta}_k^+ \tilde{\phi}^{(a)} - a^{3+\alpha} \tilde{V}_{\tilde{\phi}^{(a)}} \right) \quad (190)$$

$$b_{+0/2} = b_{-0/2} + \frac{\delta\tilde{\eta}}{3} \left(\frac{f_*}{m_p}\right)^2 a^{1+2\alpha} [(\alpha - 2)\overline{E_K} + \alpha E_G + (\alpha + 1)E_V], \quad (191)$$

$$a_{+0} = a + b_{+0/2} \delta\tilde{\eta} \quad \longrightarrow \quad a_{+0/2} \equiv (a_{+0} + a_0)/2, \quad (192)$$

$$\tilde{\phi}_{+0}^{(a)} = \tilde{\phi}^{(a)} + \delta\tilde{\eta} \tilde{\pi}_{+0/2}^{(a)} a_{+0/2}^{-(3-\alpha)}, \quad (193)$$

$$HC : \quad b_{+0/2}^2 = \frac{1}{3} \left(\frac{f_*}{m_p}\right)^2 a_{+0/2}^{2\alpha+1} (E_K + \overline{E_G} + \overline{E_V}), \quad (194)$$

IV) Iterative scheme for $\tilde{\pi}^{(a)} \equiv a^{3-\alpha} \tilde{\Delta}_0^+ \tilde{\phi}_{-0/2}^{(a)}$ and scale factor $a(n_0 + 1/2)$

$$IC : \quad \{\tilde{\pi}^{(a)}, b\} \text{ at } \tilde{\eta}_0, \quad \{\tilde{\phi}_{-0/2}^{(a)}, a_{-0/2}\} \text{ at } \tilde{\eta}_0 - 0.5\delta\tilde{\eta} \quad (195)$$

$$a_{+0/2} = a_{-0/2} + b\delta\tilde{\eta} \longrightarrow a \equiv (a_{+0/2} + a_{-0/2})/2 \quad (196)$$

$$\tilde{\phi}_{+0/2}^{(a)} = \tilde{\phi}_{-0/2}^{(a)} + \delta\tilde{\eta} \tilde{\pi}^{(a)} a^{-(3-\alpha)} \quad (197)$$

$$\tilde{\pi}_{+0}^{(a)} = \tilde{\pi}^{(a)} + a_{+0/2}^{1+\alpha} \sum_k \tilde{\Delta}_k^- \tilde{\Delta}_k^+ \tilde{\phi}_{+0/2}^{(a)} - a_{+0/2}^{3+\alpha} \tilde{V}_{\tilde{\phi}^{(a)}} \Big|_{+0/2} \quad (198)$$

$$b_{+0} = b + \frac{\delta\tilde{\eta}}{3} \left(\frac{f_*}{m_p} \right)^2 a_{+0/2}^{1+2\alpha} \left[(\alpha - 2) \overline{E_K} + \alpha E_{G,+0/2} + (\alpha + 1) E_{V,+0/2} \right], \quad (199)$$

$$HC : \quad b^2 = \frac{1}{3} \left(\frac{f_*}{m_p} \right)^2 a^{2\alpha+1} (E_K + \overline{E_G} + \overline{E_V}). \quad (200)$$

While all these iterative schemes descent from the same action (170), they are truly different algorithms, based on the choice of conjugate momenta and time domain of the scale factor. In fact, iterative schemes *I* and *II*, which are basically very similar as they are based on (discretized versions of) the same choice $\pi_a \equiv \phi'_a$, are only accurate to order $\mathcal{O}(\delta\eta)$. Iterative schemes *III* and *IV*, also very similar to each other as they are based on (discretized versions of) the choice $\pi_a \equiv a^{3-\alpha} \phi'_a$, are however accurate to order $\mathcal{O}(\delta\eta^2)$. This becomes manifest in numerical simulations by monitoring the Hubble constraint $3m_p^2 H^2 = \rho$, which in the case of schemes *I* and *II* is only verified to order $\mathcal{O}(\delta\eta)$ by Eqs. (182), (188), whereas in the schemes *III* and *IV*, Eqs. (194), (200) are verified to order $\mathcal{O}(\delta\eta^2)$. This is a first illustration of the importance of choosing the appropriate conjugate momentum to evolve the equations.

4.2.2 Staggered leapfrog à la LatticeEasy

Alternatively to discretizing action (158), like in (170), one can start from the continuum EOM for scalar fields, Eq. (162), and discretize these equations directly. Considering the EOM of N_s scalar fields canonically normalized [c.f. Eq. (162)],

$$\tilde{\phi}_b'' - a^{-2(1-\alpha)} \tilde{\nabla}^2 \tilde{\phi}_b + (3 - \alpha) \mathcal{H} \tilde{\phi}_b' + a^{2\alpha} \tilde{V}_{\tilde{\phi}_b} = 0, \quad b = 1, 2, \dots, N_s, \quad (201)$$

where $\mathcal{H} \equiv a'/a$, we could attempt to substitute here the continuum derivatives $\tilde{\partial}_\mu$ by finite difference operators $\tilde{\Delta}_\mu^\pm$, and then obtain a discretized version of the EOM. However, we would run immediately into the problem of the friction term $\propto \tilde{\phi}'$, which prevents the iterative scheme to be in the form of a Staggered leapfrog algorithm: namely, the kernel of the conjugate momenta, $\tilde{\pi}_b' = \mathcal{K}_b[\{\tilde{\phi}_c\}, \{\tilde{\pi}_c\}, \dots]$, would depend on the conjugate momenta itself $\tilde{\pi}_b = \tilde{\phi}'$, so $\partial_{\tilde{\pi}_b} \mathcal{K}_b \neq 0$.

It turns out that the problem can be easily avoided, by making a conformal re-definition of the scalar field amplitudes $\tilde{\phi}_b \longrightarrow \tilde{\varphi}_b \equiv a^\beta \tilde{\phi}_b$, so that the EOM become

$$\tilde{\varphi}_b'' + (3 - \alpha - 2\beta) \mathcal{H} \tilde{\varphi}_b' - a^{-2(1-\alpha)} \tilde{\nabla}^2 \tilde{\varphi}_b + a^{2(\alpha+\beta)} \tilde{V}_{\tilde{\varphi}_b} + m^2[\alpha, \beta] \tilde{\varphi}_b = 0, \quad (202)$$

with

$$m^2[\alpha, \beta] \equiv \beta \left((\alpha + \beta - 2) \mathcal{H}^2 - \frac{a''}{a} \right). \quad (203)$$

Choosing $\beta = (3 - \alpha)/2$ leads immediately to the elimination of the friction term, so the EOM can be finally written like

$$\tilde{\varphi}_b'' - a^{-2(1-\alpha)} \tilde{\nabla}^2 \tilde{\varphi}_b + a^{3+\alpha} \tilde{V}_{\tilde{\varphi}_b} + m_\alpha^2 \tilde{\varphi}_b = 0, \quad m_\alpha^2 \equiv \frac{(3 - \alpha)}{2} \left(\frac{(\alpha - 1)}{2} \mathcal{H}^2 - \frac{a''}{a} \right). \quad (204)$$

This corresponds to a set of equations that can be discretized with a staggered leapfrog algorithm simply by choosing $\tilde{\pi}_c \equiv \tilde{\varphi}_c'$, so that the kernel $\tilde{\pi}_c' = \mathcal{K}_c[\dots]$ depends on the field amplitudes but not on the field

momenta, $\partial_{\tilde{\pi}_a} \mathcal{K}_b = 0 \ \forall a, b$. This trick however is not enough by itself, as we still have to deal with the evolution of the scale factor through the Friedmann equations, now incorporating the conformal re-scaling of the field amplitudes. Furthermore, we notice that the new mass term m_β^2 depends actually on \mathcal{H} and a''/a , so in order for the kernel of $\tilde{\pi}_c$ to depend only say on integer times (assuming $\tilde{\pi}_c$'s live at semi-integer times), we need both \mathcal{H} and a''/a to be evaluated at the same integer time. Recalling Eq. (52) for a'' , and denoting the scale factor conjugate momentum as $b \equiv a'$, we observe that $b' = \mathcal{K}_a[a, E_K, E_G, E_V]$ with E_K, E_G and E_V representing the volume averaged kinetic, gradient and potential terms, as contributed by all scalar fields, c.f. Eq. (50), (166). We have therefore, on the one hand, EOM dictating the evolution of the conjugate momenta $\tilde{\pi}'_c$ s via kernels depending on a''/a , and on the other hand, an equation for a''/a depending on the conjugate momenta $\{\tilde{\pi}_c\}$ through the kinetic terms. This prevent us from obtaining an explicit solution. Furthermore, if we substitute the conformal redefinition of the field amplitude in the kinetic terms sourcing a''/a , we obtain that the kernel $b' = \mathcal{K}_a[\dots]$ contains terms $\propto \tilde{\pi}_c^2$, $\propto \mathcal{H}^2 \tilde{\varphi}_c^2$ and $\propto \mathcal{H} \tilde{\varphi}_c \tilde{\pi}_c$, and hence that $\mathcal{K}_a[\dots]$ depends also on \mathcal{H} . We immediately understand that implementing a staggered leapfrog algorithm is still not feasible in the current system of equations, unless we perform some extra trick.

The celebrated package *LatticeEasy* (and for this matter its parallelized version *ClusterEasy*), developed in the 2000's by Gary N. Felder and Igor I. Tkachev, circumvented the previous issue by means of the following trick: the kinetic term K_ϕ in the Friedmann equation $3m_p^2 b' = a^{1+2\alpha}((\alpha-2)E_K + \alpha E_G + (1+\alpha)E_V)$, can be substituted by its expression obtained from the other Friedmann equation $3m_p^2 \mathcal{H}^2 = a^{2\alpha}(E_K + E_G + E_V)$. That is $E_K = 3m_p^2 a^{-2\alpha} \mathcal{H}^2 - E_G - E_V$, and hence $3m_p^2 b' = 3(\alpha-2)m_p^2 a \mathcal{H}^2 + a^{1+2\alpha}(2E_G + 3E_V)$. Choosing that the scale factor lives at integer times, and introducing $b_{+0/2} \equiv \tilde{\Delta}_0^+ a$ and $\tilde{\Delta}_0^- b_{+0/2} \equiv \tilde{\Delta}_0^- \tilde{\Delta}_0^+ a$ for the first and second derivative of the scale factor, the second Friedmann equation can be written as

$$\left(\frac{b_{+0/2} - b_{-0/2}}{\delta\tilde{\eta}} \right) = \frac{(\alpha-2)}{a} \left(\frac{b_{+0/2} + b_{-0/2}}{2} \right)^2 + \frac{1}{3} \left(\frac{f_*}{m_p} \right)^2 a^{1+2\alpha} (2G_\phi + 3V), \quad (205)$$

where we have introduced an averaged Hubble rate as $\overline{\mathcal{H}} \equiv \frac{(b_{+0/2} + b_{-0/2})}{2a}$. As Eq. (205) is simply a quadratic equation for $b_{+0/2}$, we can re-arrange terms to write

$$B_2 b_{+0/2}^2 + B_1 b_{+0/2} + B_0 = 0, \quad \begin{cases} B_2 & \equiv c\delta\tilde{\eta}, & c \equiv \frac{(\alpha-2)}{4a} \\ B_1 & \equiv 2c\delta\tilde{\eta}b_{-0/2} - 1 \\ B_0 & \equiv b_{-0/2}(1 + c\delta\tilde{\eta}b_{-0/2}) + \frac{\delta\tilde{\eta}}{3} \left(\frac{f_*}{m_p} \right)^2 a^{1+2\alpha} (2E_G + 3E_V) \end{cases} \quad (206)$$

so that $b_{+0/2} = (-B_1 \pm \sqrt{B_1^2 - 4B_2 B_0})/(2B_2)$. Only by choosing the negative sign we arrive at the correct limit $b_{+0/2} \rightarrow b_{-0/2}$ when $\delta\tilde{\eta} \rightarrow 0$, so we finally obtain

$$b_{+0/2} = -b_{-0/2} + \frac{1}{2c\delta\tilde{\eta}} \left(1 - \sqrt{(1 - 2c\delta\tilde{\eta}b_{-0/2})^2 - 4c\delta\tilde{\eta}B_0} \right). \quad (207)$$

The Kernel of the second Friedmann equation $a''/a = \mathcal{K}_a[\dots]$ does not depend, in this way, on the field conjugate momenta π_c 's, while at the same time the mass term in the EOM of the $\tilde{\pi}_c$'s, Eq. (204), can now be built from $\overline{\mathcal{H}} \equiv (b_{-0/2} + b_{+0/2})/(2a)$ and $a''/a \equiv (b_{+0/2} - b_{-0/2})/(a\delta\tilde{\eta})$. Hence, a consistent staggered leapfrog algorithm can be put forward [with c, B_0 given in Eq. (206)] as

LatticeEasy staggered leapfrog scheme:

$$IC \quad : \quad \{\tilde{\varphi}_c, a\} \text{ at } \tilde{\eta}_0, \quad \{\tilde{\pi}_{-0/2}^{(c)}, b_{-0/2}\} \text{ at } \tilde{\eta}_0 - 0.5\delta\tilde{\eta} \quad (208)$$

$$b_{+0/2} = -b_{-0/2} + \frac{1}{2c\delta\tilde{\eta}} \left(1 - \sqrt{(1 - 2c\delta\tilde{\eta}b_{-0/2})^2 - 4c\delta\tilde{\eta}B_0} \right) \quad (209)$$

$$\tilde{\pi}_{+0/2}^{(c)} = \tilde{\pi}_{-0/2}^{(c)} + \delta\tilde{\eta} \left(a^{-2(1-\alpha)} \tilde{\nabla}^2 \tilde{\varphi}_c - a^{3+\alpha} \tilde{V}_{,\tilde{\varphi}_c} - m_\alpha^2(a, b_{-0/2}, b_{+0/2}) \tilde{\varphi}_c \right) \quad (210)$$

$$\tilde{\varphi}_{+0}^{(c)} = \tilde{\varphi}_{+0}^{(c)} + \delta\tilde{\eta} \tilde{\pi}_{+0/2}^{(c)} \quad (211)$$

$$a_{+0} = a + b_{+0/2} \delta\tilde{\eta} \quad (212)$$

As the field amplitudes are conformally transformed as $\tilde{\phi}_c = a^{-\beta} \phi_c$, the canonical momenta becomes $\tilde{\phi}'_c = a^{-\beta}(\pi_c - \beta \mathcal{H} \tilde{\phi}_c)$, with $\tilde{\pi}_c = \tilde{\phi}'_c$ and $\beta = (3 - \alpha)/2$. The Hubble constraint (in the continuum) then becomes

$$HC : \quad \mathcal{H}^2 = \frac{1}{3m_p^2} \left(\frac{a^{\alpha-3}}{2} \sum_c \langle (\tilde{\pi}_c - \beta \mathcal{H} \tilde{\phi}_c)^2 \rangle + \frac{a^{3\alpha-5}}{2} \sum_c \langle (\vec{\nabla} \tilde{\phi}_c)^2 \rangle + a^{2\alpha} \langle \tilde{V} \rangle \right) \quad (213)$$

which is a quadratic equation for \mathcal{H} . *LatticeEasy/ClusterEasy* presented a discretized version of Eq. (213) that is verified numerically to accuracy $\mathcal{O}(\delta\eta^2)$, as expected for a valid staggered leapfrog scheme. Discretizing the expression in Eq. (213) requires however to deal with the fact that there are terms in its *rhs* that live at integer times, others that live at semi-integer times, and there are even 'crossed' terms built from the product of the latter two. The solution *LatticeEasy/ClusterEasy* adopted for this was to synchronize the field amplitudes with the conjugate momenta, just before checking the Hubble law. In this way field amplitudes are evolved backwards in time by half time step, so that they live, during the check, at the same semi-integer step as the conjugate momenta. After the check has been done, one just evolves forward by half time step the field amplitudes, so that they are back to their appropriate value within the evolution loop.

A remark is now in order. Even though the above implementation of an $\mathcal{O}(\delta\eta^2)$ staggered leapfrog algorithm for scalar fields, works fine, it is somehow more cumbersome than our proposed schemes in Section 4.2.1. First of all, the conformal transformation of the fields leads to mix terms between amplitudes and conjugate momenta, whenever time derivatives of the original field amplitudes are calculated. Secondly, the whole method relies on the elimination of the kinetic term from the second Friedmann equation. This leads to solving the evolution of the scale factor from a quadratic equation, and generates a Hubble constraint which becomes itself also a quadratic equation for the Hubble rate \mathcal{H} . Even though one does not need to solve explicitly for \mathcal{H} to verify the Hubble law⁹, one still needs to synchronize and desynchronize the field amplitudes just before and after checking the Hubble law. Furthermore, whenever computing observables like the fields' energy density terms or the various relevant field spectra, one needs to un-do the conformal transformation of the field variables, in order to obtain physically meaningful quantities (or at least one needs to have a very clear idea of what is being obtained, and in what variables it is written down). While none of these aspects are particularly difficult to deal with, they altogether make this prescription more complicated than e.g. our iterative schemes *III* and *IV* in Section 4.2.1. Our schemes are simpler and more natural, not only because they do not require to re-define the field variables, but also because they are based on a lattice principle, i.e. in writing first a correct discretized action, from which naturally follows the dynamics and the observables. The most important caveat, however, is something that has not yet become manifest, but that we can anticipate here: the trick used to eliminate the kinetic term of the scalar fields from the Friedmann equation for a''/a , is not generalizable to gauge theories. This is simple to understand, recalling Eqs. (51),(52), we observe that the weight of the scalar and gauge field kinetic terms is the same in the Hubble constraint, but it is different in the equation for a''/a . This implies that it is impossible to eliminate both kinetic terms at the same time from the second Friedmann equation, and hence it is not possible to achieve a scale factor kernel $\mathcal{K}_a[\dots]$ free from all fields' conjugate momenta (this is actually independent of any potential conformal transformation of the gauge fields): $\mathcal{K}_a[\dots]$ is always left with the conjugate momenta of the scalar fields, or with the conjugate momenta of the gauge fields (played by the electric fields of the problem). Therefore, an approach of this kind to obtain a second order integrator for a gauge theory in an expanding background (no matter whether Abelian or non-Abelian), is simply not feasible.

4.2.3 Synchronized Leapfrog: Position- and Velocity-Verlet

While in Section 4.2.1 our starting point was a lattice action from which we derived the lattice EOM, here we will rather discretize directly the continuum EOM, without introducing a conformal rescaling, similarly to what was done in Section 4.2.1, using a re-definition of the field variables. Considering again the EOM of N_s scalar fields canonically normalized, c.f. Eq. (201), we immediately conclude that the field variables'

⁹It is enough to check that the *lhs* and the *rhs* of Eq. (213) are numerically balanced to order $\mathcal{O}(\delta\eta^2)$

kernel depend on the conjugate momenta through the friction term $(3 - \alpha)\mathcal{H}\tilde{\phi}'_b$. This seemingly appears as an impediment to apply staggered or synchronized leapfrog methods. The EOM as derived initially from the continuum action (158), can however be written as

$$(a^{(3-\alpha)}\tilde{\phi}'_b)' - a^{1+\alpha}\tilde{\nabla}^2\tilde{\phi}_b + a^{3+\alpha}\tilde{V}_{,\tilde{\phi}_b} = 0, \quad b = 1, 2, \dots, N_s, \quad (214)$$

so that only when expanding the first term (and after multiplying by $a^{-(3-\alpha)}$), the standard second derivative and friction terms $\tilde{\phi}''_b + (3 - \alpha)\mathcal{H}\tilde{\phi}'_b$ become explicit. Instead of expanding such terms, the form of Eqs. (214) invites to rather re-write them more naturally in a Hamiltonian-like scheme as

$$\tilde{\phi}'_b = a^{-(3-\alpha)}\tilde{\pi}_b, \quad (215)$$

$$\tilde{\pi}'_b = a^{1+\alpha}\tilde{\nabla}^2\tilde{\phi}_b - a^{3+\alpha}\tilde{V}_{,\tilde{\phi}_b}, \quad (216)$$

where it is manifest that the kernel does not depend on the conjugate momenta. Analogously, the second Friedmann equation (168) can then be written as

$$a' = b, \quad (217)$$

$$b' = \frac{a^{1+2\alpha}}{3} \left(\frac{f_*}{m_p} \right)^2 \left[(\alpha - 2)E_K + \alpha E_G + (\alpha + 1)E_V \right], \quad (218)$$

$$\text{where} \quad E_K \equiv \frac{1}{2a^6} \sum_i \langle (\tilde{\pi}_i)^2 \rangle, \quad E_G \equiv \frac{1}{2a^2} \sum_{i,k} \langle (\tilde{\nabla}_k \tilde{\phi}_i)^2 \rangle, \quad E_V \equiv \langle \tilde{V}(\{\tilde{\phi}_j\}) \rangle, \quad (219)$$

This immediately invites for the application of either staggered or synchronized leapfrog methods. In fact, the methods *III* and *IV* from Section 4.2.1 correspond precisely to the application of a staggered leapfrog scheme. We will thus focus now on the application of synchronized leapfrog schemes, also known as Verlet integrators, either velocity- or position-based. Following Section 4.2.3, these algorithms read:

I) Velocity-Verlet scheme for interacting scalar fields in an expanding background

$$IC : \{ \tilde{\phi}^{(i)}, \tilde{\pi}^{(i)}, a, b \} \text{ at } \tilde{\eta}_0, \quad (220)$$

$$b_{+0/2} = b + \frac{1}{3} \left(\frac{f_*}{m_p} \right)^2 a^{1+2\alpha} \left[(\alpha - 2)E_K + \alpha E_G + (\alpha + 1)E_V \right] \frac{\delta\tilde{\eta}}{2}, \quad (221)$$

$$\tilde{\pi}_{+0/2}^{(i)} = \tilde{\pi}^{(i)} + \left(a^{1+\alpha} \sum_k \tilde{\Delta}_k^- \tilde{\Delta}_k^+ \tilde{\phi}^{(i)} - a^{3+\alpha} \tilde{V}_{,\tilde{\phi}^{(i)}} \right) \frac{\delta\tilde{\eta}}{2}, \quad (222)$$

$$a_{+0} = a + b_{+0/2} \delta\tilde{\eta}, \quad (223)$$

$$a_{+0/2} = \frac{a_{+0} + a}{2}, \quad (224)$$

$$\tilde{\phi}_{+0}^{(i)} = \tilde{\phi}^{(i)} + \delta\tilde{\eta} \tilde{\pi}_{+0/2}^{(i)} a_{+0/2}^{-(3-\alpha)}, \quad (225)$$

$$\tilde{\pi}_{+0}^{(i)} = \tilde{\pi}_{+0/2}^{(i)} + \left(a_{+0}^{1+\alpha} \sum_k \tilde{\Delta}_k^- \tilde{\Delta}_k^+ \tilde{\phi}_{+0}^{(i)} - a_{+0}^{3+\alpha} \tilde{V}_{,\tilde{\phi}^{(i)}} \Big|_{+0} \right) \frac{\delta\tilde{\eta}}{2}, \quad (226)$$

$$b_{+0} = b_{+0/2} + \frac{1}{3} \left(\frac{f_*}{m_p} \right)^2 a_{+0}^{1+2\alpha} \left[(\alpha - 2)E_{K,+0} + \alpha E_{G,+0} + (\alpha + 1)E_{V,+0} \right] \frac{\delta\tilde{\eta}}{2}, \quad (227)$$

$$HC : b^2 = \frac{1}{3} \left(\frac{f_*}{m_p} \right)^2 a^{2(\alpha+1)} (E_K + E_G + E_V), \quad (228)$$

II) Position-Verlet scheme for interacting scalar fields in an expanding background

$$IC : \{ \tilde{\phi}^{(i)}, \tilde{\pi}^{(i)}, a, b \} \text{ at } \tilde{\eta}_0, \quad (229)$$

$$a_{+0/2} = a + b \frac{\delta\tilde{\eta}}{2}, \quad (230)$$

$$\tilde{\phi}_{+0/2}^{(i)} = \tilde{\phi}^{(i)} + \frac{\delta\tilde{\eta}}{2} \tilde{\pi}^{(i)} a^{-(3-\alpha)}, \quad (231)$$

$$\tilde{\pi}_{+0}^{(i)} = \tilde{\pi}^{(i)} + \left(a_{+0/2}^{1+\alpha} \sum_k \tilde{\Delta}_k^- \tilde{\Delta}_k^+ \tilde{\phi}_{+0/2}^{(i)} - a_{+0/2}^{3+\alpha} \tilde{V}_{,\tilde{\phi}^{(i)}} \Big|_{+0/2} \right) \delta\tilde{\eta}, \quad (232)$$

$$E_{K,+0/2} = \frac{E_{K,+0} + E_K}{2}, \quad (233)$$

$$b_{+0} = b + \frac{1}{3} \left(\frac{f_*}{m_p} \right)^2 a_{+0/2}^{1+2\alpha} \left[(\alpha - 2) E_{K,+0/2} + \alpha E_{G,+0/2} + (\alpha + 1) E_{V,+0/2} \right] \delta\tilde{\eta}, \quad (234)$$

$$a_{+0} = a_{+0/2} + b_{+0} \frac{\delta\tilde{\eta}}{2}, \quad (235)$$

$$\tilde{\phi}_{+0}^{(i)} = \tilde{\phi}_{+0/2}^{(i)} + \frac{\delta\tilde{\eta}}{2} \tilde{\pi}_{+0}^{(i)} a_{+0}^{-(3-\alpha)}. \quad (236)$$

$$HC : b^2 = \frac{1}{3} \left(\frac{f_*}{m_p} \right)^2 a^{2(\alpha+1)} (E_K + E_G + E_V), \quad (237)$$

Both algorithms have $\mathcal{O}(\delta\eta^2)$ accuracy and are equivalent in efficiency (number of steps per iteration, complexity of the steps), so one can equally use one or the other, and obtain the same results. Verlet integrators have however three steps per iteration (as they come in a *kick-drift-kick* or *drift-kick-drift* fashion) versus two steps of the staggered leapfrog integrators *III* and *IV* from Section 4.2.1 (which come in a *drift-kick* or *kick-drift* scheme). Verlet integrators is therefore some $\sim 30 - 40\%$ slower than staggered leapfrog algorithms. They can however be used to implement higher-order in $\delta\eta$ with the method presented in Section 3.4.1, see Section 4.3.2.

4.3 $\mathcal{O}(dt^n)$ Lattice formulation of interacting scalar fields

4.3.1 Explicit Runge-Kutta 4th order

Here we just need to specialize Eqs. (151) corresponding to the (explicit) Runge-Kutta method of order $\mathcal{O}(\delta\eta^4)$ to the EOM for N_s interacting scalar fields dictating the expansion of the universe, Eqs. (162) and (168). We first re-write the continuum EOM as

$$a' = \tilde{\pi}_a, \quad (238)$$

$$\tilde{\phi}'_i = \tilde{\pi}_i, \quad (239)$$

$$\tilde{\pi}'_i = \mathcal{K}_i[a, \tilde{\pi}_a, \{\tilde{\phi}_j\}, \tilde{\pi}_i], \quad (240)$$

$$\tilde{\pi}'_a = \mathcal{K}_a[a, E_K, E_G, E_V], \quad (241)$$

$$\text{where} \quad \begin{cases} \mathcal{K}_i[a, b, \{\tilde{\phi}_j\}, \tilde{\pi}_i] \equiv a^{-2(1-\alpha)} \tilde{\nabla}^2 \tilde{\phi}_i - (3 - \alpha) \frac{\tilde{\pi}_a}{a} \tilde{\pi}_i - a^{2\alpha} \tilde{V}_{,\tilde{\phi}_i}, \\ \mathcal{K}_a[a, E_K, E_G, E_V] \equiv \frac{1}{3} \left(\frac{f_*}{m_p} \right)^2 a^{1+2\alpha} \left[(\alpha - 2) E_K + \alpha E_G + (\alpha + 1) E_V \right], \\ E_K \equiv \frac{1}{2a^{2\alpha}} \sum_i \langle \tilde{\pi}_i^2 \rangle, \quad E_G \equiv \frac{1}{2a^2} \sum_{i,k} \langle (\tilde{\nabla}_k \tilde{\phi}_i)^2 \rangle, \quad E_V \equiv \langle \tilde{V}(\{\tilde{\phi}_j\}) \rangle. \end{cases} \quad (242)$$

It is then straightforward to adapt the explicit RK4 algorithm based on Eqs. (151), into the above system of EOM, obtaining

$$\left. \begin{aligned} \tilde{\pi}_i^{(p)} &\equiv \tilde{\pi}_i(\mathbf{n}, n_0) + \delta\tilde{\eta} b_{p,p-1} k_i^{(p-1)}, \\ \tilde{\pi}_a^{(p)} &\equiv \tilde{\pi}_a(n_0) + \delta\tilde{\eta} b_{p,p-1} k_a^{(p-1)}, \\ \tilde{\phi}_i^{(p)} &\equiv \tilde{\phi}_i(\mathbf{n}, n_0) + \delta\tilde{\eta} b_{p,p-1} \tilde{\pi}_i^{(p-1)}, \\ a^{(p)} &\equiv a(n_0) + \delta\tilde{\eta} b_{p,p-1} \tilde{\pi}_a^{(p-1)}, \\ k_i^{(p)} &\equiv \mathcal{K}_i[a^{(p)}, \{\tilde{\phi}_j^{(p)}\}, \tilde{\pi}_i^{(p)}], \\ k_a^{(p)} &\equiv \mathcal{K}_a[a^{(p)}, E_K^{(p)}, E_G^{(p)}, E_V^{(p)}], \end{aligned} \right\}_{p=1,2,3,4} \implies \begin{cases} \tilde{\Delta}_0^+ \tilde{\phi}_i(\mathbf{n}, n_0) &= \frac{1}{6} (\tilde{\pi}_i^{(1)} + 2\tilde{\pi}_i^{(2)} + 2\tilde{\pi}_i^{(3)} + \tilde{\pi}_i^{(4)}), \\ \Delta_0^+ a(n_0) &= \frac{1}{6} (\tilde{\pi}_a^{(1)} + 2\tilde{\pi}_a^{(2)} + 2\tilde{\pi}_a^{(3)} + \tilde{\pi}_a^{(4)}), \\ \tilde{\Delta}_0^+ \tilde{\pi}_i(\mathbf{n}, n_0) &= \frac{1}{6} (k_i^{(1)} + 2k_i^{(2)} + 2k_i^{(3)} + k_i^{(4)}), \\ \tilde{\Delta}_0^+ \tilde{\pi}_a(n_0) &= \frac{1}{6} (k_a^{(1)} + 2k_a^{(2)} + 2k_a^{(3)} + k_a^{(4)}), \end{cases} \quad (243)$$

where $b_{10} \equiv 0$, $b_{21} \equiv \frac{1}{2}$, $b_{32} \equiv \frac{1}{2}$, $b_{43} \equiv 1$.

Since both field amplitudes and conjugate momenta live at the same integer times (after each full iteration), the Hubble constraint is simply

$$HC : \tilde{\pi}_a^2 = \frac{1}{3} \left(\frac{f_*}{m_p} \right)^2 a^{2(\alpha+1)} (E_K + E_G + E_V), \quad (244)$$

evaluated at any integer time.

4.3.2 Verlet Integration n th order

In order to consider any of the higher-order Verlet integrators that we introduced in Section 3.4.1, we need to re-write first the EOM (215)-(218) for N_s interacting scalar fields dictating the expansion of the universe, as follows

$$a' = b, \quad (245)$$

$$\tilde{\phi}'_i = a^{-(3-\alpha)} \tilde{\pi}_i, \quad (246)$$

$$\tilde{\pi}'_i = \mathcal{K}_i[a, \{\tilde{\phi}_j\}], \quad (247)$$

$$b' = \mathcal{K}_a[a, E_K, E_G, E_V], \quad (248)$$

where

$$\mathcal{K}_i[a, \{\tilde{\phi}_j\}] \equiv a^{1+\alpha} \tilde{\nabla}^2 \tilde{\phi}_i - a^{3+\alpha} \tilde{V}_{,\tilde{\phi}_i}, \quad (249)$$

$$\mathcal{K}_a[a, E_K, E_G, E_V] \equiv \frac{1}{3} \left(\frac{f_*}{m_p} \right)^2 a^{1+2\alpha} [(\alpha-2)E_K + \alpha E_G + (\alpha+1)E_V], \quad (250)$$

$$E_K \equiv \frac{1}{2a^6} \sum_i \langle \tilde{\pi}_i^2 \rangle, \quad E_G \equiv \frac{1}{2a^2} \sum_{i,k} \langle (\tilde{\nabla}_k \tilde{\phi}_i)^2 \rangle, \quad E_V \equiv \langle \tilde{V}(\{\tilde{\phi}_j\}) \rangle. \quad (251)$$

Decomposing one time step $\delta\eta = \sum_{p=1}^s \delta\eta_p$ into s sub-steps $\delta\eta_p = w_p \delta t$, so that $\sum_{p=1}^s w_p = 1$, the idea is to iterate s -times one of the Verlet algorithms, (118) or (121), using each time the appropriate $\delta\eta_p$ sub-step. Without loss of generality we use the Velocity Verlet algorithm (118) as the building block, obtaining

$$\begin{aligned} \left\{ \begin{array}{l} \tilde{\pi}_i^{(0)} \equiv \tilde{\pi}_i(\mathbf{n}, n_0) \\ \tilde{\phi}_i^{(0)} \equiv \tilde{\phi}_i(\mathbf{n}, n_0) \\ a^{(0)} \equiv a(n_0) \\ b^{(0)} \equiv b(n_0) \end{array} \right\} &\Rightarrow \left\{ \begin{array}{l} b_{1/2}^{(p)} = b^{(p-1)} + \omega_p \frac{\delta\tilde{\eta}}{2} \mathcal{K}_a[a^{(p-1)}, E_K^{(p-1)}, E_G^{(p-1)}, E_V^{(p-1)}] \\ \tilde{\pi}_{i,1/2}^{(p)} = \tilde{\pi}_i^{(p-1)} + \omega_p \frac{\delta\tilde{\eta}}{2} \mathcal{K}_i[a^{(p-1)}, \{\tilde{\phi}_j^{(p-1)}\}] \\ a_{1/2}^{(p)} = a^{(p-1)} + b_{1/2}^{(p)} \omega_p \frac{\delta\tilde{\eta}}{2} \\ \tilde{\phi}_i^{(p)} = \tilde{\phi}_i^{(p-1)} + \omega_p \delta\tilde{\eta} \tilde{\pi}_{i,1/2}^{(p)} (a_{1/2}^{(p)})^{-(3-\alpha)}, \\ a^{(p)} = a_{1/2}^{(p)} + b_{1/2}^{(p)} \omega_p \frac{\delta\tilde{\eta}}{2}, \\ \tilde{\pi}_i^{(p)} = \tilde{\pi}_{i,1/2}^{(p)} + \omega_p \frac{\delta\tilde{\eta}}{2} \mathcal{K}_i[a^{(p)}, \{\tilde{\phi}_j^{(p)}\}] \\ b^{(p)} = b_{1/2}^{(p)} + \omega_p \frac{\delta\tilde{\eta}}{2} \mathcal{K}_a[a^{(p)}, E_K^{(p)}, E_G^{(p)}, E_V^{(p)}] \end{array} \right\}_{p=1, \dots, s} \Rightarrow \\ \Rightarrow \left\{ \begin{array}{l} \tilde{\pi}_i(\mathbf{n}, n_0 + 1) \equiv \tilde{\pi}_i^{(s)} \\ \tilde{\phi}_i(\mathbf{n}, n_0 + 1) \equiv \tilde{\phi}_i^{(s)} \\ a(n_0 + 1) \equiv a^{(s)} \\ b(n_0 + 1) \equiv b^{(s)}. \end{array} \right. \quad (252) \end{aligned}$$

By choosing the appropriate weights w_p 's from Table 1, the errors of the intermediate steps cancel up to order $\mathcal{O}(\delta\eta^n)$, with $n = 4, 6, 8$ and 10 for $s = 3, 7, 15$ and 31 , respectively.

Finally we deal with the Hubble constraint. Like in the $RK4$ case, here both field amplitudes and conjugate momenta live at the same integer times (after each full iteration over the s -subintervals), so we simply write

$$HC : b^2 = \frac{1}{3} \left(\frac{f_*}{m_p} \right)^2 a^{2(\alpha+1)} (E_K + E_G + E_V), \quad (253)$$

evaluated at any integer time. Note that a similar algorithm of accuracy $O(\delta t^6)$ has been previously introduced in Ref. [250].

4.3.3 Gauss-Legendre n th order

We can adapt the higher-order Gauss-Legendre integrators (based on implicit Runge-Kutta algorithms) introduced in Section 3.4.2, to solve the dynamics of N_s interacting scalar fields with self-consistent expansion of the universe. The continuum EOM can be written either as we did in Section 4.3.1 [here referred to as *Scheme I*], or as we did in Section 4.3.2 [here referred to as *Scheme II*]:

Scheme I :

$$a' = b, \quad (254)$$

$$\tilde{\phi}'_i = \tilde{\pi}_i, \quad (255)$$

$$\tilde{\pi}'_i = \mathcal{K}_i[a, b, \{\tilde{\phi}_j\}, \tilde{\pi}_i], \quad (256)$$

$$b' = \mathcal{K}_a[a, E_K, E_G, E_V], \quad (257)$$

$$\mathcal{K}_i[a, b, \{\tilde{\phi}_j\}, \tilde{\pi}_i] \equiv a^{-2(1-\alpha)} \tilde{\nabla}^2 \tilde{\phi}_i - (3-\alpha) \frac{b}{a} \tilde{\pi}_i - a^{2\alpha} \tilde{V}_{,\tilde{\phi}_i}, \quad (258)$$

$$\mathcal{K}_a[a, E_K, E_G, E_V] \equiv \frac{1}{3} \left(\frac{f_*}{m_p} \right)^2 a^{1+2\alpha} [(\alpha-2)E_K + \alpha E_G + (\alpha+1)E_V], \quad (259)$$

$$E_K \equiv \frac{1}{2a^{2\alpha}} \sum_i \langle \tilde{\pi}_i^2 \rangle, \quad E_G \equiv \frac{1}{2a^2} \sum_{i,k} \langle (\tilde{\nabla}_k \tilde{\phi}_i)^2 \rangle, \quad E_V \equiv \langle \tilde{V}(\{\tilde{\phi}_j\}) \rangle. \quad (260)$$

Scheme II :

$$a' = b, \quad (261)$$

$$\tilde{\phi}'_i = a^{-(3-\alpha)} \tilde{\pi}_i, \quad (262)$$

$$\tilde{\pi}'_i = \mathcal{K}_i[a, \{\tilde{\phi}_j\}], \quad (263)$$

$$b' = \mathcal{K}_a[a, E_K, E_G, E_V], \quad (264)$$

$$\mathcal{K}_i[a, \{\tilde{\phi}_j\}] \equiv a^{1+\alpha} \tilde{\nabla}^2 \tilde{\phi}_i - a^{3+\alpha} \tilde{V}_{,\tilde{\phi}_i}, \quad (265)$$

$$\mathcal{K}_a[a, E_K, E_G, E_V] \equiv \frac{1}{3} \left(\frac{f_*}{m_p} \right)^2 a^{1+2\alpha} [(\alpha-2)E_K + \alpha E_G + (\alpha+1)E_V], \quad (266)$$

$$E_K \equiv \frac{1}{2a^6} \sum_i \langle \tilde{\pi}_i^2 \rangle, \quad E_G \equiv \frac{1}{2a^2} \sum_{i,k} \langle (\tilde{\nabla}_k \tilde{\phi}_i)^2 \rangle, \quad E_V \equiv \langle \tilde{V}(\{\tilde{\phi}_j\}) \rangle. \quad (267)$$

The Gauss-Legendre integrator works in both schemes, since it can deal with field kernels that either contain or do not contain conjugate momenta. Adapting algorithm (157) into program variables, we arrive at

$$\left. \begin{aligned} \tilde{\pi}_i^{(l)} &\equiv \tilde{\pi}_i(\mathbf{n}, n_0) + \delta\tilde{\eta} \sum_{m=1}^s b_{lm} k_i^{(m)}, \\ \tilde{\pi}_a^{(l)} &\equiv \tilde{\pi}_a(n_0) + \delta\tilde{\eta} \sum_{m=1}^s b_{lm} k_a^{(m)}, \\ \tilde{\phi}_i^{(l)} &\equiv \tilde{\phi}_i(\mathbf{n}, n_0) + \delta\tilde{\eta} \sum_{m=1}^s b_{lm} \tilde{\pi}_i^{(m)}, \\ a^{(l)} &\equiv a(n_0) + \delta\tilde{\eta} \sum_{m=1}^s b_{lm} \tilde{\pi}_a^{(m)}, \\ k_a^{(l)} &\equiv \mathcal{K}_a[a^{(l)}, \bar{K}^{(l)}, \bar{G}^{(l)}, \bar{V}^{(l)}], \\ k_i^{(l)} &\equiv \begin{cases} \mathcal{K}_i[a^{(l)}, \tilde{\pi}_a^{(l)}, \{\tilde{\phi}_j^{(l)}\}, \tilde{\pi}_i^{(l)}] \text{ (Sch. I)}, \\ \mathcal{K}_i[a^{(l)}, \{\tilde{\phi}_j^{(l)}\}] \text{ (Sch. II)}, \end{cases} \end{aligned} \right\}_{l=1,2,\dots,s} \Rightarrow \begin{cases} \tilde{\Delta}_0^+ \tilde{\phi}_i(\mathbf{n}, n_0) &= \sum_{m=1}^s c_m \tilde{\pi}_i^{(m)}, \\ \tilde{\Delta}_0^+ a(n_0) &= \sum_{m=1}^s c_m \tilde{\pi}_a^{(m)}, \\ \tilde{\Delta}_0^+ \tilde{\pi}_i(\mathbf{n}, n_0) &= \sum_{m=1}^s c_m k_i^{(m)}, \\ \tilde{\Delta}_0^+ \pi_a(n_0) &= \sum_{m=1}^s c_m k_a^{(m)}, \end{cases} \quad (270)$$

where the coefficients $\{b_{lm}\}$ and $\{c_m\}$ are listed in Table 2 for the cases of $s = 2, 3, 4$ and 5 number of sub-steps (recall that a method with s -substeps has an accuracy of $\mathcal{O}(\delta\eta^{2s})$).

As both schemes *I* and *II* have field amplitudes and conjugate momenta living at the same (integer) time, the Hubble constraint can be written in both schemes simply as

$$HC \quad : \quad b^2 = \frac{1}{3} \left(\frac{f_*}{m_p} \right)^2 a^{2(\alpha+1)} (E_K + E_G + E_V), \quad (271)$$

evaluated at any integer time.

4.4 Observables

To conclude this section, we collect the main observables of interest, such as energies and power-spectra. In the case of scalar fields, we are mostly concerned with the fields and conjugate momenta themselves, $\tilde{\phi}_i$ and $\tilde{\pi}_i$. In particular, we typically monitor their mean value and their variance.

4.4.1 Energy components

We can define the kinetic and gradient energy for each field as follows,

$$E_K^{\phi_i} = \frac{1}{a^6} \left\langle (\tilde{\pi}_i)^2 \right\rangle, \quad E_G^{\phi_i} = \frac{1}{a^2} \sum_j \left\langle (\tilde{\Delta}_j^+ \tilde{\phi}_i)^2 \right\rangle, \quad (272)$$

while the total potential energy is defined as

$$E_V = \left\langle \tilde{V}(\{\tilde{\phi}_i\}) \right\rangle. \quad (273)$$

In most cases, the potential can naturally be written as a sum of p different terms $V(\{\tilde{\phi}_i\}) = \sum_a V_a(\{\tilde{\phi}_i\})$, which are typically the different mass terms and interactions of the fields. Therefore, we also measure

$$E_{V_a} = \left\langle \tilde{V}_a(\{\tilde{\phi}_i\}) \right\rangle. \quad (274)$$

4.4.2 Spectra

Finally, we can also consider the power spectrum of each individual field. Following our conventions in Eq. (65), we define

$$\mathcal{P}_{\tilde{\phi}_i}(k(\tilde{n})) = \frac{k^3(\tilde{n})}{2\pi^2} \left(\frac{\delta\tilde{x}}{N} \right)^3 \left\langle |(\tilde{\phi}_i)(\tilde{n})|^2 \right\rangle_{R(\tilde{n})}, \quad (275)$$

$$\mathcal{P}_{\tilde{\pi}_i}(k(\tilde{n})) = \frac{k^3(\tilde{n})}{2\pi^2} \left(\frac{\delta\tilde{x}}{N} \right)^3 \left\langle |\tilde{\pi}_i(\tilde{n})|^2 \right\rangle_{R(\tilde{n})}. \quad (276)$$

5 Lattice formulation of gauge fields, I: $U(1)$ interactions

We can now move on to the lattice formulation of the $U(1)$ gauge sector, which consists in developing an appropriate discretization for Eqs. (37) and (39), together with Friedmann's law (52). In particular, we will generalize the staggered leapfrog algorithm of Section 4.2.1, the velocity-Verlet one of Section 4.2.3, and its higher-order generalizations introduced in Section 4.3.2. For simplicity, we restrict the presentation to the case of a single complex scalar field φ coupled to a single Abelian gauge field A_μ , as the generalization to a larger number of fields is straightforward. Note also that for conciseness, we present explicitly only the velocity-Verlet versions of the Verlet's algorithm. The position one is straightforwardly obtained by inverting the roles of the momenta and fields, as explained in Section 4.2.3.

5.1 Continuum formulation and natural variables

We define the following *program* variables for the $U(1)$ -charged scalars and the Abelian gauge fields as

$$\tilde{\varphi} = \frac{1}{f_*} \varphi, \quad \tilde{A}_\mu = \frac{1}{\omega_*} A_\mu. \quad (277)$$

The normalization of the charged scalar is identical to the one of the scalar singlet, introduced in Eq. (160). However, the gauge field is normalized with respect ω_* , so it cancels the one coming from $\delta \tilde{x}^\mu$ in the link, i.e. $V_\mu \equiv e^{-i\delta x_\mu A_\mu} = e^{-i\delta \tilde{x}_\mu \tilde{A}_\mu} \equiv \tilde{V}_\mu$. The continuum equations of motion in these variables are, in the temporal gauge $\tilde{A}_0 = 0$,

$$(a^{3-\alpha} \tilde{\varphi}')' - a^{1+\alpha} \tilde{D}_A^2 \tilde{\varphi} = -a^{\alpha+3} \tilde{V}_{|\tilde{\varphi}|} \frac{\tilde{\varphi}}{|\tilde{\varphi}|}, \quad (278)$$

$$\tilde{\partial}_0(a^{1-\alpha} \tilde{F}_{0i}) - a^{\alpha-1} \partial_j \tilde{F}_{ji} = a^{1+\alpha} \tilde{J}_i^A, \quad (279)$$

where all field and spacetime variables are program variables, and as such, are indicated with a ‘ \sim ’. By inspecting these equations, we can naturally identify appropriate definitions for the conjugate momenta of the field variables as

$$\tilde{\pi}_\varphi \equiv a^{3-\alpha} \tilde{\varphi}', \quad (280)$$

$$(\tilde{\pi}_A)_i \equiv a^{1-\alpha} \tilde{F}_{0i}. \quad (281)$$

We define the *program* kinetic energies of the fields as

$$E_K^\varphi = \frac{1}{a^6} \langle \tilde{\pi}_\varphi^2 \rangle, \quad (282)$$

$$E_K^A = \frac{1}{2a^4} \sum_{i=1}^3 \langle (\tilde{\pi}_A)_i^2 \rangle. \quad (283)$$

For convenience, let us also define the following kernels for each of the amplitudes and momenta,

$$(\tilde{\pi}_\varphi)' = \mathcal{K}^\varphi[a, \tilde{\varphi}, \tilde{A}_i], \quad (284)$$

$$(\tilde{\pi}_A)_i' = \mathcal{K}_i^A[a, \tilde{\varphi}, \tilde{A}_i], \quad (285)$$

$$\mathcal{K}^\varphi[a, \tilde{\varphi}, \tilde{A}_i] \equiv -a^{\alpha+3} \tilde{V}_{|\tilde{\varphi}|} \frac{\tilde{\varphi}}{|\tilde{\varphi}|} + a^{1+\alpha} \tilde{D}_A^2 \tilde{\varphi}, \quad (286)$$

$$\mathcal{K}^A[a, \tilde{\varphi}, \tilde{A}_i]_i \equiv a^{1+\alpha} \tilde{J}_i^A + a^{\alpha-1} \tilde{\partial}_j \tilde{F}_{ji}. \quad (287)$$

5.2 Non-compact Lattice formulation of scalar-gauge dynamics

We first present here a spatial discretization of the kernels using non-compact variables, which means that the variables to evolve are the field amplitudes and momenta themselves, $\{\tilde{\varphi}, \tilde{\pi}_\varphi, \tilde{A}_i, (\tilde{\pi}_A)_i\}$. Using our $U(1)$ -toolkit (3.2.2), we get

$$\mathcal{K}^\varphi[a, \tilde{\varphi}, \tilde{A}_i] = -a^{\alpha+3} \tilde{V}_{|\tilde{\varphi}|} \frac{\tilde{\varphi}}{|\tilde{\varphi}|} + a^{1+\alpha} \sum_i \tilde{D}_i^- \tilde{D}_i^+ \tilde{\varphi}, \quad (288)$$

$$\mathcal{K}^A[a, \tilde{\varphi}, \tilde{A}_i]_i = a^{1+\alpha} \left(g_A Q_A^{(\tilde{\varphi})} \mathcal{I}m[\tilde{\varphi}^* \tilde{V}_i \tilde{\varphi}] + \dots \right) + a^{\alpha-1} \sum_j \left(\tilde{\Delta}_j^- \tilde{\Delta}_j^+ \tilde{A}_i - \tilde{\Delta}_j^- \tilde{\Delta}_i^+ \tilde{A}_j \right), \quad (289)$$

where the dots are here to remind the reader that any fields coupled to the $U(1)$ gauge field will contribute to its kernel through the gauge current. For example, an $SU(N)$ -doublet $\tilde{\Phi}$ would add a contribution of the sort $g_A Q_A^{(\tilde{\Phi})} \mathcal{I}m[\tilde{\Phi}^\dagger \tilde{V}_i \tilde{\Phi}]$. For conciseness, let us also define a kernel for the scale factor as

$$\mathcal{K}^b[a, \tilde{\varphi}, \tilde{\pi}_\varphi, \tilde{A}_i, (\tilde{\pi}_A)_i] = \frac{a^{2\alpha+1}}{3m_p^2} (\alpha-2)(E_K^\varphi + \dots) + \alpha(E_G^\varphi + \dots) + (\alpha+1)E_V + (\alpha-1)(E_K^A + E_G^A + \dots), \quad (290)$$

corresponding to Friedmann's equation (52). We reproduced only the terms directly relevant to the $U(1)$ gauge sector; the dots are here again to remind the reader that other contributions will enter if some other sectors are also present (e.g. scalar singlets). The kinetic energies are defined in (282) and (283). We discretize the remaining gradient and potential energies as follows,

$$E_G^\varphi = \frac{1}{a^2} \sum_i \left\langle (\tilde{D}_i^A + \tilde{\varphi})^* (\tilde{D}_i^A + \tilde{\varphi}) \right\rangle, \quad (291)$$

$$E_G^A = \frac{1}{2a^4} \sum_{i,j < i} \left\langle (\tilde{\Delta}_i^+ \tilde{A}_j - \tilde{\Delta}_i^- \tilde{A}_j)^2 \right\rangle, \quad (292)$$

$$E_V = \left\langle \tilde{V}(\tilde{\varphi}, \dots) \right\rangle. \quad (293)$$

Finally, a crucial quantity to monitor is the Gauss law, which must be obeyed at all times during the simulation. It is written in the continuum in Eq. (41). In terms of program variables, we can discretize it as follows,

$$-\sum_i \Delta_i^- (\tilde{\pi}_A)_i = g_A Q_A^{(\varphi)} \mathcal{I}m[\tilde{\varphi}^* \tilde{\pi}_\varphi]. \quad (294)$$

5.2.1 Staggered Leap-Frog

Let us now consider the time evolution of these equations. We first present an adaptation of the staggered leapfrog algorithm of order $O(\delta\eta^2)$ to our system. Momenta are evaluated at semi-integer times, while fields live at integer times. When needed, the former/latter can be evaluated at integer/semi-integer times by interpolation. In particular, this is needed in the scale-factor kernels,

$$\begin{aligned} \mathcal{K}^b[a, \tilde{\varphi}, \tilde{\pi}_\varphi, \tilde{A}_i, (\tilde{\pi}_A)_i] &= \frac{a^{2\alpha+1}}{3m_p^2} (\alpha - 2) (\overline{E_K^\varphi} + \dots) + \alpha (E_G^\varphi + \dots) + (\alpha + 1) E_V \\ &\quad + (\alpha - 1) (\overline{E_K^A} + E_G^A) \dots \end{aligned} \quad (295)$$

The algorithm to evolve the fields and their momenta by one time step proceeds as follows:

Staggered Leapfrog Non-Compact

$$IC : \left\{ a, b_{-1/2}, \tilde{\varphi}, (\tilde{\pi}_\varphi)_{-1/2}, \tilde{A}_i, (\tilde{\pi}_A)_{i,-1/2} \right\} \text{ at } \tilde{\eta}_0. \quad (296)$$

$$(\tilde{\pi}_\varphi)_{+1/2} = (\tilde{\pi}_\varphi)_{-1/2} + \delta\tilde{\eta} \mathcal{K}^\varphi[a, \tilde{\varphi}, \tilde{A}_i], \quad (297)$$

$$(\tilde{\pi}_A)_{i,+1/2} = (\tilde{\pi}_A)_{i,-1/2} + \delta\tilde{\eta} \mathcal{K}^A[a, \tilde{\varphi}, \tilde{A}_i]_i, \quad (298)$$

$$b_{+1/2} = b_{-1/2} + \delta\tilde{\eta} \mathcal{K}^b[a, \tilde{\varphi}, \tilde{\pi}_\varphi, \tilde{A}_i, (\tilde{\pi}_A)_i], \quad (299)$$

$$a_{+0} = a + \delta\tilde{\eta} b_{+1/2}, \quad (300)$$

$$a_{+1/2} = \frac{a_{+0} + a}{2}, \quad (301)$$

$$\tilde{\varphi}_{+0} = \tilde{\varphi} + \delta\tilde{\eta} \frac{(\tilde{\pi}_\varphi)_{+1/2}}{a_{+1/2}^{3-\alpha}}, \quad (302)$$

$$\tilde{A}_{i,+0} = \tilde{A}_i + \delta\tilde{\eta} \frac{(\tilde{\pi}_A)_{i,+1/2}}{a_{+1/2}^{1-\alpha}}, \quad (303)$$

$$HC : b^2 = \frac{1}{3} \left(\frac{f_*}{m_p} \right)^2 a^{2(\alpha+1)} \left(\overline{E_K^\varphi} + E_G^\varphi + \overline{E_K^A} + E_G^A + E_V \right), \quad (304)$$

where the last line is the corresponding Hubble constraint. We see that the scale factor also needs to be interpolated, as it enters into the relation between the conjugate momenta and the fields' time derivative. Note also that this scheme can be obtained from an action principle, similar to the analogous scalar singlet case.

5.2.2 Velocity-Verlet

The equations can also be solved with a velocity-Verlet scheme of order $O(\delta\tilde{\eta}^2)$, similarly to the analogous scalar case. The algorithm to update the system proceeds as follows,

Velocity-Verlet VV2 Non-Compact

$$IC : \quad \left\{ a, b, \tilde{\varphi}, \tilde{\pi}_\varphi, \tilde{A}_i, (\tilde{\pi}_A)_i \right\} \text{ at } \eta_0. \quad (305)$$

$$(\tilde{\pi}_\varphi)_{+1/2} = \tilde{\pi}_\varphi + \frac{\delta\tilde{\eta}}{2} \mathcal{K}^\varphi[a, \tilde{\varphi}, \tilde{A}_i], \quad (306)$$

$$(\tilde{\pi}_A)_{i,+1/2} = (\tilde{\pi}_A)_i + \frac{\delta\tilde{\eta}}{2} \mathcal{K}^A[a, \tilde{\varphi}, \tilde{A}_i]_i, \quad (307)$$

$$b_{+1/2} = b + \frac{\delta\tilde{\eta}}{2} \mathcal{K}^b[a, \tilde{\varphi}, \tilde{\pi}_\varphi, \tilde{A}_i, (\tilde{\pi}_A)_i], \quad (308)$$

$$a_{+0} = a + \delta\tilde{\eta} b_{+1/2}, \quad (309)$$

$$a_{+1/2} = \frac{a_{+0} + a}{2}, \quad (310)$$

$$\tilde{\varphi}_{+0} = \tilde{\varphi} + \delta\tilde{\eta} \frac{(\tilde{\pi}_\varphi)_{+1/2}}{a_{+1/2}^{3-\alpha}}, \quad (311)$$

$$\tilde{A}_{i,+0} = \tilde{A}_i + \delta\tilde{\eta} \frac{(\tilde{\pi}_A)_{+1/2}}{a_{+1/2}^{1-\alpha}}, \quad (312)$$

$$(\tilde{\pi}_\varphi)_{+0} = (\tilde{\pi}_\varphi)_{+1/2} + \frac{\delta\tilde{\eta}}{2} \mathcal{K}^\varphi[a_{+0}, \tilde{\varphi}_{+0}, \tilde{A}_{i,+0}], \quad (313)$$

$$(\tilde{\pi}_A)_{i,+0} = (\tilde{\pi}_A)_{i,+1/2} + \frac{\delta\tilde{\eta}}{2} \mathcal{K}_i^A[a_{+0}, \tilde{\varphi}_{+0}, \tilde{A}_{i,+0}]_i, \quad (314)$$

$$b_{+0} = b_{+1/2} + \frac{\delta\tilde{\eta}}{2} \mathcal{K}^b[a_{+0}, \tilde{\varphi}_{+0}, (\tilde{\pi}_\varphi)_{+0}, \tilde{A}_{i,+0}, (\tilde{\pi}_A)_{i,+0}], \quad (315)$$

$$HC : \quad b^2 = \frac{1}{3} \left(\frac{f_*}{m_p} \right)^2 a^{2(\alpha+1)} (E_K^\varphi + E_G^\varphi + E_K^A + E_G^A + E_V), \quad (316)$$

where the last line is again the Hubble constraint. Note that a similar integrator, based on a position-Verlet method, was recently presented in Ref. [154].

5.2.3 Velocity-Verlet n th order

In order to construct the higher order integrators VV4, VV6, VV8 and VV10, one simply needs to apply the method described in Section 3.4.1. Explicitly, by choosing ω_p in Table 1, it proceeds as follows,

$$\left. \begin{aligned} \tilde{\pi}_\varphi^{(0)} &\equiv \tilde{\pi}_\varphi(\mathbf{n}, n_0) \\ \tilde{\varphi}^{(0)} &\equiv \tilde{\varphi}(\mathbf{n}, n_0) \\ \tilde{A}_i^{(0)} &\equiv \tilde{A}_i(\mathbf{n}, n_0) \\ (\tilde{\pi}_A)_i^{(0)} &\equiv (\tilde{\pi}_A)_i(\mathbf{n}, n_0) \\ a^{(0)} &\equiv a(n_0) \\ b^{(0)} &\equiv b(n_0) \end{aligned} \right\} \implies \quad (317)$$

$$\Rightarrow \left\{ \begin{array}{l} (\tilde{\pi}_\varphi)_{1/2}^{(p)} = \tilde{\pi}_\varphi^{(p-1)} + \frac{\omega_p \delta \tilde{\eta}}{2} \mathcal{K}^\varphi \left[a^{(p-1)}, \tilde{\varphi}^{(p-1)}, \tilde{A}_i^{(p-1)} \right] \\ (\tilde{\pi}_A)_{i,1/2}^{(p)} = (\tilde{\pi}_A)_i^{(p-1)} + \frac{\omega_p \delta \tilde{\eta}}{2} \mathcal{K}^A \left[a^{(p-1)}, \tilde{\varphi}^{(p-1)}, \tilde{A}_i^{(p-1)} \right]_i \\ b_{1/2}^{(p)} = b^{(p-1)} + \frac{\omega_p \delta \tilde{\eta}}{2} \mathcal{K}^b \left[a^{(p-1)}, \tilde{\varphi}^{(p-1)}, \tilde{\pi}_\varphi^{(p-1)}, \tilde{A}_i^{(p-1)}, (\tilde{\pi}_A)_i^{(p-1)} \right] \\ a^{(p)} = a^{(p-1)} + \omega_p \delta \tilde{\eta} b_{1/2}^{(p)} \\ a_{1/2}^{(p)} = \frac{a^{(p)} + a^{(p-1)}}{2} \\ \tilde{\varphi}^{(p)} = \tilde{\varphi}^{(p-1)} + \delta \tilde{\eta} \frac{(\tilde{\pi}_\varphi)_{1/2}^{(p)}}{(a_{1/2}^{(p)})^{3-\alpha}} \\ \tilde{A}_i^{(p)} = \tilde{A}_i^{(p-1)} + \omega_p \delta \tilde{\eta} \frac{(\tilde{\pi}_A)_{1/2}^{(p)}}{(a_{1/2}^{(p)})^{1-\alpha}} \\ (\tilde{\pi}_\varphi)^{(p)} = (\tilde{\pi}_\varphi)_{1/2}^{(p)} + \frac{\omega_p \delta \tilde{\eta}}{2} \mathcal{K}^\varphi \left[a^{(p)}, \tilde{\varphi}^{(p)}, \tilde{A}_i^{(p)} \right] \\ (\tilde{\pi}_A)_i^{(p)} = (\tilde{\pi}_A)_{i,1/2}^{(p)} + \frac{\omega_p \delta \tilde{\eta}}{2} \mathcal{K}^A \left[a^{(p)}, \tilde{\varphi}^{(p)}, \tilde{A}_i^{(p)} \right]_i \\ b^{(p)} = b_{1/2}^{(p)} + \frac{\omega_p \delta \tilde{\eta}}{2} \mathcal{K}^b \left[a^{(p)}, \tilde{\varphi}^{(p)}, (\tilde{\pi}_\varphi)^{(p)}, \tilde{A}_i^{(p)}, (\tilde{\pi}_A)_i^{(p)} \right] , \end{array} \right\}_{p=1, \dots, s} \quad (318)$$

$$\Rightarrow \left\{ \begin{array}{l} \tilde{\pi}_\varphi(\mathbf{n}, n_0) \equiv \tilde{\pi}_\varphi^{(s)} \\ \tilde{\varphi}(\mathbf{n}, n_0) \equiv \tilde{\varphi}^{(s)} \\ \tilde{A}_i(\mathbf{n}, n_0) \equiv \tilde{A}_i^{(s)} \\ (\tilde{\pi}_A)_i(\mathbf{n}, n_0) \equiv (\tilde{\pi}_A)_i^{(s)} \\ a(n_0) \equiv a^{(s)} \\ b(n_0) \equiv b^{(s)} , \end{array} \right. \quad (319)$$

$$HC : b^2 = \frac{1}{3} \left(\frac{f_*}{m_p} \right)^2 a^{2(\alpha+1)} (E_K^\varphi + E_G^\varphi + E_K^A + E_G^A + E_V) . \quad (320)$$

5.3 Compact Lattice formulation of scalar-gauge dynamics

As presented in Section 3.2.2, the link variables V_i can also be used as “fundamental” variables to be solved, instead of the gauge field amplitudes A_i . This leads to a ‘compact’ discretization of the $U(1)$ gauge sector. In this approach, we keep the same definitions for momenta as before, (280) and (281). However, we take for the gauge fields’ kernel,

$$\mathcal{K}_i^A[a, \tilde{\varphi}, \tilde{V}_i]_i = a^{1+\alpha} \left(g_A Q_A^{(\varphi)} \mathcal{I}m[\tilde{\varphi}^* \tilde{V}_i \tilde{\varphi}] + \dots \right) + \frac{a^{\alpha-1}}{\delta \tilde{x}^3} \sum_j \left(\tilde{V}_{ij} - \tilde{V}_{ij-j} \right) . \quad (321)$$

where the second term is a backward discretization of $\tilde{\partial}_j \tilde{F}_{ji}$. This can of course be replaced by some other discretization, this precise one corresponds to a discrete action made out of a plaquettes. The magnetic energy can be approximated by

$$E_G^A = \frac{2}{a^4 \delta \tilde{x}^4} \sum_{i,j < i} (1 - \mathcal{R}e(\tilde{V}_{ij}))^2 . \quad (322)$$

The last difference with respect to the non-compact formulation is how the link variables are evolved in time. In order to understand this, let us compute the continuum time derivative of a link

$$(\tilde{V}_i)' = \partial_0 e^{-i\delta \tilde{x} \tilde{A}_i} = -i\delta \tilde{x} (\tilde{A}_i)' \tilde{V}_i , \quad (323)$$

or in terms of the conjugate momenta,

$$(\tilde{V}_i)' = -i \frac{\delta \tilde{x}}{a^{1-\alpha}} (\tilde{\pi}_A)_i \tilde{V}_i . \quad (324)$$

The scale factor kernel $\mathcal{K}^b[a, \tilde{\varphi}, \tilde{\pi}_\varphi, \tilde{V}_i, (\tilde{\pi}_A)_i]$ is then understood to be computed with these energies. Having defined all the necessary ingredients, we can write down the corresponding modified evolution algorithms for the compact formulation.

5.3.1 Staggered Leap-Frog

In this case, the only difference with respect to the non-compact formulation is how the drifts are given. The algorithm is

Staggered Leapfrog Compact

$$IC : \left\{ a, b_{-1/2}, \tilde{\varphi}, (\tilde{\pi}_\varphi)_{-1/2}, \tilde{V}_i, (\tilde{\pi}_A)_{i,-1/2} \right\} \text{ at } \eta_0. \quad (325)$$

$$(\tilde{\pi}_\varphi)_{+1/2} = (\tilde{\pi}_\varphi)_{-1/2} + \delta\tilde{\eta}\mathcal{K}^\varphi[a, \tilde{\varphi}, \tilde{V}_i], \quad (326)$$

$$(\tilde{\pi}_A)_{i,+1/2} = (\tilde{\pi}_A)_{i,-1/2} + \delta\tilde{\eta}\mathcal{K}^A[a, \tilde{\varphi}, \tilde{V}_i]_i, \quad (327)$$

$$b_{+1/2} = b_{-1/2} + \delta\tilde{\eta}\mathcal{K}^b[a, \tilde{\varphi}, \tilde{\pi}_\varphi, \tilde{V}_i, (\tilde{\pi}_A)_i], \quad (328)$$

$$a_{+0} = a + \delta\tilde{\eta}b_{+1/2}, \quad (329)$$

$$\tilde{\varphi}_{+0} = \tilde{\varphi} + \delta\tilde{\eta}\frac{(\tilde{\pi}_\varphi)_{+1/2}}{a_{+1/2}^{3-\alpha}}, \quad (330)$$

$$\tilde{V}_{i,+0} = \tilde{V}_i - i\delta\tilde{\eta}\delta\tilde{x}\frac{(\tilde{\pi}_A)_{i,+1/2}}{a_{+1/2}^{1-\alpha}}, \quad (331)$$

$$HC : b^2 = \frac{1}{3} \left(\frac{f_*}{m_p} \right)^2 a^{2(\alpha+1)} \left(\overline{E_K^\varphi} + E_G^\varphi + \overline{E_K^A} + E_G^A + E_V \right). \quad (332)$$

5.3.2 Velocity-Verlet

Again, only the drifts differ in the velocity-Verlet algorithm with respect to the non-compact case. We get

Velocity-Verlet VV2 Compact

$$IC : \left\{ a, b, \tilde{\varphi}, \tilde{\pi}_\varphi, \tilde{V}_i, (\tilde{\pi}_A)_i \right\} \text{ at } \eta_0. \quad (333)$$

$$(\tilde{\pi}_\varphi)_{+1/2} = \tilde{\pi}_\varphi + \frac{\delta\tilde{\eta}}{2}\mathcal{K}^\varphi[a, \tilde{\varphi}, \tilde{V}_i], \quad (334)$$

$$(\tilde{\pi}_A)_{i,+1/2} = (\tilde{\pi}_A)_i + \frac{\delta\tilde{\eta}}{2}\mathcal{K}^A[a, \tilde{\varphi}, \tilde{V}_i]_i, \quad (335)$$

$$b_{+1/2} = b + \frac{\delta\tilde{\eta}}{2}\mathcal{K}^b[a, \tilde{\varphi}, \tilde{\pi}_\varphi, \tilde{V}_i, (\tilde{\pi}_A)_i], \quad (336)$$

$$a_{+0} = a + \delta\tilde{\eta}b_{+1/2}, \quad (337)$$

$$a_{+1/2} = \frac{a_{+0} + a}{2}, \quad (338)$$

$$\tilde{\varphi}_{+0} = \tilde{\varphi} + \delta\tilde{\eta}\frac{(\tilde{\pi}_\varphi)_{+1/2}}{a_{+1/2}^{3-\alpha}}, \quad (339)$$

$$\tilde{V}_{i,+0} = \tilde{V}_i - i\delta\tilde{\eta}\delta\tilde{x}\frac{(\tilde{\pi}_A)_{i,+1/2}}{a_{+1/2}^{1-\alpha}}, \quad (340)$$

$$(\tilde{\pi}_\varphi)_{+0} = (\tilde{\pi}_\varphi)_{+1/2} + \frac{\delta\tilde{\eta}}{2}\mathcal{K}^\varphi[a_{+0}, \tilde{\varphi}_{+0}, \tilde{V}_{i,+0}], \quad (341)$$

$$(\tilde{\pi}_A)_{i,+0} = (\tilde{\pi}_A)_{i,+1/2} + \frac{\delta\tilde{\eta}}{2}\mathcal{K}_i^A[a_{+0}, \tilde{\varphi}_{+0}, \tilde{V}_{i,+0}]_i, \quad (342)$$

$$b_{+0} = b_{+1/2} + \frac{\delta\tilde{\eta}}{2} \mathcal{K}^b [a_{+0}, \tilde{\varphi}_{+0}, (\tilde{\pi}_\varphi)_{+0}, \tilde{V}_{i,+0}, (\tilde{\pi}_A)_{i,+0}], \quad (343)$$

$$HC : b^2 = \frac{1}{3} \left(\frac{f_*}{m_p} \right)^2 a^{2(\alpha+1)} (E_K^\varphi + E_G^\varphi + E_K^A + E_G^A + E_V) . \quad (344)$$

5.3.3 Velocity-Verlet n th order

The higher order integrators VV4, VV6, VV8 and VV10 for the compact formulation are also obtained by a simple modification of the drifts,

$$\left. \begin{aligned} \tilde{\pi}_\varphi^{(0)} &\equiv \tilde{\pi}_\varphi(\mathbf{n}, n_0) \\ \tilde{\varphi}^{(0)} &\equiv \tilde{\varphi}(\mathbf{n}, n_0) \\ \tilde{V}_i^{(0)} &\equiv \tilde{V}_i(\mathbf{n}, n_0) \\ (\tilde{\pi}_A)_i^{(0)} &\equiv (\tilde{\pi}_A)_i(\mathbf{n}, n_0) \\ a^{(0)} &\equiv a(n_0) \\ b^{(0)} &\equiv b(n_0) , \end{aligned} \right\} \Rightarrow \quad (345)$$

$$\Rightarrow \left\{ \begin{aligned} (\tilde{\pi}_\varphi)_{1/2}^{(p)} &= \tilde{\pi}_\varphi^{(p-1)} + \frac{\omega_p \delta\tilde{\eta}}{2} \mathcal{K}^\varphi [a^{(p-1)}, \tilde{\varphi}^{(p-1)}, \tilde{V}_i^{(p-1)}] \\ (\tilde{\pi}_A)_{i,1/2}^{(p)} &= (\tilde{\pi}_A)_i^{(p-1)} + \frac{\omega_p \delta\tilde{\eta}}{2} \mathcal{K}^A [a^{(p-1)}, \tilde{\varphi}^{(p-1)}, \tilde{V}_i^{(p-1)}]_i \\ b_{1/2}^{(p)} &= b^{(p-1)} + \frac{\omega_p \delta\tilde{\eta}}{2} \mathcal{K}^b [a^{(p-1)}, \tilde{\varphi}^{(p-1)}, \tilde{\pi}_\varphi^{(p-1)}, \tilde{V}_i^{(p-1)}, (\tilde{\pi}_A)_i^{(p-1)}] \\ a^{(p)} &= a^{(p-1)} + \omega_p \delta\tilde{\eta} b_{1/2}^{(p)} \\ a_{1/2}^{(p)} &= \frac{a^{(p)} + a^{(p-1)}}{2} \\ \tilde{\varphi}^{(p)} &= \tilde{\varphi}^{(p-1)} + \delta\tilde{\eta} \frac{(\tilde{\pi}_\varphi)_{1/2}^{(p)}}{(a_{1/2}^{(p)})^{3-\alpha}} \\ V_i^{(p)} &= V_i^{(p-1)} - i\delta\tilde{\eta} \delta\tilde{x} \frac{(\tilde{\pi}_A)_{i,1/2}^{(p)}}{(a_{1/2}^{(p)})^{3-\alpha}} \\ (\tilde{\pi}_\varphi)^{(p)} &= (\tilde{\pi}_\varphi)_{1/2}^{(p)} + \frac{\omega_p \delta\tilde{\eta}}{2} \mathcal{K}^\varphi [a^{(p)}, \tilde{\varphi}^{(p)}, \tilde{V}_i^{(p)}] \\ (\tilde{\pi}_A)_i^{(p)} &= (\tilde{\pi}_A)_{i,1/2}^{(p)} + \frac{\omega_p \delta\tilde{\eta}}{2} \mathcal{K}^A [a^{(p)}, \tilde{\varphi}^{(p)}, \tilde{V}_i^{(p)}]_i \\ b^{(p)} &= b_{1/2}^{(p)} + \frac{\omega_p \delta\tilde{\eta}}{2} \mathcal{K}^b [a^{(p)}, \tilde{\varphi}^{(p)}, (\tilde{\pi}_\varphi)^{(p)}, \tilde{V}_i^{(p)}, (\tilde{\pi}_A)_i^{(p)}] , \end{aligned} \right\}_{p=1, \dots, s} \quad (346)$$

$$\Rightarrow \left\{ \begin{aligned} \tilde{\pi}_\varphi(\mathbf{n}, n_0) &\equiv \tilde{\pi}_\varphi^{(s)} \\ \tilde{\varphi}(\mathbf{n}, n_0) &\equiv \tilde{\varphi}^{(s)} \\ \tilde{V}_i(\mathbf{n}, n_0) &\equiv \tilde{V}_i^{(s)} \\ (\tilde{\pi}_A)_i(\mathbf{n}, n_0) &\equiv (\tilde{\pi}_A)_i^{(s)} \\ a(n_0) &\equiv a^{(s)} \\ b(n_0) &\equiv b^{(s)} , \end{aligned} \right. \quad HC : b^2 = \frac{1}{3} \left(\frac{f_*}{m_p} \right)^2 a^{2(\alpha+1)} (E_K^\varphi + E_G^\varphi + E_K^A + E_G^A + E_V) . \quad (347)$$

As we will see in next section, an advantage of the compact formulation is that it directly generalizes to non-Abelian groups, contrary to the non-compact one. However, before moving on, let us introduce some relevant observables for the $U(1)$ gauge sector.

5.4 Observables

We group here observables whose mean value and variance are of interest,

$$U(1) \text{ matter: } \mathcal{R}e[\tilde{\varphi}] , \mathcal{I}m[\tilde{\varphi}] , \mathcal{R}e[\tilde{\pi}_\varphi] , \mathcal{I}m[\tilde{\pi}_\varphi] , |\tilde{\varphi}| , |\tilde{\pi}_\varphi| . \quad (348)$$

$$U(1) \text{ gauge fields, non-compact: } \tilde{\mathcal{E}}_i = \frac{1}{a^{1-\alpha}} (\tilde{\pi}_A)_i , \tilde{\mathcal{B}}_i = \frac{1}{2} \sum_{jk} \epsilon_{ijk} (\tilde{\Delta}_j^+ \tilde{A}_k - \tilde{\Delta}_k^+ \tilde{A}_j) , |\tilde{\mathcal{E}}| , |\tilde{\mathcal{B}}| . \quad (349)$$

$$U(1) \text{ gauge fields, compact: } \tilde{\mathcal{E}}_i = \frac{1}{a^{1-\alpha}} (\tilde{\pi}_A)_i , \tilde{\mathcal{B}}_i = -\frac{1}{2\delta\tilde{x}^4} \sum_{jk} \epsilon_{ijk} (\mathcal{R}e(\tilde{V}_{jk})) , |\tilde{\mathcal{E}}| , |\tilde{\mathcal{B}}| . \quad (350)$$

Note that, as presented in the $U(1)$ -toolkit (3.2.2), other discretizations are possible for the magnetic field.

5.4.1 Energy components

We collect here the different expressions for the energy components of the system,

$$U(1) \text{ matter: } E_K^\varphi = \frac{1}{a^6} \langle \tilde{\pi}_\varphi^2 \rangle , E_G^\varphi = \frac{1}{a^2} \sum_i \left\langle (\tilde{D}_i^{A+} \tilde{\varphi})^* (\tilde{D}_i^{A+} \tilde{\varphi}) \right\rangle . \quad (351)$$

$$U(1) \text{ gauge fields, non-compact: } E_K^A = \frac{1}{2a^4} \sum_{i=1}^3 \left\langle (\tilde{\pi}_A)_i^2 \right\rangle , E_G^A = \frac{1}{2a^4} \sum_{i,j < i} \left\langle (\tilde{\Delta}_i^+ \tilde{A}_j - \tilde{\Delta}_j^+ \tilde{A}_i)^2 \right\rangle . \quad (352)$$

$$U(1) \text{ gauge fields, compact: } E_K^A = \frac{1}{2a^4} \sum_{i=1}^3 \left\langle (\tilde{\pi}_A)_i^2 \right\rangle , E_G^A = \frac{2}{a^4 \delta\tilde{x}^4} \sum_{i,j < i} (1 - \mathcal{R}e(\tilde{V}_{ij}))^2 . \quad (353)$$

$$\text{Potential: } E_V = \left\langle \tilde{V}(\tilde{\varphi}, \dots) \right\rangle , \quad (354)$$

where ‘K’, ‘G’, and ‘V’ indicate kinetic, gradient, and potential energies.

5.4.2 Spectra

The last quantities of interest are the power spectra, which according to the discrete expression of Eq. (65), we define as follow,

$$\mathcal{P}_{\tilde{\varphi}}(k(\tilde{n})) = \frac{k^3(\tilde{n})}{2\pi^2} \left(\frac{\delta\tilde{x}}{N} \right)^3 \left\langle |\mathcal{R}e(\tilde{\varphi})(\tilde{n})|^2 + |\mathcal{I}m(\tilde{\varphi})(\tilde{n})|^2 \right\rangle_{R(\tilde{n})} , \quad (355)$$

$$\mathcal{P}_{\tilde{\pi}_\varphi}(k(\tilde{n})) = \frac{k^3(\tilde{n})}{2\pi^2} \left(\frac{\delta\tilde{x}}{N} \right)^3 \left\langle |\mathcal{R}e(\tilde{\pi}_\varphi)(\tilde{n})|^2 + |\mathcal{I}m(\tilde{\pi}_\varphi)(\tilde{n})|^2 \right\rangle_{R(\tilde{n})} , \quad (356)$$

$$\mathcal{P}_{\tilde{\mathcal{E}}}^A(k(\tilde{n})) = \frac{k^3(\tilde{n})}{2\pi^2} \left(\frac{\delta\tilde{x}}{N} \right)^3 \left\langle \sum_i |\tilde{\mathcal{E}}_i(\tilde{n})|^2 \right\rangle_{R(\tilde{n})} , \quad (357)$$

$$\mathcal{P}_{\tilde{\mathcal{B}}}^A(k(\tilde{n})) = \frac{k^5(\tilde{n})}{2\pi^2} \left(\frac{\delta\tilde{x}}{N} \right)^3 \left\langle \sum_i |\tilde{A}_i(\tilde{n})|^2 \right\rangle_{R(\tilde{n})} , [\text{non-compact}] , \quad (358)$$

$$\mathcal{P}_{\tilde{\mathcal{B}}}^A(k(\tilde{n})) = \frac{k^3(\tilde{n})}{2\pi^2} \left(\frac{\delta\tilde{x}}{N} \right)^3 \left\langle \sum_i |\tilde{\mathcal{B}}_i(\tilde{n})|^2 \right\rangle_{R(\tilde{n})} , [\text{compact}] , \quad (359)$$

with the electric and magnetic fields defined as in equations (349) and (350). The extra powers of $k(\tilde{n})$ in the non-compact magnetic field spectra come from the spatial derivative of \tilde{A}_i .

6 Lattice formulation of gauge fields, II: $SU(N)$ interactions

Let us now introduce a set of new Gauss-preserving evolution algorithms for a $SU(N)$ gauge sector with self-consistent expansion of the universe. We will follow closely what has been done for the compact $U(1)$ formulation. As in the previous section, we explicitly present only a velocity-Verlet algorithm; the corresponding position Verlet one is straightforwardly obtained from there.

6.1 Continuum formulation and natural variables

We define the following *program variables* for the non-Abelian gauge fields and complex doublet, as follows

$$\tilde{\Phi} = \frac{\Phi}{f_*}, \quad \tilde{B}_\mu^a = \frac{B_\mu^a}{\omega_*}, \quad (360)$$

mimicking the definition for the $U(1)$ gauge sector, see Eq. (277). Again, our lattice formulation will be based in these variables.

We start again by identifying an appropriate set of conjugate momenta. This is again achieved by rewriting the continuum equations (38) and (40) appropriately. In the temporal gauge, they are

$$(a^{3-\alpha}\tilde{\Phi}')' - a^{1+\alpha}\tilde{D}^2\tilde{\Phi} = -a^{\alpha+3}\tilde{V}_{|\tilde{\Phi}|}\frac{\tilde{\Phi}}{|\tilde{\Phi}|}, \quad (361)$$

$$\partial_0(a^{1-\alpha}(\tilde{G}_{0i})^a) - a^{\alpha-1}(\tilde{\mathcal{D}}_j)_{ab}(\tilde{G}_{ji})^b = a^{1+\alpha}\tilde{J}_i^a. \quad (362)$$

From here, we define the conjugate momenta as

$$\tilde{\pi}_\Phi = a^{3-\alpha}\tilde{\Phi}', \quad (363)$$

$$(\tilde{\pi}_B)^a = a^{1-\alpha}\tilde{G}_{0i}^a. \quad (364)$$

The associated kinetic energies of the two field sectors become

$$E_K^\Phi = \frac{1}{a^6} \left\langle \tilde{\pi}_\Phi^\dagger \tilde{\pi}_\Phi \right\rangle, \quad (365)$$

$$E_K^B = \frac{1}{2a^4} \sum_{a,i} \left\langle ((\tilde{\pi}_B)_i^a)^2 \right\rangle. \quad (366)$$

Finally, we define the following kernels as

$$(\tilde{\pi}_\Phi)' = \mathcal{K}^\Phi[a, \tilde{\Phi}, \tilde{U}_i], \quad (367)$$

$$((\tilde{\pi}_B)_i^a)' = \mathcal{K}^B[a, \tilde{\Phi}, \tilde{U}_i]_i^a, \quad (368)$$

$$\mathcal{K}^\Phi[a, \tilde{\Phi}, \tilde{U}_i] \equiv -a^{\alpha+3}\tilde{V}_{|\tilde{\Phi}|}\frac{\tilde{\Phi}}{|\tilde{\Phi}|} + a^{1+\alpha}\tilde{D}_A^2\tilde{\Phi}, \quad (369)$$

$$\mathcal{K}^B[a, \tilde{\Phi}, \tilde{U}_i]_i^a \equiv a^{1+\alpha}\tilde{J}_i^a + a^{\alpha-1}(\tilde{\mathcal{D}}_j)_{ab}(\tilde{G}_{ji})^b, \quad (370)$$

which allows us to proceed with the discretization and time evolution of the EOM.

6.2 Lattice formulation of scalar-gauge dynamics

For non-Abelian gauge fields, we do not have the choice between compact and non-compact variables: the compact formulation is required to maintain gauge invariance. As such, we discretize the kernels as follows,

$$\mathcal{K}^\Phi[a, \tilde{\Phi}, \tilde{U}_i] = -a^{\alpha+3}\tilde{V}_{|\tilde{\Phi}|}\frac{\tilde{\Phi}}{|\tilde{\Phi}|} + a^{1+\alpha} \sum_i \tilde{D}_i^- \tilde{D}_i^+ \tilde{\Phi}, \quad (371)$$

$$\mathcal{K}^B[a, \tilde{\Phi}, \tilde{U}_i]_i^a = a^{1+\alpha} \left(2g_B Q_B^{(\Phi)} \mathcal{Im}[\tilde{\Phi}^\dagger \tilde{U}_i \tilde{\Phi}] + \dots \right) + \frac{a^{\alpha-1}}{\delta \tilde{x}^3} \sum_j \left(\tilde{U}_{ij} - \tilde{U}_{j,-j}^\dagger \tilde{U}_{ij} - \tilde{U}_{j,-j} \tilde{U}_{ij} \right), \quad (372)$$

where the second term in the $SU(N)$ kernel is a backward finite difference approximation of the gauge covariant derivative $\tilde{D}\tilde{G}_{ij}$. We also used matrix notation, for conciseness. Using our $SU(N)$ -toolkit (80), we see that the magnetic energy can be written as

$$E_G^B = \frac{2}{g_B a^4 \delta \tilde{x}^4} \sum_{a,i,j < i} \left\langle \text{Tr}(iT_a \tilde{U}_{ij})^2 \right\rangle. \quad (373)$$

As in the compact $U(1)$ case, we need to relate our conjugate momenta to the time derivative of the link. We use the same relation in the continuum as before,

$$(\tilde{U}_i)' = \partial_0 e^{-i\delta \tilde{x} \tilde{B}_i} = -i\delta \tilde{x} (\tilde{B}_i)' \tilde{U}_i, \quad (374)$$

which in terms of the conjugate momenta is

$$(\tilde{U}_i)' = -i \frac{\delta \tilde{x}}{a^{1-\alpha}} (\tilde{\pi}_B)_i \tilde{U}_i, \quad (375)$$

with no sum intended.

Finally, a crucial quantity to monitor is the Gauss law, which must be obeyed at all times during the simulation. Based on the continuum expression in Eq. (42), we discretize it in matrix notation as

$$-\sum_i \Delta_i^- (\tilde{\pi}_B)_i = 2g_B Q_B^{(\tilde{\Phi})} \mathcal{I}m[\tilde{\Phi}^\dagger \tilde{\pi}_\Phi]. \quad (376)$$

6.2.1 Staggered Leap-Frog

Let us now consider different evolution algorithms to solve the field dynamics in the compact formulation, following closely the same script as for the $U(1)$ gauge sector. We begin with a straightforward generalization of the staggered leap-frog algorithm. It gives

Staggered Leapfrog

$$IC : \left\{ a, b_{-1/2}, \tilde{\Phi}, (\tilde{\pi}_\Phi)_{-1/2}, \tilde{U}_i, (\tilde{\pi}_B)_{i,-1/2} \right\} \text{ at } \eta_0. \quad (377)$$

$$(\tilde{\pi}_\Phi)_{i,+1/2} = (\tilde{\pi}_\Phi)_{-1/2} + \delta \tilde{\eta} \mathcal{K}^\Phi[a, \tilde{\Phi}, \tilde{U}_i]_i, \quad (378)$$

$$(\tilde{\pi}_B)_{i,+1/2} = (\tilde{\pi}_B)_{i,-1/2} + \delta \tilde{\eta} \mathcal{K}^B[a, \tilde{\Phi}, \tilde{U}_i]_i, \quad (379)$$

$$b_{+1/2} = b_{-1/2} + \delta \tilde{\eta} \mathcal{K}^b[a, \tilde{\Phi}, \tilde{\pi}_\Phi, \tilde{U}_i, (\tilde{\pi}_B)_i], \quad (380)$$

$$a_{+0} = a + \delta \tilde{\eta} b_{+1/2}, \quad (381)$$

$$a_{+1/2} = \frac{a_{+0} + a}{2}, \quad (382)$$

$$\tilde{\Phi}_{+0} = \tilde{\Phi} + \delta \tilde{\eta} \frac{(\tilde{\pi}_\Phi)_{+1/2}}{a_{+1/2}^{3-\alpha}}, \quad (383)$$

$$\tilde{U}_{i,+0} = \tilde{U}_i - i\delta \tilde{\eta} \delta \tilde{x} \frac{(\tilde{\pi}_B)_{i,+1/2}}{a_{+1/2}^{1-\alpha}}, \quad (384)$$

$$HC : b^2 = \frac{1}{3} \left(\frac{f_*}{m_p} \right)^2 a^{2(\alpha+1)} \left(\overline{E_K^\Phi} + E_G^\Phi + \overline{E_K^B} + E_G^B + E_V \right). \quad (385)$$

In particular, note that the scale factor kernel is also evaluated using semi-sums of the different kinetic energies.

6.2.2 Velocity Verlet

Mimicking the algorithm developed for the analogous U(1) gauge sector, we obtain

Velocity Verlet VV2

$$IC : \left\{ a, b, \tilde{\Phi}, \tilde{\pi}_\Phi, \tilde{U}_i, (\tilde{\pi}_B)_i \right\} \text{ at } \eta_0. \quad (386)$$

$$(\tilde{\pi}_\Phi)_{+1/2} = \tilde{\pi}_\Phi + \frac{\delta\tilde{\eta}}{2} \mathcal{K}^\Phi[a, \tilde{\Phi}, \tilde{U}_i], \quad (387)$$

$$(\tilde{\pi}_B)_{i,+1/2} = (\tilde{\pi}_B)_i + \frac{\delta\tilde{\eta}}{2} \mathcal{K}^B[a, \tilde{\Phi}, \tilde{U}_i]_i, \quad (388)$$

$$b_{+1/2} = b + \frac{\delta\tilde{\eta}}{2} \mathcal{K}^b[a, \tilde{\Phi}, \tilde{\pi}_\Phi, \tilde{U}_i, (\tilde{\pi}_B)_i], \quad (389)$$

$$a_{+0} = a + \delta\tilde{\eta} b_{+1/2}, \quad (390)$$

$$a_{+1/2} = \frac{a_{+0} + a}{2}, \quad (391)$$

$$\tilde{\Phi}_{+0} = \tilde{\Phi} + \delta\tilde{\eta} \frac{(\tilde{\pi}_\Phi)_{+1/2}}{a_{+1/2}^{3-\alpha}}, \quad (392)$$

$$U_{i,+0} = U_i - i\delta\tilde{\eta}\delta\tilde{x} \frac{(\tilde{\pi}_B)_{i,+1/2}}{a_{+1/2}^{1-\alpha}}, \quad (393)$$

$$(\tilde{\pi}_\Phi)_{+0} = (\tilde{\pi}_\Phi)_{+1/2} + \frac{\delta\tilde{\eta}}{2} \mathcal{K}^\Phi[a_{+0}, \tilde{\Phi}_{+0}, \tilde{U}_{i,+0}], \quad (394)$$

$$(\tilde{\pi}_B)_{i,+0} = (\tilde{\pi}_B)_{i,+1/2} + \frac{\delta\tilde{\eta}}{2} \mathcal{K}_i^B[a_{+0}, \tilde{\Phi}_{+0}, \tilde{U}_{i,+0}]_i, \quad (395)$$

$$b_{+0} = b_{+1/2} + \frac{\delta\tilde{\eta}}{2} \mathcal{K}^b[a_{+0}, \tilde{\Phi}_{+0}, (\tilde{\pi}_\Phi)_{+0}, \tilde{U}_{i,+0}, (\tilde{\pi}_B)_{i,+0}], \quad (396)$$

$$HC : b^2 = \frac{1}{3} \left(\frac{f_*}{m_p} \right)^2 a^{2(\alpha+1)} (E_K^\Phi + E_G^\Phi + E_K^B + E_G^B + E_V). \quad (397)$$

6.2.3 Velocity Verlet n th order

The higher-order integrators VV4, VV6, VV8 and VV10 are also obtained by a simple modification of the drifts,

$$\left. \begin{aligned} \tilde{\pi}_\Phi^{(0)} &\equiv (\tilde{\pi}_\Phi)(\mathbf{n}, n_0) \\ \tilde{\Phi}^{(0)} &\equiv \tilde{\Phi}(\mathbf{n}, n_0) \\ \tilde{U}_i^{(0)} &\equiv \tilde{U}_i(\mathbf{n}, n_0) \\ (\tilde{\pi}_B)_i^{(0)} &\equiv (\tilde{\pi}_B)_i(\mathbf{n}, n_0) \\ a^{(0)} &\equiv a(n_0) \\ b^{(0)} &\equiv b(n_0) \end{aligned} \right\} \implies \quad (398)$$

$$\Rightarrow \left\{ \begin{array}{l} (\tilde{\pi}_\Phi)_{1/2}^{(p)} = (\tilde{\pi}_\Phi)^{(p-1)} + \frac{\omega_p \delta \tilde{\eta}}{2} \mathcal{K}^\Phi [a^{(p-1)}, \tilde{\Phi}^{(p-1)}, \tilde{U}_i^{(p-1)}] \\ (\tilde{\pi}_B)_{i,1/2}^{(p)} = (\tilde{\pi}_B)_i^{(p-1)} + \frac{\omega_p \delta \tilde{\eta}}{2} \mathcal{K}^B [a^{(p-1)}, \tilde{\Phi}^{(p-1)}, \tilde{U}_i^{(p-1)}]_i \\ b_{1/2}^{(p)} = b^{(p-1)} + \frac{\omega_p \delta \tilde{\eta}}{2} \mathcal{K}^b [a^{(p-1)}, \tilde{\Phi}^{(p-1)}, \tilde{\pi}^\Phi{}^{(p-1)}, \tilde{U}_i^{(p-1)}, (\tilde{\pi}_B)_i^{(p-1)}] \\ a^{(p)} = a^{(p-1)} + \omega_p \delta \tilde{\eta} b_{1/2}^{(p)} \\ \tilde{\Phi}^{(p)} = \tilde{\Phi}^{(p-1)} + \delta \tilde{\eta} \frac{(\tilde{\pi}_\Phi)_{1/2}^{(p)}}{a_{1/2}^{(p)} \frac{1}{3-\alpha}} \\ \tilde{U}_i^{(p)} = \tilde{U}_i^{(p-1)} - i \delta \tilde{\eta} \delta \tilde{x} \frac{(\tilde{\pi}_B)_{1/2}^{(p)}}{a_{1/2}^{(p)} \frac{1}{1-\alpha}} \\ (\tilde{\pi}_\Phi)^{(p)} = (\tilde{\pi}_\Phi)_{1/2}^{(p)} + \frac{\omega_p \delta \tilde{\eta}}{2} \mathcal{K}^\Phi [a^{(p)}, \tilde{\Phi}^{(p)}, \tilde{U}_i^{(p)}] \\ (\tilde{\pi}_B)_i^{(p)} = (\tilde{\pi}_B)_{i,1/2}^{(p)} + \frac{\omega_p \delta \tilde{\eta}}{2} \mathcal{K}^B [a^{(p)}, \tilde{\Phi}^{(p)}, \tilde{U}_i^{(p)}]_i \\ b^{(p)} = b_{1/2}^{(p)} + \frac{\omega_p \delta \tilde{\eta}}{2} \mathcal{K}^b [a^{(p)}, \tilde{\Phi}^{(p)}, \tilde{\pi}^\Phi{}^{(p)}, \tilde{U}_i^{(p)}, (\tilde{\pi}_B)_i^{(p)}] , \end{array} \right\}_{p=1, \dots, s} \quad (399)$$

$$\Rightarrow \left\{ \begin{array}{l} (\tilde{\pi}_\Phi)(\mathbf{n}, n_0) \equiv (\tilde{\pi}_\Phi)_i^{(s)} \\ \tilde{\Phi}(\mathbf{n}, n_0) \equiv \tilde{\Phi}^{(s)} \\ \tilde{U}_i(\mathbf{n}, n_0) \equiv \tilde{U}_i^{(s)} \\ (\tilde{\pi}_B)_i(\mathbf{n}, n_0) \equiv (\tilde{\pi}_B)_i^{(s)} \\ a(n_0) \equiv a^{(s)} \\ b(n_0) \equiv b^{(s)} , \end{array} \right. \quad (400)$$

$$HC : b^2 = \frac{1}{3} \left(\frac{f_*}{m_p} \right)^2 a^{2(\alpha+1)} (E_K^\Phi + E_G^\Phi + E_K^B + E_G^B + E_V) . \quad (401)$$

6.3 Observables

Finally, we write here several observables that are of interest. Let us start with the following averages,

$$SU(2) \text{ matter: } \tilde{\Phi}^a, (\tilde{\pi}_\Phi)^a, |\tilde{\Phi}|, |\tilde{\pi}_\Phi| . \quad (402)$$

$$SU(2) \text{ gauge fields: } \tilde{\mathcal{E}}_i^a = \frac{1}{a^{1-\alpha}} (\tilde{\pi}_B)_i^a, \quad \tilde{\mathcal{B}}_i^a = \frac{\epsilon_{ijk}}{2\delta\tilde{x}^2} \text{Tr}[(iT_a)(\tilde{U}_{jk} - \tilde{U}_{kj})], \quad (403)$$

$$|\tilde{\mathcal{E}}^B| = \sum_{a,i} (\tilde{\mathcal{E}}_i^a)^2, \quad |\tilde{\mathcal{B}}^B| = \sum_{a,i} (\tilde{\mathcal{B}}_i^a)^2 . \quad (404)$$

6.3.1 Energy components

The different energies associated to the $SU(N)$ gauge sector are

$$SU(2) \text{ matter: } E_K^\Phi = \frac{1}{a^6} \langle \tilde{\pi}_\Phi^\dagger \tilde{\pi}_\Phi \rangle, \quad E_G^\Phi = \frac{1}{a^2} \sum_i \langle (\tilde{D}_i^+ \tilde{\Phi})^* (\tilde{D}_i^+ \tilde{\Phi}) \rangle . \quad (405)$$

$$SU(2) \text{ gauge fields: } E_K^B = \frac{1}{2a^4} \sum_{a,i} \langle ((\tilde{\pi}_B)_i^a)^2 \rangle, \quad E_G^B = \frac{2}{g_B a^4 \delta \tilde{x}^4} \sum_{a,i,j < i} \langle \text{Tr}(iT_a \tilde{U}_{ij})^2 \rangle . \quad (406)$$

$$\text{Potential: } E_V = \langle \tilde{V}(\tilde{\Phi}, \dots) \rangle , \quad (407)$$

where ‘K’, ‘G’ and ‘V’ refer to kinetic, gradient, and potential energy.

6.3.2 Spectra

We also define the associated power-spectra of each field sector as follows,

$$\mathcal{P}_{\tilde{\Phi}}(k(\tilde{n})) = \frac{k^3(\tilde{n})}{2\pi^2} \left(\frac{\delta\tilde{x}}{N} \right)^3 \left\langle \sum_a |\tilde{\Phi}^a(\tilde{n})|^2 \right\rangle_{R(\tilde{n})}, \quad (408)$$

$$\mathcal{P}_{\tilde{\pi}_\Phi}(k(\tilde{n})) = \frac{k^3(\tilde{n})}{2\pi^2} \left(\frac{\delta\tilde{x}}{N} \right)^3 \left\langle \sum_a |(\tilde{\pi}_\Phi)^a(\tilde{n})|^2 \right\rangle_{R(\tilde{n})}, \quad (409)$$

$$\mathcal{P}_{\tilde{\mathcal{E}}}^B(k(\tilde{n})) = \frac{k^3(\tilde{n})}{2\pi^2} \left(\frac{\delta\tilde{x}}{N} \right)^3 \left\langle \sum_{i,a} |\tilde{\mathcal{E}}_i^a(\tilde{n})|^2 \right\rangle_{R(\tilde{n})}, \quad (410)$$

$$\mathcal{P}_{\tilde{\mathcal{B}}}^B(k(\tilde{n})) = \frac{k^3(\tilde{n})}{2\pi^2} \left(\frac{\delta\tilde{x}}{N} \right)^3 \left\langle \sum_{i,a} |\tilde{\mathcal{B}}_i^a(\tilde{n})|^2 \right\rangle_{R(\tilde{n})}, \quad (411)$$

with the electric and magnetic fields defined as in equations (404). We note that the spectra are homogenized over all directions in space and field-space.

7 Initial conditions

We describe in this section how to set the initial conditions of the different fields, both in the continuum and in the lattice. The initial condition of any field consists of a homogeneous mode, over which a particular spectrum of fluctuations is added. In particular, let us denote the initial time of our simulations as t_* , and add the subindex “*” to any quantity evaluated at such time. The initial conditions of e.g. a scalar singlet can be written, in our notation, as

$$\phi(\mathbf{x}, t_*) \equiv \bar{\phi}_* + \delta\phi_*(\mathbf{x}), \quad (412)$$

$$\dot{\phi}(\mathbf{x}, t_*) \equiv \bar{\dot{\phi}}_* + \delta\dot{\phi}_*(\mathbf{x}), \quad (413)$$

where the bar denotes the homogeneous component of a given quantity. The numerical values of $\bar{\phi}_*$ and $\bar{\dot{\phi}}_*$ depend on the details of the specific field model being simulated. For example, in Section 8, we take the scalar field ϕ as the inflaton field sourcing the accelerated expansion of the Universe, so in this context, $\bar{\phi}_*$ and $\bar{\dot{\phi}}_*$ can be conveniently chosen as the inflaton amplitude and derivative at the end of inflation, i.e. when the inflaton oscillatory regime starts.

In this section we focus on how to set the initial fluctuations of the different fields. We first explain in Section 7.1 how to set a spectrum of scalar fluctuations in the lattice, so that they recover the expected distribution of fluctuations in the continuum limit. After that, we explain in Section 7.2 how to set the initial fluctuations of the charged fields and the (Abelian and non-Abelian) gauge fields, putting a special emphasis on achieving preservation of the Gauss constraint(s) up to machine precision.

7.1 Stochastic spectrum of scalar fluctuations

Let us consider the scalar field given in Eqs. (412)-(413). Given the homogeneous modes $\bar{\phi}_*$ and $\bar{\dot{\phi}}_*$, we want to set an appropriate set of classical fluctuations $\delta\phi_*(\mathbf{x})$ and $\delta\dot{\phi}_*(\mathbf{x})$ at time $t = t_*$, in order to mimic quantum vacuum fluctuations as well as possible. In the continuum, we can write

$$\langle \delta\phi^2 \rangle = \frac{1}{2\pi^2} \int d\log k \, k^3 \mathcal{P}_{\delta\phi}(k), \quad \langle \delta\phi_{\mathbf{k}} \delta\phi_{\mathbf{k}'} \rangle \equiv (2\pi)^3 \mathcal{P}_{\delta\phi}(k) \delta(\mathbf{k} - \mathbf{k}'), \quad (414)$$

where $\langle \dots \rangle$ represents an ensemble average, and $\mathcal{P}_{\delta\phi}(k)$ is the power spectrum. Although these quantities must obviously be evaluated at the time $t = t_*$, here we have dropped the “*” to simplify notation, as we

will do in the remainder of this section. For initial conditions representing quantum vacuum fluctuations, we choose

$$\mathcal{P}_{\delta\phi}(k) \equiv \frac{1}{2\omega_{k,\phi}} \equiv \frac{1}{2\sqrt{k^2 + m_\phi^2}} , \quad m_\phi^2 \equiv \frac{\partial^2 V}{\partial \phi^2}(\phi = \bar{\phi}) , \quad (415)$$

where $\omega_{k,\phi} \equiv \sqrt{k^2 + m_\phi^2}$ is the frequency of the mode, and m_ϕ is the effective mass of the field, evaluated in terms of the homogeneous field components.

In the lattice, we want to set the fluctuations of the scalar field so that expression (414) is recovered in the continuum limit. In the discrete we substitute the stochastic expectation value by a volume average as

$$\langle \delta\phi^2 \rangle_V = \frac{\delta x^3}{V} \sum_n \delta\phi^2(n) = \frac{1}{N^6} \sum_{\tilde{n}} |\delta\phi(\tilde{n})|^2 , \quad (416)$$

where we have used Eq. (58). Decomposing the summation into radial and angular parts, we obtain

$$\langle \delta\phi^2 \rangle_V = \frac{1}{N^6} \sum_{|\tilde{n}|} \sum_{\tilde{n}' \in R(\tilde{n})} |\delta\phi(\tilde{n})|^2 = \frac{4\pi}{N^6} \sum_{|\tilde{n}|} |\tilde{n}|^2 \langle |\delta\phi(\tilde{n})|^2 \rangle_{R(\tilde{n})} , \quad (417)$$

where $\langle (\cdots) \rangle_{R(\tilde{n})} \equiv \frac{1}{4\pi|\tilde{n}|^2} \sum_{\tilde{n}' \in R(\tilde{n})} (\cdots)$ is an angular average over the spherical shell of radius $\tilde{n}' \in [|\tilde{n}|, |\tilde{n}| + \Delta\tilde{n}]$, with $\Delta\tilde{n}$ a given radial binning. This leads to

$$\langle \delta\phi^2 \rangle_V = \frac{4\pi}{k_{\text{IR}}^3 N^6} \sum_{|\tilde{n}|} \Delta \log k(\tilde{n}) k^3(\tilde{n}) \langle |\delta\phi(\tilde{n})|^2 \rangle_{R(\tilde{n})} = \frac{1}{2\pi^2} \sum_{|\tilde{n}|} \Delta \log k(\tilde{n}) k^3(\tilde{n}) \frac{L^3}{N^6} \langle |\delta\phi(\tilde{n})|^2 \rangle_{R(\tilde{n})} \quad (418)$$

where $\Delta \log k(\tilde{n}) \equiv \frac{k_{\text{IR}}}{k(\tilde{n})}$, $\mathbf{k}(\tilde{n}) \equiv k_{\text{IR}} \tilde{n}$ and $k_{\text{IR}} \equiv \frac{2\pi}{L}$. In order to mimic in the lattice the continuum stochastic initial condition, we impose

$$\langle \delta\phi^2 \rangle_V = \frac{1}{2\pi^2} \sum_{|\tilde{n}|} \Delta \log k(\tilde{n}) k^3(\tilde{n}) \mathcal{P}_{\delta\phi}(k) , \quad (419)$$

from where we identify

$$\langle |\delta\phi(\tilde{n})|^2 \rangle_{R(\tilde{n})} = \left(\frac{N}{\delta x} \right)^3 \mathcal{P}_{\delta\phi}(k) . \quad (420)$$

The initial variance of the Fourier modes in the lattice, expressed in the program variables of Eq. (160), must be taken therefore as

$$|\delta\tilde{\phi}(\tilde{n})|^2 \equiv \left(\frac{\omega_*}{f_*} \right)^2 \left(\frac{N}{\delta \tilde{x}} \right)^3 \tilde{\mathcal{P}}_{\delta\phi}(\tilde{k}(\tilde{n})) , \quad (421)$$

where $\tilde{\mathcal{P}}_{\delta\phi} \equiv \omega_* \mathcal{P}_{\delta\phi}$ is the (dimensionless) power spectrum in program units. With this choice, we reproduce the continuum correctly,

$$\langle \delta\phi^2 \rangle_V = \frac{1}{2\pi^2} \sum_{|\tilde{n}|} \Delta \log k(\tilde{n}) k^3(\tilde{n}) \mathcal{P}_{\delta\phi}(k(\tilde{n})) \quad \longrightarrow \quad \frac{1}{2\pi^2} \int d \log k k^3 \mathcal{P}_{\delta\phi}(k) . \quad (422)$$

The key point of the identification made in Eq. (420), is that $\langle \delta\phi^2 \rangle_V$ in Eq. (422) does not depend explicitly on the volume $V = (N \cdot \delta x)^3$, as required in order to correctly reproduce the continuum result. For quantum fluctuations with distribution (415), we shall write

$$|\delta\tilde{\phi}(\tilde{n})|^2 \equiv \left(\frac{\omega_*}{f_*} \right)^2 \left(\frac{N}{\delta \tilde{x}} \right)^3 \frac{1}{2\sqrt{\tilde{k}^2(\tilde{n}) + \tilde{m}_\phi^2}} , \quad \tilde{m}_\phi^2 \equiv \frac{\partial^2 \tilde{V}}{\partial \tilde{\phi}^2}(\tilde{\phi} = \tilde{\bar{\phi}}) , \quad (423)$$

where $\tilde{k} \equiv k/\omega_*$ and $\tilde{m}_\phi \equiv m_\phi/\omega_*$ are the momentum and effective mass in program variables.

Note that this expression gives an account of the appropriate radial distribution of the amplitude of the fluctuations in the lattice, but does not describe how the amplitude changes point by point. Moreover, we also need to consider the fluctuations of the time-derivative of the field. In this regard, let us note that the field modes have a time-dependence as $\delta\phi_{\mathbf{k}} \propto (1/a)e^{\pm i\omega_k t}$, with a the scale factor. The frequency ω_k may depend on time, but we assume that the initial conditions are set in an adiabatic regime, $\dot{\omega}_k/\omega_k^2 \ll 1$. Taking the time-derivative of the field mode, we get $\delta\dot{\phi}_{\mathbf{k}} = (\pm i\omega_k - H)\delta\phi_{\mathbf{k}}$. Choosing one sign in this expression is equivalent to choosing a preferred direction in position space, so although this effect should be irrelevant in the dynamics once the non-linearities of the simulated process kick in, we follow the prescription of `Latticeeasy` to define isotropic initial conditions [246]. In particular, at each lattice point in momentum space, we add to the field amplitude in program units a sum of left-moving and right-moving waves as follows,

$$\delta\tilde{\phi}(\tilde{\mathbf{n}}) = \frac{1}{\sqrt{2}}(\delta\tilde{\phi}_1(\tilde{\mathbf{n}})e^{i\theta_1(\tilde{\mathbf{n}})} + \delta\tilde{\phi}_2(\tilde{\mathbf{n}})e^{i\theta_2(\tilde{\mathbf{n}})}) , \quad (424)$$

$$\delta\tilde{\phi}'(\tilde{\mathbf{n}}) = \frac{1}{\sqrt{2}}i\tilde{\omega}_k(\delta\tilde{\phi}_1(\tilde{\mathbf{n}})e^{i\theta_1(\tilde{\mathbf{n}})} - \delta\tilde{\phi}_2(\tilde{\mathbf{n}})e^{i\theta_2(\tilde{\mathbf{n}})}) - \tilde{H}\delta\tilde{\phi}(\tilde{\mathbf{n}}) , \quad (425)$$

where $\tilde{\omega}_k \equiv \sqrt{\tilde{k}^2(\tilde{n}) + \tilde{m}_\phi^2}$ and $\tilde{H} \equiv H/\omega_*$ are the frequency of the mode and the Hubble parameter in program units. In this expression, $\theta_1(\tilde{\mathbf{n}})$ and $\theta_2(\tilde{\mathbf{n}})$ are two random phases which vary uniformly in the range $[0, 2\pi)$ from point to point, and $\delta\tilde{\phi}_1(\tilde{\mathbf{n}})$ and $\delta\tilde{\phi}_2(\tilde{\mathbf{n}})$ are two amplitudes that also vary from point to point, according to a Gaussian distribution with the corresponding variance to reproduce (423). Note that `Latticeeasy` imposes an additional constraint $\delta\tilde{\phi}_1(\tilde{\mathbf{n}}) = \delta\tilde{\phi}_2(\tilde{\mathbf{n}})$ at each lattice site, which could pose problems in non-gaussianity studies (see the discussion in [248]). This is in principle not necessary for real scalar singlets, but the situation is different for charged scalar fields under a gauge group, see the discussion below.

7.2 Charged scalars and gauge fields

Let us now consider the initial conditions for the gauge fields, as well as of the charged fields coupled to them. In this work we are considering scalar fields charged under $U(1)$ and $SU(N) \times U(1)$ gauge groups, which we denote as φ and Φ respectively. We recall that these fields are composed of multiple real components: 2 in the case of φ , and $2N$ in the case of Φ . As the potential only depends on the absolute value of these fields, we can set the same initial amplitude to the homogeneous modes of all their components. In particular, we set for each real component φ_n of the charged field ($n = 0, 1, \dots, 2N - 1$),

$$\varphi_n(\mathbf{x}, t_*) \equiv \frac{|\varphi_*|}{2^{N/2}} + \delta\varphi_*(\mathbf{x}) , \quad (426)$$

$$\dot{\varphi}_n(\mathbf{x}, t_*) \equiv \frac{|\dot{\varphi}_*|}{2^{N/2}} + \delta\dot{\varphi}_*(\mathbf{x}) , \quad (427)$$

where $|\varphi_*|$ and $|\dot{\varphi}_*|$ are the initial homogeneous components of the complex field norm and its time derivative (which must be chosen for each particular model), and $\delta\varphi_*(\mathbf{x})$ and $\delta\dot{\varphi}_*(\mathbf{x})$ are the corresponding initial fluctuations spectra. For simplicity, we will drop the “*” notation from now on. Mimicking the functional form of the scalar singlet fluctuations (424)-(425), we impose to the charged scalar fields in the lattice the following fluctuations,

$$\delta\tilde{\varphi}_n(\tilde{\mathbf{n}}) = \frac{1}{\sqrt{2}}(\delta\tilde{\varphi}_{n1}(\tilde{\mathbf{n}})e^{i\theta_{n1}(\tilde{\mathbf{n}})} + \delta\tilde{\varphi}_{n2}(\tilde{\mathbf{n}})e^{i\theta_{n2}(\tilde{\mathbf{n}})}) , \quad (428)$$

$$\delta\tilde{\varphi}'_n(\tilde{\mathbf{n}}) = \frac{1}{\sqrt{2}}i\tilde{\omega}_{k,n}(\delta\tilde{\varphi}_{n1}(\tilde{\mathbf{n}})e^{i\theta_{n1}(\tilde{\mathbf{n}})} - \delta\tilde{\varphi}_{n2}(\tilde{\mathbf{n}})e^{i\theta_{n2}(\tilde{\mathbf{n}})}) - \tilde{H}\delta\tilde{\varphi}_n(\tilde{\mathbf{n}}) , \quad (429)$$

where $\tilde{\omega}_{k,n} \equiv \omega_{k,n}/\omega_* = \sqrt{\tilde{k}^2 + (\partial^2\tilde{V}/\partial\tilde{\varphi}_n^2)}$ is the initial effective frequency of the field mode of each component in program units. Therefore, for a charged field with $2N$ real components, there are $8N$ functions to be fixed, $(f_{n1}, f_{n2}, \theta_{n1}, \theta_{n2})$ (with $n = 0, 1, \dots, 2N - 1$). In principle, all of these functions should change from lattice point to lattice point according to the probability distributions described above, i.e. Eq. (423)

for f_{n1} and f_{n2} , and uniformly in the range $[0, 2\pi)$ for θ_{n1} and θ_{n2} . However, as we shall see, we will need to impose certain constraints to these functions in order to preserve the Gauss constraints initially.

Let us now consider the fluctuations of the Abelian and non-Abelian gauge fields. We will consider first the fluctuations in the continuum, and generalize to the discretized case later on. For the gauge fields we shall impose

$$A_i(\mathbf{x}, t_*) \equiv 0, \quad (430)$$

$$B_i^a(\mathbf{x}, t_*) \equiv 0, \quad (431)$$

$$\dot{A}_i(\mathbf{x}, t_*) \equiv \delta \dot{A}_{i*}(\mathbf{x}), \quad (432)$$

$$\dot{B}_i^a(\mathbf{x}, t_*) \equiv \delta \dot{B}_{i*}^a(\mathbf{x}), \quad (433)$$

i.e. we impose the amplitude of the gauge fields to be *exactly* zero at all lattice points, while we set an initial spectrum of fluctuations to their time-derivatives (but no homogeneous components). Because of this, the magnetic energy is exactly zero initially, while there will be some amount of electric energy, due to the fluctuations of the time-derivatives. The fluctuations of the charged scalars and gauge fields must be imposed in such a way that the Gauss constraints are initially preserved. If this is achieved, then the dynamical evolution of the field EOM will guarantee that these constraints are preserved at later times. The Gauss constraints for the $SU(2) \times U(1)$ gauge-invariant theory considered in this work are given in (41)-(42). These are

$$\partial_i F_{0i}(\mathbf{x}) = J_0^A(\mathbf{x}), \quad J_0^A(\mathbf{x}) \equiv g_A Q_A^{(\varphi)} \mathcal{I}m[\varphi^* \varphi'] + g_A Q_A^{(\Phi)} \mathcal{I}m[\Phi^\dagger \Phi'], \quad (434)$$

$$(\mathcal{D}_i)_{ab} (G_{0i})^b(\mathbf{x}) = J_0^a(\mathbf{x}), \quad J_0^a(\mathbf{x}) \equiv 2g_B Q_B \mathcal{I}m[\Phi^\dagger T_a \Phi]. \quad (435)$$

where we have set the initial scale factor to $a = 1$ for simplicity. By Fourier transforming both sides of the equation, we get

$$k^i A'_i(\mathbf{k}) = J_0^A(\mathbf{k}), \quad k^i B_i^{a'}(\mathbf{k}) = J_0^a(\mathbf{k}). \quad (436)$$

where $J_0^A(\mathbf{k})$ and $J_0^a(\mathbf{k})$ are the Fourier transforms of each current. Finally, by multiplying each side by k^i , we get

$$A'_i(\mathbf{k}) = i \frac{k_i}{k^2} J_0^A(\mathbf{k}), \quad B_i^{a'}(\mathbf{k}) = i \frac{k_i}{k^2} J_0^a(\mathbf{k}). \quad (437)$$

The complex scalar fields fluctuations $\delta\varphi_*(\mathbf{x})$ and $\delta\dot{\varphi}_*(\mathbf{x})$ are given by Eqs. (428)-(429) (we are still working in the continuum, so all involved functions must be interpreted as functions of the continuous spatial coordinate \mathbf{x} , instead of the lattice point \mathbf{n}). They generate fluctuations on the currents $J_0^A(\mathbf{x})$, and $J_0^a(\mathbf{x})$. Therefore, we can impose fluctuations to the gauge fields in momentum space via Eqs. (437), and then transform back to position space to obtain $\delta\dot{A}_{i*}(\mathbf{x})$, $\delta\dot{B}_{i*}^a(\mathbf{x})$.

The above procedure should, in principle, initially preserve the Gauss constraints. However, we must guarantee that the imposition of Eq. (437) does not add a spurious non-zero homogeneous mode to the gauge fields. We must then check that $J_0^A(\mathbf{k} = \mathbf{0}) = J_0^a(\mathbf{k} = \mathbf{0}) = 0$ (note that if this is not implicitly assumed in (437), we would be dividing the right hand side by zero). For concreteness, let us consider the case of a complex doublet Φ charged under a $U(1) \times SU(2)$ gauge group (the case of the $U(1)$ -charged field φ is just a particular case, as we explain below). The homogeneous modes of the Abelian and non-Abelian currents (434) and (435) can be written in terms of the complex field fluctuations as

$$\begin{aligned} J_0^A(\mathbf{k} = \mathbf{0}) &= \int d^3\mathbf{x} J_0^A(\mathbf{x}) \propto \int d^3\mathbf{k} \mathcal{R}e[\varphi_0^*(\mathbf{k})\varphi'_1(\mathbf{k}) - \varphi'_0(\mathbf{k})\varphi_1^*(\mathbf{k}) + \varphi_2^*(\mathbf{k})\varphi'_3(\mathbf{k}) - \varphi'_2(\mathbf{k})\varphi_3^*(\mathbf{k})] = 0, \\ J_0^1(\mathbf{k} = \mathbf{0}) &= \int d^3\mathbf{x} J_0^1(\mathbf{x}) \propto \int d^3\mathbf{k} \mathcal{R}e[\varphi_3^*(\mathbf{k})\varphi'_0(\mathbf{k}) - \varphi'_3(\mathbf{k})\varphi_0^*(\mathbf{k}) + \varphi_1^*(\mathbf{k})\varphi'_2(\mathbf{k}) - \varphi'_1(\mathbf{k})\varphi_2^*(\mathbf{k})] = 0, \\ J_0^2(\mathbf{k} = \mathbf{0}) &= \int d^3\mathbf{x} J_0^2(\mathbf{x}) \propto \int d^3\mathbf{k} \mathcal{R}e[\varphi_0^*(\mathbf{k})\varphi'_2(\mathbf{k}) - \varphi'_0(\mathbf{k})\varphi_2^*(\mathbf{k}) + \varphi_1^*(\mathbf{k})\varphi'_3(\mathbf{k}) - \varphi'_1(\mathbf{k})\varphi_3^*(\mathbf{k})] = 0, \\ J_0^3(\mathbf{k} = \mathbf{0}) &= \int d^3\mathbf{x} J_0^3(\mathbf{x}) \propto \int d^3\mathbf{k} \mathcal{R}e[\varphi_1^*(\mathbf{k})\varphi'_0(\mathbf{k}) - \varphi'_1(\mathbf{k})\varphi_0^*(\mathbf{k}) + \varphi_2^*(\mathbf{k})\varphi'_3(\mathbf{k}) - \varphi'_2(\mathbf{k})\varphi_3^*(\mathbf{k})] = 0. \end{aligned}$$

One way to guarantee these conditions are respected is to set all the integrands to zero. By solving the corresponding system of linear equations, we get the following three conditions,

$$\text{Re}[\varphi'_m(\mathbf{k})\varphi_0^*(\mathbf{k}) - \varphi_0'(\mathbf{k})\varphi_m^*(\mathbf{k})] = 0, \quad m = 1, 2, 3, \quad (438)$$

which mix the different real components of the doublet. This condition is in general *not* fulfilled when all the functions f_{n1} , f_{n2} , θ_{n1} and θ_{n2} in the scalar fluctuations (424) and (425) are unconstrained. However, by substituting these expressions into Eq. (438), we can prove that the above condition is satisfied when the following relations hold,

$$\delta\varphi_{n1}(\mathbf{k}) = \delta\varphi_{n2}(\mathbf{k}), \quad n = 0, 1, 2, 3, \quad (439)$$

$$\theta_{m2}(\mathbf{k}) = \theta_{02}(\mathbf{k}) + \theta_{m1}(\mathbf{k}) - \theta_{01}(\mathbf{k}), \quad m = 1, 2, 3. \quad (440)$$

The first relation imposes the same amplitude to the left and right waves of each real scalar component's fluctuations. The second line consists in a set of three different constraints that must be imposed to the eight phases appearing in the four components of the doublet. Therefore, in the case of the $SU(2)$ -charged doublet, one can simply generate randomly $\delta\varphi_{01}$, $\delta\varphi_{02}$, $\delta\varphi_{10}$, $\delta\varphi_{20}$, $\delta\varphi_{30}$, θ_{01} , θ_{02} , θ_{11} , θ_{21} , and θ_{31} according to the corresponding probability distributions, and then impose $\delta\varphi_{11}$, $\delta\varphi_{21}$, $\delta\varphi_{31}$, θ_{12} , θ_{22} and θ_{32} via Eqs. (439)-(440). This procedure guarantees that the homogeneous modes of the current is zero initially, and hence that the Gauss laws are preserved¹⁰.

Let us remark that a similar procedure can be applied to the simpler case of a $U(1)$ -charged field φ . In this case there are only two real scalar components, $\delta\varphi_0(\mathbf{k})$ and $\delta\varphi_1(\mathbf{k})$, so there are only three constraints to be fulfilled: $\delta\varphi_{01}(\mathbf{k}) = \delta\varphi_{02}(\mathbf{k})$, $\delta\varphi_{11}(\mathbf{k}) = \delta\varphi_{12}(\mathbf{k})$, and $\theta_{12}(\mathbf{k}) = \theta_{02}(\mathbf{k}) + \theta_{11}(\mathbf{k}) - \theta_{01}(\mathbf{k})$. The procedure to set the initial fluctuations is therefore analogous to the $SU(2) \times U(1)$ case.

Finally, let us consider the translation of this procedure developed in the continuum to the lattice. For charged scalar fields, the only difference is that the different functions $\delta\varphi_{ab}$ and θ_{ab} are only defined in each lattice point, instead of being continuum functions. Therefore, some of these parameters must be randomly generated at each lattice site $\tilde{\mathbf{n}}$ according to the corresponding probability distribution, while the others must be imposed at each lattice site via the constraint equations (439)-(440). On the other hand, for gauge fields we must start from the discrete Gauss equations. As we are not imposing fluctuations to the amplitude of the gauge fields, the discrete Gauss constraints (294) and (376) simply become, in position space and in physical variables,

$$\sum_i \Delta_i^- \Delta_0^+ A_i(\mathbf{n}) = J_0^A(\mathbf{n}), \quad \sum_i \Delta_i^- \Delta_0^+ B_i^a(\mathbf{n}) = J_0^a(\mathbf{n}), \quad (a = 1, 2, 3). \quad (441)$$

By taking a discrete Fourier transform in both sides of the equation, we get

$$\Delta_0^+ A_i(\tilde{\mathbf{n}}) = i \frac{k_{\text{Lat},i}^-}{(k_{\text{Lat},i}^-)^2} J_0^A(\tilde{\mathbf{n}}), \quad \Delta_0^+ B_i^a(\tilde{\mathbf{n}}) = i \frac{k_{\text{Lat},i}^-}{(k_{\text{Lat},i}^-)^2} J_0^a(\tilde{\mathbf{n}}), \quad (a = 1, 2, 3). \quad (442)$$

Note that, as we are taking the backward spatial derivative Δ_i^- in Eq. (441), then the corresponding complex lattice momentum $k_{\text{Lat},i}^-$ must appear in Eq. (442) after Fourier transforming, which is defined in Eq. (74). Therefore, in order to set the fluctuations of the gauge field derivatives in the lattice, we first add the fluctuations to the real components to compute the corresponding currents, then transform the currents to momentum space and impose expressions (442) to the gauge fields, and finally transform the gauge fields back to position space.

¹⁰Another possibility to guarantee constraints (438) would be to just impose the relations, $\varphi'_m(\mathbf{k}) = \varphi'_0(\mathbf{k})\varphi_m^*(\mathbf{k})/\varphi_0^*(\mathbf{k})$ directly for $m = 1, 2, 3$, where the functions in the *rhs* of this expression are to be generated according to the probability distributions (424) and (425), without imposing the constraints (439) and (440). However, using this procedure, the fluctuations generated for the 0th-component have typically very different amplitudes than for the other components, of one or more orders of magnitude of difference. Moreover, the spectra of the 0th-component depends very much on the particular random realization of the fields. This makes us prefer the procedure described in the bulk text.

8 A working example: the $SU(2) \times U(1)$ gauge invariant inflaton

In order to illustrate some of the techniques and concepts explained previously, we study in this section the dynamics of a specific scalar-gauge field theory using lattice simulations. In particular, we are going to consider an observationally viable single-field inflationary model, with monomial potential energy $V(\phi) \propto \phi^p$ around the minimum, and a 'flattening' at large field amplitudes. We will study the post-inflationary stage of preheating, which is triggered by the inflaton oscillations around the minimum of its potential. As an example of the gauge-invariant lattice techniques presented above, we will couple the inflaton to both scalar and gauge fields (which we denote indistinctly as *daughter fields* from now on), and study the transfer of energy from the inflaton to these fields.

The structure of this section is as follows. First, we present in Section 8.1 the details of how inflation and preheating proceed in the model under consideration. In particular, we will review the two resonant phenomena that govern the post-inflationary dynamics: parametric resonance of the daughter field(s), and self-resonance of the inflaton. After that, we present the results of our lattice simulations. In Section 8.2 we consider the case of a $U(1)$ gauge invariant inflaton, coupled to an Abelian gauge field through a covariant derivative. In Section 8.3 we consider the case of a $SU(2) \times U(1)$ gauge invariant inflaton, coupled simultaneously to a $SU(2) \times U(1)$ gauge sector (formed by Abelian and non-Abelian gauge fields) and a massless scalar singlet.

8.1 Model details

Let us consider a scalar field ϕ with the following potential energy,

$$V(\phi) = \frac{\Lambda^4}{p} \tanh^p \left(\frac{|\phi|}{M} \right), \quad (443)$$

where Λ and M have dimensions of energy, and p is a positive number. The particular form of this potential is based on α -attractor models of inflation, see Ref. [271]. The field amplitude is introduced as an absolute value, so the potential has a minimum at $\phi = 0$ independently of the choice of p . Similarly, the potential develops a plateau $V(\phi) \rightarrow \Lambda^4/p$ at large field amplitudes $\phi \gg M$. We take ϕ as the *inflaton* field responsible of the early inflationary stage of the Universe, and consider in detail the following stage of preheating. Although the numerical values of the model parameters (Λ , M , p) are in principle independent, they are in practice constrained by the observed amplitude of the scalar perturbations in the CMB, i.e. $\Lambda = \Lambda(M, N_{\text{CMB}}, p)$, with $N_{\text{CMB}} = 50 - 60$ the number of e-folds between the end of inflation and the horizon crossing of the relevant perturbations.

The potential (443) can be expanded around the minimum as the following monomial function,

$$V(\phi) = \frac{1}{p} \lambda \mu^{4-p} |\phi|^p, \quad \lambda \mu^{4-p} \equiv \Lambda^4 M^{-p}, \quad (444)$$

where λ is dimensionless and μ has dimensions of energy. The product of parameters $\lambda \mu^{4-p}$ in Eq. (444) is fixed in terms of (Λ , M , p) to match the exact potential (443) in the limit $\phi \ll M$. The field value that separates the monomial and plateau regimes in the exact potential can be estimated by computing its inflection point, i.e. the amplitude at which $V_{,\phi\phi}(\phi_i) = 0$. It is given by

$$\phi_i = M \operatorname{Marcsinh} \left(\sqrt{\frac{p-1}{2}} \right). \quad (445)$$

The monomial potential (444) is a very good approximation to the exact potential (443) for field amplitudes $\phi \ll M$. In particular, in the limit $M \rightarrow \infty$, the inflaton potential (443) recovers the monomial function (444) exactly, recovering this way the well-known chaotic inflation scenario.

Inflation takes place during the slow-roll decay of the inflaton, which starts at large field amplitudes and proceeds towards the minimum of the potential. The inflaton acquires a sizable effective mass approximately

when the slow-roll conditions break down, and as a consequence, starts oscillating around the minimum. The field amplitude ϕ_* when the slow-roll parameter $\epsilon_V \equiv m_{\text{pl}}^2 V_{,\phi}^2 / (2V^2)$ obeys $\epsilon_V(\phi_*) = 1$ is

$$\phi_* \equiv \frac{M}{2} \text{arcsinh} \left(\frac{\sqrt{2} p m_{\text{pl}}}{M} \right) \xrightarrow{M \rightarrow \infty} \frac{p m_{\text{pl}}}{\sqrt{2}}, \quad (446)$$

where we have also written the corresponding inflaton amplitude in the limit $M \rightarrow \infty$. In this model, inflation happens for field amplitudes $\phi \gtrsim \phi_*$, while the oscillatory regime which follows takes place for $\phi \lesssim \phi_*$. Therefore, the field amplitude $\phi = \phi_*$ constitutes a natural initial condition for our lattice simulations. If $M \gtrsim m_p$, we have that $\phi_* \ll \phi_i$, so the inflaton is already in the positive-curvature region of the potential when the slow-roll regime breaks, and does not enter into the tachyonic region during the subsequent inflaton oscillations. In that case, we can safely take the monomial potential (444) as a very good approximation to the exact potential (443) during preheating. On the other hand, if $M \lesssim m_p$ we have that $\phi_* \gg \phi_i$, so the inflaton does enter into the tachyonic region during at least the first oscillations. Here we consider only the first scenario, so our results do not depend very much on the details of the transition between the monomial function and the plateau. In particular, we will fix the value $M = 10 m_p$ in the lattice simulations, whose results we present below.

The equation of motion of the homogeneous component of the inflaton in the limit $M \rightarrow \infty$ is

$$\ddot{\phi} + 3H\dot{\phi} + \Omega^2(\phi)\phi = 0, \quad \Omega(\phi) \equiv \sqrt{\lambda} \mu^{\frac{4-p}{2}} |\phi|^{\frac{p-2}{2}}, \quad (447)$$

which corresponds to a harmonic oscillator with time-dependent effective frequency $\Omega(\phi)$ and friction term $\propto 3H\dot{\phi}$, induced by the expansion of the universe. The oscillation frequency is constant for $p = 2$, but depends explicitly on the field amplitude (and hence on time) for $p \neq 2$. This equation can be solved together with the Friedmann equation (51) in the homogeneous approximation, with initial conditions deep in slow-roll. During inflation we have $\phi \gg \phi_*$, or equivalently, $H(\phi) \gg \Omega(\phi)$. Eventually, when the field amplitude becomes approximately $\phi \simeq \phi_*$, the condition $H(\phi) = \Omega(\phi)$ holds, and the inflaton starts oscillating. The solutions for the inflaton amplitude and scale factor can be approximated during the oscillatory regime as [272]

$$\phi(t) \simeq \Phi(t) F(t), \quad \Phi(t) = \Phi_* \left(\frac{t}{t_*} \right)^{-2/p}, \quad (448)$$

$$a(t) \propto a_* \left(1 + \frac{3p}{2+p} H_* t \right)^{\frac{2+p}{3p}} \sim t^{\frac{2+p}{3p}}. \quad (449)$$

In Eq. (448), $\Phi(t)$ is a decaying amplitude that starts at a certain time t_* from some initial amplitude $\Phi_* \simeq \phi_*$, while $F(t)$ is an oscillatory function that is periodic for $p = 2$ and non-periodic for $p \neq 2$. The quantities a_* and H_* are the scale factor and Hubble parameter at time $t = t_*$. Note that this field configuration gives rise, for times $H_* t \gg 1$, to a matter/radiation-dominated equation of state for $p = 2, 4$ respectively.

In order to do lattice simulations of this system, we have to appropriately fix the program variables (f_* , α , ω_*), defined in Eq. (160). First, we want to use variables that guarantee that typical numbers of certain physical quantities (such as field amplitudes or range of excited momenta) are of order unity. And second, as the evolution algorithms discussed above assume a constant time step, we want to use a program time variable that guarantees an approximately constant oscillation frequency. This way, each oscillation period is well resolved independently of how long the simulation time is. In this regard, we get from Eqs. (448) and (449) that the inflaton oscillation frequency (defined in Eq. 447) scales with the scale factor as

$$\Omega(\phi) \sim \omega_* \left(\frac{t}{t_*} \right)^{4/p-2} \sim \left(\frac{a}{a_*} \right)^{\frac{-3(p-2)}{(p+2)}}, \quad \omega_* \equiv \sqrt{\lambda} \mu^{\frac{4-p}{2}} \phi_*^{\frac{p-2}{2}}, \quad (450)$$

where ω_* is the oscillation frequency at the onset of oscillations. Therefore, a convenient choice of program variables is

$$\alpha = 3 \frac{p-2}{p+2}, \quad f_* \equiv \phi_*, \quad \omega_* \equiv \Lambda^2 M^{-\frac{p}{2}} \phi_*^{\frac{p-2}{2}}. \quad (451)$$

Note that for this choice of units, program time corresponds to cosmic/conformal time for $p = 2, 4$ respectively, up to a dimensionful constant factor. The corresponding program potential $\tilde{V}(\tilde{\phi})$ of our model, defined in Eq. (161), can be then written as

$$\begin{aligned}\tilde{V}(\tilde{\phi}) &\equiv \frac{1}{f_*^2 \omega_*^2} V(\phi) \\ &= \frac{1}{p} \left(\frac{M}{\phi_*} \right)^p \tanh^p \left(\frac{\phi_* |\tilde{\phi}|}{M} \right),\end{aligned}\quad (452)$$

and its first and second derivatives are

$$\frac{\partial \tilde{V}}{\partial \tilde{\phi}} = 2 \left(\frac{M}{\phi_*} \right)^{p-1} \frac{\tanh^p(\phi_* |\tilde{\phi}|/M)}{\sinh(2\phi_* |\tilde{\phi}|/M)} \text{sgn}(\tilde{\phi}), \quad (453)$$

$$\frac{\partial^2 \tilde{V}}{\partial \tilde{\phi}^2} = 4 \left(\frac{M}{\phi_*} \right)^{p-2} \left(p - \cosh(2\phi_* |\tilde{\phi}|/M) \right) \frac{\tanh^p(\phi_* |\tilde{\phi}|/M)}{\sinh^2(2\phi_* |\tilde{\phi}|/M)}, \quad (454)$$

where $\text{sgn}(\tilde{\phi})$ is the sign function.

8.1.1 Preheating

Let us now review how preheating proceeds in this model. The post-inflationary dynamics of an inflaton with potential (443) has been studied with lattice simulations in the past: in the absence of inflaton interactions to other species in [164, 185], with interactions to a second scalar field with non-canonical kinetic terms in [187], and more recently, with quadratic interactions to a daughter field in [188]. In all of these studies, the fields involved were real scalars. Here, in order to illustrate the gauge-invariant lattice techniques introduced in the previous sections, we couple for the first time the inflaton field to a gauge structure.

Let us start by considering a daughter massless scalar field χ , coupled to the inflaton via a quadratic interaction. The potential of such a theory can be written as

$$V(\phi, \chi) = \frac{1}{p} \lambda \mu^{4-p} |\phi|^p + \frac{1}{2} g^2 \phi^2 \chi^2, \quad (455)$$

where g is a dimensionless coupling constant, and we have taken the limit $M \rightarrow \infty$ in the inflaton potential. When inflation ends at the amplitude $\phi = \phi_*$, the energy budget of the Universe is dominated by the homogeneous component of the inflaton. Therefore, the evolution of the inflaton amplitude and scale factor can be described approximately by Eqs. (448)-(449) during the first inflaton oscillations, and it is natural to also use the program variables defined in (451) in this context. With this choice, the program potential (again in the limit $M \rightarrow \infty$) is

$$\begin{aligned}\tilde{V}(\tilde{\phi}, \tilde{\chi}) &\equiv \frac{1}{f_*^2 \omega_*^2} V(\tilde{\phi}, \tilde{\chi}) \\ &= \frac{1}{p} |\tilde{\phi}|^p + \frac{1}{2} q_* \tilde{\phi}^2 \tilde{\chi}^2,\end{aligned}\quad (456)$$

where the *resonance parameter* q_* is defined as the following dimensionless ratio,

$$q_* \equiv \frac{g^2 \phi_*^2}{\omega_*^2}. \quad (457)$$

The first and second derivatives of the program potential with respect to the two fields are

$$\frac{\partial \tilde{V}}{\partial \tilde{\phi}} = |\tilde{\phi}|^{p-2} \tilde{\phi} + q_* \tilde{\chi}^2 \tilde{\phi}, \quad \frac{\partial \tilde{V}}{\partial \tilde{\chi}} = q_* \tilde{\phi}^2 \tilde{\chi}, \quad (458)$$

$$\frac{\partial^2 \tilde{V}}{\partial \tilde{\phi}^2} = (p-1) |\tilde{\phi}|^{p-2} + q_* \tilde{\chi}^2, \quad \frac{\partial^2 \tilde{V}}{\partial \tilde{\chi}^2} = q_* \tilde{\phi}^2. \quad (459)$$

During the first stages of preheating, the linearized fluctuations of both fields have time-dependent effective masses, induced by the oscillations of the inflaton homogeneous mode. These masses vary non-adiabatically each time the inflaton crosses zero, which triggers an exponential growth of the amplitude of the field modes for certain bands of momenta. More specifically, the post-inflationary dynamics is governed by the interplay of two different resonant phenomena, which may or may not be present for certain choices of model parameters. These are:

- **Self-resonance of the inflaton:** The inflaton has a time-dependent effective mass $m_\phi^2 \propto |\phi|^{p-2}$ for $p \neq 2$, see Eq. (455). In these cases, the (conformally rescaled) inflaton fluctuations can grow exponentially during this regime as $|\delta\tilde{\phi}_k|^2 \propto e^{2\nu_k z}$, where $\mathcal{R}e(\nu_k) > 0$ for certain momenta bands, and $\nu_k \equiv \nu_k(k; p)$ the corresponding so-called Floquet index. These bands are always narrow for all reasonable values of p , $\Delta k/\bar{k} \lesssim 0.1$ (with \bar{k} the average momentum inside the band), and the maximum Floquet index within each band is maximum $\mathcal{R}e(\nu_k) \lesssim 0.035$.
- **Parametric resonance of the daughter field:** Similarly, the daughter field also has a time-dependent mass $m^2 \propto g^2 \chi^2$ for any of choice of p as long as the quadratic interaction is present, see Eq. (455). Due to this, the (conformally rescaled) daughter field fluctuations can also grow exponentially as $|\delta\tilde{\chi}_k|^2 \propto e^{2\mu_k z}$, with $\mathcal{R}e(\mu_k) > 0$ for certain ranges of momenta, and $\mu_k \equiv \mu_k(k, q_*; p)$ the corresponding Floquet index. The key parameter signaling the strength of the resonance is the *effective resonance parameter* q_{res} , which is defined as

$$q_{\text{res}} \equiv q_* a^{\frac{6(p-4)}{p+2}}, \quad (460)$$

and evolves with the expansion of the universe. If $q_{\text{res}} \gtrsim 1$, the parametric resonance is *broad*: the width of the resonance bands for all values of p is $\Delta k/\bar{k} \sim 1$, and the maximum Floquet index within those bands is typically $\mathcal{R}e(\mu_k) \sim 0.1 - 0.2$. In this case, the maximum momenta excited by the main resonance band scales as $k \sim q_{\text{res}}^{1/4} \omega_*$, modulo some multiplying scale factor term. On the other hand, if $q_{\text{res}} \ll 1$, the width of the bands is very small $\Delta k/\bar{k} \ll 1$, and we say that the resonance is *narrow*. This second effect cannot be typically captured in the lattice due to lack of resolution. Note that q_{res} changes with time, so the type of resonance may change during preheating: it decreases with time for $p < 4$, grows for $p > 4$, and remains constant for $p = 4$. Therefore, the type of parametric resonance (either broad or narrow) can change as the Universe expands.

If broad parametric resonance of the daughter field is present (i.e. if $q_{\text{res}} > 1$), it is almost always a stronger effect than the inflaton self-resonance. However, parametric resonance eventually becomes narrow for $p < 4$, even if it was broad initially. This contrasts with inflaton self-resonance, which is always present independently of the value of p , as long as $p \neq 2$. The different behaviour of these phenomena for different model parameters is key to understand how energy distributes between the different field sectors during preheating, as well as the evolution of the post-inflationary evolution of the equation of state.

Let us now consider a scenario in which the inflaton (in this case a complex doublet Φ) is coupled to a $SU(2) \times U(1)$ gauge sector via a gauge-invariant covariant derivative. Fortunately, the simpler scalar theory described above constitutes an excellent proxy for this more complex model, as the dominant interaction term generated by the covariant derivative is also quadratic. In order to see this, let us consider the covariant derivative term in action (8), which contains the interaction between the inflaton and the gauge fields. It can be expanded as

$$(\vec{D}_\mu \Phi)^\dagger (\vec{D}^\mu \Phi) = (\partial_\mu \Phi)^\dagger \partial^\mu \Phi + \frac{1}{4} Q_A^2 g_A^2 |\Phi|^2 |\vec{A}|^2 + \frac{1}{4} Q_B^2 g_B^2 |\Phi|^2 \sum_a |\vec{B}^a|^2 + Q_A g_A Q_B g_B \sum_a \vec{A} \cdot \vec{B}^a (\Phi^\dagger T_a \Phi) \dots, \quad (461)$$

where we have ignored terms of the type $\sim (\partial_\mu \Phi) \Phi$, which are subdominant during the early linear regime. The first term in Eq. (461) gives rise to the usual Laplacian in the field equations. The second and third terms constitute quadratic interactions between the inflaton and the Abelian and non-Abelian gauge fields

Simulation	p	M/m_p	Λ^4	q_*	N	\tilde{k}_{IR}	$\delta\tilde{t}$
U(1)	2	10	$1.8 \cdot 10^{65}$	$4 \cdot 10^4$	128	4	$5 \cdot 10^{-3}$
U(1)	4	10	$4.3 \cdot 10^{65}$	10^2	128	0.6	10^{-2}
U(1)	6	10	$6.8 \cdot 10^{65}$	1	128	0.15	$7 \cdot 10^{-4}$
$SU(2) \times U(1) + \chi$	2	10	$1.8 \cdot 10^{65}$	$4 \cdot 10^4$	128	4	$3 \cdot 10^{-4}$
$SU(2) \times U(1) + \chi$	4	10	$4.3 \cdot 10^{65}$	10^2	128	0.6	10^{-2}

Table 3: Benchmark model and lattice parameters used in the U(1) and $SU(2) \times U(1) + \chi$ gauge simulations

respectively. These are analogous to the quadratic interaction of Eq. (455) between the inflaton and a secondary scalar field, with the identification $g \rightarrow Q_A g_A/2$ and $g \rightarrow Q_B g_B/2$ in each case. Mimicking the notation of Eq. (457), it is then natural to define the resonance parameters of the Abelian and non-Abelian gauge fields as

$$q_{A*} \equiv \frac{Q_A^2 g_A^2 |\Phi_*|^2}{4\omega_*^2}, \quad q_{B*} \equiv \frac{Q_B^2 g_B^2 |\Phi_*|^2}{4\omega_*^2}, \quad (462)$$

where $|\Phi_*| \equiv \phi_*$ is the amplitude of the inflaton norm at the end of inflation, which we set equal to Eq. (446). Therefore, we can use the scalar theory as a proxy to study the equivalent $U(1)$ or $SU(2)$ gauge-invariant theories, at least during the initial linear regime. In particular, in the gauge scenario the inflaton can also develop fluctuations via self-resonance, while the gauge fields can also get excited via parametric resonance. However, non-linearities become relevant at later times, so important differences between the scalar and gauge theories may appear later on. Finally, the fourth term in Eq. (461) appears when the inflaton is coupled to a full $SU(2) \times U(1)$ gauge sector. One can prove that the effect of such term is to couple the EOM of the Abelian and non-Abelian gauge fields, so that they experience parametric resonance with a common resonance parameter $q_{\text{eff}*} = q_{A*} + q_{B*}$. The details of the parametric resonance process in the presence of Abelian and non-Abelian gauge fields, as well as the relevance of that term, will be discussed in more detail in an upcoming work [273]. This goes beyond the objective of this manuscript, which is mainly to illustrate lattice gauge-invariant techniques in a specific physics model.

8.2 Lattice simulations: U(1) gauge interactions

We now proceed to discuss the results from our lattice simulations. We start by considering the post-inflationary dynamics of a complex inflaton field $\varphi \equiv \frac{1}{\sqrt{2}}(\varphi_0 + i\varphi_1)$ with potential energy (443) [where we must substitute $\phi \rightarrow \varphi$], coupled to an Abelian gauge boson A_μ via a gauge-invariant covariant derivative. The model and lattice parameters considered in the simulations are provided in Table 8.2. We have chosen a set of three representative power-law coefficients, $p = 2, 4, 6$. In each case, the resonance parameter q_{A*} is fixed to guarantee broad parametric resonances at the onset of the inflaton oscillatory regime. We have fixed the value $M = 10m_p$ as a benchmark, which guarantees that the inflationary slow-roll condition breaks down in the positive-curvature region of the potential. As described above, the initial exponential growth of the gauge field modes during broad parametric resonance takes place mainly within an infrared band of width $p \lesssim p_* \equiv q_{A*}^{1/4} \omega_*$ (modulo a multiplying scale factor term). However, when the energy transferred to the gauge fields is large enough, they backreact onto the inflaton homogeneous condensate, which triggers a propagation of the spectra of all fields to the ultraviolet. Due to this, the minimum momenta \tilde{k}_{IR} and number of points per lattice side N are chosen, in each case, to guarantee that both the initial infrared growth and the following ultraviolet propagation are well resolved in the lattice.

We start by showing in Fig. 1 the evolution of the volume-averaged inflaton norm $|\varphi| \equiv \sqrt{\varphi_0^2 + \varphi_1^2}$, equation of state $w \equiv p/\rho$, and scale factor as a function of program time $\tilde{\eta}$ [$d\tilde{\eta} \equiv a^{-\alpha} \omega_* dt$, c.f. (160)], for each of the three power-law coefficients $p = 2, 4, 6$. As described above, the inflaton can be approximated as a homogeneous condensate during its first oscillations, and the evolution of the inflaton amplitude and scale factor are approximately given by Eqs. (448)-(449). From these expressions, we deduce that the amplitude

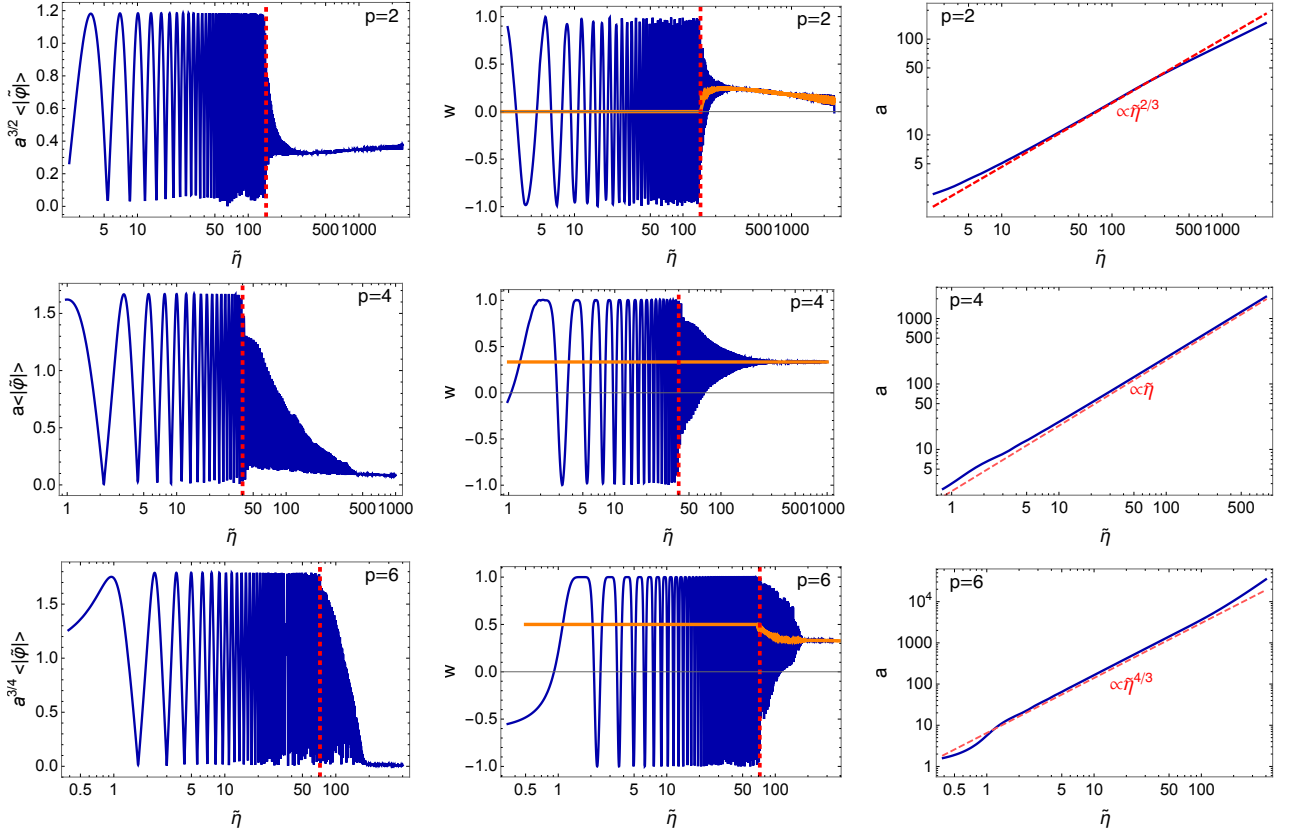


Figure 1: Average values of the scalar field norm, equation of state w , and scale factor as a function of time, for three $U(1)$ gauge simulations with $p = 2$ (top row), $p = 4$ (middle row), and $p = 6$ (bottom row). The backreaction time $\tilde{\eta}_{\text{br}}$ in indicated for the first two quantities with a vertical dashed line. In the scale factor panels we have added the prediction $a \sim \tilde{\eta}^{\frac{p+2}{6}}$, coming from the linear regime of homogeneous inflaton oscillations.

of the inflaton oscillations scales initially as $|\varphi| \sim a^{\frac{-6}{p+2}}$, so $|\varphi| \sim a^{-3/2}, a^{-1}, a^{-3/4}$ for $p = 2, 4, 6$, respectively. Therefore, in the Figure we have multiplied the inflaton norm by the inverse of these factors, so the amplitude of the rescaled inflaton oscillations is initially constant. Although the inflaton homogeneous regime holds qualitatively well during the first inflaton oscillations, the energy stored in gauge fields and inflaton gradients grows exponentially due to broad parametric resonance. Eventually, the fraction of transferred energy is so large that they backreact onto the inflaton, destroying the homogeneity of the condensate. We identify this time scale as the *backreaction time* $\tilde{\eta}_{\text{br}}$. From the simulation, we get $\tilde{\eta}_{\text{br}} \simeq 130, 40, 70$ for $p = 2, 4, 6$ respectively.

Let us now focus on the post-inflationary evolution of the equation of state $w \equiv p/\rho$, i.e. the ratio between the (volume-averaged) pressure and energy densities of the system. Initially, the inflaton oscillates coherently around the minimum, which gives rise to similar oscillations in the equation of state in the range $-1 < w < 1$. From Eqs. (448)-(449), we can compute that the *effective* (i.e. oscillation-averaged) equation of state in this regime is approximately $\bar{w} \equiv (p-2)/(p+2)$. This corresponds to $\bar{w} = 0, 1/3, 1/2$ for $p = 2, 4, 6$ respectively, which agrees with our lattice results, see the middle column of Fig. 1. After backreaction, the equation of state stops oscillating, and slowly evolves towards the asymptotic values $w \rightarrow 0$ (for $p = 2$) and $w \rightarrow 1/3$ (for $p = 4, 6$). We will be able to understand these results better in light of the evolution of the energy distribution, which we discuss below. We also show the scale factor as a function of program time in the right panels of Fig. 1. We know that during the initial linear regime, the scale factor evolves in cosmic time as $a \sim t^{\frac{2+p}{3p}}$ [c.f. (449)]. By substituting this expression in the program time definition (160), we get that the scale factor evolves as $a \sim \tilde{\eta}^{\frac{p+2}{6}}$ in terms of program time, in agreement to what we see in the lattice.

We can understand better the evolution of these quantities if we focus on the evolution of the energy distribution. In the left panels of Fig. 2 we show the total energy of the system as a function of time (Eq. 48), for the considered power-law coefficients $p = 2, 4, 6$. We also depict the evolution of each of its individual contributions: the kinetic, gradient, and potential energies of the inflaton, as well as the electric and magnetic energies of the gauge fields (see Eq. (50) for their exact expressions). As described above, the effective equation of state during the initial linear regime is $\bar{w} \simeq (p-2)/(p+2)$, so the total energy decays during the initial regime as $\rho \sim a^{-3(1+\bar{w})} = a^{\frac{-6p}{p+2}}$, which corresponds to $\rho \sim a^{-3}, a^{-4}, a^{-4.5}$ for $p = 2, 4, 6$, respectively. Therefore, we have multiplied the energies by the inverse of those factors, so that the rescaled total energy is constant initially. We also depict in the right panels of Fig. 2 the evolution of the energy ratios $\epsilon_i \equiv \tilde{\rho}_i/\tilde{\rho}$ for the same simulations, i.e. the relative contribution of each of the energy components to the total energy. By construction, the sum of all ratios is one.

As expected, the energy budget of the Universe is initially dominated by the kinetic and potential energies of the inflaton, while the other energies are subdominant, i.e. $\langle E_K^A \rangle, \langle E_G^A \rangle, \langle E_G^\varphi \rangle \ll \langle E_K^\varphi \rangle, \langle E_V \rangle$. However, a very small fraction of the initial energy is stored in the electric and inflaton gradient energies, due to the spectrum of fluctuations imposed to φ and \dot{A}_i . In contrast, the initial magnetic energy is exactly zero (up to machine precision), as we do not set fluctuations to the amplitude of the gauge field A_i , see Eqs. (430)-(433). In any case, these energies soon start growing exponentially due to parametric resonance, as seen in the three simulations. These energies become sizable approximately at the backreaction time $\tilde{\eta} \simeq \tilde{\eta}_{\text{br}}$, and the inflaton homogeneous condensate gets destroyed via backreaction effects. From then on, non-linear effects become relevant, and the system eventually achieving a stationary regime at late times. Remarkably, we observe that the inflaton gets virialized very quickly after inflation, with their oscillation-averaged energies satisfying the relation $\langle E_K^\varphi \rangle \simeq \langle E_G^\varphi \rangle + \frac{p}{2} \langle E_V \rangle$, for the three cases $p = 2, 4, 6$. Similarly, we observe equipartition between the electric and magnetic energies at late times, $\langle E_K^A \rangle \simeq \langle E_G^A \rangle$.

It is very interesting to analyze how the energy is distributed at very late times in the simulation, i.e. well within the non-linear regime. This was studied recently in Ref. [188] in the context of a real singlet inflaton with the same potential as here, coupled to a massless scalar singlet via a quadratic interaction. Although here we are considering a gauge sector, the explanation developed in Ref. [188] also applies here. In particular, we find that the energy distribution at late times is determined by the choice of p in the inflaton potential. For $p = 2$, the inflaton cannot get excited via self-resonance, but the daughter field does get excited via broad parametric resonance because $q_{A*} > 1$. However, the effective resonance parameter (460) decreases with time, so parametric resonance eventually becomes narrow. After that, the inflaton kinetic and potential energies dilute as matter, while the other ones dilute as radiation or faster. Due to this, at very late times we get the energy ratios $\epsilon_K^\varphi, \epsilon_V \rightarrow 0.5$, with the other ratios becoming negligible. This explains why the effective equation of state goes to $w \rightarrow 0$ at late times in Fig. 1. On the other hand, for $p = 4, 6$, both the inflaton and the gauge fields are always being excited resonantly at late times: inflaton self-resonance is always present for $p > 2$, while parametric resonance is always broad at late times because q_{res} is either constant (for $p = 4$) or grows with time (for $p > 4$). Therefore, the energy contributions of both field sectors are sizeable at late times. In the case $p = 4$, the inflaton possesses 60% of the total energy of the system at very late times (divided by half between kinetic and gradient energy), while the gauge fields possess the other 40% (divided also by half between electric and magnetic energy). Moreover, the inflaton potential energy becomes negligible, which explains why the effective equation of state goes to $w \rightarrow 1/3$ at late times in Fig. 1. We expect this final distribution to be quite independent on the choice of q_* , as will be seen in Ref. [273] in a slightly different context. This contrasts with the simulations of the analogous scalar theory simulated in Ref. [188], where the energy is distributed 50%-50% between the inflaton and the daughter field. On the other hand, in the gauge simulations for $p = 6$ we do observe equipartition between inflaton and gauge energies at late times, although the simulation is not long enough in this case to determine if this distribution will hold for later times, or if it will slowly evolve towards the 60%-40% distribution observed for $p = 4$.

Finally, we show in Fig. 3 the spectra of the electric and magnetic fields for the three power-law potentials $p = 2, 4, 6$ considered here. As expected from the linear analysis, mainly field modes within an infrared band $\tilde{k} \equiv k/\omega_* \lesssim q_*^{1/4}$ grow exponentially during the initial linear regime, at times $\tilde{\eta} < \tilde{\eta}_{\text{br}}$. However, when backreaction happens at time $\tilde{\eta} = \tilde{\eta}_{\text{br}}$, the growth of the infrared band saturates, and the different fields

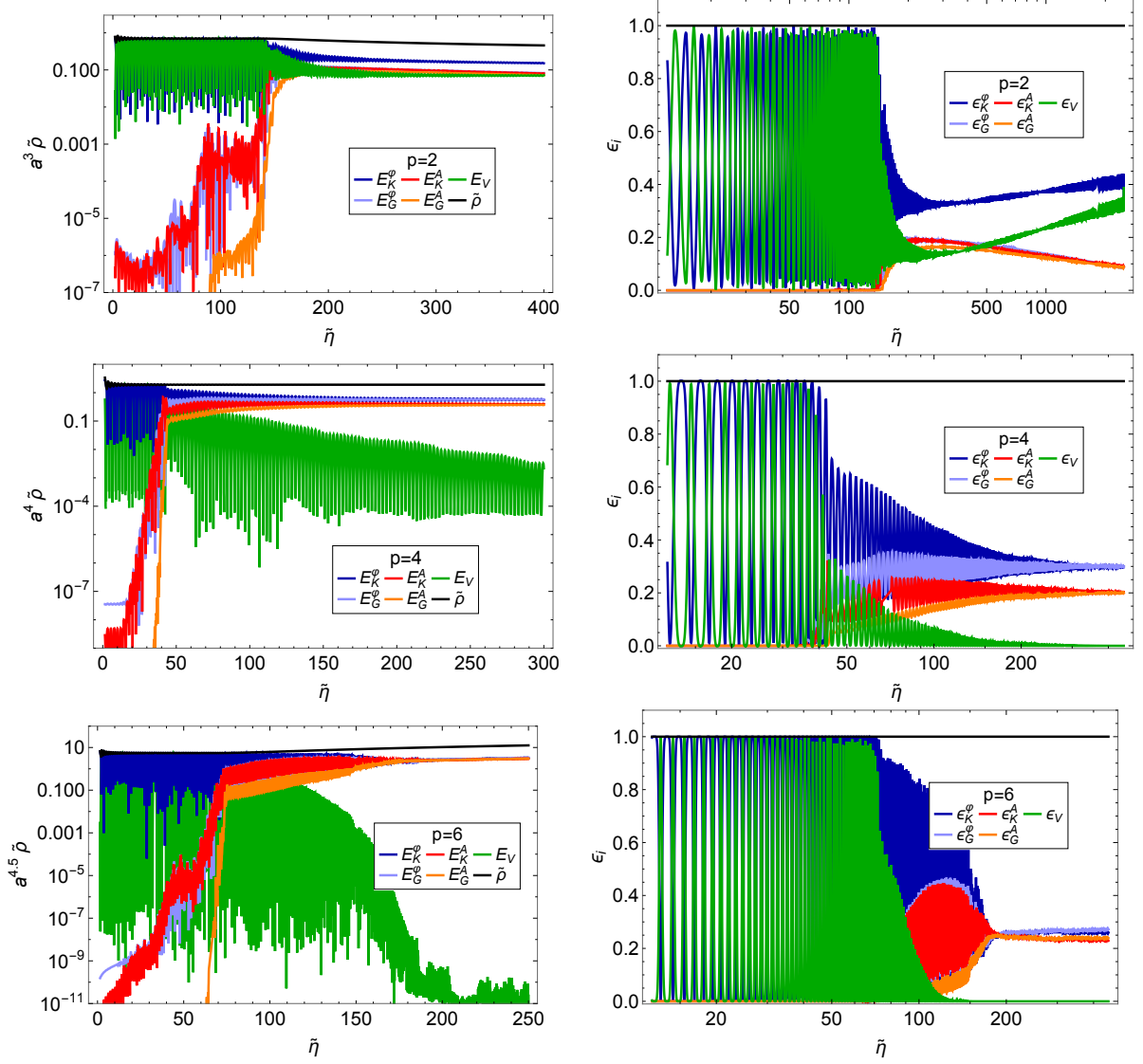


Figure 2: Left panel: Evolution of the total energy $\tilde{\rho} \equiv \rho/(f_*^2 \omega_*^2)$ for the $U(1)$ gauge simulation and $p = 2, 4, 6$, as well as of each of its individual contributions: kinetic, gradient, and potential energies of the inflaton, as well as electric and magnetic energies of the gauge field. These quantities are multiplied by the factor $\sim a^{\frac{6p}{p+2}}$. Right panel: Evolution of the energy ratios $\epsilon_i \equiv \tilde{\rho}_i / \tilde{\rho}$ for the same simulations as in corresponding left panel. The sum of all ratios is one.

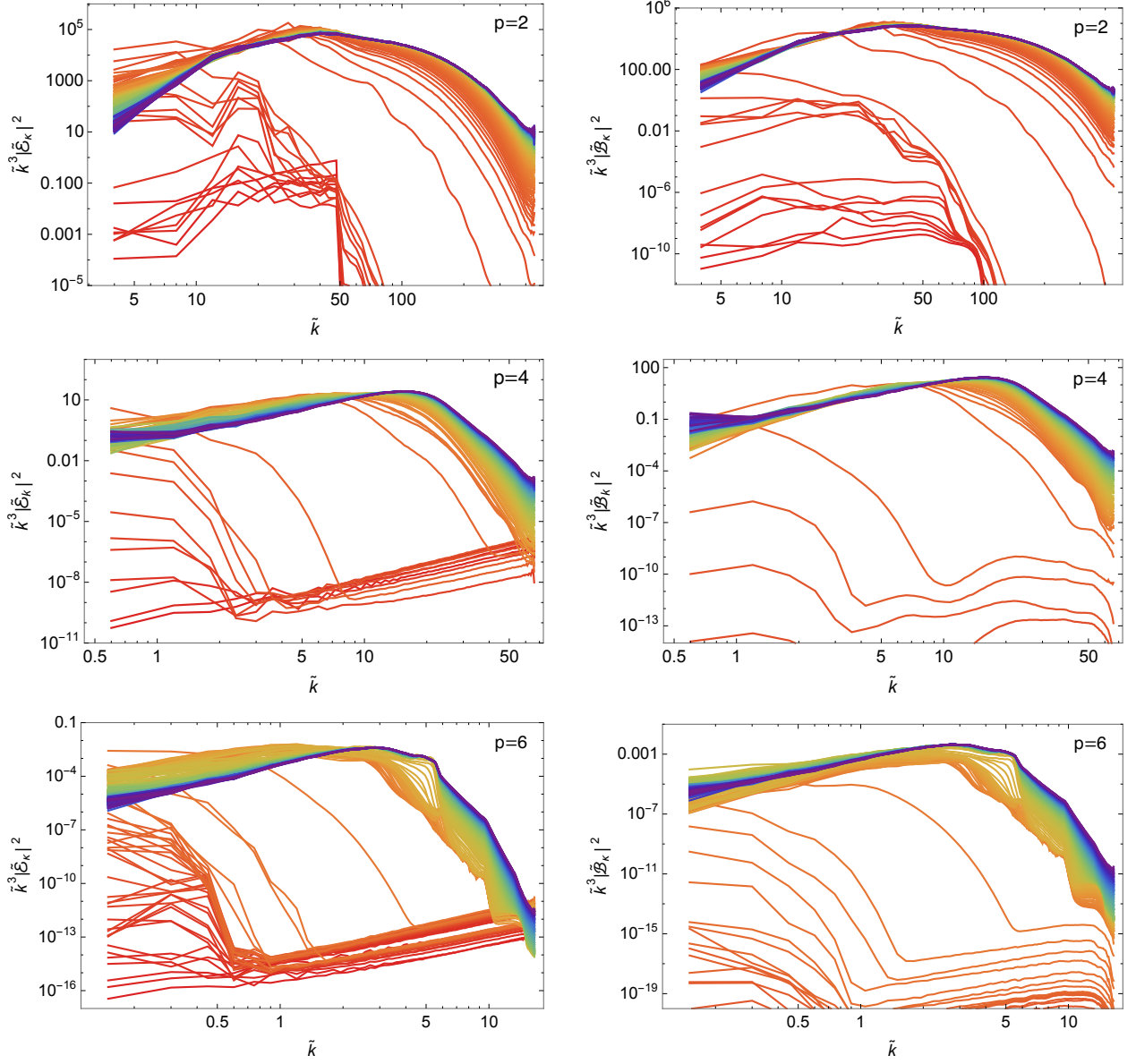


Figure 3: Spectral evolution of the electric field $\tilde{k}^3 |\tilde{\mathcal{E}}_k|^2$ (left panels) and magnetic field $\tilde{k}^3 |\tilde{\mathcal{B}}_k|^2$ (right panels), as a function of $\tilde{k} \equiv k/\omega_*$, for the $U(1)$ gauge simulations with $p = 2, 4, 6$. Each line shows the spectra at different moments of the evolution, going from red lines (early times) to purple lines (late times).

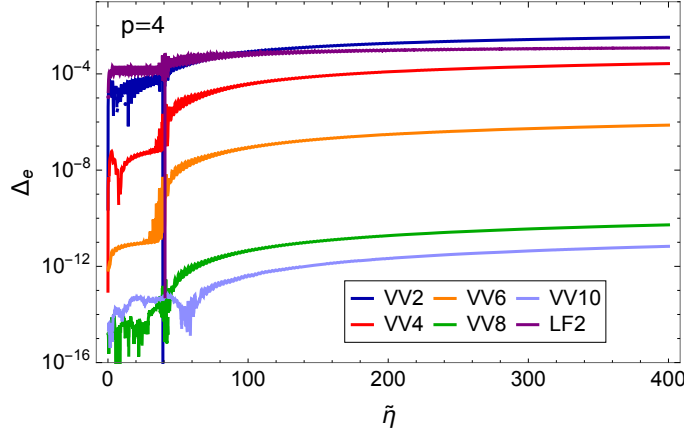


Figure 4: Comparison of “energy conservation” in the $U(1)$ gauge simulation with $p = 4$, for different evolution algorithms: velocity-Verlet (orders 2, 4, 6, 8, and 10), as well as staggered leapfrog (order 2).

start populating modes of increasingly high momenta due to rescattering. The spectra eventually saturate, showing a peak at larger scales. This process is qualitatively similar for the different choices of p considered here.

8.2.1 Accuracy tests

In flat space and in conservative systems, energy conservation can be used to monitor the precision of evolution algorithms. However, we are now considering an expanding Universe, and in particular, we are using the second Friedmann equation (168) to evolve the scale factor. In this context we can instead check that the first Friedmann equation (167) holds during the evolution. However, contrary to the Gauss laws (which are preserved by design when the discretized equations are gauge invariant), the first Friedmann’s law will be only approximately respected. We will loosely refer to this second Friedmann’s equation being respected as “energy conservation”, in analogy to the flat case. In particular, we require that the relative difference between the left and right hand sides of Eq. (167), which we denote by Δ_e , obeys always $\Delta_e \ll 1$. The better the accuracy of the evolution algorithm used to solve the lattice equations, the better “energy” is preserved. In order to illustrate this, we show in Fig. 4 the evolution of Δ_e as a function of time, for the case $p = 4$. The lattice equations have been solved with different accuracy orders of the velocity Verlet algorithm, introduced in Section 3.3.2. As expected, the higher the order, the better the “energy” is preserved: the violation of “energy conservation” at time $\tilde{\eta} \simeq 400$ is $\Delta_e \simeq 3 \cdot 10^{-3}$, $2 \cdot 10^{-4}$, $7 \cdot 10^{-7}$, $5 \cdot 10^{-11}$, and $6 \cdot 10^{-12}$, for VV2, VV4, VV6, VV8, and VV10 respectively. This means that “energy conservation” improves by factors ~ 12 , 360, 10^4 , and 8, as we increase the order of the integrator from one to the next one, i.e. from VV2 to VV4, VV4 to VV6, etc. Interestingly, the value of Δ_e saturates for VV10: in that case, the error in the scale factor constraint is due exclusively to an accumulation of machine precision errors, so using velocity-Verlet algorithms of higher-orders than VV10 will not improve the energy constraint anymore. Of course, the negative side of using higher-order iterators is the increase of the required computation time. Finally, we have also solved the field dynamics with a second-order staggered leapfrog algorithm (see Section 3.3.1), which we denote as LF2. Remarkably, this algorithm slightly improves “energy conservation” at late times with respect VV2, as observed in the Figure.

Let us now focus on the conservation of the Gauss constraint, given in Eq. (41). As already mentioned, the Gauss constraint must be always satisfied up to machine precision, *independently of the accuracy of the integrator*, as it is a direct consequence of the lattice equations of motion: a violation of the Gauss constraints is a violation of gauge invariance. We show in Fig. 5 the relative difference between the left and right hand sides of Eq. (41) as a function of time, which we denote as Δ_g . At the onset of the simulation we get $\Delta_g \sim 10^{-9}$, which is explained by the ~ 7 orders of magnitude of difference between the amplitudes of the inflaton homogeneous mode and its fluctuations. After backreaction, the relative difference decreases down to $\Delta_g \sim 10^{-13}$, and starts increasing slowly from then on, due to a constant accumulation of machine

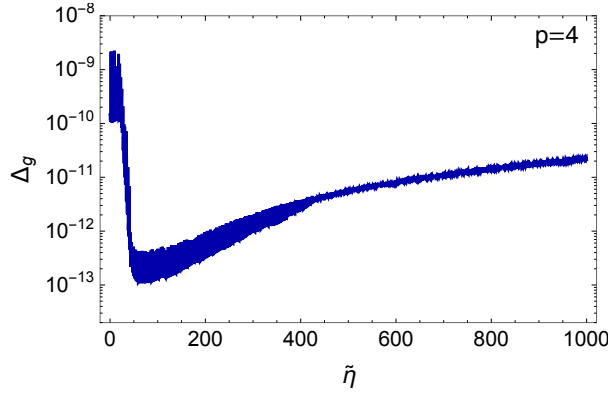


Figure 5: Conservation of the Gauss law as a function of time for the $U(1)$ gauge simulation with $p = 4$.

precision errors.

8.3 Lattice simulations: $SU(2) \times U(1)$ gauge interactions

We now consider a scenario in which a complex doublet Φ with potential (443) [where we must substitute $\phi \rightarrow \Phi$] acts as an inflaton field, and it is simultaneously coupled to 1) a $SU(2) \times U(1)$ gauge sector via a gauge-invariant covariant derivative, and 2) a massless secondary scalar field χ via a quadratic interaction $V_{\text{int}}(|\Phi|, \chi) \equiv (1/2)g^2|\Phi|^2\chi^2$, with g a dimensionless coupling constant. The strength of the parametric resonance is determined, in each case, by the corresponding resonance parameter: q_* for the scalar field (see Eq. 457), and q_{A*} and q_{B*} for the $U(1)$ and $SU(2)$ gauge fields (see Eqs. 462). Here we fix $q_{A*} = q_{B*} = q_*$ for illustrative purposes, with $q_* > 1$ to have broad parametric resonance for all daughter field sectors. We have simulated the preheating process for the power-law coefficients $p = 2, 4$, and studied the post-inflationary dynamics of the system. The lattice and model parameters chosen for the simulations are given in Table 8.2, and are similar to the analogous $U(1)$ simulations. In particular, we choose again $M = 10m_p$, which ensures that the inflaton always oscillates in the positive-curvature region of its potential. Similarly, the number of points and volume of the lattice are chosen, in each case, to resolve well both the infrared resonant bands, as well as the following propagation of the spectra towards the UV after backreaction.

The evolution of the inflaton amplitude, equation of state, and scale factor are, in this case, qualitatively similar to the examples shown for the $U(1)$ gauge simulation in the previous section. Therefore, we proceed to consider directly the evolution of the energy distribution, which differs in some aspects with respect to the $U(1)$ case. We show in Fig. 6 the evolution of the total energy of the system during preheating, as well as of each of its different contributions, for $p = 2, 4$. These are the kinetic and gradient energies of the scalars Φ and χ , the electric and magnetic energies of the $U(1)$ and $SU(2)$ gauge sectors, the inflaton potential energy $\tilde{V}_{\text{pot}} \equiv |\tilde{\Phi}|^4$, and the interaction energy $\tilde{V}_{\text{int}} \equiv (1/2)q_*|\tilde{\Phi}|^2\tilde{\chi}^2$ between Φ and χ . As in the $U(1)$ case, we have multiplied the different energies by the appropriate scale factor term, so that the (oscillation-averaged) total energy is constant during the initial linear regime. We also show the evolution of the energy ratios $\epsilon_i \equiv \tilde{\rho}_i/\tilde{\rho}$, which sum one by construction.

As expected, the energy budget is dominated by the inflaton homogeneous mode initially, so the kinetic and potential energies of the inflaton dominate over all the other energy contributions. However, the kinetic and gradient energies of all daughter fields grow exponentially due to broad parametric resonance, as well as the inflaton gradient energy. These contributions become sizeable enough at a certain time scale, destroying the inflaton homogeneous condensate via backreaction effects. As before, we denote this time scale as the *backreaction time* $\tilde{\eta}_{\text{br}}$. From the simulations, we get $\tilde{\eta}_{\text{br}} \simeq 60, 40$ for $p = 2, 4$ respectively. From then on, the non-linearities of the field EOM can no longer be ignored, and affect the dynamics of the system, achieving a stationary regime at late times. As in the $U(1)$ gauge simulation, we observe that the system gets virialized very quickly, with the inflaton energies obeying $\langle E_K^\Phi \rangle \simeq \langle E_G^\Phi \rangle + \frac{p}{2}\langle E_V \rangle + \langle E_{\text{int}} \rangle$ when averaged over oscillations. Also, we also have equipartition between the kinetic and gradient energies of all daughter field sectors at late times, as can be observed in the Figure.

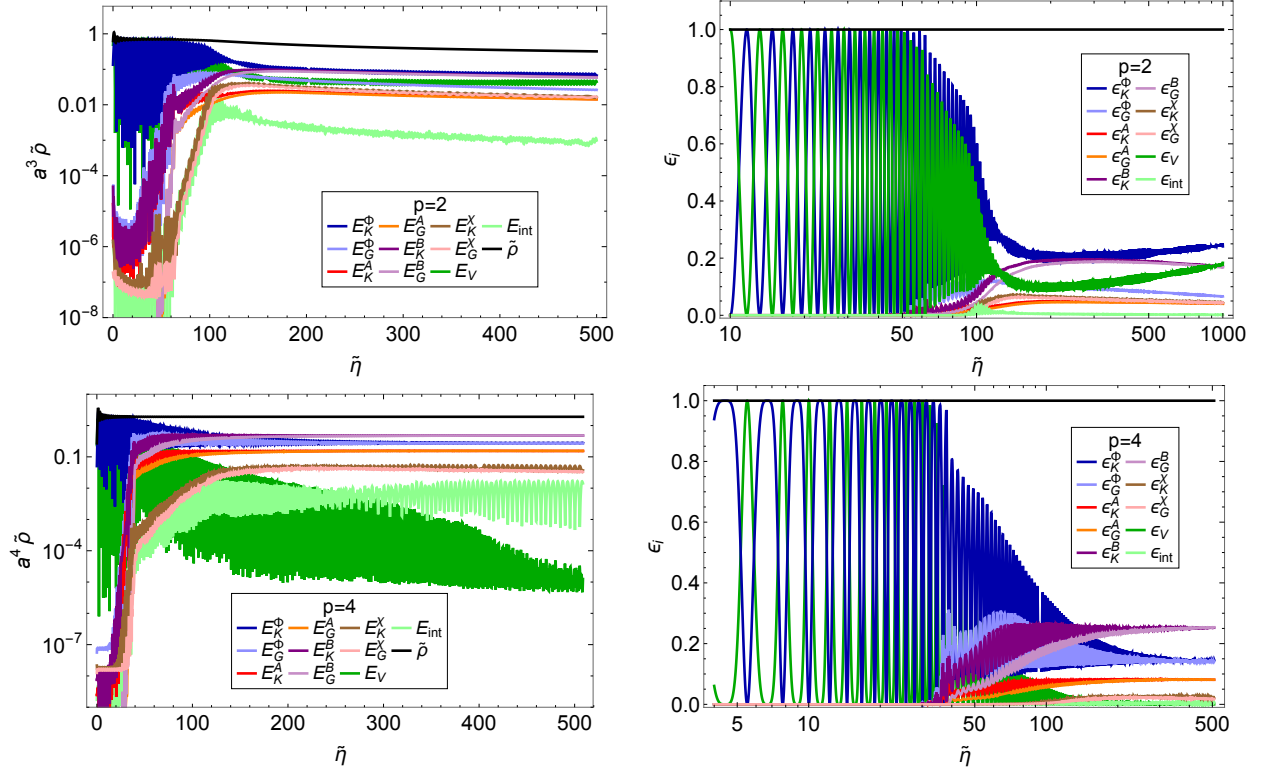


Figure 6: Left panel: Evolution of the total energy in program units, $\tilde{\rho} \equiv \rho/\omega_*$, as well as of each of its energy contributions, for the $SU(2) \times U(1) + \chi$ gauge simulations with $p = 2, 4$. Quantities are multiplied by the factor $\sim a^{\frac{6p}{p+2}}$. Right panel: Evolution of the energy ratios for the same simulations as in the left panels.

Let us now comment about how the energy distributes at very late times. Let us consider first the case $p = 2$. Here we observe a qualitatively similar behaviour than in the equivalent $U(1)$ simulation: although the inflaton kinetic and potential energy ratios decay around backreaction time, at later times they start growing again. The reason is the same as in the $U(1)$ simulations: the inflaton does not get excited via self-resonance for $p = 2$, while the parametric resonance of the daughter fields eventually becomes narrow (because the effective resonance parameter (460) decreases with time). Therefore, at very late times neither of the two resonant phenomena is present, and the inflaton slowly recovers all the energy of the system due to the different dilution rates of the energy contributions (the inflaton behaves as matter, while the daughter fields as radiation). Due to this, although our simulations are not long enough to observe this effect, we expect that $\epsilon_K^\phi, \epsilon_V \rightarrow 0.5$ at asymptotically late times. Moreover, this energy configuration also gives rise to a matter-dominated equation of state at late times, $w \rightarrow 0$.

Let us focus now on the simulation with $p = 4$. In this case, the effective resonance parameter (460) remains constant. Therefore, as we have fixed $q_* = q_{\text{eff}} > 1$ for all daughter field species (scalar χ , Abelian and non-Abelian gauge bosons), they experience a broad parametric excitation during the whole time evolution of the system, including at late times. Similarly, the inflaton is also being excited due to the oscillations of its own homogeneous mode, and develops fluctuations via self-resonance. Neither of the two effects dies out, which could explain why neither of the two field sectors (inflaton or daughter fields) possesses 100% of the total energy at asymptotically late times. In our particular scenario, we observe that at the end of the simulation, the inflaton possesses $\sim 30\%$ of the total energy, the scalar singlet $\sim 4\%$, the $U(1)$ gauge sector $\sim 16\%$, and the $SU(2)$ gauge sector $\sim 50\%$. In each of the four cases, the energy is divided half and half between kinetic and gradient contributions. These results are in contrast with the analogous $U(1)$ simulation, which show that $\sim 60\%$ of the total energy remains in the inflaton at late times. From this result, we can conclude the (somewhat expected) result that the larger the number of daughter fields, the larger the amount of energy that gets transferred to them from the inflaton. Finally, let us also observe

that the inflaton potential and inflaton- χ interaction energies go to zero at late times, $\varepsilon_V, \varepsilon_{\text{int}} \rightarrow 0$, as in the analogous $U(1)$ gauge simulation. Due to this, the effective equation of state goes to $w \rightarrow 1/3$ at late times.

We also show in Fig. 7 the evolution of the spectra of all fields involved: the norm of the inflaton $|\Phi|$, the scalar singlet χ , and the electric and magnetic energies of the $U(1)$ and $SU(2)$ sector. We observe in all cases the same qualitative behaviour: first an exponential growth of the field modes within an infrared band, which saturates at backreaction time, followed by a propagation of the spectra towards the UV, populating modes of higher and higher momenta. The initial infrared growth of the gauge fields is in agreement with the linear analysis presented above, except in the case of the inflaton, which does not experience broad parametric resonance. The inflaton growth is, instead, triggered by backreaction effects from the daughter fields.

8.3.1 Accuracy tests

Finally, it is always important to check that both “energy conservation” and the Gauss constraints are preserved at all times during the simulation. Let us consider first the left of panel of Fig. 8, where we show the relative difference between the left and right hand sides of the 1st Friedmann equation as a function of time (denoted as Δ_e), for $p = 4$. Naturally, we require $\Delta_e \ll 1$ in order to trust the results of our simulations. For illustrative purposes, we have solved the field dynamics with velocity-Verlet evolution algorithms of orders 2 and 4, for the same lattice and model parameters. As expected, the higher the accuracy of the integrator, the better “energy” is preserved: at time $\tilde{\eta} \simeq 340$ we get $\Delta_e \simeq 2.2 \cdot 10^{-3}$ for VV2, and $\Delta_e \simeq 1.1 \cdot 10^{-4}$ for VV4, i.e. VV4 preserves “energy” a factor ~ 20 better than VV2. However, the negative side is that the required simulation time for VV4 increases with respect VV2, as expected. In principle, one should be able to improve the accuracy of the integrator arbitrarily up to machine precision, as in the analogous $U(1)$ gauge simulation shown in Fig. 4. This can be useful if one wants to apply this algorithm to any particular scenario requiring extremely good energy conservation. This is always at the expense, of course, of longer simulation times.

In the right panel of Fig. 8 we show how the Gauss laws are preserved during the simulation. In this case there are two Gauss laws that must be satisfied: one for the $U(1)$ sector (given in Eq. 25), and another one for the $SU(2)$ sector (given in Eq. 26). We measure this by the parameter Δ_g , which as defined before, is the relative difference between the left and hand sides of the corresponding Gauss constraints. As explained before, these constraints must be preserved up to machine precision independently of the chosen evolution algorithm, as they are a direct consequence of the gauge invariance that our careful discretization techniques maintain in the lattice equations. We observe a similar behaviour as in the analogous $U(1)$ gauge simulations: before backreaction we have $\Delta_g \sim 10^{-9}$ for both gauge sectors, due to the large relative difference between the amplitudes of the inflaton homogeneous mode and its fluctuations. After backreaction we get $\Delta_g \simeq 10^{-13}$, and from then on, the error slowly grows due to a constant accumulation of machine precision errors in each time step. At time $\tilde{\eta} \simeq 340$ we get $\Delta_g \sim 10^{-12}$ for both $U(1)$ and $SU(2)$ gauge sectors, which shows that both Gauss constraints are exceptionally well preserved during the simulation.

9 Summary and outlook

The present document represents *Part I* of a comprehensive dissertation on lattice techniques for the simulation of non-linear dynamics in the early Universe. Here we have focused on the lattice treatment of canonical scalar-gauge field theories in an expanding Universe, considering an arbitrary number of interacting (real and complex) scalars and (Abelian and non-Abelian) gauge fields. This suffices to describe the majority of physically relevant scenarios from the early universe. In addition, we plan to discuss methods for non-canonical interactions in an upcoming *Part II* [255], like those in theories with non-minimal gravitational couplings, or in general with non-minimal kinetic terms, as well as non-canonical interactions defined by the product between field variables and their conjugate momenta.

Let us summarize the content of the present work. In Section 2 we reviewed first the field dynamics of scalar-gauge theories in a continuum space-time, both with and without expansion of the Universe. We considered a theory containing different kinds of scalars (singlets, $U(1)$ -charged, and $SU(N) \times U(1)$ -charged

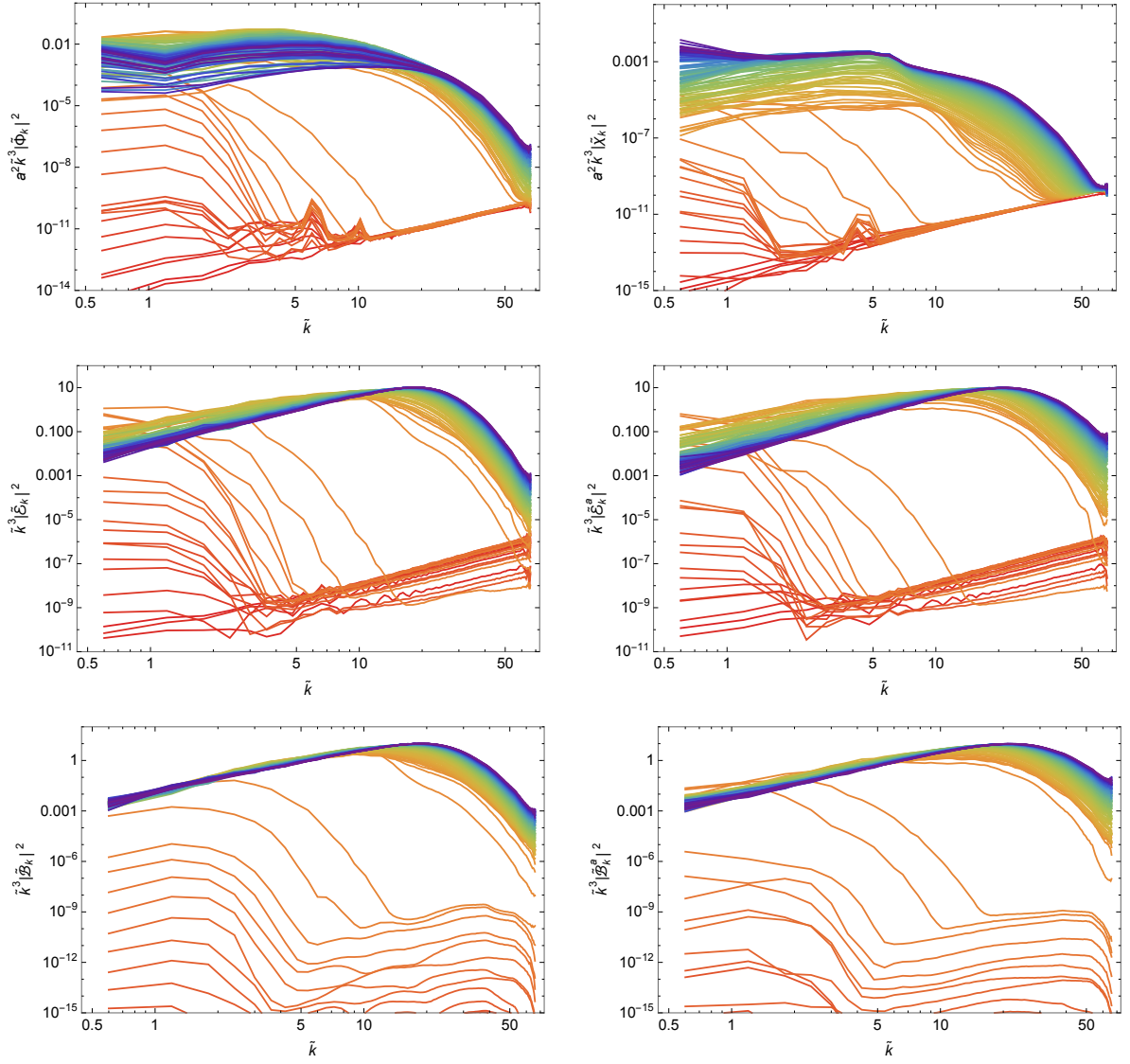


Figure 7: Spectral evolution of all the fields involved in the $SU(2) \times U(1) + \chi$ lattice simulations as a function of $\tilde{k} \equiv k/\omega_*$, for $p = 4$. From left to right and from top to bottom, we show the inflaton, the massless scalar χ , the electric and magnetic fields of the $U(1)$ gauge sector, and electric and magnetic fields of the $SU(2)$ gauge sector. Each line shows the spectra at different times during the field evolution, from red (early times) to purple (late times).

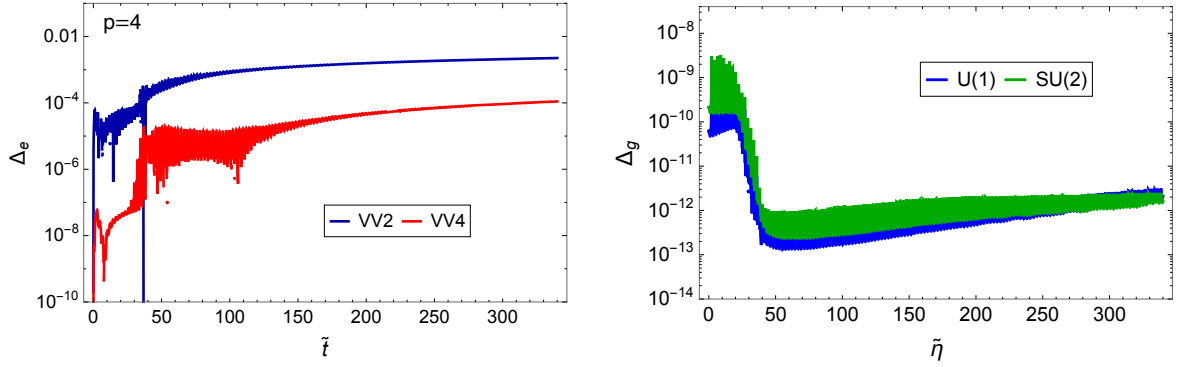


Figure 8: Left panel: Evolution of the relative error in “energy conservation” for the $SU(2) \times U(1) + \chi$ simulation with $p = 4$, obtained for the VV2 and VV4 algorithms. Right panel: Evolution of the relative error in the Gauss constraints of the $U(1)$ and $SU(2)$ gauge sectors, for the same simulation.

scalars) and (Abelian and non-Abelian) gauge fields. We wrote explicitly the EOM of such theory, as well as introduced the notation later used throughout the document. We then introduced in Section 3 basic concepts of lattice techniques, with a special emphasis on how to discretize appropriately gauge theories to preserve gauge invariance on the lattice. We then introduced basic evolution algorithms for the integration of the field EOM: staggered leapfrog and Verlet methods, with accuracy $\mathcal{O}(\delta t^2)$, and (explicit) Runge-Kutta methods with accuracy up to $\mathcal{O}(\delta t^4)$. We also showed how some of these basic algorithms can be used as building blocks for the higher-order Yoshida and Gauss-Legendre integrators, with accuracy up to $\mathcal{O}(\delta t^{10})$.

In the following three sections we focused on developing lattice formulations for the different field sectors of the canonical theories considered here. In Section 4 we considered the case of multiple interacting scalar fields. We first have introduced a set of dimensionless field and spacetime variables, which we have call the *lattice* or *program* variables. When thoughtfully defined, these variables can be very useful when working on a lattice. Our lattice algorithms are therefore written in terms of these variables. We explained how to apply different evolution algorithms to solve the scalar EOM, as well as define different useful observables. In Section 5 we developed the same ideas for gauge theories with $U(1)$ interactions, and in Section 6 we did the same for gauge theories with $SU(N)$ interactions. In Section 7 we described how to set the initial conditions for the different kinds of fields, both in the continuum and in the lattice. For scalar fields, we imposed a spectrum of classical vacuum fluctuations, which mimics the expected spectrum of quantum fluctuations in a FLRW Universe. For gauge fields, we discussed how to set their initial conditions so that Gauss constraint is preserved from the beginning.

Finally, in Section 8, we simulated the dynamics of a specific scalar-gauge field model with *CosmoLattice*, to illustrate some of the techniques presented in the previous sections. In particular, we considered the preheating dynamics of a charged inflaton, with monomial shape around the minimum of its potential. We considered two different scenarios: 1) a $U(1)$ -charged scalar coupled to an Abelian gauge field, and 2) a $SU(2) \times U(1)$ charged scalar coupled to Abelian and non-Abelian gauge fields simultaneously, as well as to a scalar singlet. We considered different model parameters, and in particular, we studied different power-law coefficients in the monomial function. We studied the evolution during preheating of several relevant observables: the inflaton mean amplitude value, the evolution of the scale factor and of the equation of state, the energy distributions among field components, and the relevant field spectra. We showed explicitly how each Gauss constraint is preserved to machine precision during the evolution of the system. We also demonstrated the power of the higher-order Verlet evolution algorithms implemented in *CosmoLattice*, which can be used to obtain energy conservation up to machine precision in simulations of scalar-gauge theories in an expanding Universe.

Let us emphasize here that, to the best of our knowledge, we are presenting for the first time an algorithm for non-Abelian $SU(N)$ gauge theories, which is symplectic, explicit in time, and preserving exactly the Gauss constraint, while solving for the expansion of the universe self-consistently. Furthermore, it can be made of arbitrary order. Besides, we also present higher-order integration algorithms for Abelian $U(1)$ gauge theories, similar to those in *GFiRe* [154], demonstrating explicitly for the first time their numerical implementation for the highest orders, in particular for $\mathcal{O}(\delta t^6)$, $\mathcal{O}(\delta t^8)$ and $\mathcal{O}(\delta t^{10})$. Similarly, we also present higher-order integration algorithms for interacting scalar theories, similar to those in *HLattice* [250], but going also to higher-orders, in particular building explicit implementations for $\mathcal{O}(\delta t^8)$ and $\mathcal{O}(\delta t^{10})$.

The concepts and techniques discussed in this dissertation, in particular the explicit-in-time algorithms presented in Sections 4-6, are already implemented in our present code *CosmoLattice*, a *user – friendly* and highly modular C++ MPI-based code for lattice simulations of non-linear classical dynamics in an expanding universe, that we plan to publicly release before the end of 2020. Most of the algorithms presented in this work are bundled in a high-level interface which allows the user to add almost effortlessly models with different interaction potentials, and easily add new integration algorithms. Moreover, the library has been designed in such a way to allow the user to use complex, vectorial and matricial representation of fields, to keep the lattice equations resembling as much as possible to the continuum ones. This level of abstraction is achieved through the use of compile-time code generation, using C++ expression templates, so that performance is never sacrificed.

The aim of this manuscript has been to illustrate different concepts of lattice gauge-invariant techniques and of general integration methods, which we have then specialized and adapted for their use in the context

of canonical scalar-gauge field theories. We expect that the work we have developed so far here (soon to be complemented by *Part II* [255]) shall be useful for a large fraction of the research community interested in the early universe, let it be completely inexperienced researchers in lattice field theory simulations, or very experienced ones.

To conclude, we comment on several aspects that we plan to explore in forthcoming works (either in *Part II* or elsewhere), both in the near and in the mid-term future:

- The development of lattice techniques for the discretization of theories with non-minimal kinetic terms. As the *drift* and *kick* functionals in these theories typically contain a linear combination of conjugate momenta of other fields, explicit-in-time symplectic integrators (such as staggered leapfrog or Verlet integrators) are not appropriate. However, one can resort to explicit (non-symplectic) Runge-Kutta methods like those presented in Section 3.3.3 (this has been done in e.g. [252]), or even to higher-order implicit (yet symplectic) integrators like the Gauss-Legendre methods, presented in Section 3.4.2. As mentioned before, we postpone a specialized discussion of these problems to *Part II* of our dissertation on lattice techniques [255]. The implementation of the corresponding algorithms in *CosmoLattice* will also be made publicly available in that moment.
- In a similar spirit, the axial couplings of a pseudo-scalar field with a gauge sector is also of great interest. An implicit method for the interaction of an axion-like field ϕ with a $U(1)$ -gauge sector through a shift invariant coupling $\phi F^{\mu\nu} \tilde{F}_{\mu\nu}$, has been in fact explored in [90–96]. In particular, an exactly lattice-shift-symmetric formulation was developed in [96], and was later on generalized to an expanding background in [93]. We could revisit and generalize this kind of approaches in light of the algorithms presented here in Section 3, coming possibly with many potential outlooks. We plan to present a specialized discussion on these interactions in *Part II* [255].
- The creation of tensor perturbation representing gravitational waves [94, 95, 109, 134–151], as well as the dynamics of scalar metric perturbations [115–124] (possibly leading to the formation of primordial black holes [125–133]) are all topics of great interest. In the case of tensor perturbations, we plan to follow [262] (based on an idea originally proposed in [137]), as this technique allows for generic sources independently of the field content of the theory studied. Although we have not decided about a clear strategy for a general solver of scalar metric perturbations yet, one possibility would be to follow [250].
- The inclusion of fermions in the simulations. Of course, the notion of ‘classical fermions’ does not exist due to Pauli-blocking, and hence a straightforward discretization and evolution of the Dirac equation would not be useful. However, as first realised in [260], one can still study real-time fermions’ dynamics in a semi-classical formulation of the out-of-equilibrium Schwinger-Keldysh formulation, see also references [235, 237, 274]. Combining the lattice implementation proposed in [260], with the ‘low cost’ fermions introduced in [261], [256–259] have succeeded in simulating out-of-equilibrium dynamics of classical scalar fields coupled to quantum fermions. These simulations are however very costly in terms of computer memory, and only very small lattices have been considered until now.
- The addition of other initialization procedures. Depending on the problem, initializing fields in real space might be more convenient than imposing a certain mode spectrum in Fourier space, as we did in Section 7. As mentioned in the introduction, to simulate e.g. the dynamics of field string networks or any other type of cosmic defects, one needs to create in first place the defect network in configuration space, see e.g. [155–162, 210, 211, 263], and then evolve the field configuration from then onward (typically after a diffusion phase to force the system to reach a scaling regime as fast as possible). Although different problems may require completely different initializers, it might be useful to consider making a library for specialized ones for cosmic strings, other topological defects, and other circumstances.
- The addition of ‘cooling’ procedures for the initial condition for gauge fields. Another improvement would be to use cooling algorithms to initialize gauge fields. Instead of imposing the Gauss constraints by hand as we have done in Section 7.2, one can impose completely unconstrained fluctuations to

the gauge fields, and then remove the unwanted transverse degree's of freedom by a minimization procedure [275,276]. For thermal initial conditions, one can also thermalize the system while exactly preserving Gauss law through some Langevin dynamics [277]. Studying such algorithms will allow us to consider different initial conditions and thus study yet another variety of models.

Acknowledgments

The authors would like to thank Andrei Frolov for useful discussions, and in particular for pointing us out the Gauss-Legendre methods. D.G.F. and F.T. acknowledge hospitality from KITP-UCSB, where part of this work was carried out under support by the National Science Foundation under Grant No. NSF PHY-1748958. F.T. thanks M. Shaposhnikov for his kind invitation to EPFL during the development of this work. A.F. wants to thank S. Antusch for his kind invitation to Basel. D.G.F. (ORCID 0000-0002-4005-8915) is supported by a Ramón y Cajal contract by Spanish Ministry MINECO, with Ref. RYC-2017-23493. A.F. acknowledges support from the Swiss National Science Foundation. F.T. also acknowledges support from the Swiss National Science Foundation (project number 200020/175502).

References

- [1] Y. Akrami *et al.*, “Planck 2018 results. X. Constraints on inflation,” 7 2018.
- [2] A. H. Guth, “The Inflationary Universe: A Possible Solution to the Horizon and Flatness Problems,” *Adv. Ser. Astrophys. Cosmol.*, vol. 3, pp. 139–148, 1987.
- [3] A. D. Linde, “A New Inflationary Universe Scenario: A Possible Solution of the Horizon, Flatness, Homogeneity, Isotropy and Primordial Monopole Problems,” pp. 185–195, 10 1981.
- [4] A. Albrecht and P. J. Steinhardt, “Cosmology for Grand Unified Theories with Radiatively Induced Symmetry Breaking,” *Adv. Ser. Astrophys. Cosmol.*, vol. 3, pp. 158–161, 1987.
- [5] R. Brout, F. Englert, and E. Gunzig, “The Creation of the Universe as a Quantum Phenomenon,” *Annals Phys.*, vol. 115, p. 78, 1978.
- [6] A. A. Starobinsky, “A New Type of Isotropic Cosmological Models Without Singularity,” *Adv. Ser. Astrophys. Cosmol.*, vol. 3, pp. 130–133, 1987.
- [7] D. Kazanas, “Dynamics of the Universe and Spontaneous Symmetry Breaking,” *Astrophys. J. Lett.*, vol. 241, pp. L59–L63, 1980.
- [8] K. Sato, “First Order Phase Transition of a Vacuum and Expansion of the Universe,” *Mon. Not. Roy. Astron. Soc.*, vol. 195, pp. 467–479, 1981.
- [9] V. F. Mukhanov and G. V. Chibisov, “Quantum Fluctuations and a Nonsingular Universe,” *JETP Lett.*, vol. 33, pp. 532–535, 1981.
- [10] A. H. Guth and S. Pi, “Fluctuations in the New Inflationary Universe,” *Phys. Rev. Lett.*, vol. 49, pp. 1110–1113, 1982.
- [11] A. A. Starobinsky, “Dynamics of Phase Transition in the New Inflationary Universe Scenario and Generation of Perturbations,” *Phys. Lett. B*, vol. 117, pp. 175–178, 1982.
- [12] S. Hawking, “The Development of Irregularities in a Single Bubble Inflationary Universe,” *Phys. Lett. B*, vol. 115, p. 295, 1982.
- [13] J. M. Bardeen, P. J. Steinhardt, and M. S. Turner, “Spontaneous Creation of Almost Scale - Free Density Perturbations in an Inflationary Universe,” *Phys. Rev. D*, vol. 28, p. 679, 1983.

- [14] D. H. Lyth and A. Riotto, “Particle physics models of inflation and the cosmological density perturbation,” *Phys. Rept.*, vol. 314, pp. 1–146, 1999.
- [15] A. Riotto, “Inflation and the theory of cosmological perturbations,” *ICTP Lect. Notes Ser.*, vol. 14, pp. 317–413, 2003.
- [16] A. D. Linde, “Inflationary Cosmology,” *Lect. Notes Phys.*, vol. 738, pp. 1–54, 2008.
- [17] D. Baumann, “Inflation,” in *Theoretical Advanced Study Institute in Elementary Particle Physics: Physics of the Large and the Small*, pp. 523–686, 2011.
- [18] B. A. Bassett, S. Tsujikawa, and D. Wands, “Inflation dynamics and reheating,” *Rev. Mod. Phys.*, vol. 78, pp. 537–589, 2006.
- [19] R. Allahverdi, R. Brandenberger, F.-Y. Cyr-Racine, and A. Mazumdar, “Reheating in Inflationary Cosmology: Theory and Applications,” *Ann. Rev. Nucl. Part. Sci.*, vol. 60, pp. 27–51, 2010.
- [20] M. A. Amin, M. P. Hertzberg, D. I. Kaiser, and J. Karouby, “Nonperturbative Dynamics Of Reheating After Inflation: A Review,” *Int. J. Mod. Phys. D*, vol. 24, p. 1530003, 2014.
- [21] K. D. Lozanov, “Lectures on Reheating after Inflation,” 7 2019.
- [22] J. H. Traschen and R. H. Brandenberger, “Particle Production During Out-of-equilibrium Phase Transitions,” *Phys. Rev. D*, vol. 42, pp. 2491–2504, 1990.
- [23] L. Kofman, A. D. Linde, and A. A. Starobinsky, “Reheating after inflation,” *Phys. Rev. Lett.*, vol. 73, pp. 3195–3198, 1994.
- [24] Y. Shtanov, J. H. Traschen, and R. H. Brandenberger, “Universe reheating after inflation,” *Phys. Rev. D*, vol. 51, pp. 5438–5455, 1995.
- [25] D. I. Kaiser, “Post inflation reheating in an expanding universe,” *Phys. Rev. D*, vol. 53, pp. 1776–1783, 1996.
- [26] L. Kofman, A. D. Linde, and A. A. Starobinsky, “Towards the theory of reheating after inflation,” *Phys. Rev. D*, vol. 56, pp. 3258–3295, 1997.
- [27] P. B. Greene, L. Kofman, A. D. Linde, and A. A. Starobinsky, “Structure of resonance in preheating after inflation,” *Phys. Rev. D*, vol. 56, pp. 6175–6192, 1997.
- [28] D. I. Kaiser, “Preheating in an expanding universe: Analytic results for the massless case,” *Phys. Rev. D*, vol. 56, pp. 706–716, 1997.
- [29] D. I. Kaiser, “Resonance structure for preheating with massless fields,” *Phys. Rev. D*, vol. 57, pp. 702–711, 1998.
- [30] P. B. Greene and L. Kofman, “Preheating of fermions,” *Phys. Lett. B*, vol. 448, pp. 6–12, 1999.
- [31] P. B. Greene and L. Kofman, “On the theory of fermionic preheating,” *Phys. Rev. D*, vol. 62, p. 123516, 2000.
- [32] M. Peloso and L. Sorbo, “Preheating of massive fermions after inflation: Analytical results,” *JHEP*, vol. 05, p. 016, 2000.
- [33] J. Berges, D. Gelfand, and J. Pruschke, “Quantum theory of fermion production after inflation,” *Phys. Rev. Lett.*, vol. 107, p. 061301, 2011.
- [34] S. Khlebnikov and I. Tkachev, “Classical decay of inflaton,” *Phys. Rev. Lett.*, vol. 77, pp. 219–222, 1996.

- [35] T. Prokopec and T. G. Roos, “Lattice study of classical inflaton decay,” *Phys. Rev. D*, vol. 55, pp. 3768–3775, 1997.
- [36] K. Enqvist and M. S. Sloth, “Adiabatic CMB perturbations in pre - big bang string cosmology,” *Nucl. Phys. B*, vol. 626, pp. 395–409, 2002.
- [37] D. H. Lyth and D. Wands, “Generating the curvature perturbation without an inflaton,” *Phys. Lett. B*, vol. 524, pp. 5–14, 2002.
- [38] T. Moroi and T. Takahashi, “Effects of cosmological moduli fields on cosmic microwave background,” *Phys. Lett. B*, vol. 522, pp. 215–221, 2001. [Erratum: *Phys.Lett.B* 539, 303–303 (2002)].
- [39] A. Mazumdar and J. Rocher, “Particle physics models of inflation and curvaton scenarios,” *Phys. Rept.*, vol. 497, pp. 85–215, 2011.
- [40] K. Enqvist, S. Nurmi, and G. Rigopoulos, “Parametric Decay of the Curvaton,” *JCAP*, vol. 10, p. 013, 2008.
- [41] K. Enqvist, D. G. Figueroa, and R. N. Lerner, “Curvaton Decay by Resonant Production of the Standard Model Higgs,” *JCAP*, vol. 01, p. 040, 2013.
- [42] K. Enqvist, R. N. Lerner, and S. Rusak, “Reheating dynamics affects non-perturbative decay of spectator fields,” *JCAP*, vol. 11, p. 034, 2013.
- [43] K. Enqvist, R. N. Lerner, and T. Takahashi, “The minimal curvaton-higgs model,” *JCAP*, vol. 01, p. 006, 2014.
- [44] A. A. Starobinsky and J. Yokoyama, “Equilibrium state of a selfinteracting scalar field in the De Sitter background,” *Phys. Rev. D*, vol. 50, pp. 6357–6368, 1994.
- [45] K. Enqvist, T. Meriniemi, and S. Nurmi, “Generation of the Higgs Condensate and Its Decay after Inflation,” *JCAP*, vol. 10, p. 057, 2013.
- [46] A. De Simone and A. Riotto, “Cosmological Perturbations from the Standard Model Higgs,” *JCAP*, vol. 02, p. 014, 2013.
- [47] M. Herranen, T. Markkanen, S. Nurmi, and A. Rajantie, “Spacetime curvature and Higgs stability after inflation,” *Phys. Rev. Lett.*, vol. 115, p. 241301, 2015.
- [48] D. G. Figueroa and C. T. Byrnes, “The Standard Model Higgs as the origin of the hot Big Bang,” *Phys. Lett. B*, vol. 767, pp. 272–277, 2017.
- [49] K. Enqvist, S. Nurmi, and S. Rusak, “Non-Abelian dynamics in the resonant decay of the Higgs after inflation,” *JCAP*, vol. 10, p. 064, 2014.
- [50] D. G. Figueroa, “A gravitational wave background from the decay of the standard model Higgs after inflation,” *JHEP*, vol. 11, p. 145, 2014.
- [51] A. Kusenko, L. Pearce, and L. Yang, “Postinflationary Higgs relaxation and the origin of matter-antimatter asymmetry,” *Phys. Rev. Lett.*, vol. 114, no. 6, p. 061302, 2015.
- [52] D. G. Figueroa, J. Garcia-Bellido, and F. Torrenti, “Decay of the standard model Higgs field after inflation,” *Phys. Rev. D*, vol. 92, no. 8, p. 083511, 2015.
- [53] K. Enqvist, S. Nurmi, S. Rusak, and D. Weir, “Lattice Calculation of the Decay of Primordial Higgs Condensate,” *JCAP*, vol. 02, p. 057, 2016.
- [54] F. L. Bezrukov and M. Shaposhnikov, “The Standard Model Higgs boson as the inflaton,” *Phys. Lett. B*, vol. 659, pp. 703–706, 2008.

- [55] F. Bezrukov, A. Magnin, M. Shaposhnikov, and S. Sibiryakov, “Higgs inflation: consistency and generalisations,” *JHEP*, vol. 01, p. 016, 2011.
- [56] F. Bezrukov, D. Gorbunov, and M. Shaposhnikov, “On initial conditions for the Hot Big Bang,” *JCAP*, vol. 06, p. 029, 2009.
- [57] J. Garcia-Bellido, D. G. Figueroa, and J. Rubio, “Preheating in the Standard Model with the Higgs-Inflaton coupled to gravity,” *Phys. Rev. D*, vol. 79, p. 063531, 2009.
- [58] D. G. Figueroa, “Preheating the Universe from the Standard Model Higgs,” *AIP Conf. Proc.*, vol. 1241, no. 1, pp. 578–587, 2010.
- [59] J. Repond and J. Rubio, “Combined Preheating on the lattice with applications to Higgs inflation,” *JCAP*, vol. 07, p. 043, 2016.
- [60] Y. Ema, R. Jinno, K. Mukaida, and K. Nakayama, “Violent Preheating in Inflation with Nonminimal Coupling,” *JCAP*, vol. 02, p. 045, 2017.
- [61] E. I. Sfakianakis and J. van de Vis, “Preheating after Higgs Inflation: Self-Resonance and Gauge boson production,” *Phys. Rev. D*, vol. 99, no. 8, p. 083519, 2019.
- [62] T. Gherghetta, C. F. Kolda, and S. P. Martin, “Flat directions in the scalar potential of the supersymmetric standard model,” *Nucl. Phys. B*, vol. 468, pp. 37–58, 1996.
- [63] K. Enqvist and A. Mazumdar, “Cosmological consequences of MSSM flat directions,” *Phys. Rept.*, vol. 380, pp. 99–234, 2003.
- [64] M. Dine, L. Randall, and S. D. Thomas, “Baryogenesis from flat directions of the supersymmetric standard model,” *Nucl. Phys. B*, vol. 458, pp. 291–326, 1996.
- [65] I. Affleck and M. Dine, “A New Mechanism for Baryogenesis,” *Nucl. Phys. B*, vol. 249, pp. 361–380, 1985.
- [66] M. K. Gaillard, H. Murayama, and K. A. Olive, “Preserving flat directions during inflation,” *Phys. Lett. B*, vol. 355, pp. 71–77, 1995.
- [67] K. A. Olive and M. Peloso, “The Fate of SUSY flat directions and their role in reheating,” *Phys. Rev. D*, vol. 74, p. 103514, 2006.
- [68] A. Basboll, D. Maybury, F. Riva, and S. M. West, “Non-Perturbative Flat Direction Decay,” *Phys. Rev. D*, vol. 76, p. 065005, 2007.
- [69] A. Gumrukcuoglu, K. A. Olive, M. Peloso, and M. Sexton, “The Nonperturbative decay of SUSY flat directions,” *Phys. Rev. D*, vol. 78, p. 063512, 2008.
- [70] A. D. Linde, “Hybrid inflation,” *Phys. Rev. D*, vol. 49, pp. 748–754, 1994.
- [71] G. N. Felder, J. Garcia-Bellido, P. B. Greene, L. Kofman, A. D. Linde, and I. Tkachev, “Dynamics of symmetry breaking and tachyonic preheating,” *Phys. Rev. Lett.*, vol. 87, p. 011601, 2001.
- [72] G. N. Felder, L. Kofman, and A. D. Linde, “Tachyonic instability and dynamics of spontaneous symmetry breaking,” *Phys. Rev. D*, vol. 64, p. 123517, 2001.
- [73] E. J. Copeland, S. Pascoli, and A. Rajantie, “Dynamics of tachyonic preheating after hybrid inflation,” *Phys. Rev. D*, vol. 65, p. 103517, 2002.
- [74] J. Garcia-Bellido, M. Garcia Perez, and A. Gonzalez-Arroyo, “Symmetry breaking and false vacuum decay after hybrid inflation,” *Phys. Rev. D*, vol. 67, p. 103501, 2003.

- [75] B. A. Bassett and S. Liberati, “Geometric reheating after inflation,” *Phys. Rev. D*, vol. 58, p. 021302, 1998. [Erratum: *Phys.Rev.D* 60, 049902 (1999)].
- [76] S. Tsujikawa, K.-i. Maeda, and T. Torii, “Resonant particle production with nonminimally coupled scalar fields in preheating after inflation,” *Phys. Rev. D*, vol. 60, p. 063515, 1999.
- [77] S. Tsujikawa, K.-i. Maeda, and T. Torii, “Preheating with nonminimally coupled scalar fields in higher curvature inflation models,” *Phys. Rev. D*, vol. 60, p. 123505, 1999.
- [78] S. Tsujikawa, K.-i. Maeda, and T. Torii, “Preheating of the nonminimally coupled inflaton field,” *Phys. Rev. D*, vol. 61, p. 103501, 2000.
- [79] J. Crespo and H. de Oliveira, “Aspects of wave turbulence in preheating. Part II. Rebirth of the nonminimal coupled models,” *JCAP*, vol. 12, p. 045, 2019.
- [80] J. Crespo and H. de Oliveira, “Aspects of wave turbulence in preheating III: The case of the two-fields models,” 6 2019.
- [81] M. P. DeCross, D. I. Kaiser, A. Prabhu, C. Prescod-Weinstein, and E. I. Sfakianakis, “Preheating after Multifield Inflation with Nonminimal Couplings, I: Covariant Formalism and Attractor Behavior,” *Phys. Rev. D*, vol. 97, no. 2, p. 023526, 2018.
- [82] M. P. DeCross, D. I. Kaiser, A. Prabhu, C. Prescod-Weinstein, and E. I. Sfakianakis, “Preheating after multifield inflation with nonminimal couplings, II: Resonance Structure,” *Phys. Rev. D*, vol. 97, no. 2, p. 023527, 2018.
- [83] M. P. DeCross, D. I. Kaiser, A. Prabhu, C. Prescod-Weinstein, and E. I. Sfakianakis, “Preheating after multifield inflation with nonminimal couplings, III: Dynamical spacetime results,” *Phys. Rev. D*, vol. 97, no. 2, p. 023528, 2018.
- [84] R. Nguyen, J. van de Vis, E. I. Sfakianakis, J. T. Giblin, and D. I. Kaiser, “Nonlinear Dynamics of Preheating after Multifield Inflation with Nonminimal Couplings,” *Phys. Rev. Lett.*, vol. 123, no. 17, p. 171301, 2019.
- [85] J. van de Vis, R. Nguyen, E. I. Sfakianakis, J. T. Giblin, and D. I. Kaiser, “Time-Scales for Nonlinear Processes in Preheating after Multifield Inflation with Nonminimal Couplings,” 5 2020.
- [86] D. Battefeld, “Preheating after Multi-field Inflation,” *Nucl. Phys. B Proc. Suppl.*, vol. 192-193, pp. 126–127, 2009.
- [87] D. Battefeld and S. Kawai, “Preheating after N-flation,” *Phys. Rev. D*, vol. 77, p. 123507, 2008.
- [88] D. Battefeld, T. Battefeld, and J. T. Giblin, “On the Suppression of Parametric Resonance and the Viability of Tachyonic Preheating after Multi-Field Inflation,” *Phys. Rev. D*, vol. 79, p. 123510, 2009.
- [89] J. Braden, L. Kofman, and N. Barnaby, “Reheating the Universe After Multi-Field Inflation,” *JCAP*, vol. 07, p. 016, 2010.
- [90] P. Adshead, J. T. Giblin, T. R. Scully, and E. I. Sfakianakis, “Gauge-preheating and the end of axion inflation,” *JCAP*, vol. 12, p. 034, 2015.
- [91] P. Adshead, J. T. Giblin, T. R. Scully, and E. I. Sfakianakis, “Magnetogenesis from axion inflation,” *JCAP*, vol. 10, p. 039, 2016.
- [92] P. Adshead, J. T. Giblin, and Z. J. Weiner, “Gravitational waves from gauge preheating,” *Phys. Rev. D*, vol. 98, no. 4, p. 043525, 2018.
- [93] J. R. C. Cuissa and D. G. Figueroa, “Lattice formulation of axion inflation. Application to preheating,” *JCAP*, vol. 06, p. 002, 2019.

- [94] P. Adshead, J. T. Giblin, M. Pieroni, and Z. J. Weiner, “Constraining axion inflation with gravitational waves from preheating,” *Phys. Rev. D*, vol. 101, no. 8, p. 083534, 2020.
- [95] P. Adshead, J. T. Giblin, M. Pieroni, and Z. J. Weiner, “Constraining axion inflation with gravitational waves across 29 decades in frequency,” *Phys. Rev. Lett.*, vol. 124, no. 17, p. 171301, 2020.
- [96] D. G. Figueroa and M. Shaposhnikov, “Lattice implementation of Abelian gauge theories with Chern–Simons number and an axion field,” *Nucl. Phys. B*, vol. 926, pp. 544–569, 2018.
- [97] D. G. Figueroa, A. Florio, and M. Shaposhnikov, “Chiral charge dynamics in Abelian gauge theories at finite temperature,” *JHEP*, vol. 10, p. 142, 2019.
- [98] J. Deskins, J. T. Giblin, and R. R. Caldwell, “Gauge Field Preheating at the End of Inflation,” *Phys. Rev. D*, vol. 88, no. 6, p. 063530, 2013.
- [99] P. Adshead, J. T. Giblin, and Z. J. Weiner, “Non-Abelian gauge preheating,” *Phys. Rev. D*, vol. 96, no. 12, p. 123512, 2017.
- [100] A. Rajantie, P. Saffin, and E. J. Copeland, “Electroweak preheating on a lattice,” *Phys. Rev. D*, vol. 63, p. 123512, 2001.
- [101] E. J. Copeland, D. Lyth, A. Rajantie, and M. Trodden, “Hybrid inflation and baryogenesis at the TeV scale,” *Phys. Rev. D*, vol. 64, p. 043506, 2001.
- [102] J. Smit and A. Tranberg, “Chern-Simons number asymmetry from CP violation at electroweak tachyonic preheating,” *JHEP*, vol. 12, p. 020, 2002.
- [103] J. Garcia-Bellido, M. Garcia-Perez, and A. Gonzalez-Arroyo, “Chern-Simons production during preheating in hybrid inflation models,” *Phys. Rev. D*, vol. 69, p. 023504, 2004.
- [104] A. Tranberg and J. Smit, “Baryon asymmetry from electroweak tachyonic preheating,” *JHEP*, vol. 11, p. 016, 2003.
- [105] J.-I. Skullerud, J. Smit, and A. Tranberg, “W and Higgs particle distributions during electroweak tachyonic preheating,” *JHEP*, vol. 08, p. 045, 2003.
- [106] M. van der Meulen, D. Sexty, J. Smit, and A. Tranberg, “Chern-Simons and winding number in a tachyonic electroweak transition,” *JHEP*, vol. 02, p. 029, 2006.
- [107] A. Diaz-Gil, J. Garcia-Bellido, M. Garcia Perez, and A. Gonzalez-Arroyo, “Magnetic field production during preheating at the electroweak scale,” *Phys. Rev. Lett.*, vol. 100, p. 241301, 2008.
- [108] A. Diaz-Gil, J. Garcia-Bellido, M. Garcia Perez, and A. Gonzalez-Arroyo, “Primordial magnetic fields from preheating at the electroweak scale,” *JHEP*, vol. 07, p. 043, 2008.
- [109] J.-F. Dufaux, D. G. Figueroa, and J. Garcia-Bellido, “Gravitational Waves from Abelian Gauge Fields and Cosmic Strings at Preheating,” *Phys. Rev. D*, vol. 82, p. 083518, 2010.
- [110] A. Tranberg, S. Thtinen, and D. J. Weir, “Gravitational waves from non-Abelian gauge fields at a tachyonic transition,” *JCAP*, vol. 04, p. 012, 2018.
- [111] K. D. Lozanov and M. A. Amin, “The charged inflaton and its gauge fields: preheating and initial conditions for reheating,” *JCAP*, vol. 06, p. 032, 2016.
- [112] K. Kohri and H. Matsui, “Higgs vacuum metastability in primordial inflation, preheating, and reheating,” *Phys. Rev. D*, vol. 94, no. 10, p. 103509, 2016.
- [113] D. G. Figueroa, A. Rajantie, and F. Torrenti, “Higgs field-curvature coupling and postinflationary vacuum instability,” *Phys. Rev. D*, vol. 98, no. 2, p. 023532, 2018.

- [114] Y. Ema, M. Karciauskas, O. Lebedev, and M. Zatta, “Early Universe Higgs dynamics in the presence of the Higgs-inflaton and non-minimal Higgs-gravity couplings,” *JCAP*, vol. 06, p. 054, 2017.
- [115] B. A. Bassett, D. I. Kaiser, and R. Maartens, “General relativistic preheating after inflation,” *Phys. Lett. B*, vol. 455, pp. 84–89, 1999.
- [116] B. A. Bassett, F. Tamburini, D. I. Kaiser, and R. Maartens, “Metric preheating and limitations of linearized gravity. 2.,” *Nucl. Phys. B*, vol. 561, pp. 188–240, 1999.
- [117] B. A. Bassett, C. Gordon, R. Maartens, and D. I. Kaiser, “Restoring the sting to metric preheating,” *Phys. Rev. D*, vol. 61, p. 061302, 2000.
- [118] F. Finelli and R. H. Brandenberger, “Parametric amplification of metric fluctuations during reheating in two field models,” *Phys. Rev. D*, vol. 62, p. 083502, 2000.
- [119] A. Chambers and A. Rajantie, “Lattice calculation of non-Gaussianity from preheating,” *Phys. Rev. Lett.*, vol. 100, p. 041302, 2008. [Erratum: *Phys. Rev. Lett.* 101, 149903 (2008)].
- [120] J. Bond, A. V. Frolov, Z. Huang, and L. Kofman, “Non-Gaussian Spikes from Chaotic Billiards in Inflation Preheating,” *Phys. Rev. Lett.*, vol. 103, p. 071301, 2009.
- [121] S. V. Imrith, D. J. Mulryne, and A. Rajantie, “Primordial curvature perturbation from lattice simulations,” *Phys. Rev. D*, vol. 100, no. 4, p. 043543, 2019.
- [122] N. Musoke, S. Hotchkiss, and R. Easther, “Lighting the Dark: Evolution of the Postinflationary Universe,” *Phys. Rev. Lett.*, vol. 124, no. 6, p. 061301, 2020.
- [123] J. T. Giblin and A. J. Tishue, “Preheating in Full General Relativity,” *Phys. Rev. D*, vol. 100, no. 6, p. 063543, 2019.
- [124] J. Martin, T. Papanikolaou, L. Pinol, and V. Vennin, “Metric preheating and radiative decay in single-field inflation,” *JCAP*, vol. 05, p. 003, 2020.
- [125] E. Cotner, A. Kusenko, M. Sasaki, and V. Takhistov, “Analytic Description of Primordial Black Hole Formation from Scalar Field Fragmentation,” *JCAP*, vol. 10, p. 077, 2019.
- [126] J. Martin, T. Papanikolaou, and V. Vennin, “Primordial black holes from the preheating instability in single-field inflation,” *JCAP*, vol. 01, p. 024, 2020.
- [127] J. Garcia-Bellido, A. D. Linde, and D. Wands, “Density perturbations and black hole formation in hybrid inflation,” *Phys. Rev. D*, vol. 54, pp. 6040–6058, 1996.
- [128] A. M. Green and K. A. Malik, “Primordial black hole production due to preheating,” *Phys. Rev. D*, vol. 64, p. 021301, 2001.
- [129] J. Hidalgo, L. Urena-Lopez, and A. R. Liddle, “Unification models with reheating via Primordial Black Holes,” *Phys. Rev. D*, vol. 85, p. 044055, 2012.
- [130] E. Torres-Lomas, J. C. Hidalgo, K. A. Malik, and L. A. Urea-Lpez, “Formation of subhorizon black holes from preheating,” *Phys. Rev. D*, vol. 89, no. 8, p. 083008, 2014.
- [131] T. Suyama, T. Tanaka, B. Bassett, and H. Kudoh, “Are black holes over-produced during preheating?,” *Phys. Rev. D*, vol. 71, p. 063507, 2005.
- [132] T. Suyama, T. Tanaka, B. Bassett, and H. Kudoh, “Black hole production in tachyonic preheating,” *JCAP*, vol. 04, p. 001, 2006.
- [133] E. Cotner, A. Kusenko, and V. Takhistov, “Primordial Black Holes from Inflaton Fragmentation into Oscillons,” *Phys. Rev. D*, vol. 98, no. 8, p. 083513, 2018.

- [134] S. Khlebnikov and I. Tkachev, “Relic gravitational waves produced after preheating,” *Phys. Rev. D*, vol. 56, pp. 653–660, 1997.
- [135] R. Easther and E. A. Lim, “Stochastic gravitational wave production after inflation,” *JCAP*, vol. 04, p. 010, 2006.
- [136] R. Easther, J. Giblin, John T., and E. A. Lim, “Gravitational Wave Production At The End Of Inflation,” *Phys. Rev. Lett.*, vol. 99, p. 221301, 2007.
- [137] J. Garcia-Bellido, D. G. Figueroa, and A. Sastre, “A Gravitational Wave Background from Reheating after Hybrid Inflation,” *Phys. Rev. D*, vol. 77, p. 043517, 2008.
- [138] J. F. Dufaux, A. Bergman, G. N. Felder, L. Kofman, and J.-P. Uzan, “Theory and Numerics of Gravitational Waves from Preheating after Inflation,” *Phys. Rev. D*, vol. 76, p. 123517, 2007.
- [139] J.-F. Dufaux, G. Felder, L. Kofman, and O. Navros, “Gravity Waves from Tachyonic Preheating after Hybrid Inflation,” *JCAP*, vol. 03, p. 001, 2009.
- [140] S.-Y. Zhou, E. J. Copeland, R. Easther, H. Finkel, Z.-G. Mou, and P. M. Saffin, “Gravitational Waves from Oscillon Preheating,” *JHEP*, vol. 10, p. 026, 2013.
- [141] L. Bethke, D. G. Figueroa, and A. Rajantie, “Anisotropies in the Gravitational Wave Background from Preheating,” *Phys. Rev. Lett.*, vol. 111, no. 1, p. 011301, 2013.
- [142] L. Bethke, D. G. Figueroa, and A. Rajantie, “On the Anisotropy of the Gravitational Wave Background from Massless Preheating,” *JCAP*, vol. 06, p. 047, 2014.
- [143] S. Antusch, F. Cefala, and S. Orani, “Gravitational waves from oscillons after inflation,” *Phys. Rev. Lett.*, vol. 118, no. 1, p. 011303, 2017. [Erratum: *Phys.Rev.Lett.* 120, 219901 (2018)].
- [144] S. Antusch, F. Cefala, S. Krippendorff, F. Muia, S. Orani, and F. Quevedo, “Oscillons from String Moduli,” *JHEP*, vol. 01, p. 083, 2018.
- [145] S. Antusch, F. Cefala, and S. Orani, “What can we learn from the stochastic gravitational wave background produced by oscillons?,” *JCAP*, vol. 03, p. 032, 2018.
- [146] J. Liu, Z.-K. Guo, R.-G. Cai, and G. Shiu, “Gravitational wave production after inflation with cuspy potentials,” *Phys. Rev. D*, vol. 99, no. 10, p. 103506, 2019.
- [147] D. G. Figueroa and F. Torrenti, “Gravitational wave production from preheating: parameter dependence,” *JCAP*, vol. 10, p. 057, 2017.
- [148] C. Fu, P. Wu, and H. Yu, “Production of gravitational waves during preheating with nonminimal coupling,” *Phys. Rev. D*, vol. 97, no. 8, p. 081303, 2018.
- [149] K. D. Lozanov and M. A. Amin, “Gravitational perturbations from oscillons and transients after inflation,” *Phys. Rev. D*, vol. 99, no. 12, p. 123504, 2019.
- [150] C. Armendariz-Picon, “On the Expected Production of Gravitational Waves During Preheating,” *JCAP*, vol. 08, p. 012, 2019.
- [151] C. Caprini and D. G. Figueroa, “Cosmological Backgrounds of Gravitational Waves,” *Class. Quant. Grav.*, vol. 35, no. 16, p. 163001, 2018.
- [152] M. Hindmarsh and T. Kibble, “Cosmic strings,” *Rept. Prog. Phys.*, vol. 58, pp. 477–562, 1995.
- [153] E. J. Copeland and T. Kibble, “Cosmic Strings and Superstrings,” *Proc. Roy. Soc. Lond. A*, vol. A466, pp. 623–657, 2010.

- [154] K. D. Lozanov and M. A. Amin, “GFIRE: a Gauge Field integrator for Reheating,” *JCAP*, vol. 04, p. 058, 2020.
- [155] G. Vincent, N. D. Antunes, and M. Hindmarsh, “Numerical simulations of string networks in the Abelian Higgs model,” *Phys. Rev. Lett.*, vol. 80, pp. 2277–2280, 1998.
- [156] N. Bevis, M. Hindmarsh, M. Kunz, and J. Urrestilla, “CMB power spectrum contribution from cosmic strings using field-evolution simulations of the Abelian Higgs model,” *Phys. Rev. D*, vol. 75, p. 065015, 2007.
- [157] M. Hindmarsh, K. Rummukainen, T. V. I. Tenkanen, and D. J. Weir, “Improving cosmic string network simulations,” *Phys. Rev. D*, vol. 90, no. 4, p. 043539, 2014. [Erratum: *Phys.Rev.D* 94, 089902 (2016)].
- [158] D. Daverio, M. Hindmarsh, M. Kunz, J. Lizarraga, and J. Urrestilla, “Energy-momentum correlations for Abelian Higgs cosmic strings,” *Phys. Rev. D*, vol. 93, no. 8, p. 085014, 2016. [Erratum: *Phys.Rev.D* 95, 049903 (2017)].
- [159] J. Lizarraga, J. Urrestilla, D. Daverio, M. Hindmarsh, and M. Kunz, “New CMB constraints for Abelian Higgs cosmic strings,” *JCAP*, vol. 10, p. 042, 2016.
- [160] M. Hindmarsh, J. Lizarraga, J. Urrestilla, D. Daverio, and M. Kunz, “Type I Abelian Higgs strings: evolution and Cosmic Microwave Background constraints,” *Phys. Rev. D*, vol. 99, no. 8, p. 083522, 2019.
- [161] M. Hindmarsh, J. Lizarraga, A. Lopez-Eiguren, and J. Urrestilla, “Scaling Density of Axion Strings,” *Phys. Rev. Lett.*, vol. 124, no. 2, p. 021301, 2020.
- [162] D. G. Figueroa, M. Hindmarsh, and J. Urrestilla, “Exact Scale-Invariant Background of Gravitational Waves from Cosmic Defects,” *Phys. Rev. Lett.*, vol. 110, no. 10, p. 101302, 2013.
- [163] M. A. Amin, R. Easther, H. Finkel, R. Flauger, and M. P. Hertzberg, “Oscillons After Inflation,” *Phys. Rev. Lett.*, vol. 108, p. 241302, 2012.
- [164] K. D. Lozanov and M. A. Amin, “Self-resonance after inflation: oscillons, transients and radiation domination,” *Phys. Rev. D*, vol. 97, no. 2, p. 023533, 2018.
- [165] M. A. Amin, J. Braden, E. J. Copeland, J. T. Giblin, C. Solorio, Z. J. Weiner, and S.-Y. Zhou, “Gravitational waves from asymmetric oscillon dynamics?,” *Phys. Rev. D*, vol. 98, p. 024040, 2018.
- [166] N. Kitajima, J. Soda, and Y. Urakawa, “Gravitational wave forest from string axiverse,” *JCAP*, vol. 10, p. 008, 2018.
- [167] S. Antusch, F. Cefal, and F. Torrent, “Properties of Oscillons in Hilltop Potentials: energies, shapes, and lifetimes,” *JCAP*, vol. 10, p. 002, 2019.
- [168] S. Kasuya, M. Kawasaki, F. Otani, and E. Sonomoto, “Revisiting oscillon formation in KKLT scenario,” 1 2020.
- [169] K. Enqvist, S. Kasuya, and A. Mazumdar, “Inflatonic solitons in running mass inflation,” *Phys. Rev. D*, vol. 66, p. 043505, 2002.
- [170] M. A. Amin and P. Mocz, “Formation, gravitational clustering, and interactions of nonrelativistic solitons in an expanding universe,” *Phys. Rev. D*, vol. 100, no. 6, p. 063507, 2019.
- [171] J. C. Niemeyer and R. Easther, “Inflaton Clusters and Inflaton Stars,” 11 2019.
- [172] A. Diaz-Gil, J. Garcia-Bellido, M. Garcia Perez, and A. Gonzalez-Arroyo, “Magnetic field production after inflation,” *PoS*, vol. LAT2005, p. 242, 2006.

- [173] A. Diaz-Gil, J. Garcia-Bellido, M. Garcia Perez, and A. Gonzalez-Arroyo, “Primordial magnetic fields at preheating,” *PoS*, vol. LATTICE2007, p. 052, 2007.
- [174] T. Fujita and R. Namba, “Pre-reheating Magnetogenesis in the Kinetic Coupling Model,” *Phys. Rev. D*, vol. 94, no. 4, p. 043523, 2016.
- [175] S. Vilchinskii, O. Sobol, E. Gorbar, and I. Rudenok, “Magnetogenesis during inflation and preheating in the Starobinsky model,” *Phys. Rev. D*, vol. 95, no. 8, p. 083509, 2017.
- [176] E. W. Kolb, A. D. Linde, and A. Riotto, “GUT baryogenesis after preheating,” *Phys. Rev. Lett.*, vol. 77, pp. 4290–4293, 1996.
- [177] E. W. Kolb, A. Riotto, and I. I. Tkachev, “GUT baryogenesis after preheating: Numerical study of the production and decay of X bosons,” *Phys. Lett. B*, vol. 423, pp. 348–354, 1998.
- [178] J. Garcia-Bellido, D. Y. Grigoriev, A. Kusenko, and M. E. Shaposhnikov, “Nonequilibrium electroweak baryogenesis from preheating after inflation,” *Phys. Rev. D*, vol. 60, p. 123504, 1999.
- [179] R. Allahverdi, B. A. Campbell, and J. R. Ellis, “Reheating and supersymmetric flat direction baryogenesis,” *Nucl. Phys. B*, vol. 579, pp. 355–375, 2000.
- [180] J. Cornwall, D. Grigoriev, and A. Kusenko, “Resonant amplification of electroweak baryogenesis at preheating,” *Phys. Rev. D*, vol. 64, p. 123518, 2001.
- [181] A. Tranberg, A. Hernandez, T. Konstandin, and M. G. Schmidt, “Cold electroweak baryogenesis with Standard Model CP violation,” *Phys. Lett. B*, vol. 690, pp. 207–212, 2010.
- [182] K. Kamada, K. Kohri, and S. Yokoyama, “Affleck-Dine baryogenesis with modulated reheating,” *JCAP*, vol. 01, p. 027, 2011.
- [183] K. D. Lozanov and M. A. Amin, “End of inflation, oscillons, and matter-antimatter asymmetry,” *Phys. Rev. D*, vol. 90, no. 8, p. 083528, 2014.
- [184] D. I. Podolsky, G. N. Felder, L. Kofman, and M. Peloso, “Equation of state and beginning of thermalization after preheating,” *Phys. Rev. D*, vol. 73, p. 023501, 2006.
- [185] K. D. Lozanov and M. A. Amin, “Equation of State and Duration to Radiation Domination after Inflation,” *Phys. Rev. Lett.*, vol. 119, no. 6, p. 061301, 2017.
- [186] D. G. Figueroa and F. Torrenti, “Parametric resonance in the early Universe—a fitting analysis,” *JCAP*, vol. 02, p. 001, 2017.
- [187] T. Krajewski, K. Turzyński, and M. Wieczorek, “On preheating in α -attractor models of inflation,” *Eur. Phys. J. C*, vol. 79, no. 8, p. 654, 2019.
- [188] S. Antusch, D. G. Figueroa, K. Marschall, and F. Torrenti, “Energy distribution and equation of state of the early Universe: matching the end of inflation and the onset of radiation domination,” 5 2020.
- [189] M. A. Garcia and M. A. Amin, “Prethermalization production of dark matter,” *Phys. Rev. D*, vol. 98, no. 10, p. 103504, 2018.
- [190] M. Hindmarsh and A. Rajantie, “Phase transition dynamics in the hot Abelian Higgs model,” *Phys. Rev. D*, vol. 64, p. 065016, 2001.
- [191] A. Rajantie and E. J. Copeland, “Phase transitions from preheating in gauge theories,” *Phys. Rev. Lett.*, vol. 85, p. 916, 2000.
- [192] D. G. Figueroa and M. Shaposhnikov, “Anomalous non-conservation of fermion/chiral number in Abelian gauge theories at finite temperature,” *JHEP*, vol. 04, p. 026, 2018.

- [193] A. Brandenburg, T. Kahniashvili, S. Mandal, A. Roper Pol, A. G. Tevzadze, and T. Vachaspati, “Evolution of hydromagnetic turbulence from the electroweak phase transition,” *Phys. Rev. D*, vol. 96, no. 12, p. 123528, 2017.
- [194] A. Brandenburg, T. Kahniashvili, S. Mandal, A. R. Pol, A. G. Tevzadze, and T. Vachaspati, “The dynamo effect in decaying helical turbulence,” *Phys. Rev. Fluids.*, vol. 4, p. 024608, 2019.
- [195] M. Hindmarsh, S. J. Huber, K. Rummukainen, and D. J. Weir, “Gravitational waves from the sound of a first order phase transition,” *Phys. Rev. Lett.*, vol. 112, p. 041301, 2014.
- [196] M. Hindmarsh, S. J. Huber, K. Rummukainen, and D. J. Weir, “Numerical simulations of acoustically generated gravitational waves at a first order phase transition,” *Phys. Rev. D*, vol. 92, no. 12, p. 123009, 2015.
- [197] M. Hindmarsh, S. J. Huber, K. Rummukainen, and D. J. Weir, “Shape of the acoustic gravitational wave power spectrum from a first order phase transition,” *Phys. Rev. D*, vol. 96, no. 10, p. 103520, 2017. [Erratum: *Phys.Rev.D* 101, 089902 (2020)].
- [198] D. Cutting, M. Hindmarsh, and D. J. Weir, “Gravitational waves from vacuum first-order phase transitions: from the envelope to the lattice,” *Phys. Rev. D*, vol. 97, no. 12, p. 123513, 2018.
- [199] D. Cutting, M. Hindmarsh, and D. J. Weir, “Vorticity, kinetic energy, and suppressed gravitational wave production in strong first order phase transitions,” 6 2019.
- [200] A. Roper Pol, S. Mandal, A. Brandenburg, T. Kahniashvili, and A. Kosowsky, “Numerical Simulations of Gravitational Waves from Early-Universe Turbulence,” 3 2019.
- [201] D. Cutting, E. G. Escartin, M. Hindmarsh, and D. J. Weir, “Gravitational waves from vacuum first order phase transitions II: from thin to thick walls,” 5 2020.
- [202] M. Hindmarsh and A. Rajantie, “Defect formation and local gauge invariance,” *Phys. Rev. Lett.*, vol. 85, pp. 4660–4663, 2000.
- [203] A. Rajantie, “Formation of topological defects in gauge field theories,” *Int. J. Mod. Phys. A*, vol. 17, pp. 1–44, 2002.
- [204] A. Rajantie, “Magnetic monopoles from gauge theory phase transitions,” *Phys. Rev. D*, vol. 68, p. 021301, 2003.
- [205] M. Donaire, T. Kibble, and A. Rajantie, “Spontaneous vortex formation on a superconductor film,” *New J. Phys.*, vol. 9, p. 148, 2007.
- [206] T. Hiramatsu, M. Kawasaki, K. Saikawa, and T. Sekiguchi, “Axion cosmology with long-lived domain walls,” *JCAP*, vol. 01, p. 001, 2013.
- [207] M. Kawasaki, K. Saikawa, and T. Sekiguchi, “Axion dark matter from topological defects,” *Phys. Rev. D*, vol. 91, no. 6, p. 065014, 2015.
- [208] L. M. Fleury and G. D. Moore, “Axion String Dynamics I: 2+1D,” *JCAP*, vol. 05, p. 005, 2016.
- [209] G. D. Moore, “Axion dark matter and the Lattice,” *EPJ Web Conf.*, vol. 175, p. 01009, 2018.
- [210] B. Eggemeier, J. Redondo, K. Dolag, J. C. Niemeyer, and A. Vaquero, “First simulations of axion minicluster halos,” 11 2019.
- [211] M. Gorghetto, E. Hardy, and G. Villadoro, “Axions from Strings: the Attractive Solution,” *JHEP*, vol. 07, p. 151, 2018.

- [212] T. Hiramatsu, M. Kawasaki, and K. Saikawa, “On the estimation of gravitational wave spectrum from cosmic domain walls,” *JCAP*, vol. 02, p. 031, 2014.
- [213] E. W. Kolb and I. I. Tkachev, “Nonlinear axion dynamics and formation of cosmological pseudosolitons,” *Phys. Rev. D*, vol. 49, pp. 5040–5051, 1994.
- [214] M. Buschmann, J. W. Foster, and B. R. Safdi, “Early-Universe Simulations of the Cosmological Axion,” *Phys. Rev. Lett.*, vol. 124, no. 16, p. 161103, 2020.
- [215] H. Fukunaga, N. Kitajima, and Y. Urakawa, “Efficient self-resonance instability from axions,” *JCAP*, vol. 06, p. 055, 2019.
- [216] T. Patel, H. Tashiro, and Y. Urakawa, “Resonant magnetogenesis from axions,” *JCAP*, vol. 01, p. 043, 2020.
- [217] J. T. Giblin, G. Kane, E. Nesbit, S. Watson, and Y. Zhao, “Was the Universe Actually Radiation Dominated Prior to Nucleosynthesis?,” *Phys. Rev. D*, vol. 96, no. 4, p. 043525, 2017.
- [218] M. A. Amin, J. Fan, K. D. Lozanov, and M. Reece, “Cosmological dynamics of Higgs potential fine tuning,” *Phys. Rev. D*, vol. 99, no. 3, p. 035008, 2019.
- [219] O. Philipsen, “The Sphaleron rate in the ‘symmetric’ electroweak phase,” *Phys. Lett. B*, vol. 358, pp. 210–216, 1995.
- [220] J. Ambjorn and A. Krasnitz, “The Classical sphaleron transition rate exists and is equal to $1.1 (\alpha(w) T)^{**4}$,” *Phys. Lett. B*, vol. 362, pp. 97–104, 1995.
- [221] P. B. Arnold and L. G. Yaffe, “The NonAbelian Debye screening length beyond leading order,” *Phys. Rev. D*, vol. 52, pp. 7208–7219, 1995.
- [222] P. B. Arnold, D. Son, and L. G. Yaffe, “The Hot baryon violation rate is $O(\alpha-w^{**5} T^{**4})$,” *Phys. Rev. D*, vol. 55, pp. 6264–6273, 1997.
- [223] P. B. Arnold, “Hot B violation, the lattice, and hard thermal loops,” *Phys. Rev. D*, vol. 55, pp. 7781–7796, 1997.
- [224] G. D. Moore, C.-r. Hu, and B. Muller, “Chern-Simons number diffusion with hard thermal loops,” *Phys. Rev. D*, vol. 58, p. 045001, 1998.
- [225] D. Bodeker, “On the effective dynamics of soft nonAbelian gauge fields at finite temperature,” *Phys. Lett. B*, vol. 426, pp. 351–360, 1998.
- [226] G. D. Moore, “The Sphaleron rate: Bodeker’s leading log,” *Nucl. Phys. B*, vol. 568, pp. 367–404, 2000.
- [227] G. D. Moore and K. Rummukainen, “Classical sphaleron rate on fine lattices,” *Phys. Rev. D*, vol. 61, p. 105008, 2000.
- [228] D. Bodeker, G. D. Moore, and K. Rummukainen, “Chern-Simons number diffusion and hard thermal loops on the lattice,” *Phys. Rev. D*, vol. 61, p. 056003, 2000.
- [229] P. B. Arnold and L. G. Yaffe, “High temperature color conductivity at next-to-leading log order,” *Phys. Rev. D*, vol. 62, p. 125014, 2000.
- [230] W.-H. Tang and J. Smit, “Chern-Simons diffusion rate near the electroweak phase transition for $m(H)$ approximates $m(W)$,” *Nucl. Phys. B*, vol. 482, pp. 265–285, 1996.
- [231] J. Ambjorn and A. Krasnitz, “Improved determination of the classical sphaleron transition rate,” *Nucl. Phys. B*, vol. 506, pp. 387–403, 1997.

- [232] G. D. Moore, “Sphaleron rate in the symmetric electroweak phase,” *Phys. Rev. D*, vol. 62, p. 085011, 2000.
- [233] M. D’Onofrio, K. Rummukainen, and A. Tranberg, “The Sphaleron Rate through the Electroweak Cross-over,” *JHEP*, vol. 08, p. 123, 2012.
- [234] M. D’Onofrio and K. Rummukainen, “Standard model cross-over on the lattice,” *Phys. Rev. D*, vol. 93, no. 2, p. 025003, 2016.
- [235] P. Buividovich and M. Ulybyshev, “Numerical study of chiral plasma instability within the classical statistical field theory approach,” *Phys. Rev. D*, vol. 94, no. 2, p. 025009, 2016.
- [236] P. Buividovich and S. Valgushev, “First experience with classical-statistical real-time simulations of anomalous transport with overlap fermions,” *PoS*, vol. LATTICE2016, p. 253, 2016.
- [237] M. Mace, N. Mueller, S. Schlichting, and S. Sharma, “Chiral instabilities & the onset of chiral turbulence in QED plasmas,” *Phys. Rev. Lett.*, vol. 124, no. 19, p. 191604, 2020.
- [238] M. Mace, N. Mueller, S. Schlichting, and S. Sharma, “Chirality transfer & chiral turbulence in gauge theories,” in *28th International Conference on Ultrarelativistic Nucleus-Nucleus Collisions*, 3 2020.
- [239] Y. Akamatsu, A. Rothkopf, and N. Yamamoto, “Non-Abelian chiral instabilities at high temperature on the lattice,” *JHEP*, vol. 03, p. 210, 2016.
- [240] K. Boguslavski, A. Kurkela, T. Lappi, and J. Peuron, “Spectral function for overoccupied gluodynamics from real-time lattice simulations,” *Phys. Rev. D*, vol. 98, no. 1, p. 014006, 2018.
- [241] S. Schlichting, D. Smith, and L. von Smekal, “Spectral functions and critical dynamics of the $O(4)$ model from classical-statistical lattice simulations,” *Nucl. Phys. B*, vol. 950, p. 114868, 2020.
- [242] M. Laine, G. D. Moore, O. Philipsen, and M. Tassler, “Heavy Quark Thermalization in Classical Lattice Gauge Theory: Lessons for Strongly-Coupled QCD,” *JHEP*, vol. 05, p. 014, 2009.
- [243] M. Laine and A. Rothkopf, “Light-cone Wilson loop in classical lattice gauge theory,” *JHEP*, vol. 07, p. 082, 2013.
- [244] M. Panero, K. Rummukainen, and A. Schfer, “Lattice Study of the Jet Quenching Parameter,” *Phys. Rev. Lett.*, vol. 112, no. 16, p. 162001, 2014.
- [245] K. Boguslavski, A. Kurkela, T. Lappi, and J. Peuron, “Heavy quark diffusion in an overoccupied gluon plasma,” 5 2020.
- [246] G. N. Felder and I. Tkachev, “LATTICEEASY: A Program for lattice simulations of scalar fields in an expanding universe,” *Comput. Phys. Commun.*, vol. 178, pp. 929–932, 2008.
- [247] G. N. Felder, “CLUSTEREASY: A program for lattice simulations of scalar fields in an expanding universe on parallel computing clusters,” *Comput. Phys. Commun.*, vol. 179, pp. 604–606, 2008.
- [248] A. V. Frolov, “DEFROST: A New Code for Simulating Preheating after Inflation,” *JCAP*, vol. 11, p. 009, 2008.
- [249] J. Sainio, “CUDA EASY - a GPU Accelerated Cosmological Lattice Program,” *Comput. Phys. Commun.*, vol. 181, pp. 906–912, 2010.
- [250] Z. Huang, “The Art of Lattice and Gravity Waves from Preheating,” *Phys. Rev. D*, vol. 83, p. 123509, 2011.
- [251] J. Sainio, “PyCOOL - a Cosmological Object-Oriented Lattice code written in Python,” *JCAP*, vol. 04, p. 038, 2012.

- [252] H. L. Child, J. Giblin, John T., R. H. Ribeiro, and D. Seery, “Preheating with Non-Minimal Kinetic Terms,” *Phys. Rev. Lett.*, vol. 111, p. 051301, 2013.
- [253] R. Easther, H. Finkel, and N. Roth, “PSpectRe: A Pseudo-Spectral Code for (P)reheating,” *JCAP*, vol. 10, p. 025, 2010.
- [254] M. Pippig, “PFFT - An extension of FFTW to massively parallel architectures,” *SIAM J. Sci. Comput.*, vol. 35, pp. C213 – C236, 2013.
- [255] D. G. Figueroa, A. Florio, and F. Torrenti *In preparation*.
- [256] P. M. Saffin and A. Tranberg, “Real-time Fermions for Baryogenesis Simulations,” *JHEP*, vol. 07, p. 066, 2011.
- [257] P. M. Saffin and A. Tranberg, “Dynamical simulations of electroweak baryogenesis with fermions,” *JHEP*, vol. 02, p. 102, 2012.
- [258] Z.-G. Mou, P. M. Saffin, and A. Tranberg, “Ensemble fermions for electroweak dynamics and the fermion preheating temperature,” *JHEP*, vol. 11, p. 097, 2013.
- [259] Z.-G. Mou, P. M. Saffin, and A. Tranberg, “Cold Baryogenesis from first principles in the Two-Higgs Doublet model with Fermions,” *JHEP*, vol. 06, p. 163, 2015.
- [260] G. Aarts and J. Smit, “Real time dynamics with fermions on a lattice,” *Nucl. Phys. B*, vol. 555, pp. 355–394, 1999.
- [261] S. Borsanyi and M. Hindmarsh, “Low-cost fermions in classical field simulations,” *Phys. Rev. D*, vol. 79, p. 065010, 2009.
- [262] D. G. Figueroa, J. Garcia-Bellido, and A. Rajantie, “On the Transverse-Traceless Projection in Lattice Simulations of Gravitational Wave Production,” *JCAP*, vol. 11, p. 015, 2011.
- [263] A. Lopez-Eiguren, J. Lizarraga, M. Hindmarsh, and J. Urrestilla, “Cosmic Microwave Background constraints for global strings and global monopoles,” *JCAP*, vol. 07, p. 026, 2017.
- [264] openQCD, <https://luscher.web.cern.ch/luscher/openQCD/>.
- [265] M. Clark, R. Babich, K. Barros, R. Brower, and C. Rebbi, “Solving Lattice QCD systems of equations using mixed precision solvers on GPUs,” *Comput. Phys. Commun.*, vol. 181, pp. 1517–1528, 2010.
- [266] N. Aghanim *et al.*, “Planck 2018 results. VI. Cosmological parameters,” 7 2018.
- [267] V. Vlasov, V. Matveev, A. Tavkhelidze, S. Khlebnikov, and M. Shaposhnikov, “Canonical Quantization of Gauge Theories With Scalar Condensate and the Problem of Spontaneous Symmetry Breaking. (In Russian),” *Fiz. Elem. Chast. Atom. Yadra*, vol. 18, pp. 5–38, 1987.
- [268] H. Yoshida, “Construction of higher order symplectic integrators,” *Phys. Lett. A*, vol. 150, pp. 262–268, 1990.
- [269] W. Kahan and R.-C. Li, “Composition constants for raising the orders of unconventional schemes for ordinary differential equations,” *Mathematics of Computation*, vol. 66, pp. 1089–1099, July 1997.
- [270] J. C. Butcher, “Implicit runge-kutta processes,” *Mathematics of Computation*, vol. 18, no. 85, pp. 50–64, 1964.
- [271] R. Kallosh and A. Linde, “Universality Class in Conformal Inflation,” *JCAP*, vol. 07, p. 002, 2013.
- [272] M. S. Turner, “Coherent Scalar Field Oscillations in an Expanding Universe,” *Phys. Rev. D*, vol. 28, p. 1243, 1983.

- [273] D. G. Figueroa, J. Garcia-Bellido, and F. Torrenti *In preparation*.
- [274] V. Kasper, F. Hebenstreit, and J. Berges, “Fermion production from real-time lattice gauge theory in the classical-statistical regime,” *Phys. Rev. D*, vol. 90, no. 2, p. 025016, 2014.
- [275] J. Ambjorn, T. Askgaard, H. Porter, and M. Shaposhnikov, “Sphaleron transitions and baryon asymmetry: A Numerical real time analysis,” *Nucl. Phys. B*, vol. 353, pp. 346–378, 1991.
- [276] G. D. Moore, “Motion of Chern-Simons number at high temperatures under a chemical potential,” *Nucl. Phys. B*, vol. 480, pp. 657–688, 1996.
- [277] A. Krasnitz, “Thermalization algorithms for classical gauge theories,” *Nucl. Phys. B*, vol. 455, pp. 320–338, 1995.